CHARLES UNIVERSITY

Faculty of Science

Department of Physical and Macromolecular Chemistry

RNDr. Veronika Gajdošová (born Sutrová)

NEW PATHWAYS TO PLASMONIC NANOPARTICLE ASSEMBLING INTO 2D AND 3D HYBRID ACTIVE SYSTEMS FOR SERS OF GRAPHENE AND SERS, SERRS AND GERS + SERS OF AROMATIC MOLECULES

Nové přístupy k uspořádávání plasmonických nanočástic do 2D a 3D hybridních aktivních systémů pro SERS grafenu a pro SERS, SERRS a SERS + GERS aromatických molekul

Doctoral Thesis

of study program Physical Chemistry

Supervisor: Prof. RNDr. Blanka Vlčková, CSc.

Consultant: RNDr. Ivana Šloufová, Ph.D.

doc. RNDr. Miroslav Šlouf, Ph.D.

Prague, 2019

Prohlášení

Prohlašuji, že jsem závěrečnou práci zpracovala samostatně pod vedením své školitelky prof. RNDr. Blanky Vlčkové, CSc. a že jsem uvedla všechny použité informační zdroje a literaturu. Tato práce ani její podstatná část nebyla předložena k získání jiného nebo stejného akademického titulu.

V Praze,

Podpis

Poděkování

Nejprve bych ráda poděkovala své školitelce prof. RNDr. Blance Vlčkové, CSc. a mé konzultantce RNDr. Ivaně Šloufové, Ph.D., za velice přátelskou a rodinnou atmosféru, kterou vytvářely ve skupině po celou dobu mého studia. Vždy jsem se ve skupině cítila dobře, a ačkoliv věda není jednoduchá, nikdy jsem v jejich přítomnosti neměla pocit, že bychom společně něco nezvládly.

Své školitelce prof. RNDr. Blance Vlčkové, CSc. bych ráda dále poděkovala za její laskavý a velice přátelský přístup. Ráda bych ji poděkovala za pomoc a za rady, jak profesní, tak osobní, které měla nejen při vypracovávání této práce, ale i v průběhu celého mého studia.

Neméně velký dík patří mé konzultantce RNDr. Ivaně Šloufové, Ph.D., která mi vždy byla ochotna pomoci a to nejen s experimenty. Velice ji děkuji za pomoc při výpočtech použitých v této práci, zejména za obrazovou analýzu TEM snímků. Další velký dík patří mému druhému konzultantovi doc. RNDr. Miroslavu Šloufovi, Ph.D., který mi umožnil nejen přístup k elektronovým mikroskopům, ale umožnil mi i získávat praxi, a to nejen v oboru elektronové mikroskopie.

Ráda bych poděkovala mým dalším kolegyním RNDr. Sabině Krejčíkové a Jiřině Hromádkové za zaučení při práci s elektronovými mikroskopy.

V neposlední řadě bych ráda poděkovala své rodině za podporu. Z mých blízkých bych ráda nejvíce poděkovala svému manželovi, za to, že mi byl v průběhu celého mého doktorského studia obrovskou oporou a podporou a v těžkých chvílích mi dával sílu jít dál.

Děkuji.

Abstrakt

První část práce se zabývá vývojem a testováním nových typů aktivních systémů pro SERS a SERRS měření hydrofobních molekul. Byly vyvinuty 3D nanohoubovité agregáty s včleněnými hydrofobními molekulami do vnitřní struktury. Jako hydrofobní testovací molekuly byl zvolen fulleren C_{60} a H_2TPP. Byly určeny meze SERS a SERRS spektrální detekce (LODs) fullerenu C_{60} na 4 excitačních vlnových délkách, přičemž LODs fullerenu C_{60} byly ve všech případech o řád nižší než v případě referenčního systému, který napodoboval již dříve využité Ag nanohoubovité agregáty pro SERS a SERRS spektrální měření. Zlepšení detekčních schopností agregátu je způsobeno efektivní lokalizací hydrofobních molekul do „hot spotů“ ve 2D fraktálních agregátech Ag nanočástic (NČ). Diprotonace molekul H_2TPP v průběhu přípravy, způsobená použitím HCl jako preagregačního činidla byla eliminována nahrazením NaCl za HCl během přípravy agregátu. Na druhou stranu, studium mechanismu diprotonace ukázalo na možnost využití agergátu jako nanoreaktoru.

Druhá část práce se zabývá přípravou 2D struktur tvořených Ag nanočásticemi jakožto vhodnějšími substráty pro SERS monovrstevného grafenu (SLG) než jakými jsou 3D struktury. 2D nanočásticové (NČ) struktury modifikované ethanthiolátovým spacerem, nanesené na povrch SLG umožňovaly získat SERS spektra neporušeného grafenu. Byl připraven i inverzní hybridní systém označovaný jako soubor AgNČ/SLG, u kterého bylo pozorováno SERS spektrálním testováním slabé negativní dopování grafenu, které bylo způsobeno přítomnými Ag nanočásticemi.

Třetí část práce se zabývá hybridním systémem tvořeným soubory AgNČ/SLG/H_2Pc(MV) [MV = monovrstva] a využívaným ke zkoumání mechanismu kombinovaného povrchem a grafenem zesíleného Ramanova rozptylu (SERS + GERS) monovrstvy molekul H_2Pc. Pomocí mikro-Ramanova spektrálního testování hybridního systému a referentního vzorku na 5 excitačních vlnových délkách byly určeny SERS, GERS a SERS + GERS faktory zesílení. Rovněž byly vytovřeny SERS + GERS excitační profily molekuly H_2Pc. Byly prokázány dva mechanismy GERSu (i) první mechanismus je založen na modifikaci polohy a lokalizace $Q_y(0,1)$ elektronového přechodu a (ii) druhý mechanismus představuje přenose náboje z Fermiho hladiny SLG do LUMO hladiny H_2Pc. Rovněž bylo prokázáno jejich aditivní působení s elektromagnetickcým mechanismem SERSu.

Abstract

In the first part of the Thesis, a new type of active system for SERS and SERRS of hydrophobic molecules, namely a 3-dimensional (3D) nanosponge aggregate with incorporated hydrophobic molecules has been developed, and tested by fullerene C_{60} and hydrophobic free-base tetraphenylporfine (H_2TPP). The SERS and SERRS (surface enhanced /resonance/ Raman scattering) limits of detection (LODs) of C_{60} at four excitation wavelengths spanning the visible spectral region were found to be by one order of magnitude lower than in the reference system, which mimics the previously reported ways of utilization of Ag nanosponges as substrates for SERS and SERRS. The superiority of the newly developed sample is attributed to the efficient localization of the hydrophobic molecules into hot spots in 2D fractal aggregates of Ag nanoparticles (NPs). Diprotonation of H_2TPP during the procedure using HCl as the preaggregation agent has been eliminated by employment of NaCl. On the other hand, investigation of the mechanism of H_2TPP protonation during the former preparation procedure opened a possibility to employ Ag nanosponge aggregate as nanoreactor.

In the second part of the Thesis, 2D assemblies of AgNPs were found to be better substrates for SERS of single layer graphene (SLG) than the 3D ones. In particular, the 2D assembly of Ag NPs modified by ethanethiolate spacer deposited on SLG on glass enabled to obtain SERS of unperturbed SLG. By inversion of the preparation procedure, AgNPs array/SLG hybrid systems were prepared, and a weak negative doping of SLG by Ag NPs was revealed by SERS spectral probing.

In the third part, the last mentioned hybrid system was employed as a platform for assembling of AgNPs arrays/SLG/H_2Pc (ML) [H_2Pc = free base phthalocyanine, ML = monolayer] hybrid system for investigation of the mechanism of combined surface- and graphene-enhanced Raman scattering (SERS+GERS) of a monolayer of planar aromatic molecule, namely H_2Pc. By micro-Raman spectral probing of the hybrid sample as well as of the appropriate reference systems at 5 excitation wavelengths, SERS, GERS and SERS + GERS enhanced factors and SERS + GERS excitation profiles of H_2Pc spectral bands were determined. Two mechanisms of GERS, in particular (i) modification of the position and localization of the $Q_y(0,1)$ electronic transition in the visible region and (ii) a charge transfer from Fermi level of SLG (positioned at -4.4 eV) to LUMO of H_2Pc and their additive operation with the electromagnetic mechanism of SERS were established.

List of publications

Sutrová, V.; Šloufová, I.; Mojzeš, P.; Melníková, Z.; Kalbáč, M.; Vlčková, B. Excitation Wavelenght Dependence of Combined Surface- and Graphene-Enhanced Raman Scattering Experienced by Free-Base Phthalocyanine Localized on Single-Layer Graphene-Covered Ag Nanoparticle Arrays, *J. Phys. Chem. C*, **2018**, *122*, 20850 – 20860 (IF 4.484).

Sutrová, V.; Šloufová, I.; Melníková, Z.; Kalbáč, M.; Pavlova, E.; Vlčková, B. Effect of Ethanethiolate Spacer on Morphology and Optical Responses of Ag Nanoparticle Array-Single Layer Graphene Hybrid Systems, *Langmuir*, **2017**, *33 (50)*, 14414 – 14424 (IF 3.833).

Uhlířová, T.; Mojzeš, P.; Melníková, Z.; Kalbáč, M.; **Sutrová, V.,** Šloufová, I.; Vlčková, B. Raman excitation profiles of hybrid systems constituted by single layer graphene and free base phthalocyanine: Manifestations of two mechanisms of graphene-enhanced Raman scattering, *J. Raman. Spectr.,* **2017,** *48 (10)*, 1270 – 1281 (IF 2.969).

Further publications:

Prusková, M.; **Sutrová, V.;** Šlouf, M.; Vlčková, B.; Vohlídal, J.; Šloufová, I. Arrays of Ag and Au Nanoparticles with Terpyridine- and Thiophene-Based Ligands: Morphology and Optical Responses, *Langmuir*, **2017**, *33 (17)*, 4146 – 4156 (IF 3.833).

Sutrová, V., Šloufová, I., Nevoralová, M., Vlčková, B., SERS microRaman spectral probing of adsorbate-containing, liyuid-overlayed nanosponge Ag aggregates assembled from fractal aggregates, *J. Raman. Spectr.*, **2015**, *46 (6)*, 559 – 565 (IF 2.671).

Šlouf, M.; Michálková, D.; **Gajdošová, V.**; Dybal, J.; Pilař, J. Prooxidant activity of phenolic stabilizers in polyolefins during accelerated photooxidation. *Polym. Degrad. Stab*., MS in the review process

Šloufová, I.; Šlouf, M.; Vlčková, B.; **Gajdošová, V.**; Zedník, J.; Vohlídal, J. Controlled tuning of the size of Ag-hydrosol nanoparticles by non-stabilized THF and detection of peroxides in THF, *Langmuir*, MS in the review process

Table of Contents

Prohlášení 2

Poděkování 3

Abstrakt 4

Abstract 5

List of publications 6

1. Introduction 11

1.1. Focus of the Thesis 11

1.2. Fundamentals of surface-enhanced Raman scattering (SERS) and graphene-enhanced Raman scattering (GERS) 12

1.3. Mechanisms of SERS 13

1.4. SERS active surfaces and systems relevant for the Thesis 14

1.4.1. Ag nanoparticle hydrosols 14

1.4.2. Localization of hydrophobic molecules into Ag NPs assemblies originating from Ag NP hydrosols 16

1.4.3. Nanoporous Ag networks as substrates for SERS 17

1.5. Testing adsorbates 19

1.5.1. Fullerene C_{60} 19

1.5.2. 5,10,15,20-Tetraphenyl-21H, 23H-porphine 20

1.5.3. 29,31H-Phthalocyanine 21

1.5.4. Single layer graphene (SLG) 22

1.6. Mechanisms of GERS 25

1.7. Hybrid systems for combined SERS and GERS 25

2. Objectives 27

3. Experimental 29

3.1. Materials 29

3.1.1. Chemicals 29

3.1.2. Chemical glassware and cuvettes 29

3.2. Preparations of AgNPs hydrosols 30
3.2.1. Preparation of HA-AgNPs hydrosol 30
3.2.2. Preparation of AgNPs hydrosol denoted as BH1 30
3.2.3. Preparation of AgNPs hydrosol denoted as BH2 31
3.3. Preparations of 3D AgNPs aggregates 32
3.3.1. Preparation of an empty Ag nanosponge aggregate - 32
3.3.2. Preparation of 3D Ag nanosponge aggregate with attempted incorporation of hydrophobic adsorbates by adapting the procedure used for hydrophilic adsorbates 33
3.3.3. Preparations of 3D Ag nanosponge aggregates with incorporated hydrophobic testing adsorbates 34
3.4 Preparation of hybrid systems for SERS of SLG 36
3.4.1 Glass/SLG/Ag aggregate hybrid system preparation 36
3.4.2 Glass/SLG/AgNPs-ET film hybrid system preparation 37
3.4.3 Glass/AgNPs/SLG hybrid system preparation 38
3.5 Preparation of hybrid systems for combined GERS and SERS of selected aromatic molecules and of the appropriate reference systems 39
3.5.1 Graphite/H_2Pc hybrid system preparation (reference system for GERS) . 39
3.5.2 Preparation of glass/SLG/H_2Pc(ML) hybrid system as reference system for SERS + GERS 39
3.5.3 Glass/AgNPs/SLG/H_2Pc hybrid system preparation 40
3.6 Instrumentation 41
3.6.1 Raman spectral measurements 41
3.6.2 UV/Vis spectral measurement 41
3.6.3 Transmission electron microscopy 41
3.6.4 Scanning electron microscopy 41
4. Results and discussion 42

4.1. Ag nanosponge aggregates as substrates and samples for SERS and SERRS of hydrophobic molecules 42

4.1.1. Searching for the best type of preparation of 3D aggregate with incorporated hydrophobic adsorbate 42

4.1.2. 3D Ag nanosponge aggregate with incorporated fullerene C_{60} into the internal structure 47

4.1.3. SERS spectral testing of H_2TPP incorporated into and overlayed over the Ag nanosponge aggregate 53

4.1.4. Ag nanosponge aggregate with incorporated hydrophobic molecules as a new samples for SERS ans SERRS: advantages and drawbacks 73

4.2. 2D and 3D AgNPs assemblies as substrates for SERS of SLG 77

4.2.3. 3D AgNPs aggregates as a samples for SERS of SLG 77

4.2.4. AgNPs-ET film as a substrate for SERS of SLG 83

4.2.5. 2D and 3D AgNPs assemblies as substrates for SERS of SLG: their advantages and drawbacks 105

4.3. Glass/AgNPs/SLG/H_2Pc(ML) hybrid system as sample for SERS + GERS of H_2Pc 106

4.3.3. Characterization and spectral probing of glass/AgNPs/SLG/H_2Pc(ML) hybrid system and of the reference system. 106

4.3.4. Searching of reference system for GERS of H_2Pc 113

4.3.5. GERS, SERS and SERS + GERS enhancement factors 115

4.3.6. SERS +GERS excitation profiles of selected spectral bands of H_2Pc localized in the glassI/AgNPs/SLG/H_2Pc(ML) hybrid system 118

4.3.7. Specification of the mechanisms of GERS and of their operation in GERS and SERS+GERS of H_2Pc in the 532-830 nm range 120

4.3.8. Combined SERS + GERS of H2Pc: conditions of the additivity of two enhancement mechanisms 122

5. Conclusion 125

6. References 128

7. List of abbreviation 138

8. Supplement 139

8.1. Publication I: Raman excitation profiles of hybrid systems constituted by single-layer graphene and free base phthalocyanine: Manifestation of two mechanisms of graphene-enhanced Raman scattering 139

8.2. Publication II: Effect of ethanethiolate spacer presence and/or removal on morphology and optical responses of hybrid systems constituted by single layer graphene and Ag nanoparticle arrays 166

8.3. Publication III: Excitation wavelength dependence of combined surface- and graphene-enhanced Raman scattering experienced by free-base phthalocyanine localized on single layer graphene-covered Ag nanoparticle array 184

1. Introduction

1.1. Focus of the Thesis

Design, preparation and utilization of plasmonic metal nanostructures (NSs) have been the subject of interest for more than 40 years [1–17]. First, it was closely connected with the development of surface-enhanced Raman scattering (SERS) spectroscopy, and, in the last two decades, with the broad and rapidly evolving field of plasmonics, into which SERS spectroscopy has been included as well [2–17]. Among a variety of plasmonic metal nanostructures, Ag nanoparticle (NP) assemblies have been in the forefront of interest for several reasons: (i) nanostructured Ag is the most efficient plasmonic enhancer of visible radiation, (ii) Ag nanoparticles (NPs) can be easily prepared by simple chemical procedures which allow for at least some control over their sizes and size-distributions, and, (iii) Ag NPs can be assembled to 2-dimensional (2D) and/or 3D of various morphologies [2–17]. There is thus a challenging possibility to tailor Ag NPs assemblies for particular research tasks and/or applications.

Several important issues are currently addressed in SERS spectroscopy. One of them is an efficient localization of molecules into strong, nanoscale localized optical fields dubbed "hot spots" generated by an external optical excitation in the abovementioned 2D and 3D assemblies of Ag NPs. The importance of "hot spots" generation in Ag NP assemblies for achievement of large SERS enhancement by the electromagnetic (EM) mechanism (with the enhancement factors up to 1×10^{11}) has been established by numerous theoretical and experimental studies [13–17]. On the other hand, localization of certain types of molecules, in particular of the hydrophobic molecules insoluble in water or in a water – miscible solvent into the "hot spots" in Ag NP assemblies still remains a challenge. Another challenging task for SERS spectroscopy is SERS of graphene, particularly of the single layer graphene (SLG), for which Raman spectroscopy is an excellent characterization tool [18,19]. SLG as a single sheet of sp^2 hybridized carbon atoms represents a very unusual type of "adsorbate", for which achievement of SERS enhancement by the EM mechanism with a minimum perturbation of its native structure is requested.

Preservation of the native structure of the adsorbates (particularly of the biologically important molecules) in hybrid systems with Ag NP assemblies has been an important issue since the early days of SERS spectroscopy, and motivated development of various

types of molecular spacers [20–22]. Recently, it was proposed and demonstrated that SLG can not only act as a spacer between planar aromatic molecules and plasmonic metal NS, but that it is the first type of spacer which can further enhance SERS of planar aromatic molecules by means of graphene-enhanced Raman scattering (GERS) [23–26]. The systematic research on the mechanisms of GERS recently summarized in [25,26] arises an important question about the simultaneous operation of the EM mechanism of SERS [2–17] and of one of the four proposed mechanisms of GERS [24] for a particular type of planar aromatic molecules localized in a hybrid system with SLG and Ag NP assembly, i.e. on the top of a combined Ag NP assembly-SLG platform.

1.2. Fundamentals of surface-enhanced Raman scattering (SERS) and graphene-enhanced Raman scattering (GERS)

SERS spectroscopy is a widely used spectro-analytical method, which utilizes enhancement of Raman scattering by plasmonic metal NSs such as plasmonics nanoparticles (NPs) and their assemblies. SERS spectroscopy is used in qualitative and quantitative analytical analysis, surface chemistry, medical and environmental research, and also in material science, art conservation and archeology [2–12]. SERS spectroscopy allows studying molecules at single molecule level, which further increases its applications [13–17].

SERS was first observed by Fleischmann et al. in 1974 [27]. The study was focused on Raman spectral studies of pyridine at a roughened Ag electrode. They observed that the signal intensity of pyridine was unusually high. However, Fleischmann explained this phenomenon as a consequence of localization of more molecules of pyridine to the roughened (enlarged) surface of the electrode. In 1977, Van Duyne et al. and Creighton et al. proved and described, that increasing of the Raman signal is caused by a new effect called surface-enhanced Raman scattering [28,29]. One year later, Moskovits attributed this effect to excitations of dipolar surface plasmons on nanostructured surfaces of free-electron metals (namely Ag, Au or Cu) and to emission of the resulting dipoles [30]. Only later, when this mechanism, dubbed the electromagnetic (EM) mechanisms of SERS, has been firmly established, these metals started to be called the plasmonic metals. At the beginning of 21st century, SERS spectroscopy provided and important input into a new branch of nanoscale optics dubbed plasmonics, and became an inherent part of this research field [8]. In addition to

the roughened electrodes, a variety of nanostructured surfaces has been tested and employed for SERS spectroscopy, e.g. aggregated hydrosols of plasmonic metal NPs island films, etc. It has been established that aggregates of plasmonic NPs amplify Raman scattering of molecules more efficiently than the isolated metal plasmonics NPs. Particularly efficient light amplifiers have been the nanostructures in which "hot spots", (strong nanoscale localized optical fields) are generated by an optical excitation [13–17].

For many years, Raman signal of molecules has been amplified only by plasmonics metals, but in recent years, graphene, and, in particular, single layer graphene (SLG) emerged as another light amplifier. A new phenomenon dubbed graphene-enhanced Raman scattering (GERS) was discovered and described by Ling et al. in 2010 [23]. After this discovery, many scientists have focused on the study of the mechanisms of GERS [25,26]. Another major step on this research field has been done by Barros and Dresselhaus who described four conditions and two basic rules for GERS observation [24].

A very promising and interesting field of research appears to be the combination of both effects, i.e. of SERS and GERS.

1.3. Mechanisms of SERS

Surface-enhanced Raman scattering (SERS) originates from coupled optical responses of plasmonic metal nanostructures and of molecules located on (or in a close vicinity of) their surfaces. In this coupled system, both the incident light and the light inelastically scattered by the molecules in the Raman scattering process are enhanced by the resonance optical responses of the plasmonic metal nanostructures [2–17]. These resonance optical responses are based on a resonance excitation of dipolar surface plasmons localized on the individual NS (such as an Ag NP represented by a simplified single sphere model) followed by the resulting dipoles emission. In classical physics terms, the process is known as resonance Mie scattering of light. This enhancement mechanism is denoted as the electromagnetic (EM) mechanism of SERS. The EM mechanism is the principal mechanism of SERS and operates independently on the nature of the target molecular species. For explanation of EM mechanism, the model of an isolated, spherical NP with size about 5 – 20 nm was chosen (Figure 1). The enhancement factors achieved by operation of the EM mechanism are dependent on the optical characteristics (namely on the n and k components of the complex refraction

index N) of the metal, on the morphology of the nanostructured surface and on the wavelength of the exciting radiation, and their values range from 10^4 – 10^{11} [2–17].

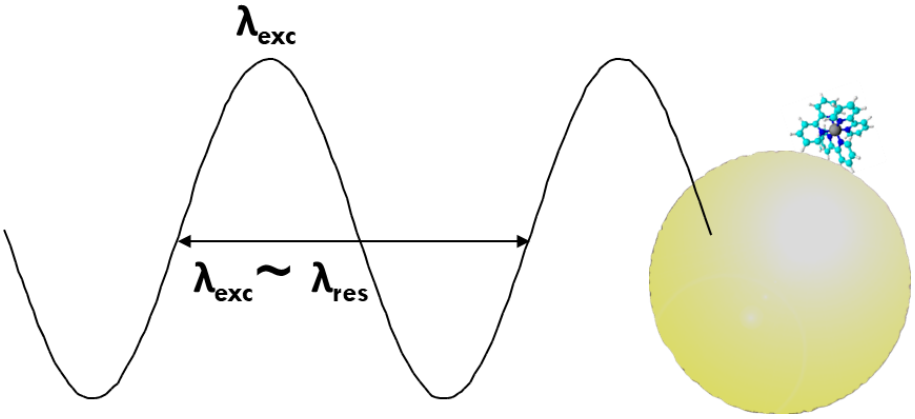

Figure 1: *Schematic depiction of the model of plasmonic NP – molecule system.*

Provided that the wavelength of incident light obeys simultaneously with the EM resonance condition also a molecular resonance condition defined by an overlap between the SERS excitation wavelength and an electronic absorption band involving the molecular orbitals of the studied molecule, the molecular resonance mechanism also contributes to the overall enhancement of Raman scattering. In the case that the resonant electronic transition is inherent to the molecule itself, the overall scattering process is dubbed surface-enhanced resonance Raman scattering (SERRS). Provided that the resonant electronic transition originates from the metal surface-molecule bonding (chemisorption), the molecular resonance contribution is referred to as the chemical mechanism of SERS. The mechanisms and applications of SERS have been the subject of several monographs, reviews and feature articles [2–17, 31–35].

1.4. SERS active surfaces and systems relevant for the Thesis

1.4.1. Ag nanoparticle hydrosols

Ag NP hydrosols are the most commonly used surfaces for SERS spectral measurements. Ag NPs hydrosols are popular due to their easy preparation by several types of chemical procedures [20,36–39], and they are also commercially available. Hydrosols of Ag NPs can be prepared also by laser ablation of a Ag target in an aqueous ambient [40–43], however, the most common type of preparation is a chemical reduction of $AgNO_3$ by a suitable reducing agents such as $NaBH_4$, $NH_2OH{\cdot}HCl$ etc. in the aqueous ambient [20,21,36–39]. The type of the reducing agent and of the

preparation procedure affects morphological, optical and chemical properties of the hydrosols such as the average size, size distribution and concentration of the NPs, surface potential and/or the oxidation state of adsorption sites on AgNPs surfaces. The presence of the particular adsorption sites affects the type and strength of adsorption of the molecules onto the AgNPs surface.

The largest SERS enhancement is provided by Ag NP hydrosols which contain aggregated NPs [2–17]. Aggregation of NPs can be caused by addition of testing adsorbate with or without a preaggregating agent (e.g. Cl^- ions). Aggregation of metal NPs in hydrosols causes changes in the plasmon resonance, and this effect manifests itself by changes of SPE (surface plasmon extinction) spectrum. Interaction of individual spherical particles in an AgNPs aggregate leads to splitting of the original SPE spectral band of an assembly of isolated Ag NPs (parent Ag NP hydrosol) due to dipole-dipole interactions of individual optical excitations of the NPs in the aggregates. The original SPE band is split into two bands, the maximum of the first band is localized close to the maximum of the original SPE band, the second band is shifted to the higher wavelengths (i.e. red – shifted) and broadened.

The largest amplification of radiation is obtained by localization of molecules into specific locations of interacting NPs such as dimers and/or fractal aggregates (Figure 2). The largest enhancements by the EM mechanism are provided by the assemblies of AgNPs containing "hot spots" (strong optical fields localized into the nanometer dimensions). Existence of "hot spots" has been predicted theoretically and proved experimentally both in large fractal aggregates of Ag nanoparticles and in dimers and very small aggregates of these nanoparticles [13–17].

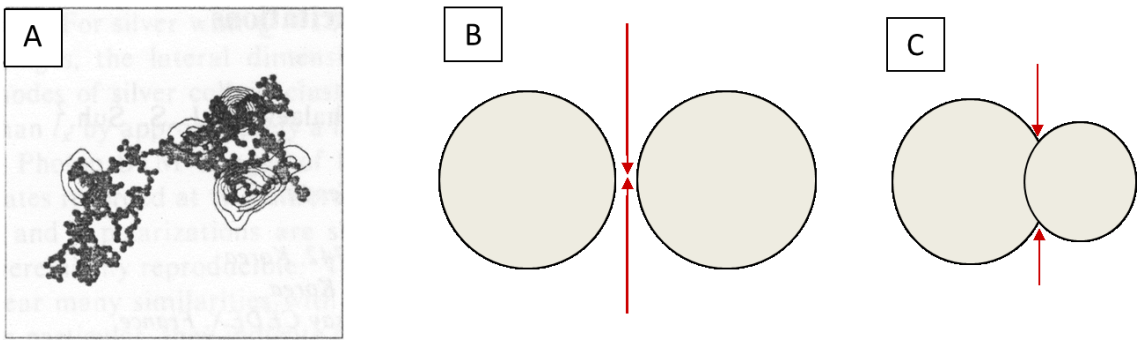

Figure 2: *Depiction of localization of "hot spots" in (A) fractal aggregates (B) dimer of closely spaced NPs and (C) intergrown NPs dimer. Adopted from* [13–16].

1.4.2. Localization of hydrophobic molecules into Ag NPs assemblies originating from Ag NP hydrosols

Localization of hydrophobic molecules into Ag NP assemblies originating from Ag NP hydrosols (earlier denoted as Ag colloids) has been a challenge for more than 20 years. First, amphiphilic adsorbates have been efficiently incorporated into Ag colloid – adsorbate films constituted by 9 – 10 nm sized Ag NPs (originating from Ag NP hydrosols, i.e. Ag colloids prepared by reduction of $AgNO_3$ by $NaBH_4$) and formed at the interface between the Ag NPs hydrosol and a solution of an amphiphilic adsorbate in dichloromethane (CH_2Cl_2). These Ag NPs – amphiphilic adsorbate films deposited on glass slides were shown to be good quality and stable samples for SERS and/or SERRS [44]. In contrast to that, employment of the same preparation procedure for a hydrophobic adsorbate (namely tetraphenylporhine, H_2TPP) resulted into formation of 2D fractal aggregates with the extremely low fractal (Hausdorff) dimension of D=1.2. After deposition on glass slides, no SERRs or SERRS signal of the hydrophobic porphyrin could be obtained [44].

Furthermore, interfacial Ag colloid – ethanethiol films were prepared in the two-phase system constituted by an Ag NP hydrosol (aqueous Ag colloid prepared by a modification of the original procedure of the reduction of $AgNO_3$ by $NaBH_4$) and a solution of ethanethiol in dichloromethane [21]. SERS spectra of the glass – deposited films confirmed modification of Ag NPs by the chemisorbed thiol. The deposited films were used as substrates for adsorption of hydrophobic, water insoluble species, namely H_2TPP and β-carotene, from their 1×10^{-5} M dichloromethane solutions. Good quality SERRS spectra of the chemically unperturbed hydrophobic adsorbates have demonstrated that these films can be employed as spacer – modified substrates for SERRS of water insoluble chromophoric molecules [21]. In addition to that, TEM images of the deposited Ag NPs – ethanethiol films have shown the slightly irregular 2D morphology of these films [22].

Finally, incorporation of hydrophobic adsorbates, namely β-carotene, H_2TPP and C_{60}, into multilayer interfacial Ag colloid (H_2SO_4) – adsorbate films has been successfully accomplished at the interface between Ag NP hydrosol modified by addition of sulphuric acid and a 1×10^{-4} M solution of the hydrophobic adsorbate in dichloromethane. TEM images of the films show enlargement and sintering of parent Ag nanoparticles (prepared by reduction of $AgNO_3$ by $NaBH_4$). SERS and SERRS

spectra of the unperturbed adsorbates were obtained from the films at 514.5 nm excitation with the excitation power as low as tens of mW [45].

1.4.3. Nanoporous Ag networks as substrates for SERS

In connection with the development of micro – Raman spectroscopy, macroscopic 3D Ag nanostructures started to be of interest as substrates for SERS. The highest benefits of their microRaman probing include the possibility to obtain the optical image of the measured substrate and/or sample and to localize the excitation laser beam onto a particular spot on the sample with a ~1 μm resolution. Another benefit is the possibility of Raman spectral mapping, which enables to assess the homogeneity or inhomogeneity of the sample [2–9].

Currently, nanoporous metallic networks are at the forefront of the research, because they exhibit unique optical properties which make them applicable in many fields such as materials for photonics and optoelectronics, catalysis, sensing applications etc. [1]. Their sensing applications have been focused also on SERS and/or SERRS spectral detection of analytes [46–48]. The pores in the networks can be ordered or distributed randomly. Many research groups focus on preparation of highly ordered nanoporous networks. These types of networks can be prepared mostly by lithographic techniques or by templating. Colloidal crystals build up from dielectric materials such as silica, block-copolymers or imprinted polymers can be used as templates. In the case that polymer is used as a carrier, metal NPs are incorporated into the polymer internal structure. The disordered (sponge-like) networks have been prepared by dealloying, colloidal assembling combined with supercritical drying, non – sacrificial templating and /or physical vapor deposition. [1]

For example, Ron et al. [49] developed a method for preparation of the pure 3D nanoporous metallic networks based on physical vapor deposition (PVD) of a metal on an electrostatic silica aerogel substrate.

Although by using the PVD methods, pure and relatively large nanosponge/ nanoporous structures are obtained, this method is relatively expensive for producing of SERS substrates. Much cheaper are preparations of nanosponge/nanoporous networks by chemical procedures.

Tang et al. [46] prepared several types of metal nanosponges by reducing of metal ions complexes ($AgNO_3$, $HAuCl_4$, K_2PdCl_4 etc.) by hydrazine to obtain metal NPs. Then they prepared metal nanosponge/nanoporous structures by reducing of NPs by

ethanol in temperature control oscillator. They were able to prepare large discs with nanoporous/nanosponge structure, and they tested them as SERS and/or SERRS substrates. In particular, Rhodamine B was detected by SERRS at 1×10^{-7} M concentration. Furthermore, Ag-bacterial cellulosic sponges were prepared and tested as SERS – active substrates using thiosalycylic acid and 2,2-dithiodipyridine as analytes and obtaining the 1×10^{-4} M limit of their detection [47]. Determination of pesticides by capillary chromatography and SERS detection using Ag – quantum dots nanocomposites as substrates has been reported and the limits of the pesticides detection were found to range from 0.2 to 0.5 ng [48].

In summary, Ag nanoporous networks, particularly the disordered ones with sponge-like morphologies, appear to be prospective substrates for SERS. On the other hand, some of the currently employed procedures of their preparation are synthetically quite demanding. Moreover, in all cases of their SERS spectral testing, the Ag nanosponges were employed as substrates, into which adsorbates were deposited by soaking into the pores from their solutions. The testing was done by hydrophilic and/or amphiphilic adsorbates. Nevertheless, one can assume that deposition by soaking from a solution could be applicable for hydrophobic species as well.

A markedly different approach to assembling of Ag nanosponges, and, in particular to incorporation of the hydrophilic and amphiphilic adsorbates into these nanosponges has been developed and reported in my Bachelor and Master thesis [50,51] and in ref. [52]. The approach is based on formation of 2D fused fractal aggregates by modification of ~30 nm Ag NPs in hydrosol (prepared by reduction of $AgNO_3$ by $NH_2OH\cdot HCl$) by addition of aqueous solutions of HCl and the testing adsorbate, and on their subsequent 3D assembling into a Ag nanosponge aggregate with the adsorbate incorporated into its internal structure. In this Thesis, I have undertaken a challenging task to develop a new preparative strategy which would enable to incorporate the hydrophobic adsorbates into a similar Ag nanosponge structure.

1.5. Testing adsorbates

1.5.1. Fullerene C_{60}

Fullerenes are significant molecules belonging to the group of carbon allotropes. Fullerenes are molecules formed from carbon atoms arranged to pentagons or hexagons, which are mostly closely packed into the spheres of ellipsoids. One of the most famous fullerenes is fullerene C_{60} also called Buckminster fullerene. Its structure is depicted in Figure 3. The name was given after the American architect Buckminster Fuller, which designed geodetic domes of similar shape as fullerene C_{60}. Fullerene C_{60} was discovered in 1985 by Richard Smalley, Robert Curl, James Health, Sean O´Brien and Harold Kroto [53].

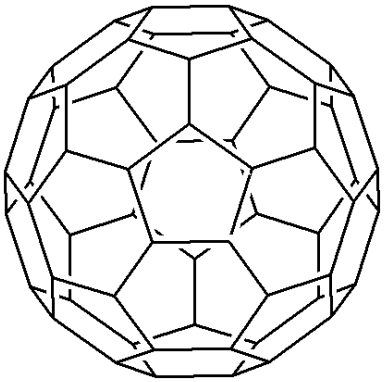

***Figure 3**: Structure of fullerene C_{60}*

The shape of fullerene C_{60} molecule is a truncated icosahedron (the I_h symmetry). The fullerene samples have been prepared mostly by a thermal evaporation of graphite in an electric arc in an inert gas atmosphere. Fullerene C_{60} was studied and used in many applications such as biological sensing, drug delivery, organic light emitting diodes, organics photovoltaics or organic field effect transistors [54].

Fullerene C_{60} was also studied first by Raman spectroscopy [55,56] and then by SERS spectroscopy [57,58]. Comparison of the Raman spectra of a solid C_{60} film with the SERS spectra of C_{60} adsorbed on roughened (nanostructured) Ag surfaces has shown an interesting effect. The strongest Raman band attributed to the pentagonal pinch mode of C_{60} molecule and observed at 1470 cm^{-1} in the solid C_{60} film [55], was shifted to 1435 cm^{-1} in the SERS spectra [57]. Similar shifts were observed also in other SERS spectral studies [58] and explained by interaction between the π electrons of fullerene C_{60} and Ag aggregates. By contrast, SERS spectrum of unperturbed C_{60} was obtained from Ag colloid (H_2SO_4) – C_{60} films prepared in a two phase system constituted by H_2SO_4 – modified Ag NP hydrosol and a dichloromethane solution of C_{60} [45].

1.5.2. 5,10,15,20-Tetraphenyl-21H, 23H-porphine

Porphyrins belong to a large group of heterocyclic and macrocyclic organic compounds, and they are known as biologically important chromophores, e.g. in chromophoric proteins. Porphyrins are used in molecular biology for specific sensing of DNA, in solar energy conversion as sensitizers in dye-sensitized solar cells, and, most importantly, as sensitizers in photodynamic therapy of cancer. [59,60]

One of the widely studied hydrophobic (water insoluble) free – base porphyrins is 5,10,15,20-tetraphenyl-21H,23H-porphine (H_2TPP). The structure of H_2TPP is shown in Figure 4.

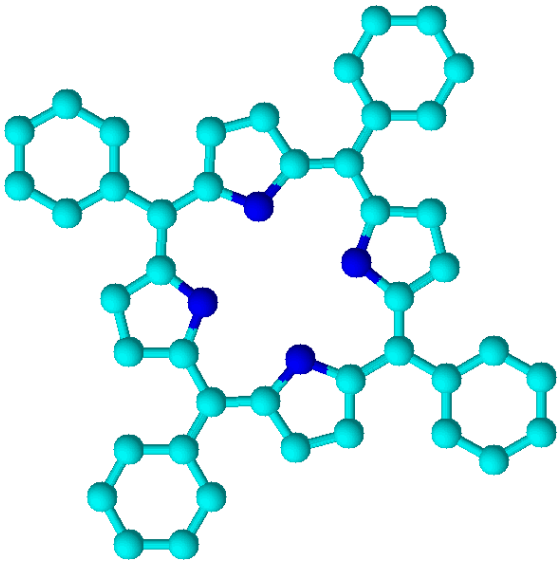

Figure 4: *Structure of H_2TPP*

Electronic absorption spectra of H_2TPP show the very intense Soret (B) band at 419 nm and four Q bands (due to D_{2h} molecule symmetry). The strongest $Q_y(1,0)$ band maximum is located at 514 nm, and the other three Q – bands are $Q_y(0,0)$ at 549 nm, $Q_x(1,0)$ at 592 nm and $Q_x(0,0)$ at 647 nm.

Resonance Raman (RR) spectra of H_2TPP measured upon excitation into the Soret band were reported e.g. in ref. [61,62]. Raman spectral bands of solid H_2TPP in a KBr pellet were found at 198, 330, 636, 961, 1001, 1075, 1232, 1292, 1330, 1361, 1487, 1497 and 1550 cm^{-1} [62].

In SERS and SERRS spectroscopy of free – base porphyrins in systems with Ag nanostructures, in particular with Ag NP assemblies, preservation of the native structure of the porphyrins and prevention of their Ag metallation is an important issue [20]. Good quality SERRS spectra of unperturbed H_2TPP were obtained first from the Ag colloid – ethanethiol – H_2TPP films, in which Ag colloid (NPs) – ethanethiol film was employed as a spacer – modified substrate for SERRS of H_2TPP [21]. SERRS spectrum of unperturbed H_2TPP was obtained also from Ag colloid (H_2SO_4) – H_2TPP films prepared in a two phase system constituted by H_2SO_4 – modified Ag NP hydrosol and a dichloromethane solution of H_2TPP [45]. Hajdukova et al. [63] reported SERRS spectra of native H_2TPP deposited from a solution onto Ag NPs immobilized on a glass slide by aminopropyltrimethoxysilane (APTMS). They found, that APTMS also serves as a

molecular spacer, and they achieved a relatively low, 8×10^{-8} M limit of SERRS spectral detection of the porphyrin. All these SERRS spectral measurements were performed at 514.5 nm excitation [21,45,63].

Interestingly, molecules of the hydrophobic H_2TPP can be diprotonated yielding the diacid form of the porphyrin, H_4TPP^{2+}. The diacid form can be prepared either chemically by a very strong acidification of H_2TPP solutions, or by a complex photoexcited radical reaction of H_2TPP with a chlorinated solvent, e.g. chloroform [64]. RR spectra of H_4TPP^{2+} measured upon excitation into the Soret band were reported e.g. in ref. [61,62]. In the later paper, assignment of both Raman and IR spectral bands of H_4TPP^{2+} supported by DFT calculations has been provided [62].

1.5.3. 29,31H-Phthalocyanine

Phthalocyanines are planar aromatic molecules characteristic by a high degree of symmetry and electron delocalization. Phthalocyanines are formed from isoindole rings at the four corners linked together by four nitrogen atoms. The central macrocycle consists of a 16 membered ring in which the two imino-hydrogen atoms are replicable by metal.

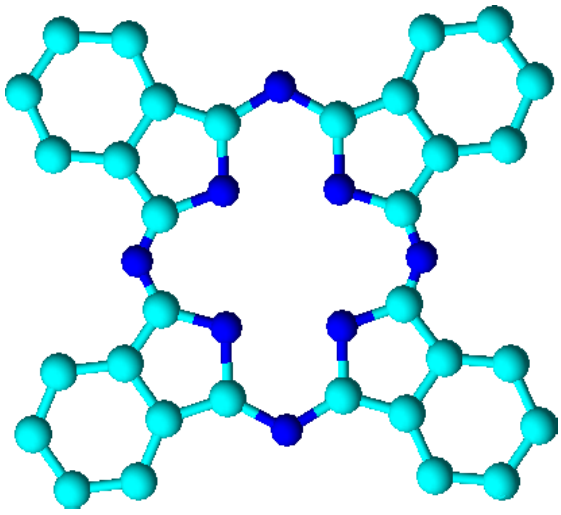

***Figure 5**: Structure of H_2Pc*

Free – base phthalocyanine H_2Pc is an aromatic planar centrosymmetric molecule of D_{2h} symmetry. Its structure is depicted in Figure 5.

H_2Pc is studied for its utilization in optics and photonics such as optical switching and limiting devices, light-emitting devices, dye – sensitized solar cells, and as a photosensitizer in photodynamic therapy of cancer [65].

Molecules of H_2Pc exhibit strong fluorescence, which has complicated measurements of Raman spectra in solutions and polymer matrices [66]. On the other hand, when thin films of phthalocyanine were used for measurements, no interference of fluorescence was observed [67]. A detailed assignment of infrared (IR) and Raman spectral bands of H_2Pc obtained from H_2Pc molecules in isolated matrices and supported by DFT calculations has been reported in ref. [68].

In the electronic absorption spectra of H_2Pc, the Soret (B) band is observed in the near ultraviolet region. The Q band in the visible spectral region is split into the Q_x and Q_y bands due to removal of the degeneracy between the first and the second excited states caused by the D_{2h} symmetry of the H_2Pc molecule [69]. It was found, that the electronic transitions giving rise to Q bands are localized mainly on the macrocycle, while the Soret (B) band is delocalized over the benzene rings. [67]. The absorption maxima of the Q_x and Q_y bands in the visible region depend on the ambient in which the H_2Pc molecules are located. In particular, the Q_x bands are located in the 670 – 702 nm range and the Q_y bands in the 627 – 666 nm range in the systems reported previously [66,69], namely in isolation matrices [70], a chloronaphtalene solution [66], and in polysiloxane films [66].

As mentioned above, Raman spectral measurements of H_2Pc are complicated by intense fluorescence. On the other hand, when H_2Pc is adsorbed onto the roughened metal surface, fluorescence is strongly quenched, and SERS and SERRS spectra of H_2Pc have been measured [69,71]. In the later paper, detailed SERRS excitation profiles of both Q_y and Q_x electronic absorption bands were reported.

Importantly, H_2Pc has also been among the very first molecules probed for GERS in 2010 [23]. Raman spectra of $Si/SiO_2/SLG/H_2Pc$ hybrid samples prepared by H_2Pc sputtering onto the SLG surface were measured at 488.0, 514.5 and 633 nm wavelength and quenching of the H_2Pc luminescence has been demonstrated. GERS enhancement of H_2Pc spectral bands by factors 5 – 15 has been determined in relation to the $Si/SiO_2/H_2Pc$ reference sample at 633 nm excitation. On the other hand, the actual mechanism of GERS enhancement has not been established, and the LUMO and HOMO energies considered in that paper [23] were not appropriate, because the value of their difference corresponded with the B (Soret) electronic transition (in the UV spectral region) rather than with the Q_x electronic transition which represents the actual HOMO – LUMO transition.

1.5.4. Single layer graphene (SLG)

Graphene is a relatively new material, which is at the forefront of interest of many research groups. In general, it is a 2D sheet of sp^2 – hybridized carbon, which is honeycomb structured as demonstrated in Figure 6. Especially single layer graphene (SLG) exhibits special thermal, mechanical and electrical properties [72].

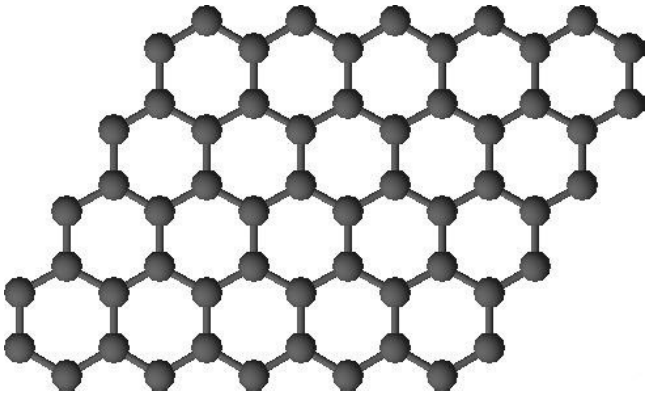

Figure 6: *Structure of SLG*

In 2004, SLG was first isolated by Novoselov and co-workers at Manchester University by exfoliation from graphite [73].

Since that time, novel types of preparation procedures were developed and tested. Nowadays, the chemical vapor deposition (CVD) is the most frequently employed procedure of SLG preparation [74,75]. With the increasing of number of single graphene layers and formation bi- or multilayer layer graphene samples, the unique properties of graphene change markedly [72]. Raman spectroscopy has emerged as a suitable non – destructive tool for probing and characterization of graphene samples, with the ability to reveal strain, defects, doping as well as the actual number of single layers within a particular graphene sample [18,19].

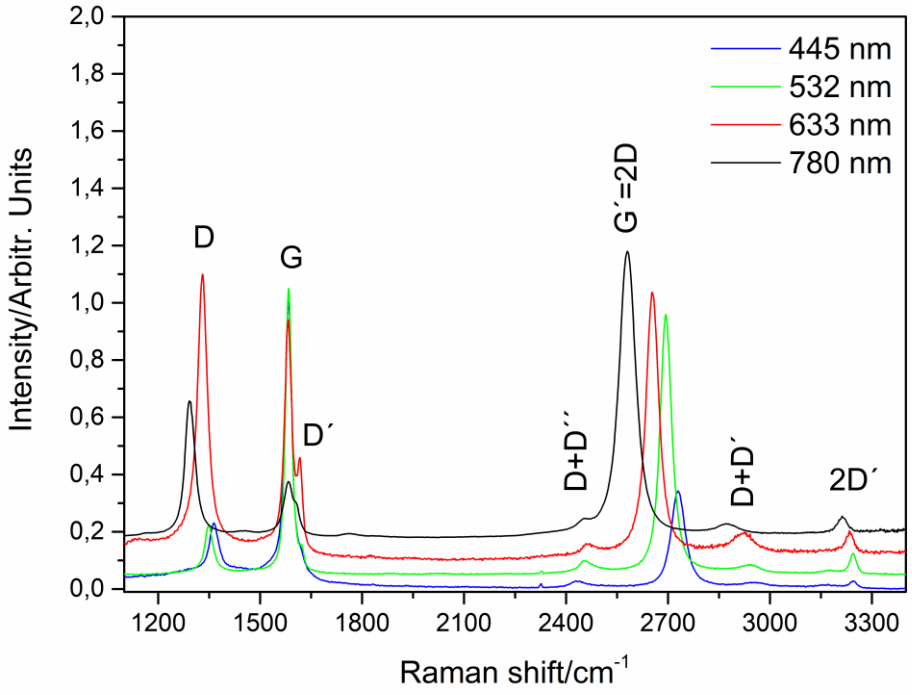

Figure 7: *SERS spectra of graphene at four excitation wavelengths showing shifts and disorder of graphene sample.*

The Raman spectrum of pristine graphene contains only two bands – the G mode and the 2D mode sometimes called G´ mode. All other bands are spectral features of

defects. Typical SERS spectra of SLG are shown in Figure 7.The G band is a sharp band that appears around 1585 cm^{-1}. The band is an in-plane vibrational mode of C – C bond stretching. The wavenumber position of the G mode band is very sensitive to strain and doping. The D band, mostly known as the disorder or the defect band appears in the 1250 – 1400 cm^{-1} range. This band corresponds to the breathing of the six – atom rings and it is strongly related to the defect presence. The intensity of the D band in highly ordered pristine graphene is typically weak, in an ideal case, no D band is observed. With the increase of the D band intensity, decrease the quality of the graphene sample decreases, since a strong D band indicates a high amount of defects in the sample. The D′ band is another band pointing to the defects in the structure. The presence of defects is necessary for its activation. The D′ mode position is around 1620 cm^{-1}. The 2D band appears around 2500 – 2800 cm^{-1} and this band is result of two phonon lattice vibration process. Sometimes is the 2D band referred as an overtone of the D band, but unlike the D band, no defects are required for its activation. Analogously to the D band position, also the 2D band position strongly depends on the excitation wavelength used for measurement, i.e. both these modes are dispersive. 2D′ band is the overtone of the D′ band and its position is around 3240 cm^{-1}.

Finally, the combination bands can be observed. The first, D + D′′ band is usually observed at 2450 cm^{-1}, and the second D + D′ band usually appears at 2970 cm^{-1} [18,19].

Furthermore, SERS spectroscopy of SLG has been successfully employed for revealing of the effect of coupling of SLG with plasmonic metal nanostructures, e.g. Ag or Au NPs arrays, on doping, strain and/or defects formation experienced by SLG in the plasmonic metal NPs/SLG hybrid systems. [76–84]. The SERS enhancement experienced by the SLG modes has been attributed to the EM, i.e. the localized plasmon resonance mechanism of SERS [79]. SERS spectra of SLG were obtained from hybrid systems constituted by SLG and the overdeposited plasmonic NPs as well as from the assemblies of plasmonic NPs overlayed by SLG [76–83]. A comparison of SERS of SLG from these two types of hybrid systems has been attempted, however, it was hampered by different morphologies of the Ag NPs and of their assemblies in each of them [84].

Graphene can be also used as a platform for the enhancement of Raman scattering of molecules, preferably of the planar aromatic ones. This process is called Graphene –

enhanced Raman scattering (GERS) and it is a quite new tool in Raman sensing [23–26].

1.6. Mechanisms of GERS

Graphene – enhanced Raman scattering (GERS) spectroscopy is relatively new phenomenon, which was first observed in 2010 by Ling et al.[23] and after this discovery, this effect is booming in its study [25,26]. GERS is observed from a monolayer of aromatic molecules localized on the surface of graphene. The theoretical background of GERS was developed by Barros and Dresselhaus [24]. They defined four conditions for which GERS provides the largest enhancement.

$$\hbar\omega_0 = E_L - E_H \quad \text{or} \quad \hbar\omega_0 = E_L - E_H + \hbar\omega_q \qquad 1.a$$

$$E_F = E_H \pm \hbar\omega_q \quad \text{or} \quad E_F = E_L \pm \hbar\omega_q \qquad 1.b$$

$$\hbar\omega_0 = E_F - E_H \quad \text{or} \quad \hbar\omega_0 = E_F - E_H + \hbar\omega_q \qquad 1.c$$

$$\hbar\omega_0 = E_L - E_F \quad \text{or} \quad \hbar\omega_0 = E_L - E_F - \hbar\omega_q \qquad 1.d$$

Where $\hbar\omega_0$ is excitation energy, E_L is the energy of the lowest unoccupied molecular orbital (LUMO) state and E_H is the energy of the highest occupied molecular orbital (HOMO) state of the molecule. E_F is the energy of Fermi level of graphene and $\hbar\omega_q$ is the phonon energy.

Based on equations 1.a – 1.d., Barros and Dresselhaus formulated two basic selectivity rules for GERS – the Energy Level Rule and the Structure Rule.

The first rule says that HOMO and LUMO levels of the molecule need to be in the appropriate energy range with respect to graphene Fermi level to be probed by a given set of laser excitation wavelengths. The conditions, under which the largest GERS enhancements will be observed, are defined by equations 1.a – 1.d listed above. The second rule predicts that the largest GERS enhancement will be achieved for molecules with the symmetry compatible to the symmetry of the graphene units (D_{6h}) i.e. for those with the D_{nh} symmetry [24].

1.7. Hybrid systems for combined SERS and GERS

Hybrid systems constituted by plasmonic nanostructures and SLG, as well as their employment as platforms for surface – enhanced Raman scattering (SERS) of molecular species, has recently become a subject of interest due to a possible contribution of SERS

as well as GERS enhancement to Raman signal of detected molecules. [85 – 89] On the other hand, only very few studies were targeted specifically on investigation of the mechanism of the combined SERS+GERS of aromatic molecules, e.g. [85]. In this study, regular Au nanostructures constituted by Au nanoparticles (NPs) and/or nanohole arrays were employed for a comparison of SERS+GERS spectra of methylene blue (MB) dye obtained from the Au nanostructure/ SLG/MB hybrid system with its SERS spectra from the Au nanostructure/MB hybrid at 647 nm excitation. A 3 fold and/or 9 fold additional average GERS enhancement of MB vibrational modes was established in the former system with the nanoholes and the nanoparticles, respectively [85].

2. Objectives

I. New strategy of incorporation of hydrophobic molecules into fractal aggregates of Ag NPs, 3D assembling of the fractal aggregates, and SERS and SERRS microRaman spectral probing of the importance of the molecules localization into "hot spots"

(i) Design, development and optimization of preparation procedures enabling localization of hydrophobic molecules (insoluble both in water and in water – miscible solvents), namely fullerene C_{60} and 5,10,15,20-tetraphenyl-21H,23H-porphine (H_2TPP) into 2D fractal aggregates of Ag NPs originating from Ag NP hydrosols. Characterization of the aggregates by transmission electron microscopy (TEM) imaging, including determination of their fractal (Hausdorff) dimension.

(ii) 3D assembling of the 2D fractal aggregates (both with and without incorporated hydrophobic molecules) into macroscopic (~ $1mm^3$) aggregates. Characterization of the aggregates morphology by scanning electron microscopy (SEM).

(iii) SERS and SERRS micro-Raman spectral probing of the 3D aggregates with incorporated C_{60} or H_2TPP molecules and of the reference samples with the same molecules adsorbed from solutions into the pre-prepared empty aggregates. Determination and mutual comparison of the concentration values of the SERS spectral limits of detection (LODs) of C_{60} and/or H_2TPP in both types of aggregates. Quantitative evaluation of the impact of C_{60} and/or H_2TPP incorporation into the parent 2D fractal aggregates for achievement of the low LOD values.

II. New Ag NPs assemblies as platforms for SERS of single layer graphene (SLG)

(i) Design, preparation and optimization of Ag NP assemblies – SLG hybrid systems for SERS of SLG.

(ii) Acquisition and interpretation of SERS spectra of SLG from the hybrid systems with Ag NP assemblies, and with and without a molecular spacer.

(iii) Development of an optimized Ag NP assembly – SLG platform for combined SERS+GERS (GERS = graphene – enhanced Raman scattering) of planar aromatic molecules with a broad surface plasmon extinction (SPE) spectral band of the Ag NP assembly spanning the visible spectral region.

III. **Probing combined surface- and graphene-enhanced Raman scattering experienced by a planar aromatic molecule, namely free-base phthalocyanine (H_2Pc) in Ag NP assembly-SLG-H_2Pc hybrid system**

(i) Preparation of a 3 – component hybrid system constituted by Ag NP assembly on a glass substrate overdeposited first by SLG and, subsequently, by a monolayer of H_2Pc molecules, as well as of the appropriate reference systems.

(ii) Micro-Raman spectral mapping of the 3 – component hybrid system as well as of the reference systems at multiple excitation wavelengths. Probing of observation of the combined SERS+GERS by determination of GERS, SERS and SERS+GERS enhancement factors and their mutual comparison.

(iii) Construction and a mutual comparison of SERS+GERS and GERS excitation profiles of H_2Pc spectral bands. Determination of the actual mechanism(s) of GERS experienced by H2Pc in the Ag NP assembly – SLG – H_2Pc hybrid system and in the SLG – H_2Pc reference system and exploration of the additivity of SERS and GERS of H_2Pc in the 3 – component hybrid system.

3. Experimental

3.1. Materials

3.1.1. Chemicals

- Silver nitrate – $AgNO_3$ (Merck, p.a.)
- Hydroxylamine hydrochloride – $NH_2OH \cdot HCl$ (Sigma Aldrich)
- Sodium borohydride – $NaBH_4$ (Merck, p.a.)
- Sodium hydroxide – NaOH (Merck, p.a.)
- Ethanethiol (Sigma Aldrich)
- Toluene for spectroscopy – C_7H_8 (Merck)
- Dichloromethane for spectroscopy – CH_2Cl_2 (Merck)
- 29, 31H-Phthalocyanine – H_2Pc (Sigma Aldrich)
- Fullerene C_{60} (Sigma Aldrich)
- 5,10,15,20-tetraphenyl-21H,23H-porphine – H_2TPP (Sigma Aldrich)
- Nitric acid – HNO_3 (Lach-Ner, p.a.)
- Hydrochloric acid – HCl (Lach-Ner, p.a.)
- Sulphuric acid – H_2SO_4 (Lach-Ner, p.a.)
- Hydrogen peroxide – H_2O_2 (Lach-Ner, p.a.)
- Chromsulfuric acidic mixture (Lach-Ner, a.)
- Doubly distilled deionized water
- Single – layer graphene (SLG): samples containing SLG were prepared at the Heyrovsky Institute of Physical Chemistry, by members of the Dr. Kalbáč´s group.

3.1.2. Chemical glassware and cuvettes

All glassware was cleaned by a double distilled water, dilute nitric acid (1:1), peroxymonosulfuric acid, aqua regia and once again by the doubly distilled water. In each bath, the glassware was soaked at least for 30 minutes. Cuvettes for UV/Vis measurements were also washed by chromsulfuric acid. Between immersions into each bath, the glassware was rinsed by deionized water and the final rinse was done by the doubly distilled water.

3.2. Preparations of AgNPs hydrosols

3.2.1. Preparation of HA-AgNPs hydrosol

HA-AgNPs hydrosols were prepared by reduction of $AgNO_3$ by Hydroxylamin hydrochloride ($NH_2OH{\cdot}HCl$). This procedure was described in ref. [37] and modified in ref. [38]. Briefly, 90.0 mL of 1.6×10^{-3} M $NH_2OH{\cdot}HCl$ was mixed with 0.3 mL of aqueous solution of 1M NaOH. Subsequently, 10.0 mL of 1×10^{-2} M $AgNO_3$ was added. Specifically, 10.4 mg of $NH_2OH{\cdot}HCl$ was dissolved in 90.0 mL of doubly distilled water and started to be stirred. To this solution, 30 µL of 1M aqueous solution of NaOH (prepared by dissolving of 0.2 g NaOH in 5.0 mL of double distilled water) were added. After addition of NaOH, the solution pH changes into slightly alkaline. Subsequently, 10.0 mL of aqueous solution of $AgNO_3$ (prepared by dissolving of 33.9 mg of $AgNO_3$ in 20.0 mL of doubly distilled water) were added dropwise. Stirring of the reaction mixture was continued for 45 minutes. A glass stirring bar and 350 rpm rotation speed of the magnetic stirrer was used for the preparation.

HA-AgNPs hydrosol is yellow – brown colored and opalescent with average size of AgNPs about 27 nm as demonstrated in Figure. 8.

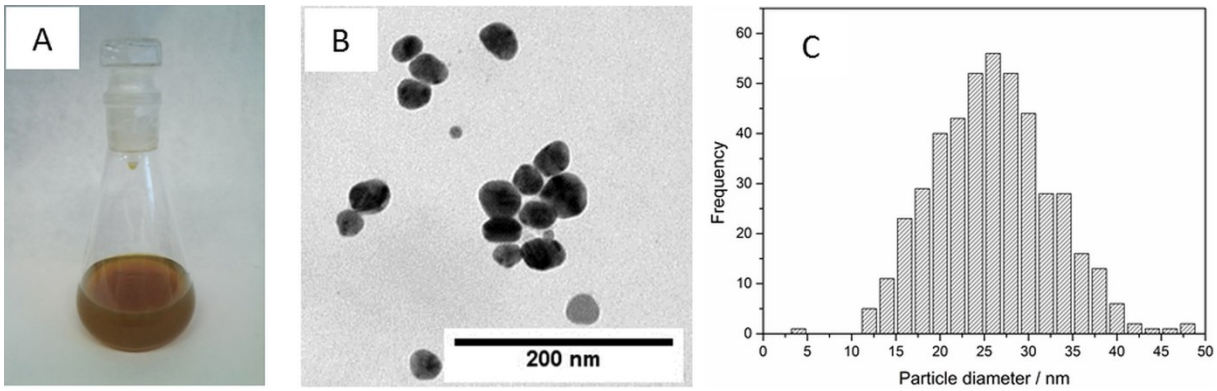

Figure 8: *(A) HA-AgNPs hydrosol (B) TEM images of AgNPs from HA-AgNPs hydrosol (C) Particle size distribution of HA-AgNPs hydrosol*

3.2.2. Preparation of AgNPs hydrosol denoted as BH1

AgNPs hydrosols denoted as BH1 were prepared by reduction of $AgNO_3$ by $NaBH_4$. This procedure was described in ref. [36] and modified in ref. [20]. Briefly, into the 75.0 mL of 1.2×10^{-3} M $NaBH_4$, 9.0 mL of 2.2×10^{-3} M $AgNO_3$ was added. Specifically, 3.5 mg of $NaBH_4$ was dissolved in 75 mL of doubly distilled water. This solution was cooled to 2.0 °C. After cooling down, the solution of $NaBH_4$ started to be stirred. Into

the pre-cooled and stirred solution, 9.0 mL of the aqueous solution of $AgNO_3$ were added dropwise. The aqueous solution of $AgNO_3$ was prepared by dissolving of 6.7 mg of $AgNO_3$ in 18.0 mL of double distilled water. Stirring of the reaction mixture was continued for 45 minutes. A glass stirring bar and 350 rpm rotation speed of the magnetic stirrer was used for stirring.

BH1 AgNPs hydrosol is transparent, yellow colored with the 10 nm average size as is shown in Figure 9.

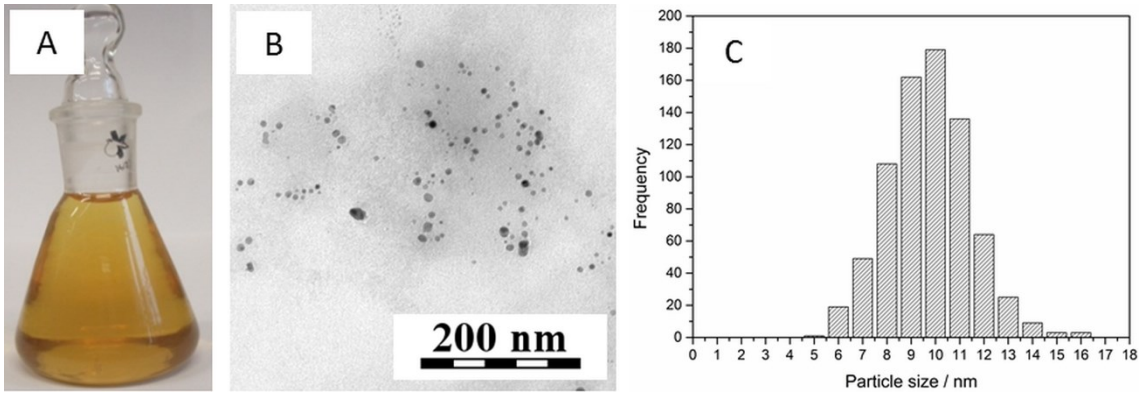

Figure 9: *(A) BH1 AgNPs hydrosol (B) TEM images of AgNPs from BH1 AgNPs hydrosol (C) Particle size distribution of BH1 AgNPs hydrosol*

3.2.3. Preparation of AgNPs hydrosol denoted as BH2

AgNPs hydrosols denoted as BH2 were prepared by reduction of $AgNO_3$ by $NaBH_4$. This procedure was described in ref. [21]. Briefly, into the 75.0 mL of 1.2×10^{-3} M $NaBH_4$, 9.0 mL of 4.6×10^{-3} M $AgNO_3$ was added. Subsequently, 3.5 mg of $NaBH_4$ was dissolved in 75 mL of doubly distilled water. This solution was cooled to 2.0 °C. After cooling down, the solution of $NaBH_4$ was stirred. To the cooled solution, 9.0 mL of the aqueous solution of $AgNO_3$ were added dropwise. The aqueous solution of $AgNO_3$ was prepared by dissolving of 13.4 mg of $AgNO_3$ in 18.0 mL of double distilled water. Stirring of the reaction mixture was continued for 45 minutes. A glass stirring bar and 350 rpm rotation speed of the magnetic stirrer was used for stirring.

BH2 AgNPs hydrosol is transparent, yellow colored with the 13 nm average size as demonstrated in Figure 10.

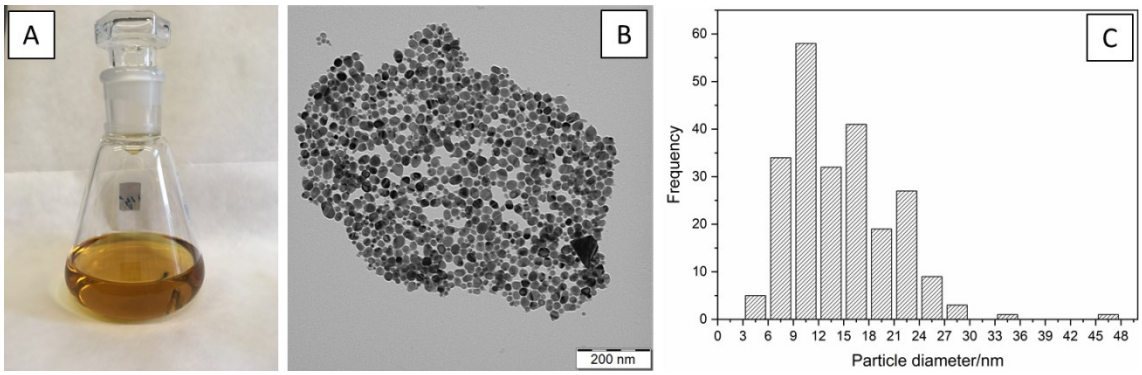

Figure 10: *(A) BH2 AgNPs hydrosol (B) TEM images of AgNPs from BH2 AgNPs hydrosol (C) Particle size distribution of BH2 AgNPs hydrosol.*

3.3. Preparations of 3D AgNPs aggregates

3.3.1. Preparation of an empty Ag nanosponge aggregate -

Empty Ag nanosponge aggregates (i.e. those without any incorporated adsorbate) were prepared by modification of HA-AgNPs hydrosol by 1M HCl during the procedure developed by adaption of the preparation procedure described in ref. [52] for Ag nanosponge aggregates with the incorporated hydrophilic adsorbates.

In a glass vial, 2 mL of HA-AgNPs hydrosol were modified by 10 µL of 1M HCl and the closed vial was intensively manually shaken, till the formation of small fused aggregates was observed by a naked eye. A single 3D nanosponge Ag aggregate was prepared by merging of the fused aggregates by a pipette tip (1 – 1000 µL). Finally, the 3D Ag nanosponge aggregate was transferred by a pipette tip onto a glass microscopic slide with residual aqueous phase and let to dry.

Alternatively, the residues of the acidified aqueous phase were purposefully left in the aggregate pores and used for diprotonation of H_2TPP into H_4TPP^{2+} (Chapter 4.1.3.4.).

Schematic depiction of the aggregate preparation is shown in Figure 11.

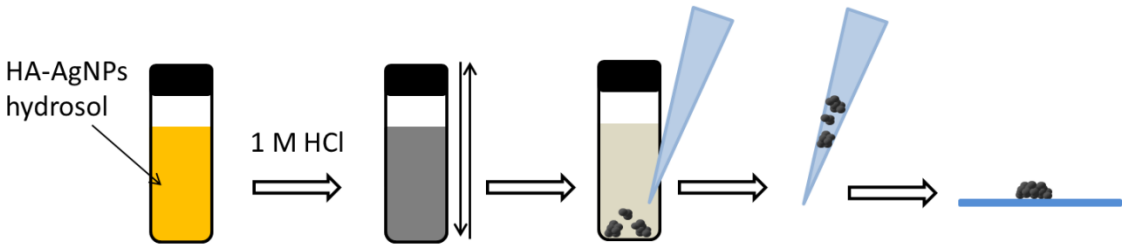

Figure 11: *Schematic depiction of the empty Ag nanosponge aggregate.*

3.3.2. Preparation of 3D Ag nanosponge aggregate with attempted incorporation of hydrophobic adsorbates by adapting the procedure used for hydrophilic adsorbates

This preparation procedure was based on adapting the procedure developed for incorporation of the hydrophilic adsorbates into 3D Ag nanosponge aggregates and reported in refs [50–52] for the hydrophobic adsorbates, namely H_2TPP and C_{60}. The procedure has been denoted as type A. In particular, Into a 5 mL weighting bottle, 2 mL of HA-AgNPs hydrosol, 10.0 µL of 1M HCl aqueous solution and 20 µL of the testing adsorbates (C_{60} or H_2TPP) dichloromethane solution were added. The final concentration of testing adsorbate in the active system was varied in the 1×10^{-4} – 1×10^{-10} M range. The final concentration of HCl in the system was 5×10^{-3} M. The closed weighting bottle was intensively manually shaken for 30 – 60 s, i.e. until formation of small fused aggregates which was detected by the naked eye. A single 3D nanosponge Ag aggregate was prepared by merging of the fused aggregates by a pipette tip (1 – 1000 µL). Finally, the 3D Ag nanosponge aggregate was transferred by a pipette tip onto a glass microscopic slide with residual aqueous phase and let to dry.

Nevertheless, the subsequent SERS and SERRS spectral testing of these aggregates (Chapter 4.1.1.) has shown a highly irregular distribution of the hydrophobic adsorbate within the aggregate. For this reason, other preparation procedures were developed and tested (Chapter 3.3.3.).

Schematic depiction of the aggregate preparation is shown in Figure 12.

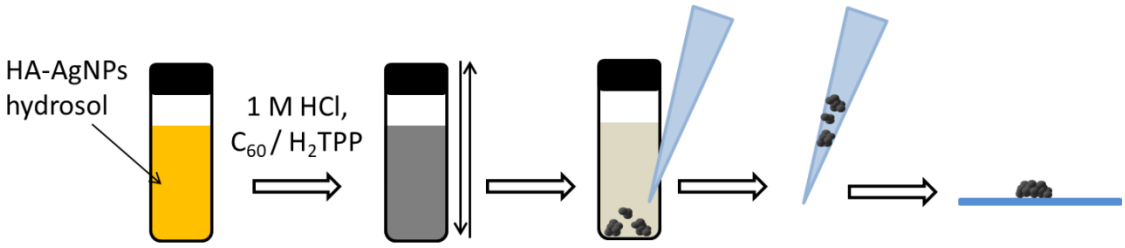

Figure 12: *Schematic depiction of preparation of 3D Ag nanosponge aggregate with attempted incorporation of a hydrophobic testing adsorbate.*

3.3.3. Preparations of 3D Ag nanosponge aggregates with incorporated hydrophobic testing adsorbates

Preparation of Ag nanosponge aggregates from a two – phase system was based on the procedure described for the BH-AgNPs hydrosol (10 nm average NP size) in refs. [44,45] and modified for the purpose of the Thesis by employment of the HA-AgNPs hydrosol (27 nm average NP size).

The general principle of the Ag aggregate preparation was always the same, but the pre-aggregating agent (PA), its concentration and its adding before and after addition of the dichloromethane solution of the adsorbate varied depending on the type of the Ag aggregates preparation.

In a vial, HA-AgNPs hydrosol with dichloromethane solution of selected hydrophobic testing adsorbate was mixed in the 1:1 ratio (typically 2 mL of HA-AgNPs hydrosol and 2 mL of the dichloromethane solution of testing adsorbate) and then, the HA-AgNPs hydrosol was modified by the selected pre-aggregating agent. Based on pre-aggregation agent used for preparation, different types of Ag nanosponge aggregates were prepared. Types of preparation are listed in Table 1.

The concentration of dichloromethane solution of the testing adsorbate in the preparation system varied in the 1×10^{-4} – 1×10^{-10} M range. The closed vial was intensively manually shaken for 30 – 60 s, i.e. until formation of small fused aggregates on the interface, which was detected by the naked eye. A single 3D nanosponge Ag aggregate was prepared by merging of the fused aggregates by a pipette tip (1 – 1000 µL). Finally, the 3D nanosponge aggregate was transferred by a pipette tip onto a glass microscopic slide and let to dry. Schematic depiction and photographical evidence of the sample preparation are shown in Figures 13 – 15.

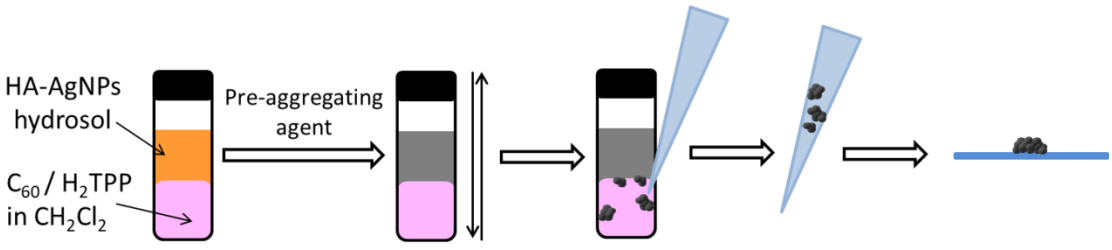

Figure 13: *Schematic depiction of 3D Ag nanosponge aggregate preparation with incorporated hydrophobic testing adsorbate into its internal structure*

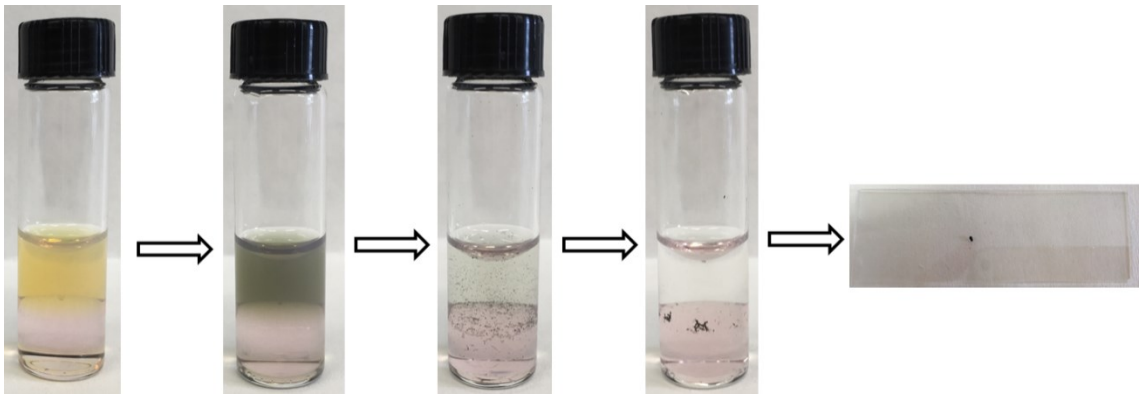

Figure 14: *Photographical evidence of formation of 3D Ag nanosponge aggregate with incorporated hydrophobic testing adsorbate into its internal structure (testing adsorbate: H_2TPP, $c_M = 1\times10^{-5}M$, PA = 0.1 M HCl)*

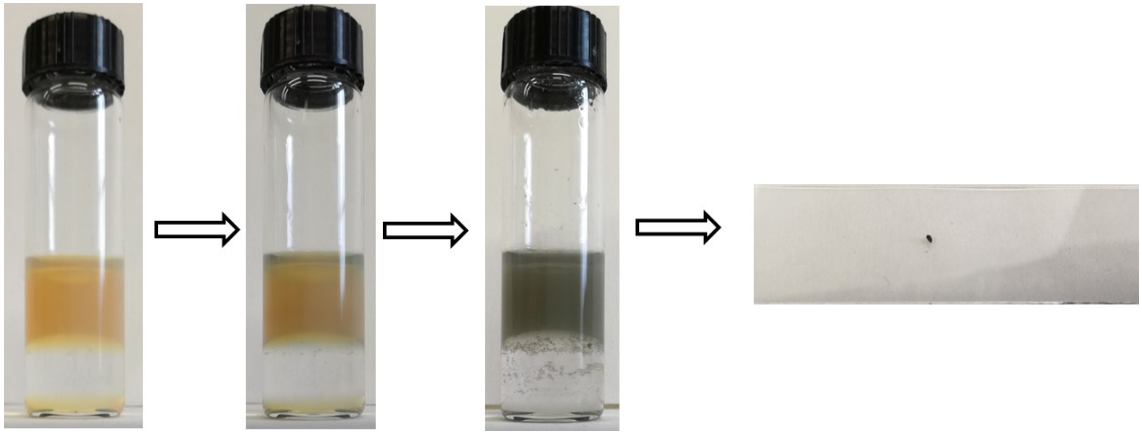

Figure 15: *Photographical evidence of formation of 3D Ag nanosponge aggregate with incorporated hydrophobic testing adsorbate into its internal structure (testing adsorbate: H_2TPP, $c_M = 1\times10^{-6}M$, PA = 0.1 M HCl)*

Decreasing of the testing adsorbate concentration in dichloromethane allows for a better and more effective formation of small, fused fractal aggregates from which 3D Ag nanosponge aggregates are formed.

Table 1: *Types of 3D Ag nanosponge aggregates preparation*

Sample name	***PA***	***Amount and addition of PA^{+}***	***Final concentration of PA****	***Testing adsorbate$^{\#}$***
B	1M HCl	10 µL before	5×10^{-3} M	Fullerene C_{60}
C	1 M HCl	10 µL after	5×10^{-3} M	Fullerene C_{60}, H_2TPP
D	0.1 M HCl	50 µL after	2.5×10^{-3} M	Fullerene C_{60}, H_2TPP
E	1 M NaCl	50 µL after	2.5×10^{-2} M	Fullerene C_{60}, H_2TPP
F	1 M H_2SO_4	50 µL after	2.5×10^{-2} M	Fullerene C_{60}

* Final concentration of the pre-aggregating agent is the smallest amount which caused the formation of small fused Ag aggregates.

$^{+}$ i.e. before or after adding of dichloromethane solution of testing adsorbate.

$^{\#}$ Testing adsorbate for which the preparation procedure was tested.

3.4 Preparation of hybrid systems for SERS of SLG

3.4.1 Glass/SLG/Ag aggregate hybrid system preparation

As the first, the free AgNPs aggregates were prepared. Into the vial 2 mL of HA-AgNPs hydrosol was added and modified by 10 µL of 1M HCl. The closed vial was intensively shaken using a side to side laboratory shaker with interval of mixing 750 rpm. This type of preparation provides small 2D/3D fused aggregates which float on the aqueous phase surface. Aggregates from the aqueous phase were transferred onto a glass slide by a cut pipette tip. Then, SLG was transferred onto the Ag aggregates in two ways. The Ag aggregates were imprinted onto SLG deposited on a glass slide (a) or SLG was transferred onto the Ag aggregates surface (b) as shown in Figure 16.

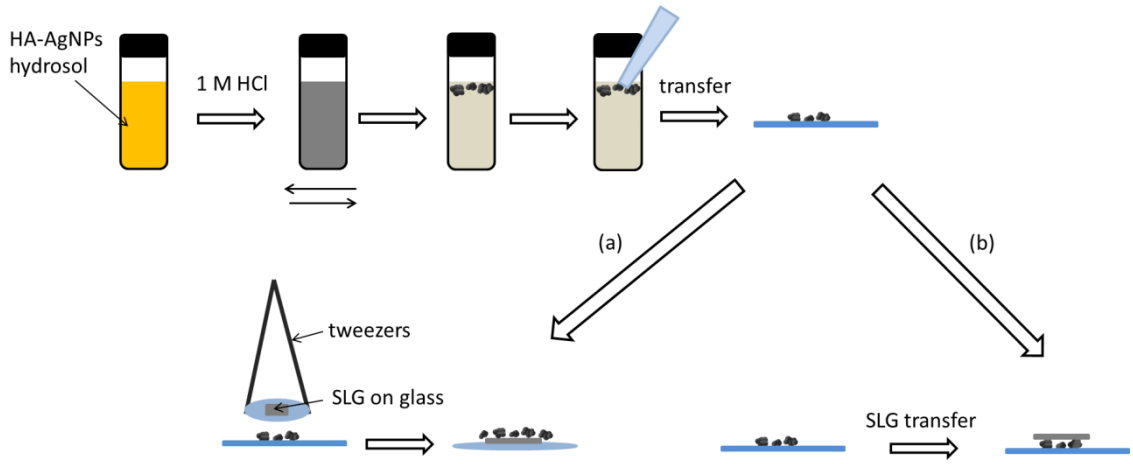

Figure 16: *Schematic depiction of glass/SLG/Ag aggregate hybrid system preparation*

SLG samples were prepared and deposited onto the glass slide or onto the microscopic cover glass slide/AgNPs aggregate hybrid system at the Heyrovsky Institute of Physical Chemistry, ASCR, by members of the Dr. Kalbáč´s group.

3.4.2 Glass/SLG/AgNPs-ET film hybrid system preparation

AgNPs-ET interfacial film was prepared by the procedure described in ref. X [21]. Briefly, into the vial, 2 mL of BH2-AgNPs hydrosol and 2 mL of 1×10^{-3} M dichloromethane solution of ethanethiol was added. The closed weighting bottle was intensively manually shaken till the formation of the metallic blue interfacial AgNPs-ET film. AgNPs-ET film was transferred by a pipette tip onto a glass slide with a small amount of residual aqueous phase. Then the AgNPs-ET film was imprinted onto a microscopic cover glass slide covered by SLG and let to dry.

Schematic depiction and photographical evidence of the sample preparation is shown in Figures 17 and 18.

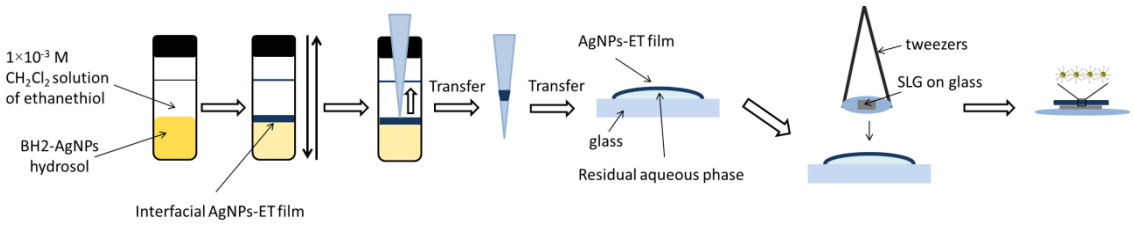

Figure 17: *Schematic depiction of glass/SLG/AgNPs-ET film hybrid system preparation.*

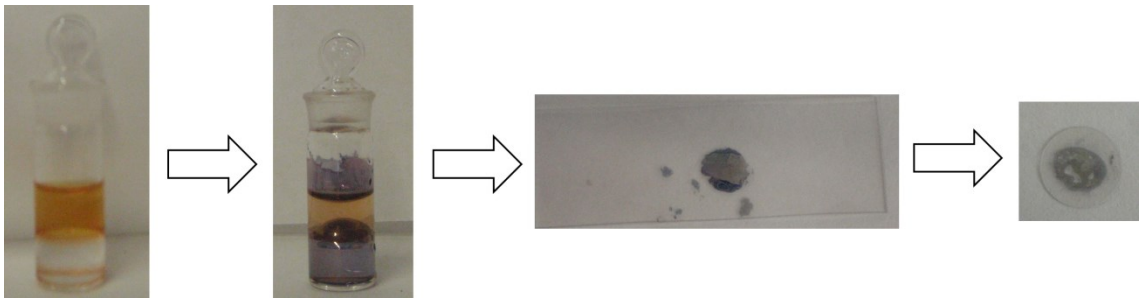

Figure 18: *Photographical evidence of formation of AgNPs-ET film and its deposition onto a glass slide.*

3.4.3 Glass/AgNPs/SLG hybrid system preparation

As the precursor, AgNPs-ET film was used and the preparation procedure of AgNPs-ET film was described in Chapter 3.4.2. The SLG was transferred onto the AgNPs-ET film by the NC procedure. The as-grown graphene [74] was transferred to the glass substrate using cellulose nitrate (NC) [75]. The majority of the NC layer was removed by methanol drops at room temperature. Then the glass/AgNPs-ET/SLG sample was annealed at 160^{o} C for 30 min. in order to remove the NC residuals from the SLG surface. SERS spectral testing (Chapter 4.2.2.2.) has shown that ET was removed from AgNPs surface during this process, hence the final system is denoted as glass/AgNPs/SLG. SLG preparation and transfer was done at the Heyrovsky Institute of Physical Chemistry, ASCR, by members of the Dr. Kalbáč´s group. Schematic depiction of sample preparation is shown in Figure 19.

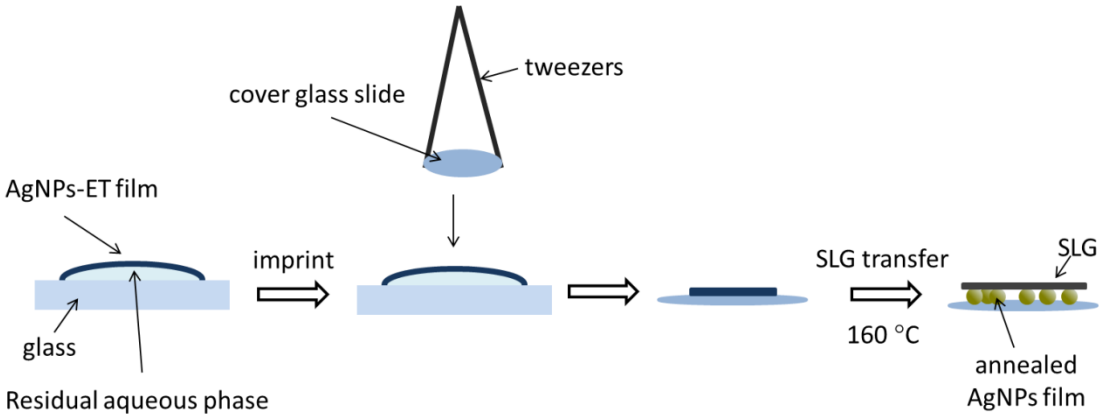

Figure 19: *Schematic depiction of glass/AgNPs/SLG hybrid system preparation*

3.5 Preparation of hybrid systems for combined GERS and SERS of selected aromatic molecules and of the appropriate reference systems

3.5.1 Graphite/H_2Pc hybrid system preparation (reference system for GERS)

The graphite electrode (GE) was overlayed by saturated ($<5\times10^{-5}$ M) solution of H_2Pc in toluene (which was filtered by the 1 μm filter prior to use). Subsequently, GE was kept in the toluene – saturated atmosphere in a sealed weighting bottle for 24 h to accomplish adsorption of H_2Pc onto the surface. The sample was then extracted from the weighting bottle to the new, clean weighing bottle. The second step aimed at the removal of excess H_2Pc molecules was performed by soaking the as-prepared GE/H_2Pc sample in a pure toluene and by keeping it in the same setup as described above for 10 min. The GE was then removed, new pure toluene was added onto the weighting bottle and GE was sunk again. This process was repeated 10 times. Schematic of sample preparation is shown in Figure 20.

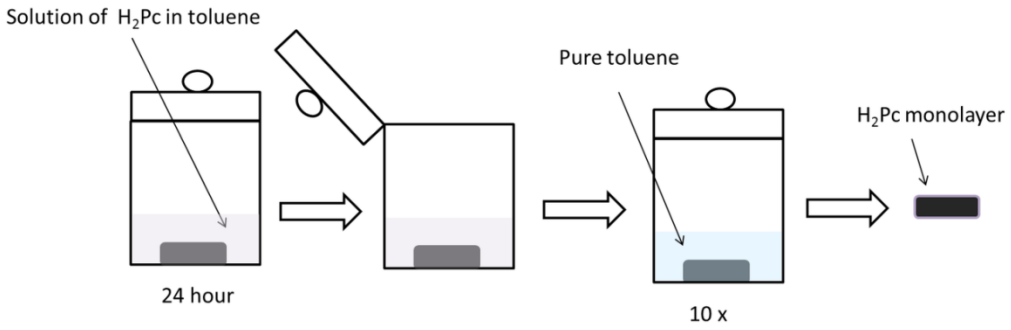

Figure 20: *Schematic depiction of the GE/H_2Pc (reference) sample preparation.*

3.5.2 Preparation of glass/SLG/H_2Pc(ML) hybrid system as reference system for SERS + GERS

Preparation of the glass/SLG/H_2Pc hybrid system was prepared by the procedure described in the ref [90] and modified by the using a different type of the glass slide for the sample preparation. The purpose was to mimic doping of SLG by Ag by doping of SLG by the special microsopy glass substrate as described in Chaper 4.3.1.

Briefly, onto the large weighting bottle, the smaller was placed (upside down) and the large weighting bottle was filled by the pure toluene to the half of the hight of the smaller one. To the bottom of the small weighting bottle, glass/SLG sample was placed

and the glass/SLG sample was covered by the solution of the H_2Pc toluene. The weighting bottle was closed and sealed with parafilm, and left standing for 24 hours. Then the residues of H_2Pc in toluene solution were dried by the filter paper. By the same procedure as described above, the glass/SLG/H_2Pc sample was covered by the pure toluene for 10 minutes, to wash out the residues of the H_2Pc. This process was repeated 10×. By this procedure, the glass/SLG/H_2Pc(ML) (ML = monolayer) sample was prepared. The preparation procedure is demonstrated in Figure 21.

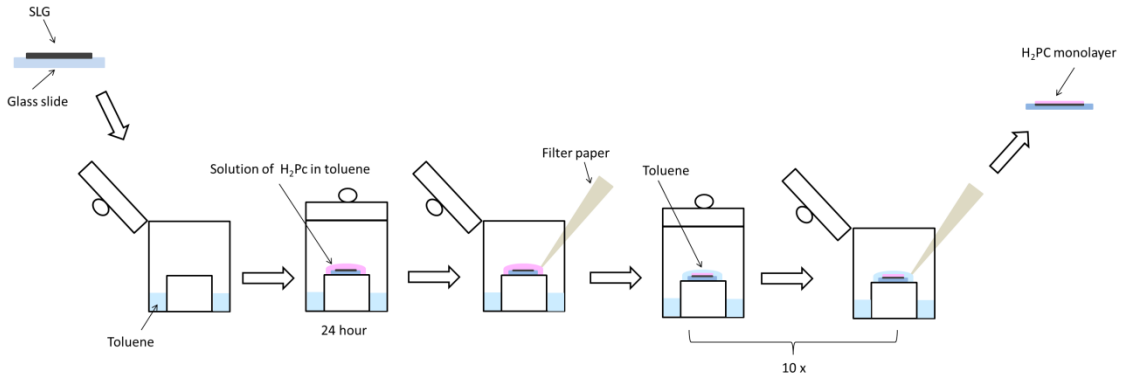

Figure 21: *Schematic depiction of the glass/SLG/H_2Pc(ML) sample preparation.*

3.5.3 Glass/AgNPs/SLG/H_2Pc hybrid system preparation

Preparation of glass/AgNPs/SLG/H_2Pc hybrid system consists from 3 steps. First, AgNPs-ET film was prepared by the procedure described in Chapter 3.4.2. according to ref. [21]. Secondly, AgNPs-ET film was overdeposited by the SLG [74] using the nitrocellulose method [75] described in Chapter 3.4.3. During this procedure, ET was removed from AgNPs surface (Chapter 4.2.2.2.).

In the third step, H_2Pc monolayer was deposited onto the SLG surface by the procedure described in Chapter 4.5.1.

Schematic depiction of the sample is shown in Figure 22.

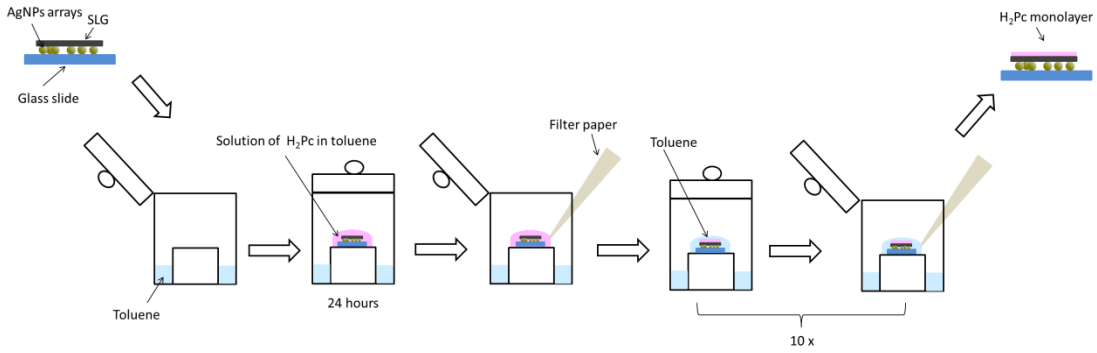

Figure 22*: Schematic depiction of the glass/AgNPs-ET/SLG/H_2Pc hybrid system*

3.6 Instrumentation

3.6.1 Raman spectral measurements

SERS and SERRS spectra were recorded on a DXR Raman microscope (Thermo Scientific) interfaced to an Olympus microscope. For SERS measurements, an objective with the 50x magnification was used. The 445 nm (diode laser), 532 nm (diode-pumped solid state laser), 633 (He-Ne laser) and 780 nm (diode laser) excitation lines were used. The maximal laser power ranged from 8 to 24 mW. Full range gratings were used for all measurements.

Combined SERS + GERS spectra of 3 – component hybrid samples as well as GERS and Raman spectra of reference samples were recorded on WITec alpha300 Raman micro-spectrometer. An objective (Zeiss) with 100× magnification was used for all the above mentioned Raman spectral measurements performed at 532, 633, 647, 785 and 830 nm excitations. For measurements on WITec alpha300, two spectrographs equipped with charge-coupled device (CCD) detectors optimized for the blue-green and for the red-NIR (near infrared) spectral ranges have been used, the first one for collection of spectra at 532 nm excitation and the second one for the other four excitation wavelengths, i.e. 633, 647, 785 and 830 nm. Excitation was provided by the following lasers at the respective wavelengths and laser power values (at the sample): SHG Nd:YVO_4 , 532 nm (2.3 mW); He-Ne, 633 nm (2.5 mW); Kr^+ ion, 647 nm (5.0 mW), diode, 785 nm (50.0 mW), diode, 830 nm (11.0 mW). Raman spectral mapping was performed by using the 25 μm x 25 μm area scans with 50 x 50 points.

3.6.2 UV/Vis spectral measurement

UV/Vis spectra were recorded on a Specord s600 (Analytik Jena) or on a Schimadzu UV-2401 PC UV/Vis (Schimadzu corporation) recording spectrometer.

3.6.3 Transmission electron microscopy

TEM images were obtained with TECNAI G2 Spirit (FEI) transmission electron microscope with the acceleration voltage 120 keV.

3.6.4 Scanning electron microscopy

SEM images were obtained with Quanta 200 FEG (FEI) and MAIA 3 (TESCAN) scanning electron microscope.

4. Results and discussion

4.1. Ag nanosponge aggregates as substrates and samples for SERS and SERRS of hydrophobic molecules

4.1.1. Searching for the best type of preparation of 3D aggregate with incorporated hydrophobic adsorbate

Six ways of preparation of 3D Ag nanosponge aggregates with incorporated hydrophobic adsorbate were developed and denoted as A – F. Preparation of type A aggregates has been described in Chapter 3.3.2, that of B – F aggregates in Chapter 3.3.3. and Table 1. All types of the Ag aggregates were tested by SEM imaging, and by SERS spectral measurements.

SEM microscopy revealed the morphology of Ag aggregate surface and the shape of the aggregate. As demonstrated in Figure 23: A.2 – F.2 the surface morphology of all aggregates is almost the same, only with small differences. The overall shape of the aggregates is always different as demonstrated in Figure 23: A.1 – F.1. The final shape and the size of the Ag aggregate is mostly affected by the amount and type of pre-aggregating agent, which causes the formation of small fused aggregates.

The shape and size of the aggregates affects the resulting SERS signal. In particular, the small aggregates provide less intensive SERS signal than the larger and thicker aggregates.

By the SERS spectral testing, the aggregate with the best SERS signal to noise ratio was searched. As the testing molecule for establishing of the best preparation procedure, fullerene C_{60} was selected, and the aggregates with incorporated C_{60} prepared from a 1×10^{-4}M solution of C_{60} in dichloromethane solution by procedures A – F were probed. The resulting SERS spectra are shown in Figure 24.

From all types of aggregates, SERS spectra of C_{60} were obtained. However, the Ag nanosponge aggregate – type A provides any SERS signal very sparsely at very few locations within the aggregate. For obtaining of any SERS signal, SERS spectral mapping of the whole aggregate volume was necessary. On the other hand, when the positive signal was obtained, relatively intense SERS spectrum of fullerene C_{60} was obtained – Figure 24.

Ag nanosponge aggregates – types C and E provide the positive SERS signal through the whole volume, but the signal was very weak and noisy. Due to these facts, these three types of aggregates were excluded from further testing.

Type B, D and F aggregates provide relatively intense SERS signal of fullerene C_{60} through the whole volume of the aggregate. For the determination of the "best" preparation procedure, limits of SERS spectral detection (SERS LODs) of C_{60} were determined at λ_{exc} = 532 nm. The lowest limit of SERS spectral detection was obtained from the aggregate – type D and it was determined as 1×10^{-7} M.

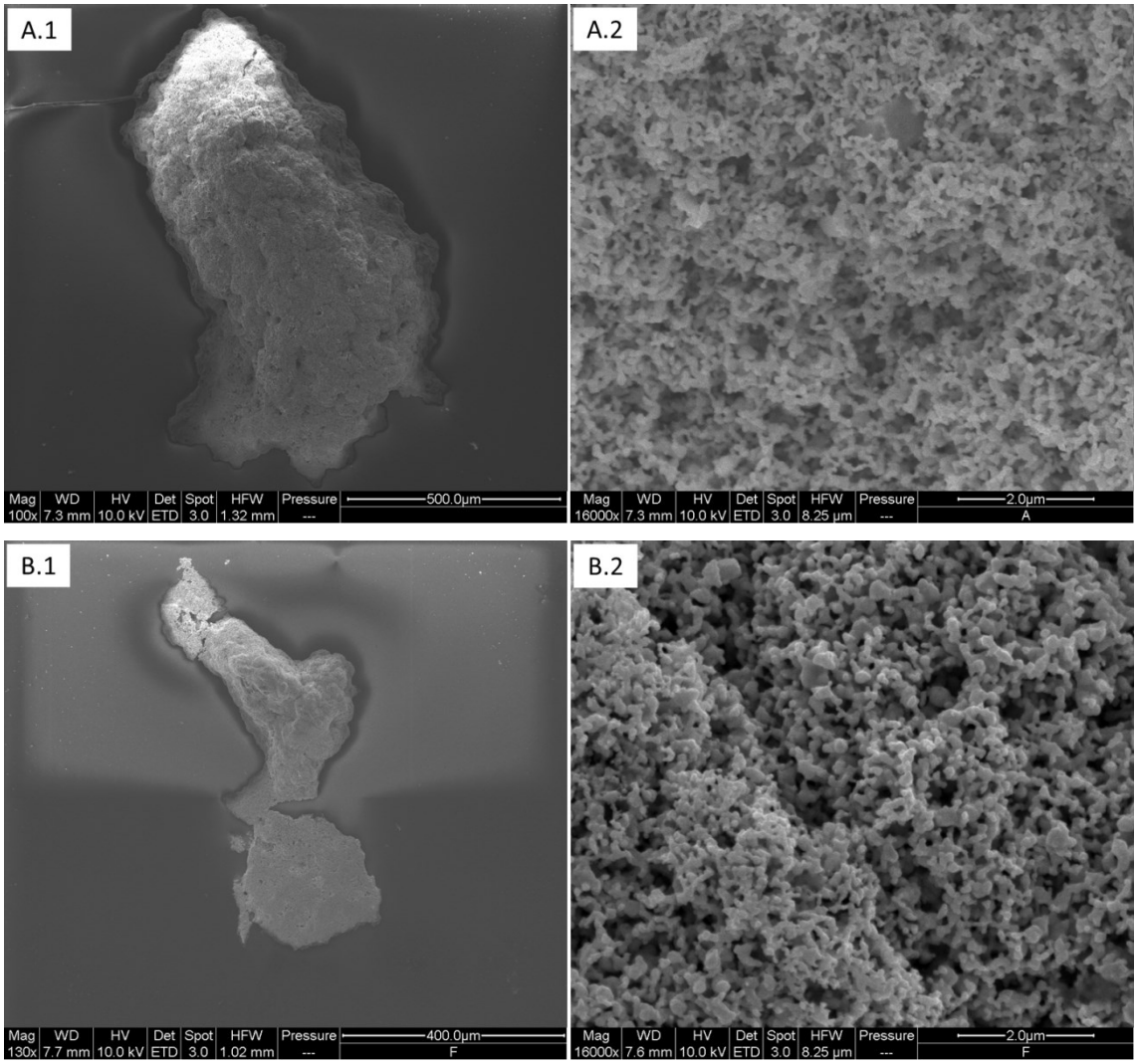

Continue on next page

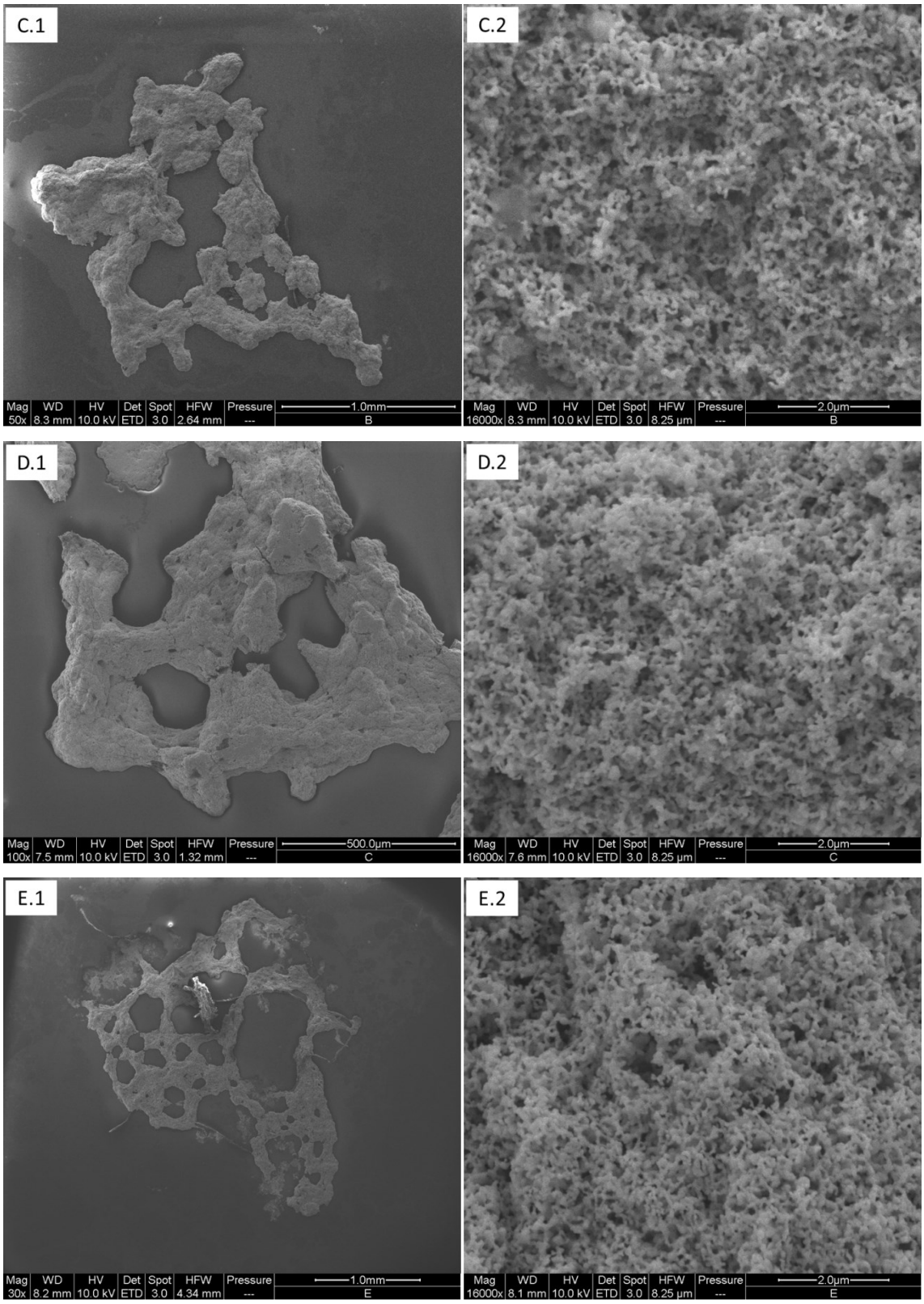

Continue on next page

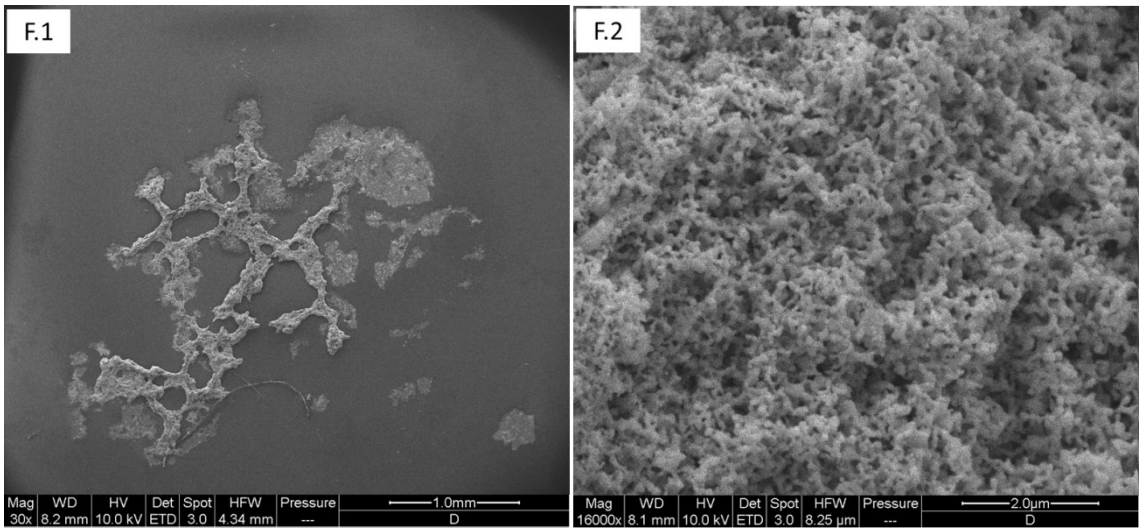

Figure 23: *SEM images of 6 types of Ag nanosponge aggregates. As a testing adsorbate, 1×10^{-4} M dichloromethane solution of fullerene C_{60} was used. Images A – F.1 shows the whole aggregates. Images A – F.2 shows the nanosponge morphology of its surface.*

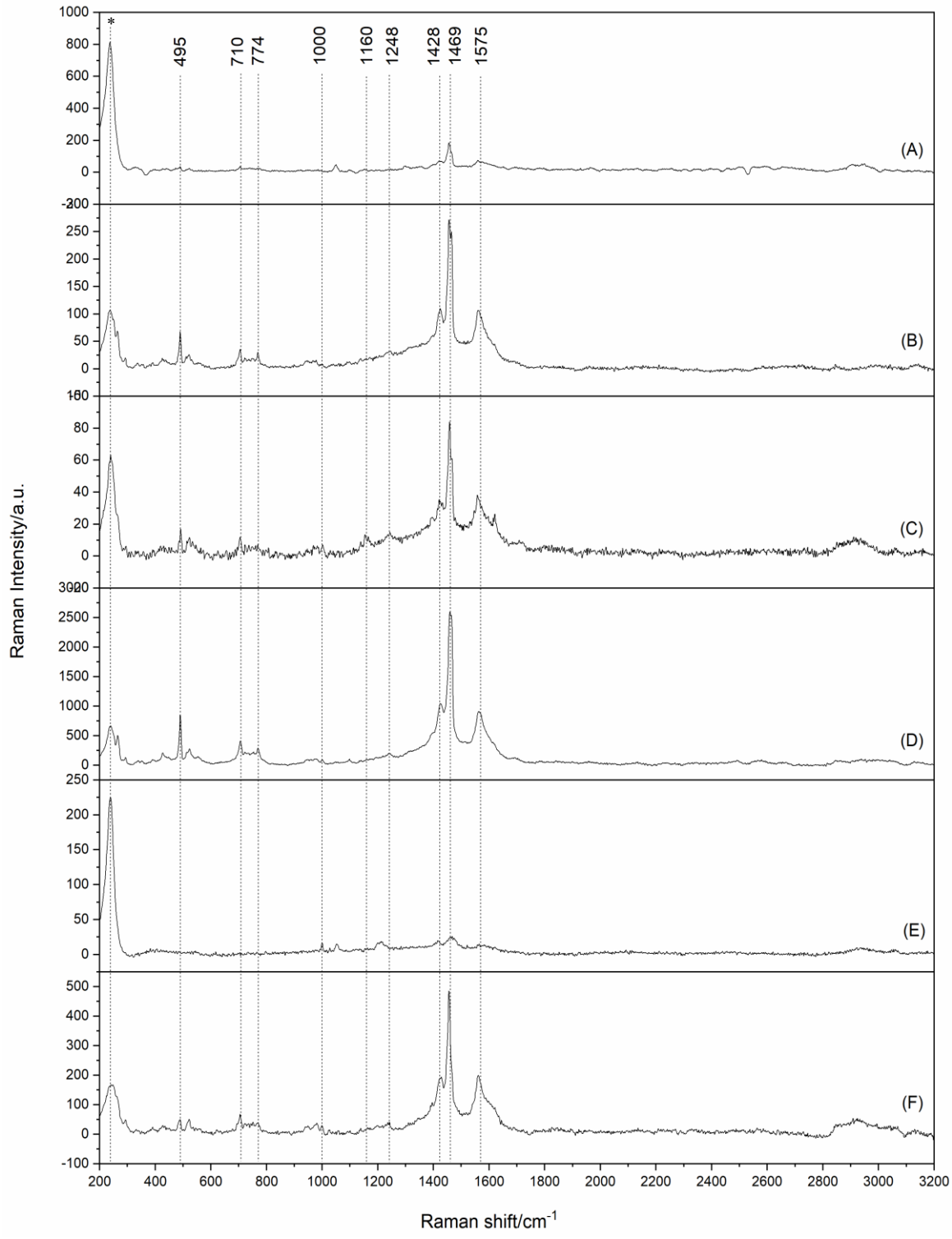

Figure 24: *SERS spectra of fullerene C_{60} incorporated into different types of 3D Ag nanosponge aggregates (A – F) at λ_{exc}= 532 nm. Dichloromethane solution of 1×10^{-4} M fullerene C_{60} was used for the samples preparation. All spectra were baseline corrected. The Ag-Cl spectral band at 241 cm^{-1} is denoted by an asterisk.*

In conclusion, the preparation procedure – type D was established as the best type of preparation of the Ag nanosponge aggregate with incorporated C_{60} molecules. In this procedure (described in detail in Chapter 3.3.3, 0.1 M HCl was added as a pre-aggregation agent into the two phase system, i.e. after mixing of the Ag NP hydrosol with the 1×10^{-4}M solution of C_{60} in dichloromethane (Table 1 in Chapter 3.3.3). This preparation procedure leads to the formation of Ag aggregates with the 1.5×1×0.025 mm average size, and this aggregate provides the best SERS signal to noise ratio of the incorporated hydrophobic C_{60} molecules.

4.1.2. 3D Ag nanosponge aggregate with incorporated fullerene C_{60} into the internal structure

4.1.2.1. Morphological studies of 3D Ag nanosponge aggregate and its 2D fused AgNPs aggregate precursors

First, morphological study of the 3D Ag nanosponge aggregate and of its 2D fused Ag NP aggregate precursor with incorporated fullerene C_{60} into the internal structure was done by the SEM and TEM imaging. Figure 25 – A shows the TEM image of fused 2D aggregates from which the resulting 3D aggregate is formed. TEM images of the 2D fused aggregates were used for the calculation of the average value of the fractal dimension, which was determined as $D = 1.89 \pm 0.05$. The fractal character of these aggregates indicates that after optical excitation, "hot spots" will be generated in them [13,14].

The resulting shape and morphology of 3D Ag aggregate is demonstrated in Figure 25 (B – D). Figure 25 – B shows the overall shape of the Ag aggregate, Figure 25 – C and D shows the internal nanosponge morphology of the Ag aggregate at various magnifications. The internal morphology of the nanosponge aggregates was studied and characterized by the measurement of the pore size distribution (Figure 26). The pore size distribution is very broad. However, two main types of sizes can be distinguished, namely the smaller pores with the sizes of approximately 60 nm and the larger pores with the sizes of approximately 250 nm.

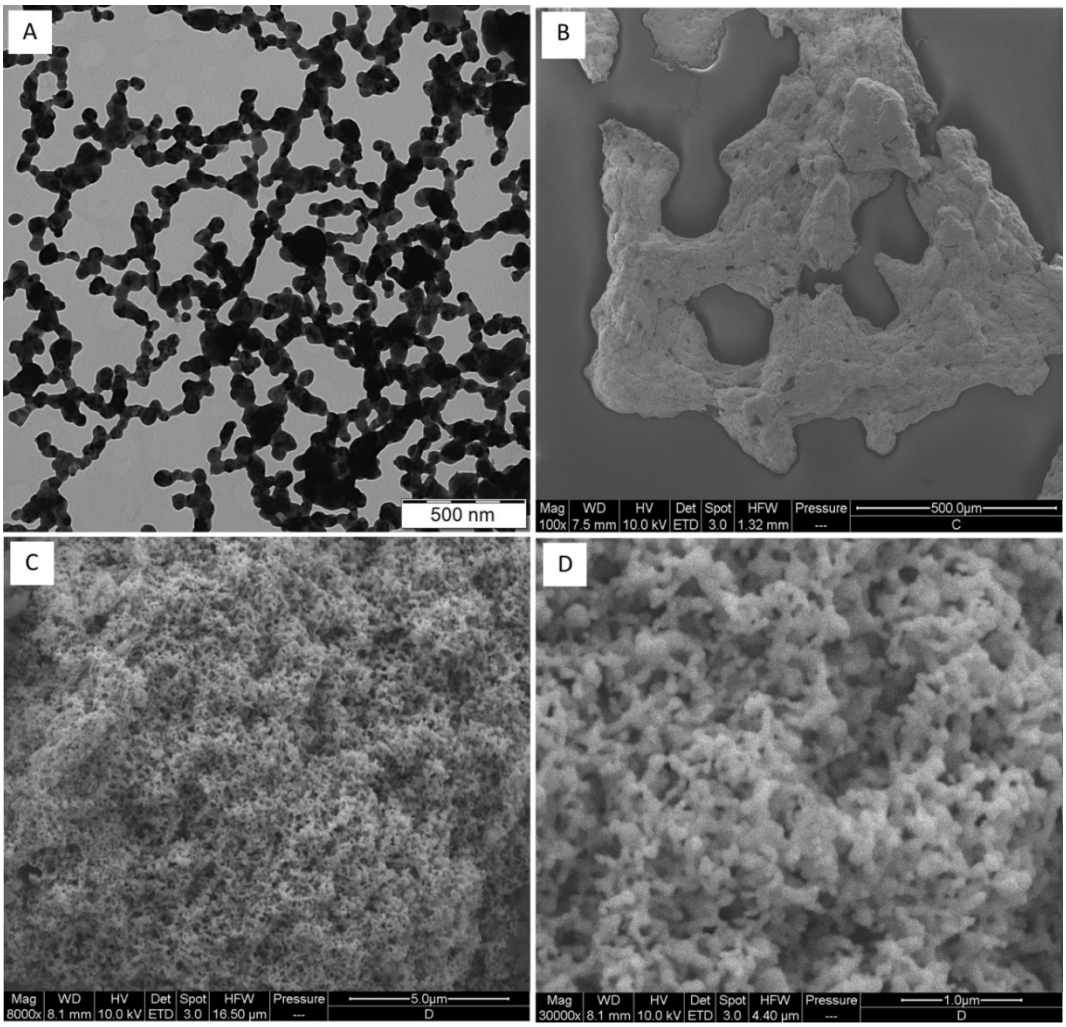

Figure 25: *(A) TEM image of 2D fused Ag aggregates and (B) – (D) SEM images of 3D AgNPs aggregate with incorporated fullerene C_{60} into the internal structure prepared from the 2-phase system in different magnifications.*

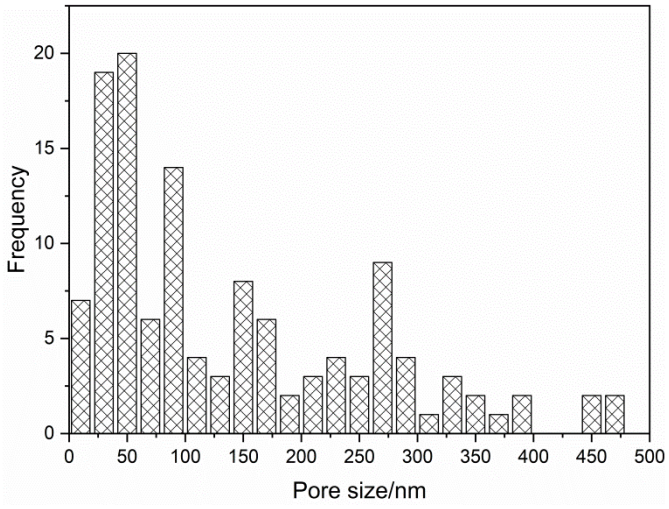

Figure 26: *Histogram of pore size distribution of the 3D Ag nanosponge aggregate with incorporated fullerene C_{60} into the internal structure.*

4.1.2.2. Spectral testing of fullerene C60 incorporated into and overlayed over the Ag aggregate

First, electronic absorption spectra were measured. Figure 27 demonstrates the electronic absorption spectrum of a 1×10^{-4} M dichloromethane solution of fullerene C_{60} with projection of excitation wavelength used for SERS measurements. The absorption maximum is located at 340 nm, in the 450 – 650 nm range the spectrum shows broad increase of absorption.

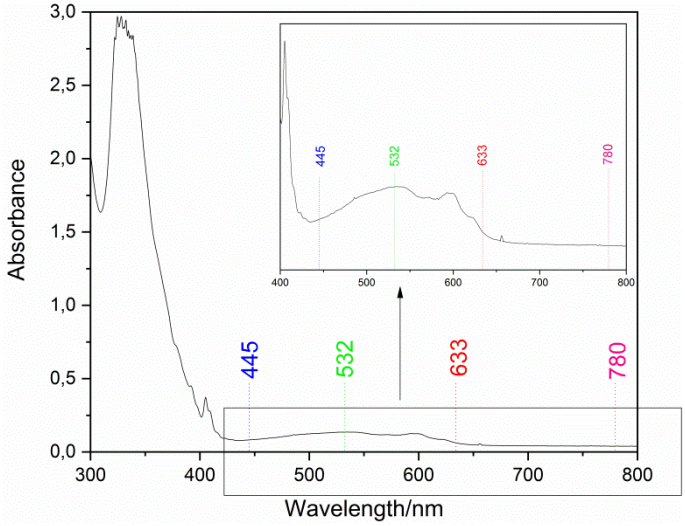

Figure 27: *UV/VIS spectrum of 1×10^{-4} M solution of fullerene C_{60} in CH_2Cl_2. Excitation wavelength used for SERS and SERRS spectral testing are shown.*

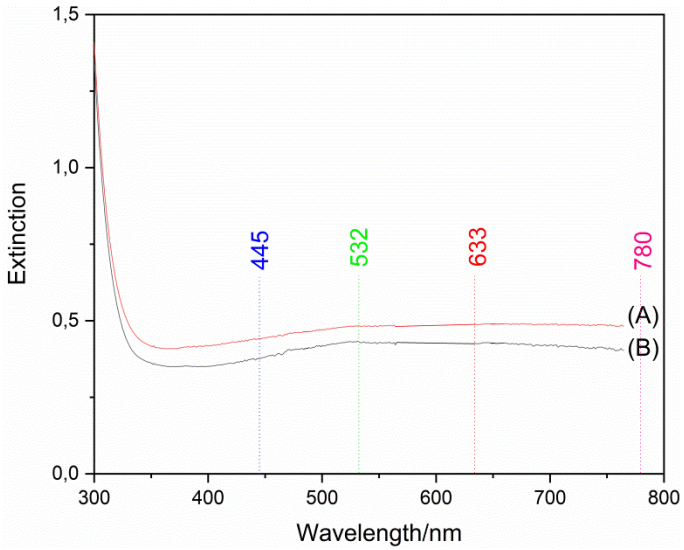

Figure 28: *SPE spectra of (A) empty AgNPs aggregate (B) AgNPs aggregate with incorporated C_{60} into the internal structure. Excitation wavelengths used for SERS and SERRS spectral testing are shown.*

Figure 28 demonstrates the SPE spectrum of (A) empty Ag nanosponge aggregate and (B) Ag nanosponge aggregate with incorporated C_{60} into the internal structure. SPE spectrum of the empty Ag nanosponge aggregate shows a small increase of extinction in the 400 – 800 nm range. SPE spectrum of the Ag nanosponge aggregate with incorporated fullerene C_{60} shows the small increase of extinction in the 400 – 600 nm range, while the value of extinction in the 600 – 800 nm range very slightly decreases with the increasing wavelength.

SERS and SERRS spectra of fullerene C_{60} were measured at four excitation wavelengths (445, 532, 633 and 780 nm) in two hybrid systems: (i) fullerene C_{60} was incorporated into the internal structure of the Ag aggregate and (ii) surface of the tempy Ag aggregate was overlayed by the dichloromethane solution of the fullerene C_{60}. From both systems, SERS and/or SERRS spectra were measured as a function of decreasing C_{60} concentration in the parent dichloromethane solution and the limits of SERS and SERRS spectral detection (LODs) were determined.

Figure 29 demonstrates SERS spectra of the fullerene C_{60} incorporated into the Ag aggregate internal structure at 445, 532, 633 and 780 nm excitations at the limits of their spectral detection. The characteristic bands at 496, 709, 738, 772, 1248, 1426, 1468 and 1575 cm^{-1} were used for determination of SERS and SERRS LODs. According to ref. [56,91] these bands belong to modes of A_g and H_g symmetry in the I_h symmetry point group. Spectra of fullerene C_{60} measured from the Ag aggregate which was overlayed by the dichloromethane solution of fullerene C_{60} show the same characteristic spectral bands (Figure 30).

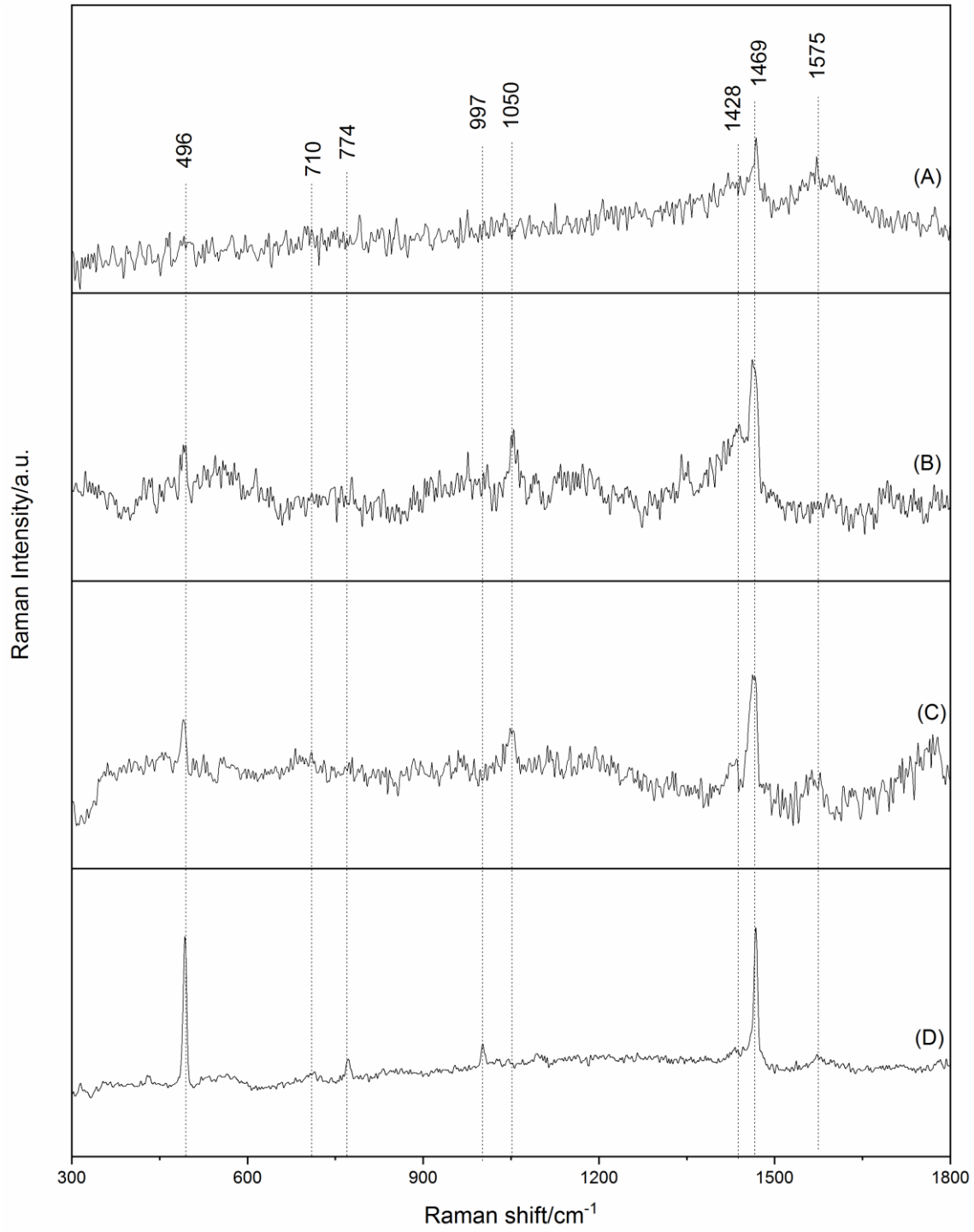

***Figure 29**: SERS spectra of fullerene C_{60} incorporated into the Ag aggregate internal structure in limits of SERS spectral detection (LOD) at four excitation wavelengths. (A) λ_{exc} = 445 nm, LOD = 1×10^{-6} M (B) λ_{exc} = 532 nm, LOD = 1×10^{-7} M (C) λ_{exc} = 633 nm, LOD = 1×10^{-5} M (D) λ_{exc} = 780 nm, LOD = 1×10^{-6} M. All spectra were baseline corrected.*

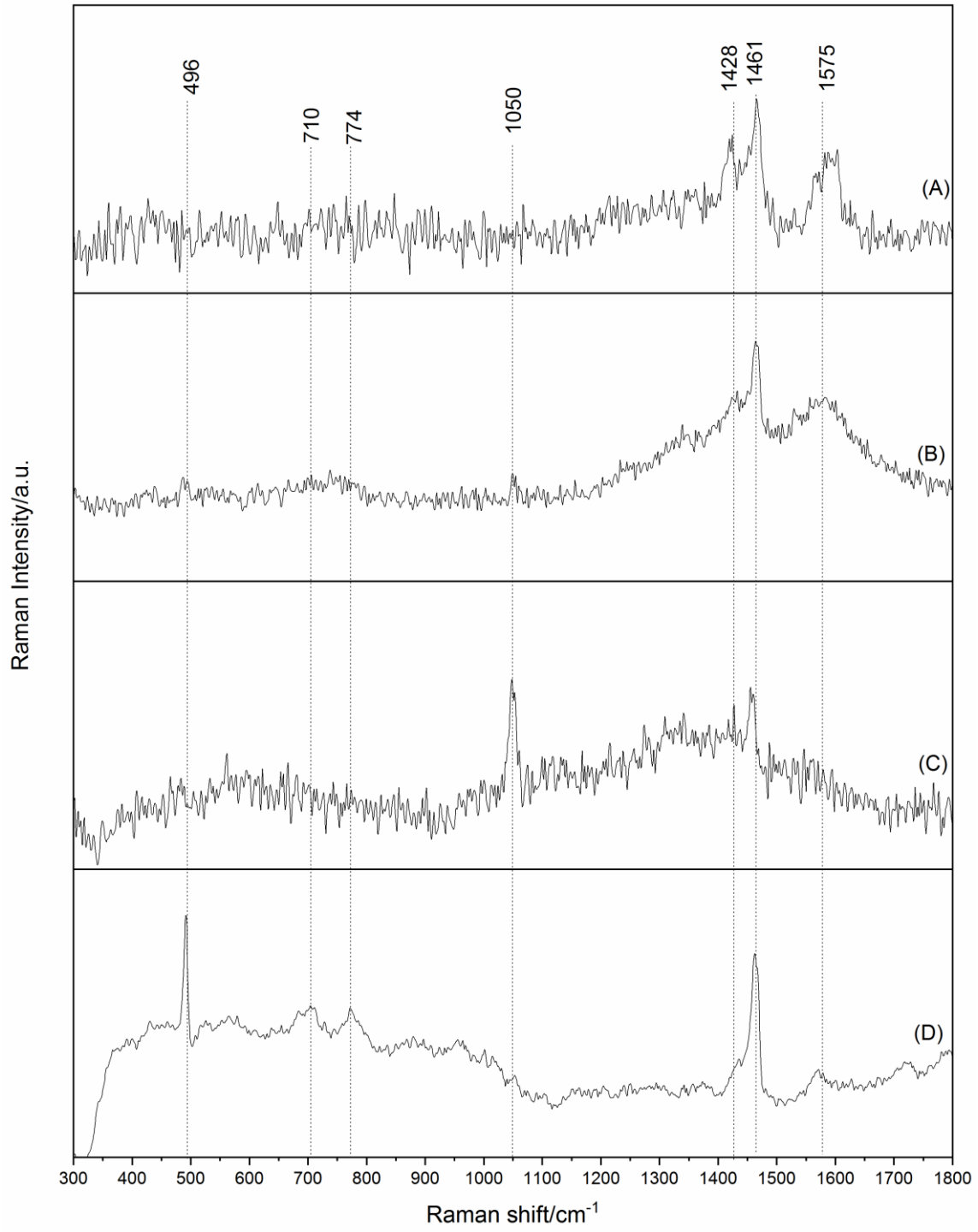

***Figure 30**: SERS spectra of fullerene C60 overlayed over the Ag aggregate in limits of SERS spectral detection (LOD) at four excitation wavelengths. (A) λ_{exc} = 445 nm, LOD = 1×10^{-5} M (B) λ_{exc} = 532 nm, LOD = 1×10^{-6} M (C) λ_{exc} = 633 nm, LOD = 1×10^{-4} M (D) λ_{exc} = 780 nm, LOD = 1×10^{-5} M. All spectra were baseline corrected.*

Limits of SERS and SERRS spectral detection of fullerene C_{60} in case of incorporation into the internal structure of the aggregates are by one order of magnitude lower than in case of overlaying of the aggregate by the solution of fullerene C_{60}, as shown in Table 2.

Table 2: *Comparison of SERS and SERRS LODs for fullerene C_{60}*

λ_{exc}	**445 nm**	**532 nm**	**633 nm**	**780 nm**
C_{60} incorporated into the internal structure of Ag aggregate	1×10^{-6} M	1×10^{-7} M	1×10^{-5} M	1×10^{-6} M
C_{60} overlayed over the Ag aggregate	1×10^{-5} M	1×10^{-6} M	1×10^{-4} M	1×10^{-5} M

Both samples provide SERS spectra of fullerene C_{60} in the native form, but the limits of detection are by one order of magnitude lower for the fullerene incorporated into the aggregate than for the soaked one.

The resultst demonstrates that incorporation of C_{60} into 2D fused fractal and, subsequently into 3D nanosponge aggregate is superior to C_{60} deposition by soaking of the C_{60} solution into the pores of the aggregates. The superiority results from efficient incorporation of C_{60} molecules into "hot spots" in the fused fractal 2D aggregates from which the 3D Ag aggregate are assembled.

4.1.3. SERS spectral testing of H_2TPP incorporated into and overlayed over the Ag nanosponge aggregate

4.1.3.1. Morphological study

5. Analogously to the case of fullerene C_{60}, the 3D Ag nanosponge aggregate with incorporated H_2TPP into the internal structure SEM images and TEM images of parent 2D fused fractal aggregates with incorporated H_2TPP were obtained as demonstrate Figure 31. From TEM images, fractal dimension of 2D fused AgNPs aggregates was determined as 1.95 ± 0.07, again the fractal character of these aggregates indicates that after optical excitation, "hot spots" will be generated in them [13,14]. The resulting shape and morphology of the 3D Ag aggregate demonstrates Figure 31 (B – D). Figure 31 – B shows the overall shape of the Ag aggregate, Figure 31 – C and D shows the internal nanosponge morphology of the

Ag aggregate at various magnifications. Also, the pore size distribution of was done and 3 main types of pores can be distinguished as shows the histogram in Figure 32: the small pores with the size approximately 50 nm, the middle pores with the size approximately 170 nm and the large pores with the size approximately 360 nm.

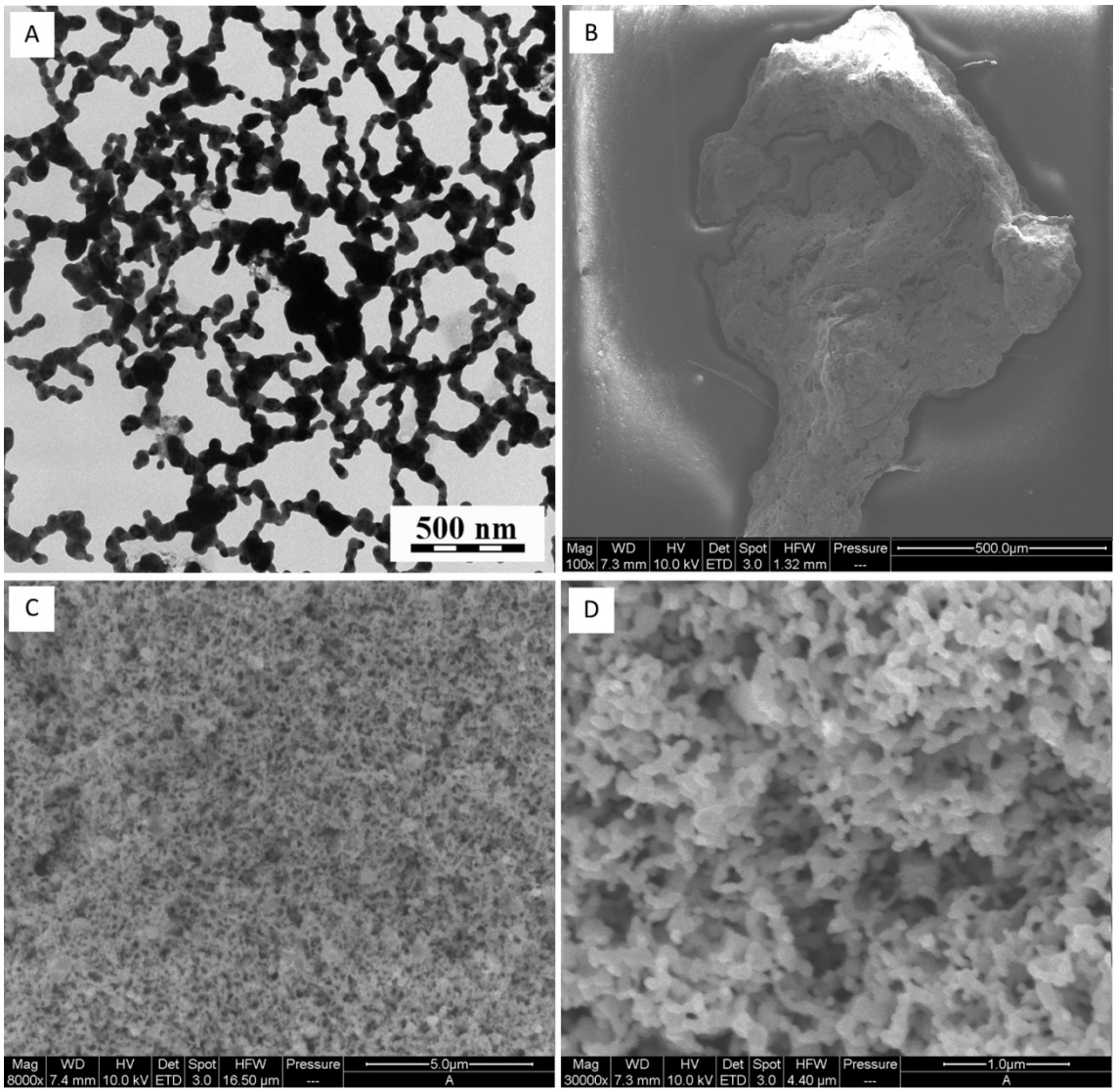

Figure 31: *(A) TEM image of 2D fused Ag aggregates and (B) – (D) SEM images of 3D AgNPs aggregate with incorporated H_2TPP into the internal structure in different magnifications.*

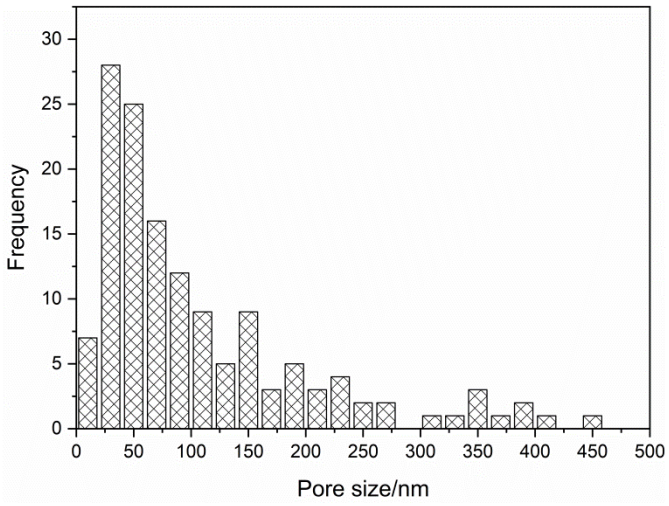

Figure 32: *Histogram of pore size distribution of the 3D Ag nanosponge aggregate with incorporated H_2TPP into the internal structure.*

4.1.3.2. Spectral testing of H_2TPP incorporated into and overlayed over the Ag nanosponge aggregate

First, the UV/Vis spectral measurements were done for the better understanding and characterization of the systems. Figure 33 shows the UV/Vis spectrum of 1×10^{-5} M dichloromethane solution of H_2TPP and Figure 34 shows SPE spectrum of 3D Ag nanosponge aggregate with incorporated H_2TPP into its internal structure.

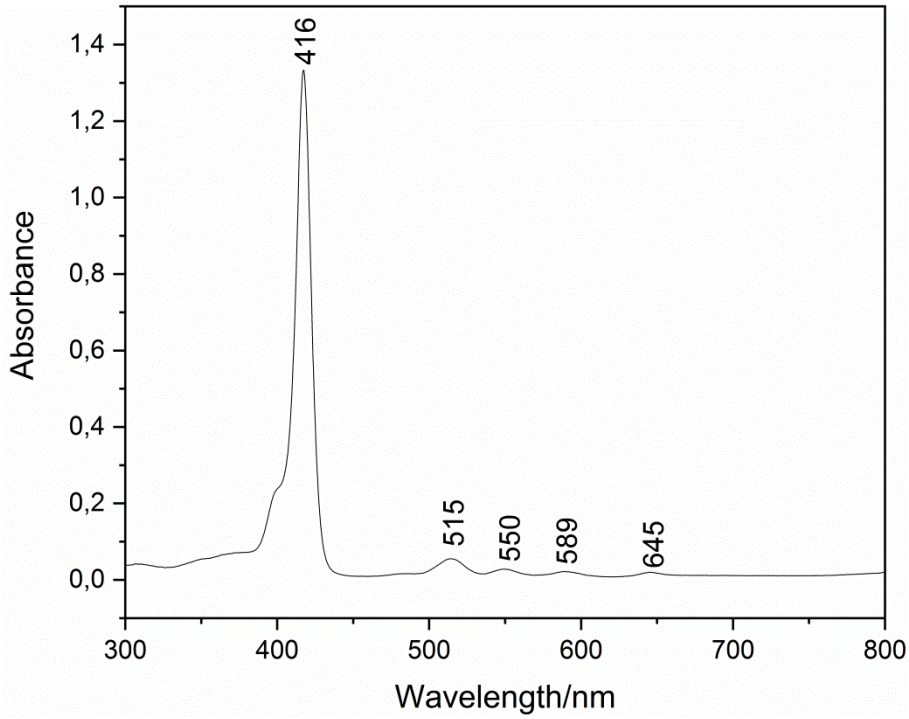

Figure 33: *UV/Vis spectrum of 1×10^{-5} M dichloromethane solution of H_2TPP.*

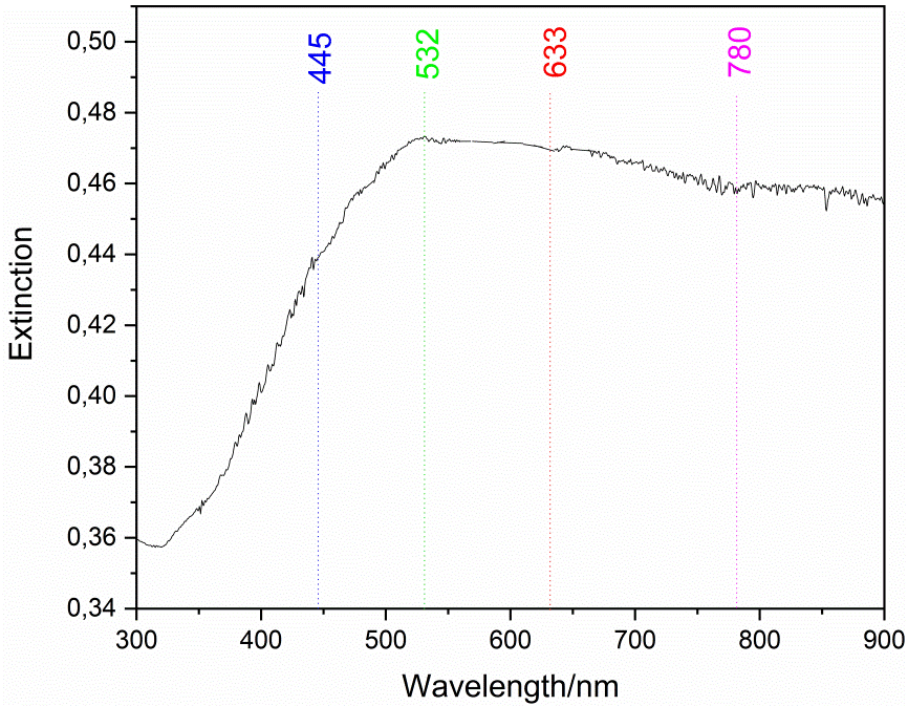

Figure 34: *SPE spectrum of 3D Ag nanosponge aggregate with incorporated H_2TPP into the internal structure with the projection of wavelengths used for SERS measurements.*

SPE spectrum of Ag nanosponge aggregate with incorporated H_2TPP into the internal structure shows an increase of the extinction in the 350 – 650 nm range, while the value of extinction in the 650 – 800 nm range only slightly decreases with the increasing wavelength.

Subsequently, SERS and SERRS spectral testing and determination of SERS and/or SERRS LODs of H_2TPP were done. Figure 35 shows SERS and SERRS spectra of H_2TPP incorporated into the Ag nanosponge aggregate internal structure from the 1×10^{-5} M parent solution of H_2TPP in dichloromethane. The spectra were measured at 445, 532, 633 and 780 nm excitations.

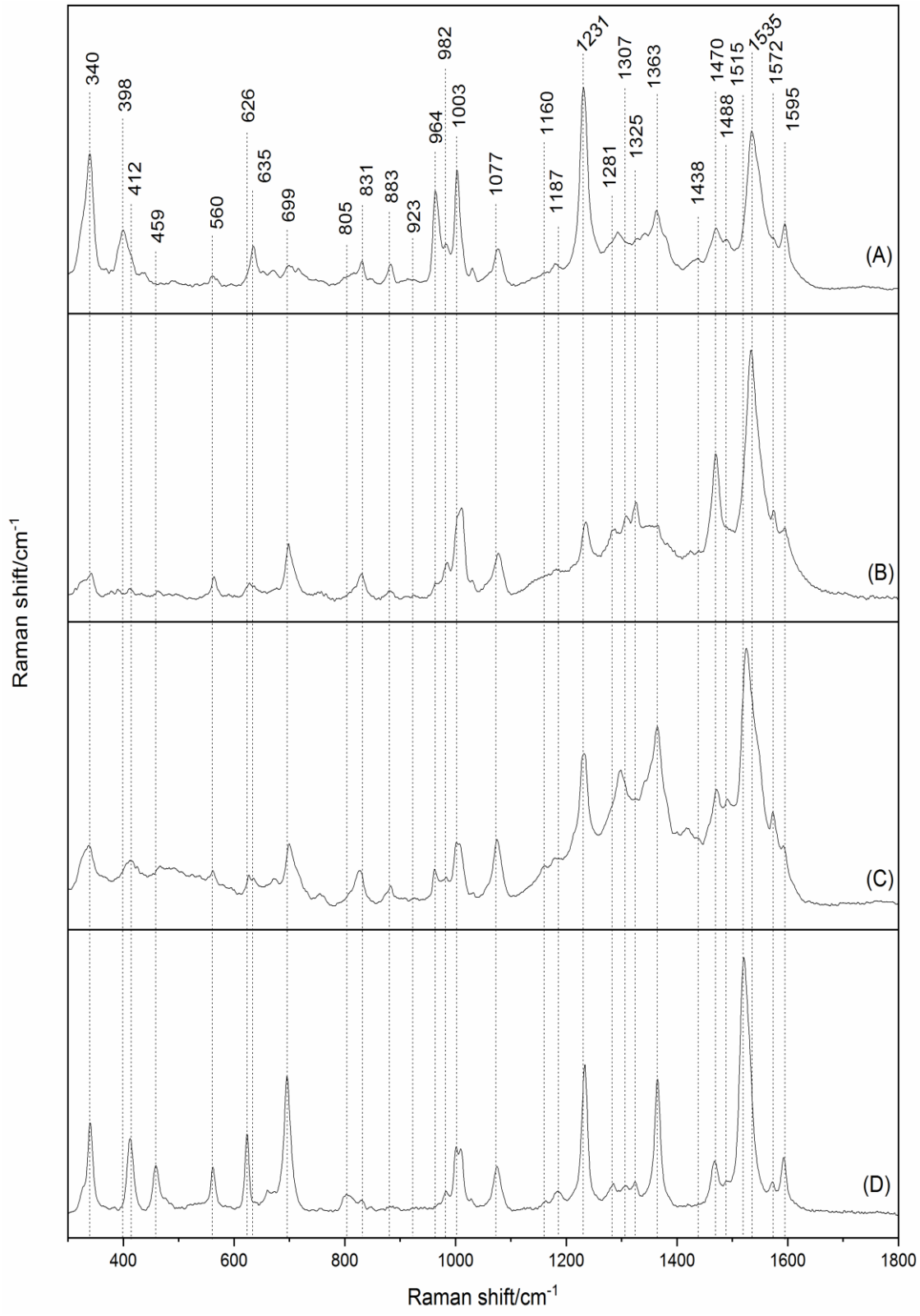

Figure 35: *SERS spectra of H_2TPP (c_M = 1×10^{-5} M) incorporated into the Ag aggregate at (A)λ_{exc} = 445 mn, (B) λ_{exc} = 532 mn, (C) λ_{exc} = 633 mn and (D) λ_{exc} = 780 mn. All spectra were baseline corrected.*

Figure 36 demonstrates the SE(R)RS spectra of H_2TPP incorporated into the internal structure of Ag aggregate at the limits of detection in the 200 – 1800 cm^{-1} range. The limits of SERS spectral detection of H_2TPP solution overlayed over the empty Ag aggregate were also determined and the SERS spectra at the limits of SERS spectral detection are shown in Figure 37. SERS spectra at λ_{exc} = 633 nm from the aggregate soaked in the H_2TPP solution could not be measured due to strong fluorescence.

The limits of SERS spectral detection of both systems were determined and their values are listed in Table 3.

Table 3**:** *Comparison of SERS and SERRS LODs of H_2TPP in two types of aggregates*

λ_{exc}	**445 nm**	**532 nm**	**633 nm**	**780 nm**
H_2TPP incorporated into the internal structure of Ag aggregate and partially converted into H_4TPP^{2+}	1×10^{-9} M	1×10^{-7} M	1×10^{-6} M	1×10^{-7} M
H_2TPP solution overlayed over the Ag aggregate	1×10^{-6} M	1×10^{-4} M	×	1×10^{-4} M

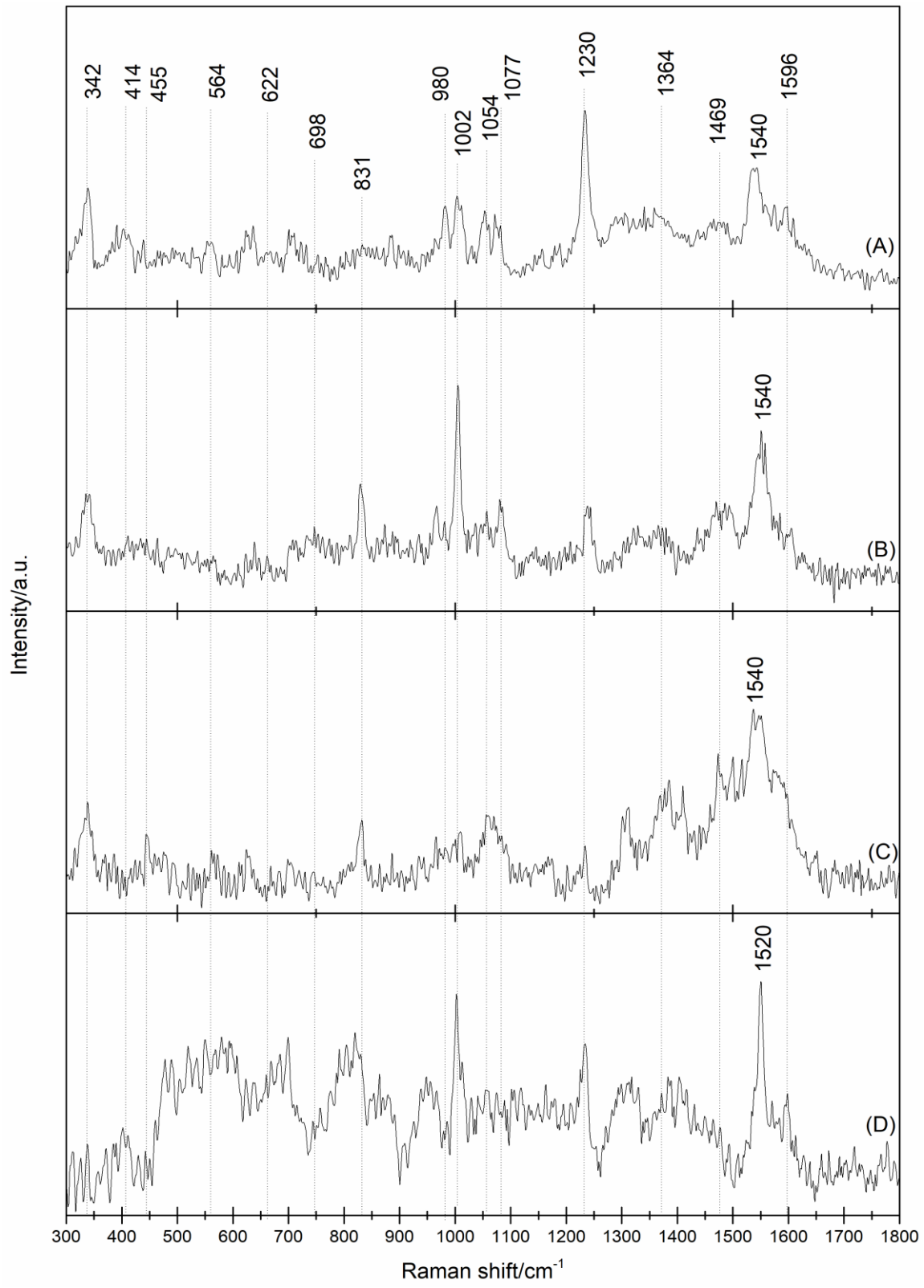

Figure 36: *SE(R)RS spectra of H_2TPP incorporated into the Ag aggregate at the limits of SERS spectral detection at (A) λ_{exc} = 445 mn, (B) λ_{exc} = 532 mn, (C) λ_{exc} = 633 mn and (D) λ_{exc} = 780 mn. All spectra were baseline corrected.*

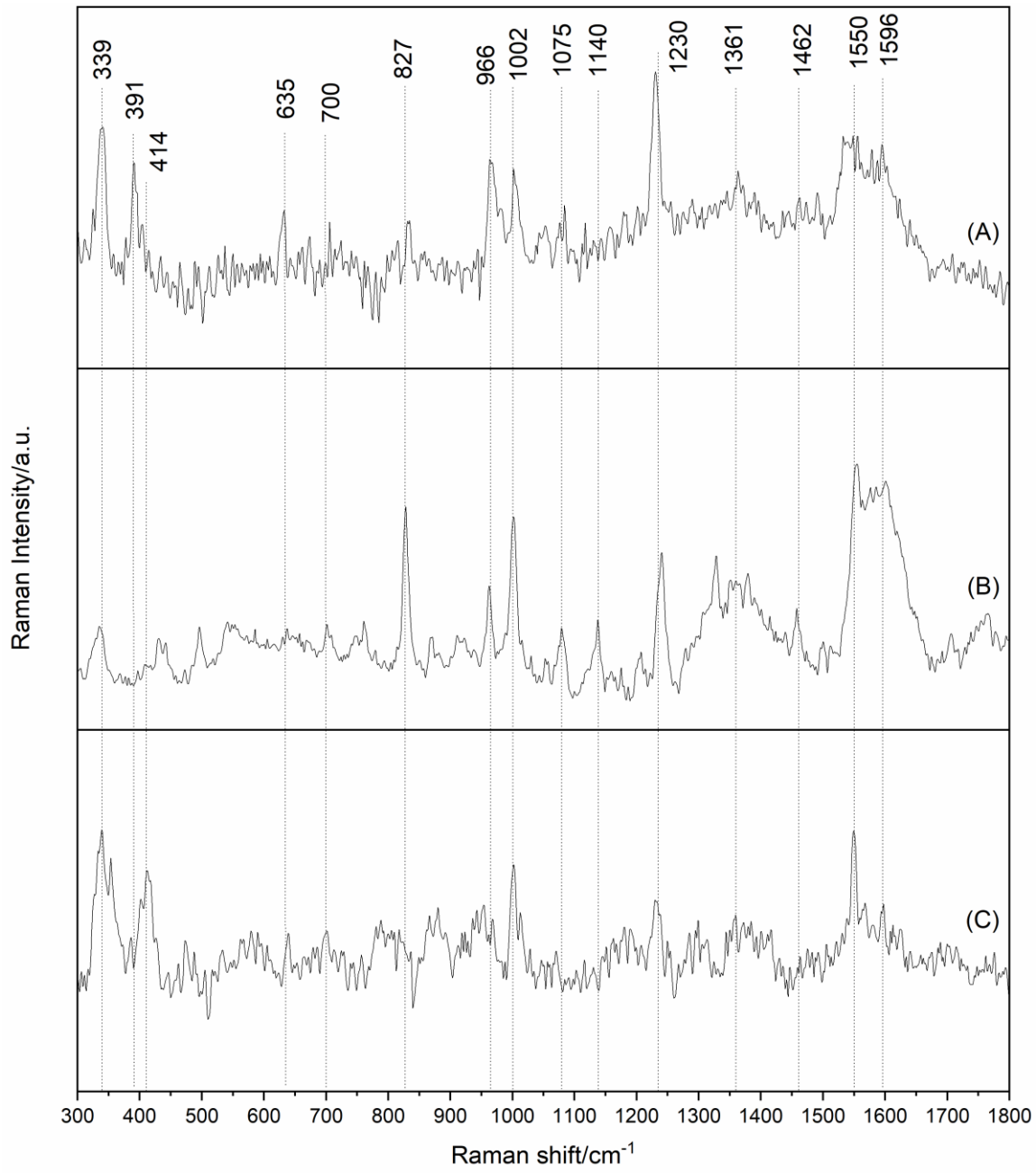

***Figure 37**: SERS spectra of H_2TPP overlayed over the Ag aggregate at the limits of their SERS spectra detection at (A) λ_{exc} = 445 nm (B) λ_{exc} = 532 nm and (C) λ_{exc} = 780 nm. All spectra were baseline corrected.*

In the SERS and SERRS spectra of system, where the H_2TPP was incorporated into the Ag nanosponges (denoted as System I in Table 4), only two characteristic H_2TPP spectral marker bands were found at 1364 and 1522 cm^{-1} while all the additional markers bands have been tentatively attributed to the diprotonated form of H_2TPP i.e. to H_4TPP^{2+} on the basis of the previously published RR spectra of H_4TPP^{2+} in solid state

sample and in solution [61,62] (details in Table 4). In particular, the most important marker bands of H_4TPP^{2+} appear to be the 340, 562, 625, 984, 1371 and 1540 cm^{-1} bands, and 5 of these 6 marker bands were identified in the SERRS spectra of System I (Table 4). Nevertheless, an unequivocal confirmation that these marker bands are, indeed, also the SERRS spectral markers of H_4TPP^{2+} remained to be established, and this has been done in Chapter (4.1.3.4.) by using the photochemically generated and UV/Vis tested H_4TPP^{2+} as the adsorbate for SERRS at 445 nm excitation.

In contrast to System I, in the system, where the dried Ag nanosponge aggregate was soaked in the dichloromethane solution of H_2TPP (system II in Table 4), predominantly the spectral marker bands of H_2TPP were found in the SERS and SERRS spectra (9 of 11 bands, Table 4). The most important bands characteristic for H_2TPP are the 339, 635, 966, 1002, 1361 and 1550 cm^{-1} bands (all of them observed in the SERRS spectrum). In addition to the bands specific for the free base and the diacid (diprotonated) form of the porphyrin, there are also the bands common to both spectral form, the most typical of them being the 1175, 1230 and 1596 cm^{-1} bands. It should be noted that SERRS spectra of H_2TPP have been reported, however, they were obtained at 514.5 nm excitation [45,63]. Nevertheless, they were found to match the RR spectra measured at these excitations and they were attributed to the unperturbed H_2TPP.

Detection of different porphyrin species as in System I and II has hampered the mutual comparison of the limits of SERS spectral detection of the porphyrin in both samples. In general, the limits of SERS spectral detection of H_2TPP incorporated into the Ag aggregate internal structure (and detected as predominantly the H_4TPP^{2+} species) are by 3 orders of magnitude lower than those of H_2TPP from the Ag nanosponge aggregate overlayed by its solution at all four excitations.

RR of H_2TPP [61,62]*	RR of H_4TPP^{2+} [61,62]*	SERRS of System I λ_{exc} = 445 nm	SERRS of System II λ_{exc} = 445 nm	SERRS of System III λ_{exc} = 445 nm	SERRS of System IV λ_{exc} = 445 nm	SERRS of System V λ_{exc} = 445 nm
335				335	339	
	340	342	339			340
392				388		
410		414	414	407	410	
432					434	
	459	455				
541						
	562	564			562	561
	623	622				625
636			635	634		638
	697	698	700		696	
	707				709	703
822			827	828		
	838					
	878				879	
884				883		
921	920				921	
961			966	961	962	
	984				984	983
1001		1002	1002	1001	1002	1002
	1016				1012	
	1033				1030	
1053		1054				1053
1075	1078	1077	1075	1079	1077	1072
	1140		1140			
	1183				1181	
1232	1234	1230	1230	1231	1233	1234
	1285				1285	
1292				1293		
	1326			1330		
1361		1364	1361	1363		
	1370				1371	1370
	1386					
	1428				1433	
1461			1462			
	1468	1469			1470	
1487				1487		
1497						
1522		1522				
	1534					
	1543				1540	1540
1551			1550	1550		
1560		1562				
	1576					1574
1597	1596	1596	1596	1593	1593	1595

*RR spectra of H_2TPP and H_4TPP^{2+} were excited at 441.6, 476.5 and 488.0 nm in ref. 61 and 488.0 in ref. 62

4.1.3.3. The role of the HCl in the H_4TPP^{2+} formation during incorporation of H_2TPP into Ag nanosponge aggregate

Observation of the spectral bands tentatively attributed to H_4TPP^{2+} in the SERS and SERRS spectra of Ag nanosponge aggregate into which H_2TPP molecules have been incorporated during its preparation (Table 4, System I and RR of H_4TPP^{2+} from ref. 62) indicates that the diprotonation of H_2TPP to H_4TPP^{2+} is most probably caused by presence of the HCl employed as the pre-aggregation agent in the 2D fused fractal aggregates preparation. For verification of this hypothesis, Ag nanosponge aggregate with incorporated H_2TPP molecules was prepared in the absence of HCl, i.e. by using NaCl as pre-aggregating agent, as is described in Chapter 3.3.3., as the E – type preparation). The SERRS spectral testing of this aggregate at λ_{exc} = 445 nm excitation was done (Figru 38 and Table 4, System III), and only H_2TPP marker bands and no markers of H_4TPP^{2+} were found. This result thus confirms the abovementioned hypothesis and indicates the chemical origin of the diprotonation reaction. Nevertheless, further experiments targeted on obtaining SERRS spectra of H_4TPP^{2+} generated by an alternative procedure, e.g. photochemically, and on probing of the role of the presence of Ag NPs during the diprotonation reaction were done to get a better insight into the mechanism of H_4TPP^{2+} formation during the Ag nanosponge aggregate preparation.

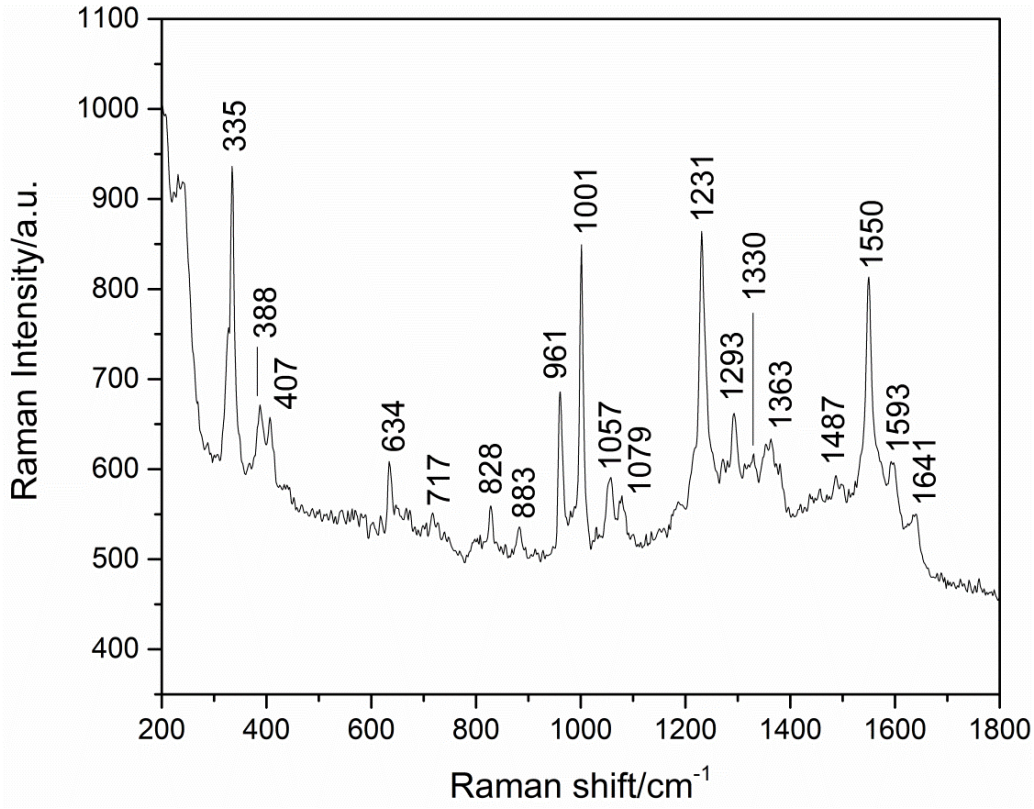

Figure 38: *Ag nanosponge aggregate with incorporated H_2TPP into the internal structure, prepared by using NaCl instead of HCl as the pre-aggregating agent.* λ_{exc} *= 445 nm.*

4.1.3.4. Photochemical generation of H_4TPP^{2+} and its SERS spectral measurements

The photochemical generation of the diacid form of the porphyrin from its parent free-base form the in dichloromethane solution has been performed and followed by the time-dependent UV/Vis spectral measurements. Characteristic UV/Vis spectra of H_2TPP and H_4TPP^{2+} are shown in Figure 39.

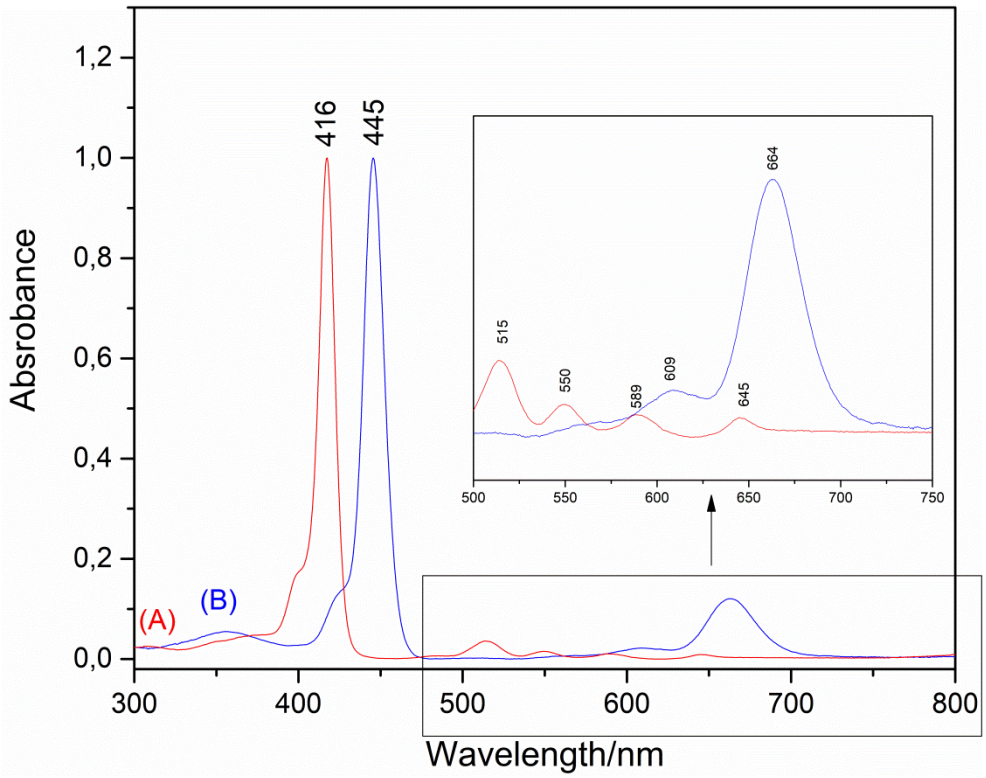

Figure 39: *UV/VIS spectra of 1×10^{-5} M dichloromethane solution of (A) H_2TPP and (B) H_4TPP^{2+}.In the inset, enlarged spectral bands in the 500 – 750 nm range are shown. Spectra were normalized.*

Conversion of H_2TPP to H_4TPP^{2+} is a relatively fast process, it means that a full conversion of H_2TPP to H_4TPP^{2+} takes several minutes (typically 10 – 15min.). Figure 40 demonstrates conversion of H_2TPP to H_4TPP^{2+} in dichloromethane solution followed by time-evolution of UV/Vis spectra. The conversion is accompanied by the decrease of the Soret band of the free base form at 416 nm, and by the increase of the Soret band of the diacid form at 445 nm. The changes are obvious also in the Q bands region, the most obvious is the increase of the 664 nm Q band of the diacid form.

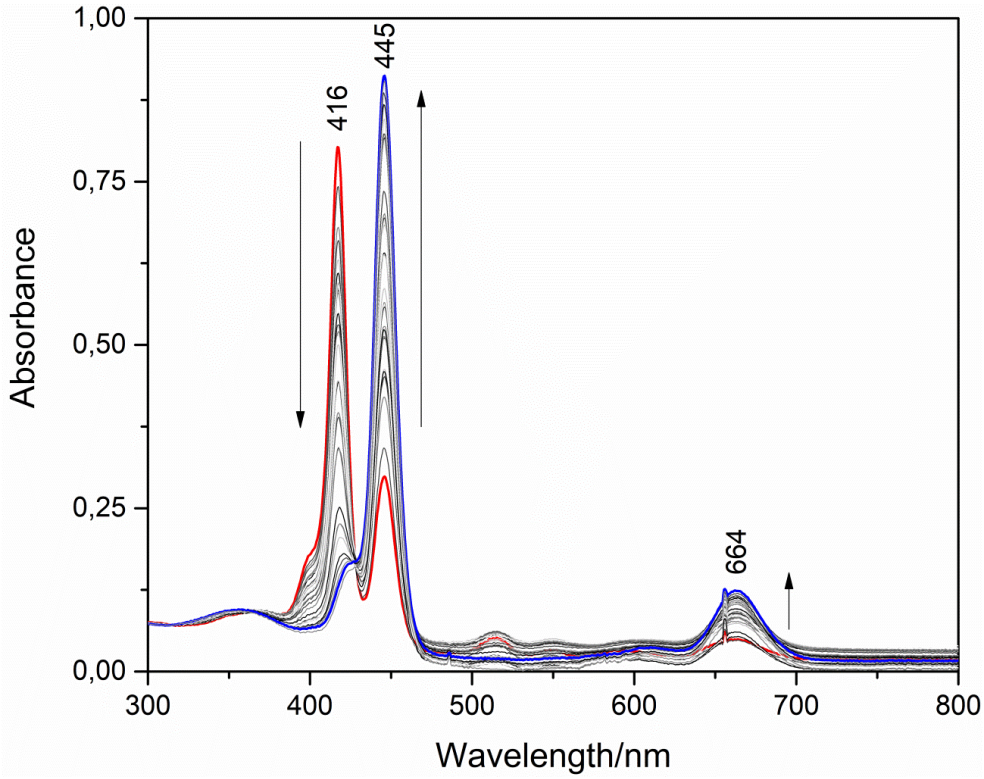

Figure 40: *Time evolution of conversion of H_2TPP to H_4TPP^{2+} form.*

Conversion of H_2TPP to H_4TPP^{2+} is also accompanied by a change of solutions colour from the violet (Figure 41 – A) to the green one (Figure 41 – B). The structure of H_4TPP^{2+} is depicted in Figure 41 – C.

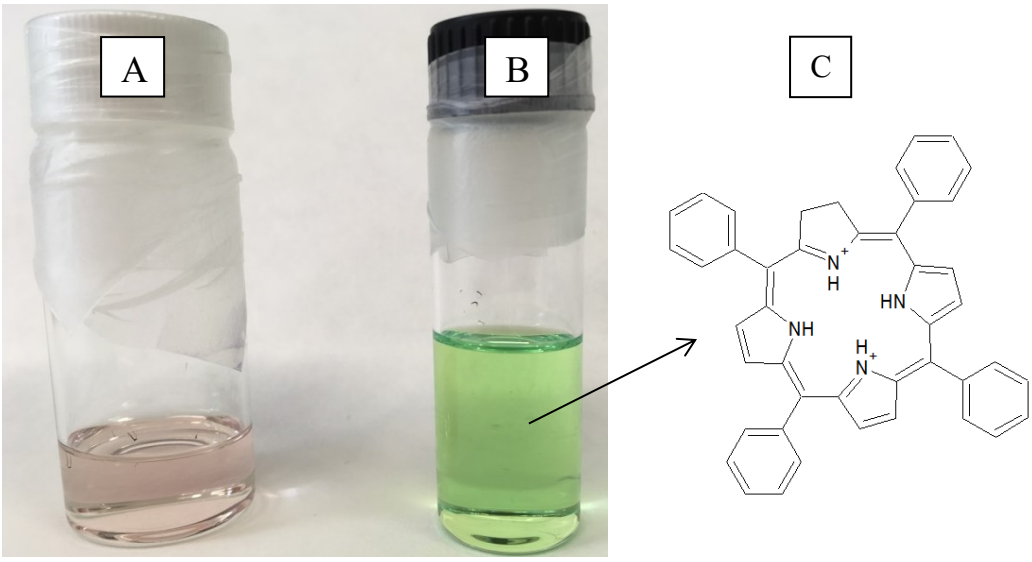

Figure 41: *1×10^{-5} M dichloromethane solution of (A) H_2TPP, (B) H_4TPP^{2+} and (C) structure of the H_4TPP^{2+}.*

Conversion of H_2TPP to H_4TPP^{2+} has been observed during the UV/Vis measurements. For the sake of comparison, the efficiency of an external UV light source in performing this conversion was tested. 50 mL of 1×10^{-5} M dichloromethane solution of H_2TPP in the quartz beaker was placed on the top of an UV lamp (180 – 340 nm range) for 30 minutes. After 15 minutes, the solution changed the colour from violet to the green. For accomplishment of a complete conversion, the solution was exposed to the UV light for another 15 minutes. After this time, the UV/Vis spectrum was measured and it is shown in Figure. 42. The spectrum after 30 minutes illumination by the UV light is virtually identical with the spectrum of H_4TPP^{2+} in *Figure. 39 – B.*

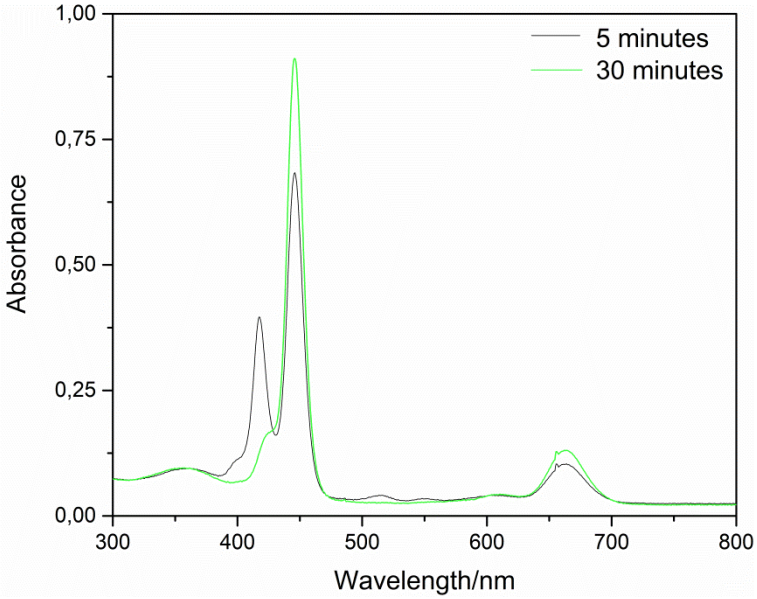

Figure 42: *Absorption spectrum of the 1×10^{-5} M dichloromethane solution of H_2TPP (H_4TPP^{2+} respectively) after 5 and 30 minutes of irradiation by UV light.*

In addition to the UV/Vis spectral testing, the pH changes were studied. The average pH value of the pure dichloromethane solution of H_2TPP was 4.5. However, after the 30 minutes of irradiation by the UV light, the average pH value of the solution decreased to the 2.7. The change of the pH indicates that HCl has been formed as product of a photoinduced radical reaction of CH_2Cl_2, as proposed in ref [64].

Finally, a possibility to employ daylight (i.e. the solar radiation source) for photogenerated conversion of H_2TPP to H_4TPP^{2+} was probed. During a sunny day, 50 mL of 1×10^{-4} M and 1×10^{-5} M dichloromethane solution of H_2TPP in a quartz flask was placed on a window sill. After 15 minutes, the colour of the solution started to change from violet to green-violet and after another 15 minutes, the 1×10^{-5} M solution

completely changed its colour to green. The complete colour change of the 1×10^{-4}M solution lasted for another 20 minutes. This experiment did not work during the cloudy days, which indicates that intense sunlight is required for this conversion, the time of which was found to be also porphyrin concentration-dependent. The photoinduced conversion of H_2TPP to H_4TPP^{2+} represent a new example of reaction which converts the solar energy into the chemical bond energy.

In this work, all these experiments were targeted primarily on production of solutions of H_4TPP^{2+} in dichloromethane which could be employed for obtaining SERS and SERRS spectra of H_4TPP^{2+} which have not be reported previously. In this experiment, the empty and completely dried Ag nanosponge aggregate was overlayed by the 1×10^{-5} M dichloromethane solution of photochemically generated H_4TPP^{2+} and the SERRS spectra were measured at λ_{exc} = 445 nm excitation. The majority of spectral bands in this SERRS spectrum (Figure 43 and Table 4, System IV) is consistent with the RR spectra of H_4TPP^{2+} reported in ref. 62 and listed in Table 4, however, a weak 960 cm^{-1} marker band attributed to H_2TPP [62] was also observed, together with two other weak markers of this form. Upon a detailed inspection of the UV/Vis spectra of the photogenerated H_4TPP^{2+}, one can see a residual band at ca 420 nm, in addition to the main band at 445 nm. There is thus a possibility, that photoconversion of H_2TPP to H_4TPP^{2+} is not complete, which, in turn, could explain observation of the three weak residual band of H_2TPP in the SERRS spectra of the System IV (Figure 43 and Table 4).

Importantly, in the case of System IV, generation of H_4TPP^{2+} was evidenced by the exact match between the UV/Vis spectra presented in this Thesis in Figures 39 and 42 and the previously published UV/Vis spectra of H_4TPP^{2+} after its photochemical generation in a chloroform solution [64,92]. Therefore, there is thus an independent evidence of the presence of H_4TPP^{2+} in System IV, and its SERRS spectral marker bands Table 4, System IV can be reliably compared with those in the previously published RR spectra [61,62] (Table 4, second column). For 14 RR spectral marker bands of H_4TPP^{2+}, a match with the SERRS spectral bands of H_4TPP^{2+} has been found, with an average difference of ~1.5 cm^{-1}. There are thus virtually no meaningful differences between the band wavenumbers in the RR and in the SERRS spectra of H_4TPP^{2+} which indicates that SERRS spectra of the native, unperturbed H_4TPP^{2+} species have been obtained. Furthermore, these results confirm the validity of the selection of the most important marker bands of H_4TPP^{2+} on the basis of its RR spectra (namely the 340, 562, 625, 984, 1371 and 1540 cm^{-1} bands), and, consequently, also the

presence of H_4TPP^{2+} as the dominant spectral form in SERRS spectra obtained from the Ag nanosponge aggregate into which H_2TPP was incorporated during its preparation (Table 4, System I)

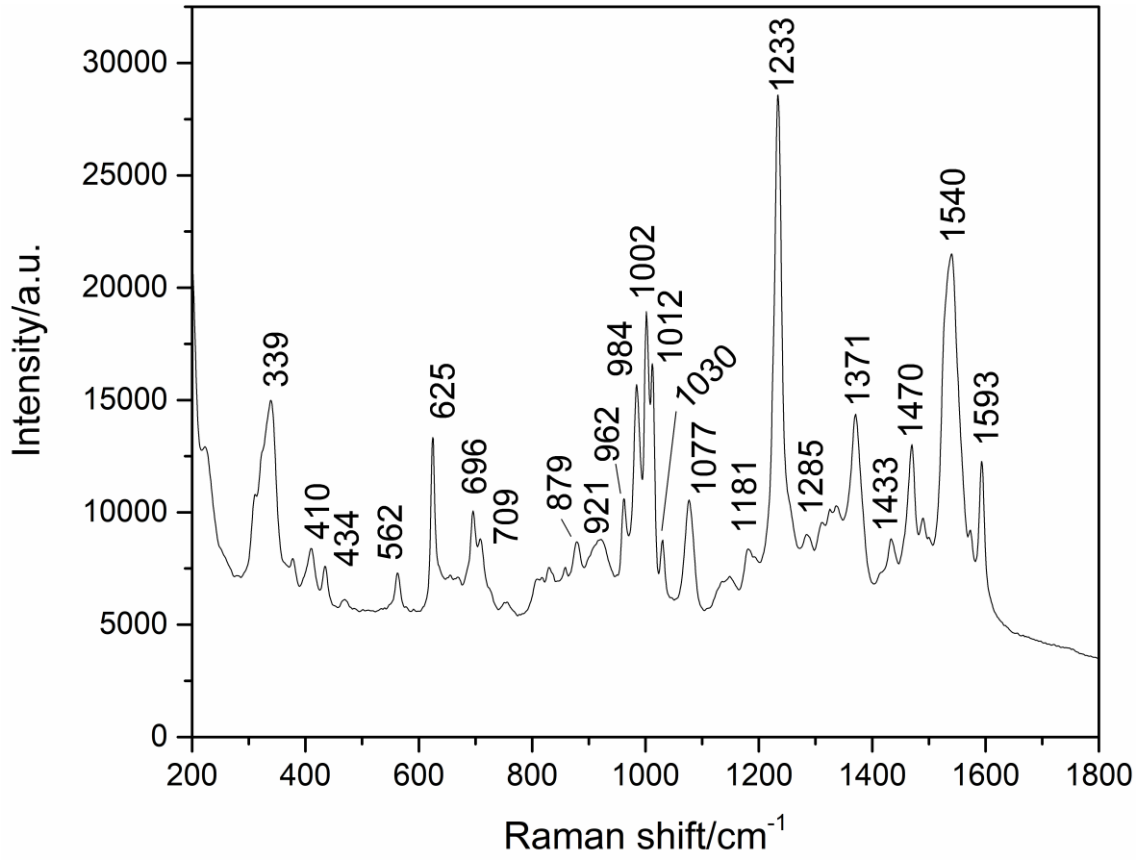

Figure 43: *SERRS spectrum Ag nanosponge aggregate overlayed by the 1×10^{-5} M solution of the photochemically generated H_4TPP^{2+} in dichloromethane. λ_{exc} = 445 nm.*

4.1.3.5. The role of the adsorption sites: Probing of the presence of Ag(0) and Ag(+) adsorption sites available upon incorporation of the testing adsorbate into Ag nanosponge aggregate and upon its soaking into the pores of a dried empty Ag nanosponge aggregate by using 2,2´-bipyridine as the spectral probe

The unequivocal SERRS spectral evidence of H_4TPP^{2+} presence in Ag nanosponge aggregate into which H_2TPP molecules were incorporated during its preparation, in contrast to the absence of this form and detection of parent H_2TPP in the dried empty Ag nanosponge aggregate overlayed by a solution of H_2TPP in dichloromethane

motivated probing of the presence of Ag (0) and/or Ag^+ adsorption sites in each of the two systems (Systems I and II, respectively, in Table 4).

As the established SERS spectral probe of Ag (0) and/or Ag^+ adsorption sites, 2,2´- bipyridine (bpy) was used [94]. Depending on the presence of Ag adsorption sites, bpy can be detected in two forms Ag(+)-bpy or Ag(0)-bpy which indicates the presence of Ag^+ or Ag^0 adsorption sites, respectively. Both surface species originate from the bidentate coordination of bpy in cis conformation to each of the two types of Ag adsorption sites, and their SERS spectra differ markedly in the bands position and also in relative intensities. Ag(+)-bpy typical markers bands are located at 763, 1008, 1058, 1302, 1482, 1567 and 1588 cm^{-1}. On the other hand, Ag(0)-bpy typical markers bands are located at 659, 765, 1022, 1169, 1318, 1486, 1558 and 1601 cm^{-1}.

For the determination of the adsorption sites, Ag nanosponge aggregates with incorporated bpy and with bpy soaked from its dichloromethane solution were prepared by the same procedures as described for H_2TPP in Chapters 3.3.1. and 3.3.3. The resulting spectra are shown in Figure 44, A and B. In the case of the Ag nanosponge aggregate soaked in the CH_2Cl_2 solution of bpy, marker bands of Ag(+)-bpy surface species have been found, indicating the presence of Ag^+ adsorption sites. On the other hand, in the Ag nanosponge aggregate with incorporated bpy, the spectral markers of Ag(0)-bpy sites have been detected, and they indicate the presence of Ag(0) adsorption sites.

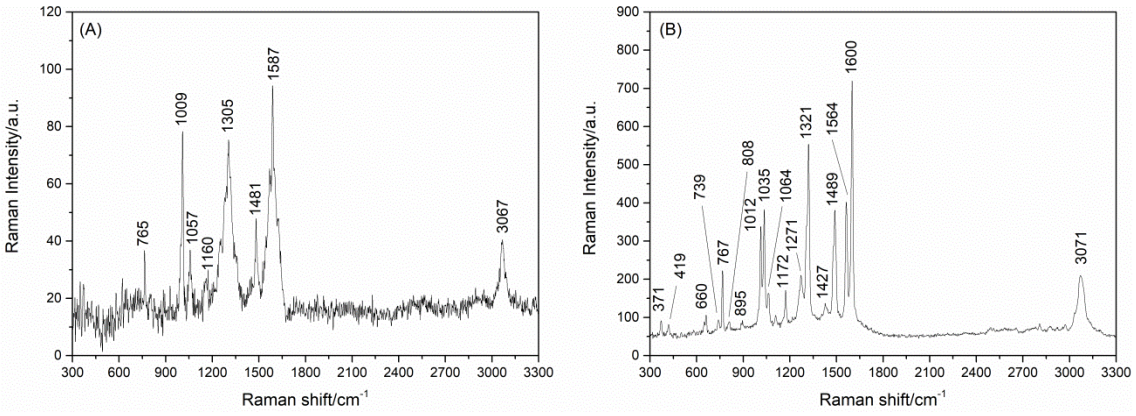

Figure 44: *SERS spectra of (A) Ag nanosponge aggregate overlayed by dichloromethane solution of bpy and (B) Ag nanosponge aggregate with incorporated bpy into the internal structure.*

4.1.3.6. The role of the presence of Ag NPs in H_4TPP^{2+} generation

To clarify the role of the presence of Ag NPs in the H_4TPP^{2+} formation in the two phase system constituted by HCl – modified Ag NPs hydrosol and a solution of H_2TPP in dichloromethane, several control experiments without Ag NPs were done.

First, pure dichloromethane was shaken against the 2.5×10^{-3} M aqueous solution of HCl (the same concentration which has been used in the Ag nanosponge aggregate preparation in Chapter 3.3.3, but here in the absence of Ag NPs). After 2 minutes, the dichloromethane was separated from the aqueous phase and used for preparation of the H_2TPP solution. The resulting 1×10^{-5} M solution of H_2TPP was violet coloured and its UV/Vis spectrum confirmed presence of the free-base form of the porphyrin. Very similar test was done with 1×10^{-5} M dichloromethane solution of H_2TPP. This solution was manually shaken against the 2.5×10^{-3} M aqueous solution of HCl and then, again, the UV/Vis spectrum of 1×10^{-5} M dichloromethane solution was measured. The solution was again violet coloured and the UV/Vis spectrum shows the presence of H_2TPP only. These experiments have demonstrated that the concentration of HCl used for the Ag nanosponge aggregates preparation is not high enough for the conversion of H_2TPP to H_4TPP^{2+} in the two phase system in the absence of Ag NPs.

Consequently, a higher concentration of HCl was used in the attempt to generate H_4TPP^{2+} in the two phase system in the absence of Ag NPs. The two experiments described above were repeated using 1M HCl. In that case, H_4TPP^{2+} was generated, as confirmed by the UV/Vis spectra and the observed colour change of the dichloromethane phase from the violet to the green. For the conversion of the H_2TPP to H_4TPP^{2+} in the two phase system without Ag NPs, markedly higher (by 2 or 3 orders of magnitude) concentration of the HCl is required than that needed for the same conversion in the presence of Ag NPs.

Furthermore, important implications follow from the successful realization of the latter experiment. First, the diprotonated porphyrin H_4TPP^{2+} remains in the dichloromethane phase, as witnessed by its green color, while the aqueous phase remains colorless. Therefore, the diprotonation of the porphyrin has to take place at (or in the close vicinity) the water – dichloromethane interface by the interface proton transfer, presumably by the following reaction:

$2H_3O^+$ (aq.) + H_2TPP (org.) → $2H_2O$ (aq.) + H_4TPP^{2+} (org.)

This tentative explanation is in accord with characterization of the water – dichloromethane interface molecular structure in ref. 93.

4.1.3.7. Chemical generation of H_4TPP^{2+} in wet empty Ag nanosponge aggregate: Ag nanosponge aggregate as a prospective nanoreactor

Another attempt to generate chemically H_4TPP^{2+}, i.e. the diacid (diprotonated) form of the porphyrin from the parent solution of H_2TPP in dichloromethane was done using a wet Ag nanosponge aggregate. After preparation and transfer onto a glass slide, the empty Ag nanosponge aggregate contains residues of the acidified (i.e. HCl containing) aqueous phase in its pores (Chapter 3.3.1). In the previous testing (System II, Chapter 4.1.3.2.), a completely the dried Ag nanosponge aggregate was employed as substrate. In contrast to that, the as transferred, wet empty Ag nanosponge aggregate (with the residues of acidic aqueous phase) has been tested as a substrate for SERRS and a potential nanoreactor. The wet Ag aggregate was overlayed by dichloromethane solution of H_2TPP (violet coloured), and after evaporation of the CH_2Cl_2, used as a sample for SERRS spectral testing (denoted System V) at λ_{exc} = 445 nm excitation. The resulting SERRS spectrum is shown in Figure 45.

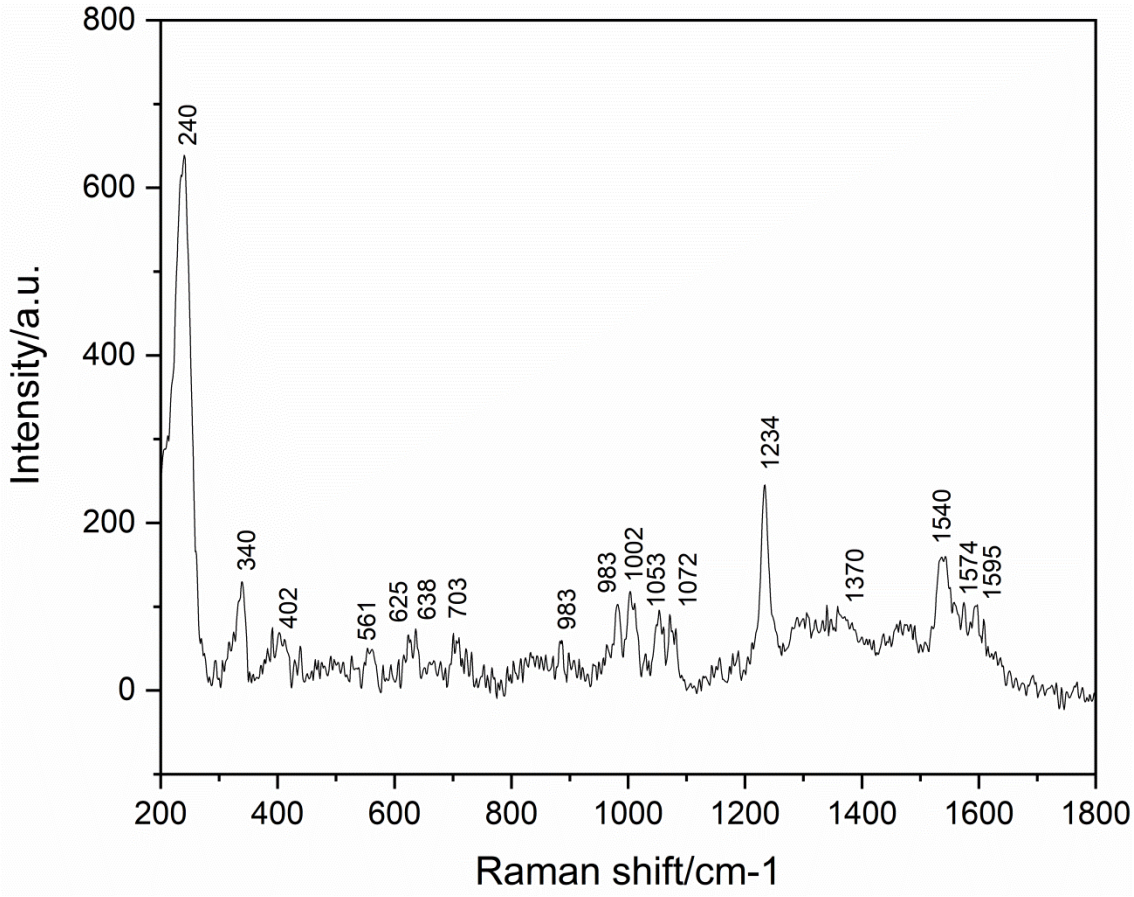

Figure 45: *SERS spectrum of H_2TPP/H_4TPP^{2+} respectively, measured from Ag nanosponge aggregate nanoreactor.*

The spectrum of System V in Figure 45 is strongly dominated by spectral bands consistent with the spectral marker bands of H_4TPP^{2+} obtained from the RR spectra reported in ref. 62, as well as with the SERRS spectral marker bands of this form obtained from System IV (Table 4). In particular, all 6 important SERRS spectral markers of H_4TPP^{2+}, namely the 340, 561, 625, 983, 1370 and 1540 cm^{-1} bands, are present in the spectrum (Figure 45). Several tests with wet aggregates were done and the resulting SERRS spectra from the wet aggregates always contained the diacid form, i.e. H_4TPP^{2+} marker bands, while the SERRS spectra measured from the completely dried Ag nanosponge aggregates overlayed by the dichloromethane solution of H_2TPP contained only the free-base form, i.e. the H_2TPP spectral markers. (Chapter 4.1.3.3.)

Furthermore, with the increasing time period of the wet aggregate drying in air, the H_4TPP^{2+} spectral markers decrease in the relative intensity with respect to those of H_2TPP. These results indicate that H_2TPP is converted to the H_4TPP^{2+} in a two phase system formed in the pores of the aggregate, i.e. at the interface between the HCl – containing aqueous phase already present in the pores of the wet aggregate and H_2TPP – containing dichloromethane phase delivered into the wet aggregate by its overdeposition by the dichloromethane solution of H_2TPP. In addition to that, the concentration of HCl in the system, from which the empty Ag nanosponge aggregate was prepared, has been 5×10^{-3} M, i.e. 200× lower than that required for the H_2TPP to the H_4TPP^{2+} conversion in the two phase system constituted by the 1M aqueous solution of HCl and the solution of H_2TPP in dichloromethane. One of the possible explanation of this difference could be formation of a relatively large interface area resulting as a sum of numerous interfaces formed inside the irregular pores of the Ag nanosponge. In a broader scope, the presented results outline the possibilities to employ Ag nanosponge aggregate as a nanoreactor.

4.1.4. Ag nanosponge aggregate with incorporated hydrophobic molecules as a new samples for SERS ans SERRS: advantages and drawbacks

Ag nanosponge aggregate with incorporated fullerene C_{60} molecules prepared by the bottom-up 3D assembling of 2D fused fractal aggregates of Ag NPs with incorporated C_{60} molecules was demonstrated to be a highly advantageous new sample for SERS and SE(R)RS spectral detection of unperturbed (native) C_{60} molecules. In particular, SERS and SE(R)RS spectra of C_{60} obtained from this sample at four excitation wavelengths: 445, 532, 633 and 780 nm are in full agreement with the previously published RR

spectra of this molecule [55,56], and, in contrast to the previously reported SERS spectral studies [57,58], no downward shift of the principal totally symmetric (A_g) pentagonal pinch mode at 1470 cm^{-1} has been observed in SERS and or SE(R)RS obtained from this new sample. Furthermore, the concentration values of SERS and SE(R)RS spectral limits of detection (LODs) of C_{60} obtained from these samples (using the C_{60} solutions of various concentrations for the sample preparation) are, at all excitations, by one order of magnitude lower than those obtained from the reference sample, which was prepared by overlaying of a well dried, empty Ag nanosponge aggregate by dichloromethane solutions of C_{60} of various concentrations (Table 2). The latter (reference) procedure of SERS and SE(R)RS sample preparation mimics the previously reported procedures of preparation of samples for SERS and SERRS of various hydrophilic and amphiphilic molecules by using Ag nanosponges as substrates [46–48]. The one order of magnitude lower SERS and SE(R)RS LODs in the former system in comparison to the latter one are attributed to an efficient incorporation of C_{60} molecules into 2D fused fractal aggregates formed at the interface between the Ag NPs hydrosol modified by addition of HCl and the dichloromethane solution of H_2TPP, and, consequently, into hot spots generated in the fractal Ag NPs aggregates by the laser excitation during the SERS and SE(R)RS spectral measurements. SERS spectral probing of the Ag nanosponge aggregate with incorporated 2,2-bipyridine as the spectral probe for neutral and cationic adsorption sites on Ag NPs surfaces revealed, that neutral Ag(0) adsorption sites are available on the surfaces of fusing Ag NPs. Availability of the neutral Ag(0) adsorption sites for adsorption of C_{60} molecules can contribute to the efficient incorporation of C_{60} into 2D fused fractal aggregates, from which the 3D Ag nanosponges have been assembled.

Furthermore, the lowest C_{60} LOD=1×10^{-7} M was obtained for Ag nanosponge aggregate with incorporated C_{60} at 532 nm excitation which coincides simultaneously with the maximum of a rather weak electronic absorption band of C_{60} (Figure 27) and with the region of slightly increased extinction on a rather flat SPE of the nanosponge aggregate (Figure 28). Therefore, the lowest LOD of C_{60} at this excitation (as compared to those obtained at the other three excitations), and consequently, the relatively largest enhancement of Raman scattering, has its origin in the largest contributions of both the electromagnetic and the molecular resonance mechanisms to the overall enhancement of Raman signal of C_{60}. Therefore, the spectra of C_{60} measured at 532 nm excitation are denoted as SE(R)RS spectra.

SERS and SERRS spectra testing of Ag nanosponge aggregate prepared by the 3D assembling of fused fractal 2D aggregates formed at the interface between HCl – modified Ag NPs hydrosol and the dichloromethane solution of a hydrophobic free base porphyrin H_2TPP (denoted as System I) revealed the presence of the diprotonated form of this porphyrin, i.e. H_4TPP^{2+} as the major spectral component, and of the parent H_2TPP as the minor spectral component (Figure 36 and Table 4). The presence of the SERRS spectral marker bands of H_4TPP^{2+} in the SERRS spectrum of System I was confirmed by SERRS spectral measurements of photochemically generated H_4TPP^{2+} in dichloromethane overlayed over a well dried, empty Ag nanosponge aggregate (System IV, Table 4). In contrast to System I, only spectral marker bands of the parent H_2TPP molecule were detected by SERS and SERRS spectral testing of System II prepared by overlaying of a well dried empty Ag nanosponge aggregate by dichloromethane solutions of H_2TPP of various concentrations. The SERS and SERRS spectral testing of both System I and System II was performed at four excitation wavelengths, namely 445, 532, 633 and 780 nm, and limits of the SERS and/or SERRS spectral detection of the porphyrin species were determined (Table 3). A direct comparison of LODs of the porphyrin species in System I and System II is hampered by the fact that different porphyrin species, namely H_4TPP^{2+} as the major spectral component in System I and H_2TPP as the only spectral component in System II, are detected in each of the two systems. Nevertheless, it is worth mentioning that the LOD of H_4TPP^{2+} in System I is by three orders of magnitude lower than that of H_2TPP in System II at all four excitation wavelengths. The lowest SERRS LOD=1×10^{-9} M (Table 3) was established for H_4TPP^{2+} in System I at 445 nm excitation, which coincides with the maximum of the Soret electronic absorption band of this diprotonated porphyrin species (Figure 39). This SERRS LOD is nearly by 2 orders of magnitude lower that that reported for H_2TPP adsorbed from solution on Ag NPs attached to silanized glass slides (8×10^{-8} M) and determined at 514.5 nm excitation coincident with the maximum of the $Q_y(1,0)$ electronic absorption band in ref 63. However, from the analytical point of view, the SERRS LOD established from System I has a certain disadvantage in detecting a chemically altered porphyrin species. The SERRS and SERS LODs of the parent H_2TPP in System II are at least one order of magnitude higher than that established in ref.63, hence, from the analytical point of view, the system reported in ref.63 is more advantageous for detection of H_2TPP than the System II reported in this Thesis.

On the other hand, a challenging question about the mechanism of H_4TPP^{2+} generation upon incorporation of parent H_2TPP into the internal structure of Ag nanosponge aggregate emerged from the abovementioned results, and several experiments targeted on its answering were done. First, it was shown that upon replacing of HCl in the preparation procedure of Ag nanosponge aggregate by NaCl, i.e. substituting the preparation procedure D by the procedure E (both of them described in Chapter 3.3.3 and listed in Table 1), the SERRS spectral testing of the resulting Ag nanosponge aggregate (System III, Table 4) has revealed the presence of only the parent H_2TPP porphyrin. This experiment thus points towards HCl as the source of H^+ ions in the process of the porphyrin diprotonation. Therefore, H_4TPP^{2+} species incorporated into the Ag nanosponge aggregate has to be generated chemically by H^+ ions (protons) originating from H_3O^+ ions produced by dissociation of HCl added as a pre-aggregation agent to Ag NPs hydrosol (aqueous phase) in the presence of the second, water immiscible organic phase, namely the solution of H_2TPP in dichloromethane. Furthermore, diprotonation of H_2TPP into H_4TPP^{2+} has been accomplished in the two phase system also in the absence of Ag NPs, however, at concentrations of HCl by ca 2-3 orders of magnitude higher than that used for the preparation of 2D fused Ag NP aggregates (as precursors of the 3D Ag nanosponge aggregate), i.e. in the presence of Ag NPs. This result indicates, that the presence of Ag NPs, and probably also adsorption of the parent H_2TPP onto Ag(0) adsorption sites available on their surfaces upon formation of fused 2D aggregates at the interface (as revealed by the bpy spectral probe) has a catalytic effect on the process of diprotonation of the hydrophobic porphyrin.

Another example of chemical generation of H_4TPP^{2+} emerged from the SERRS spectral testing of System V (Table 4) prepared by overlaying a wet empty Ag nanosponge aggregate by a solution of H_2TPP in dichloromethane. In this case, H_2TPP has been converted to the H_4TPP^{2+} in a two phase system formed in the pores of the aggregate, i.e. at the interface between the HCl – containing, residual aqueous phase already present in the pores of the wet aggregate and the H_2TPP – containing dichloromethane phase delivered into the wet aggregate by its overlaying by the dichloromethane solution of H_2TPP. Furthermore, the concentration of HCl in the residual aqueous phase was also markedly lower than that required for H_4TPP^{2+} generation in the two phase system in the absence of Ag NPs. Both the catalytic effect of Ag nanostructured surface and formation of a relatively large interface area resulting

as a sum of numerous interfaces formed inside the irregular pores of the Ag nanosponge could be responsible for this difference. The results of this experiment open the possibilities to employ Ag nanosponge aggregate as a nanoreactor.

4.2. 2D and 3D AgNPs assemblies as substrates for SERS of SLG

4.2.3. 3D AgNPs aggregates as a samples for SERS of SLG

AgNPs aggregates prepared from 2D fused interfacial aggregates were used as substrates for SERS of SLG. For the measurements, two types of samples were prepared and tested – the first (Figure 46A), glass/SLG/AgNPs aggregate and the second (Figure 46B), glass/AgNPs aggregate/SLG. The schematic depictions of the sample and measurement setup demonstrate Figure 46.

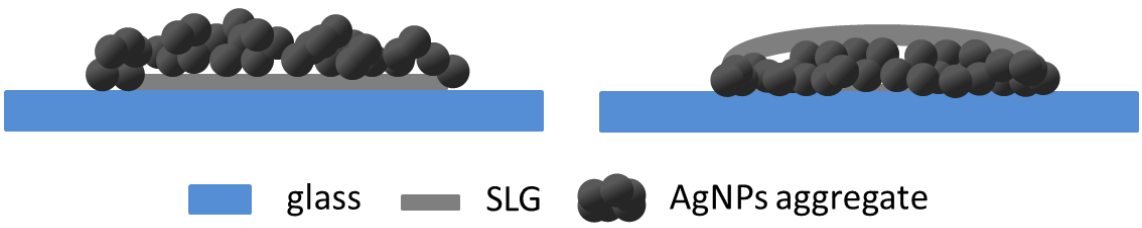

Figure 46: *Schematic depiction of (A) glass/SLG/AgNPs aggregate and (B) glass/AgNPs aggregate/SLG hybrid system.*

SERS spectral measurements were complicated by the thickness of AgNPs aggregate and its rough surface. The contact between SLG and AgNPs surface was limited, which caused that the intensity of the SLG signal was different at different spots on the sample. The glass/SLG/AgNPs aggregate hybrid system was measured in inverted geometry, while the glass/AgNPs aggregate/SLG hybrid system was measured in the straight geometry, as demonstrated in Figure 47. The different sample geometries were chosen to minimize the loses of the SERS signal of SLG by its absorption by thick Ag NP aggregates. Therefore, the samples were always measured in such a way that SLG was on the top of the AgNPs aggregate surface.

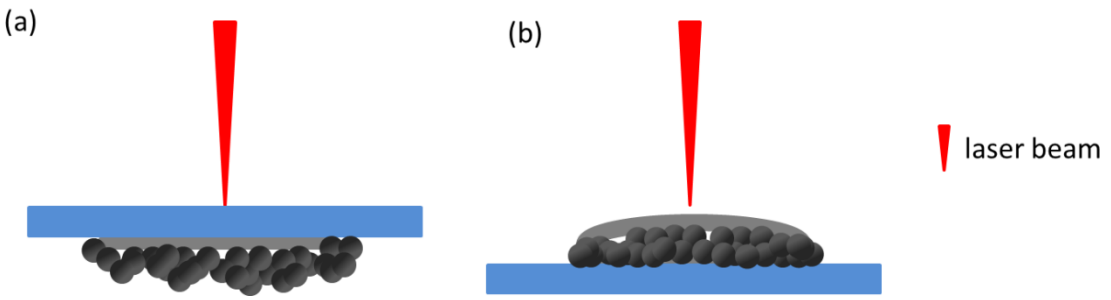

Figure 47: *Schematic depiction of sample measurement geometries.*

During the hybrid systems preparations, several problems were found. (i) For the obtaining of the pure SLG sample, the thermal treatment (180 °C) after the SLG transfer is necessary. Therefore, when the AgNPs aggregate is already present on the surface, the thermal treatment damages the AgNPs aggregate surface by its oxidation. In this respect, the glass/SLG/AgNPs hybrid system seems to be better, because SLG is transferred onto the glass slide before the aggregate deposition. (ii) On the other hand, SLG is very sensitive sample and it is easy to to perturb it by contact with water. AgNPs aggregates have to be transferred from the aqueous phase, and this step complicated the sample preparation due to a possible SLG damage. In this respect, the glass/AgNPs aggregate/SLG hybrid system seems to be better for the preparation, because the AgNPs aggregate is transferred onto the glass slide before the SLG.

Thermal treatment after the transfer by nitrocellulose was found as the crucial step for the obtaining of the pure SLG sample. SLG has been previously transferred to the substrate by several polymers (mostly PMMA). The washing out by many solvent was several times tested, but a pure SLG sample without polymer residues has not been obtained. Since SERS is such a sensitive method, these small impurities complicated the sample measurement, because the SLG signal was masked by the SERS spectrum of the polymer carrier.

The hybrid systems described above were characterized by UV/Vis (SPE) spectral measurements and then by SERS spectral mapping. During the SERS spectral sampling, the homogeneity of the G mode wavenumbers of SLG was checked and also the homogeneous/heterogeneous distribution of SERS spectral intensities of 2D and D bands of SLG within the linear sampling across the Ag NP aggregate was tested.

Typically, small part of AgNPs aggregate which covered the SLG or SLG covered the AgNPs aggregate was used for SERS spectral sampling (Figure 48) and across this area, the linear sampling was done.

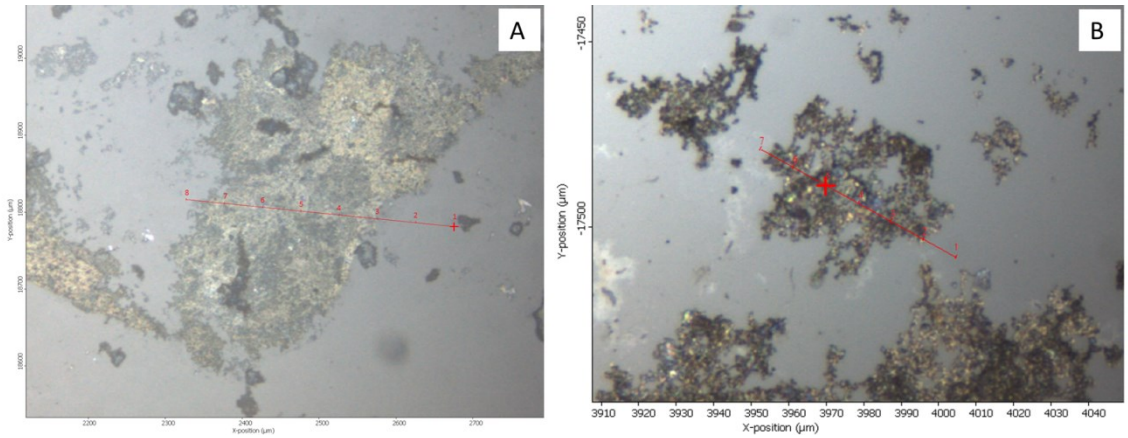

Figure 48: *Example of glass/SLG/AgNPs aggregate hybrid system (A) and glass/AgNPs aggregate/SLG hybrid system(B) with the projection of the map line. Numbers over the line correspond to the spectra in Figure 49 and Figure 50.*

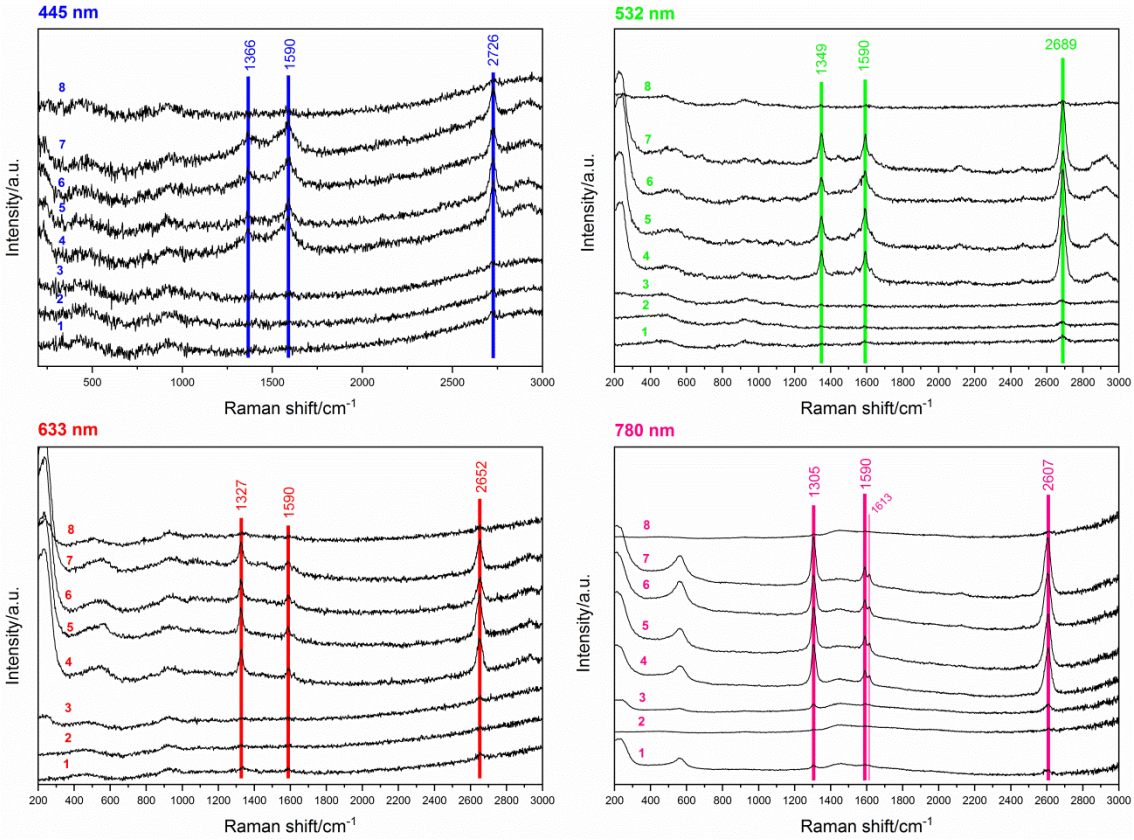

Figure 49: *The SERS spectra of glass/SLG/AgNPs aggregate hybrid system at excitation wavelengths used for measurement. Spectral number markers correspond to the numbers of positions in Figure 48.*

The SERS spectra of the glass/SLG/Ag NPs aggregate measured in the inverted sample geometry are shown in Figure 49 and those of glass/AgNPs aggregate/SLG hybrid system measured in the straight geometry shows Figure 50.

During the linear sampling, several spectra were measured also from the glass/SLG part of the sample, and these spectra were used as the reference for calculation of the SERS enhancement factors of the SLG.

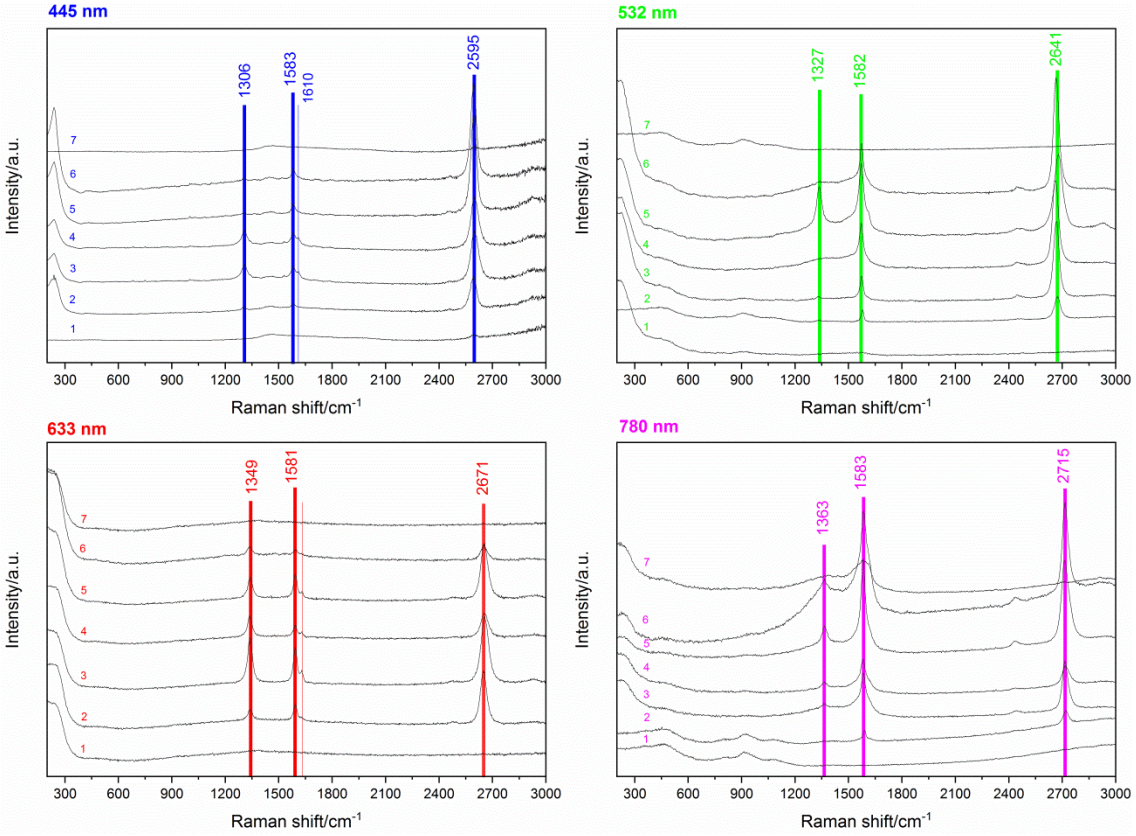

Figure 50: *SERS spectra of glass /AgNPs aggregate/SLG hybrid system at excitation wavelengths used for measurement. Spectral number markers correspond to the numbers in Figure 48, which belong to the points at the sampling line.*

SLG is very sensitive to doping or strain. The most sensitive bands to the strain and the doping those of the G mode and the 2D mode. The D mode apperance corresponds to the occurrence of defects. The positions of these bands are listed in Tables 5 – 7 .

Table 5: *Position of the G mode in SERS spectra of SLG obtained from the hybrid systems*

λ_{exc} / nm	Glass/AgNPs aggregate/SLG	Glass/ SLG/AgNPs aggregate/
445	1590	1583
532	1590	1582
633	1590	1581
780	1590	1583

Table 6: *Position of the 2D mode in SERS spectra of SLG obtained from the hybrid systems*

λ_{exc}/nm	Glass/AgNPs aggregate/SLG	Glass/ SLG/AgNPs aggregate/
445	2607	2595
532	2652	2641
633	2689	2671
780	2726	2715

Table 7: *Position of the D mode in SERS spectra of SLG obtained from the hybrid systems*

λ_{exc}/nm	Glass/AgNPs aggregate/SLG	Glass/ SLG/AgNPs aggregate/
445	1305	1306
532	1327	1326
633	1349	1349
780	1366	1367

The position of the G and 2D modes in the glass/SLG/AgNPs aggregate hybrid system is different from the glass/AgNPs aggregate/SLG hybrid systems as is shown in listed tables above

The position of the G/2D mode in the glass/AgNPs aggregate/SLG hybrid system on average decreases by 7/13 cm^{-1}, respectively, against the position of the glass/SLG/AgNPs aggregate hybrid system. This wavenumber decreasing of G and 2D mode bands is attributed to the biaxial strain in SLG over the AgNPs aggregate sample,

particularly in the contact areas between SLG and the AgNPs aggregate [94]. For the D mode, no wavenumber shift was observed.

For both hybrid system, enhancement factors of the 2D mode were calculated and they are listed in Table 8. Furthermore, the SPE spectra of both hybrid systems were measured and they are presented in Figure 51. To the SPE spectra, the dependence of the E_f of the 2D mode on the excitation wavelength has been related

Table 8: *Enhancement factors of the 2D mode at both geometries*

λ_{exc}/nm	*Glass/SLG/AgNPs aggregate* *Ef of the 2D mode*	*Glass/AgNPs aggregate/SLG* *Ef of the 2D mode*
445	10	171
532	23	288
633	49	182
780	97	162

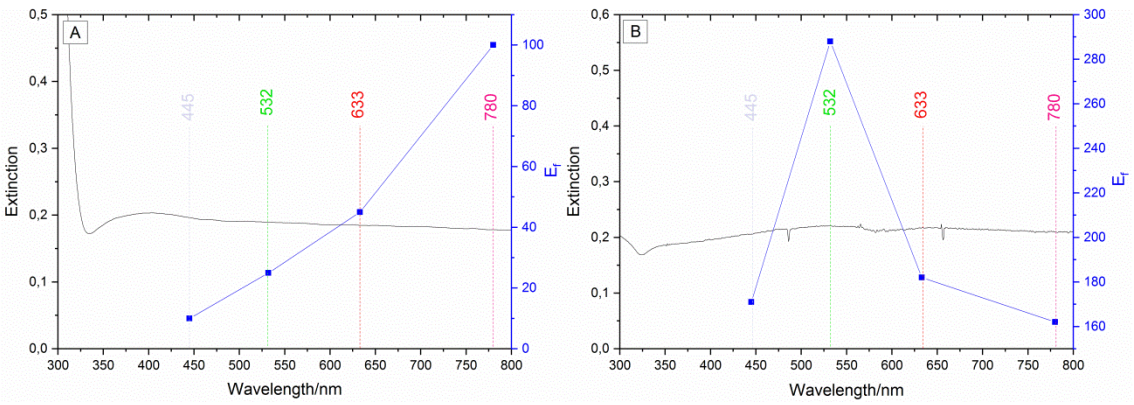

Figure 51: *SPE spectra of (A) glass/SLG/AgNPs aggregate hybrid system and (B) glass/AgNPs aggregate/SLG hybrid system with the projection of enhancement factors (Ef) and projection of excitation wavelength used for measurement.*

The differences in the Efs obtained for the two hybrid systems are obvious. The glass/SLG/AgNPs aggregate hybrid system measured in inverted geometry provides the largest Ef at 780 nm excitation (1×10^2). On the other hand glass/AgNPs aggregate/SLG hybrid system provides the largest Ef at 532 nm excitation (3×10^2). The difference is attributed to the different sample preparation, in conjunction with the fractal

morphology (D=1.84) of the fused AgNPs aggregates and the 2D monolayer structure of SLG as the "adsorbate". Localization/delocalization of modes in fractal aggregates depends on the excitation wavelength. Localization length increases with the increasing excitation wavelength [13]. Larger contact areas between SLG and AgNPs aggregate provide the largest SERS enhancement which originates from the more delocalized fractal modes excited at 780 nm. On the other hand, smaller contact areas between SLG and AgNPs aggregate provide the largest SERS enhancement originating from the more localized fractal modes excited at 532 nm.

4.2.4. AgNPs-ET film as a substrate for SERS of SLG

4.2.2.1 Surface plasmon extinction, SERS spectra and morphology of glass/SLG/AgNPs-ET hybrid system: The effect of the ET spacer presence

The glass/SLG/AgNPs-ET hybrid system as the sample for SERS microRaman spectral measurement is schematically depicted in Figure 52. AgNPs-ET film was deposited over SLG on glass by the procedure described in Chapter 3.4.2.

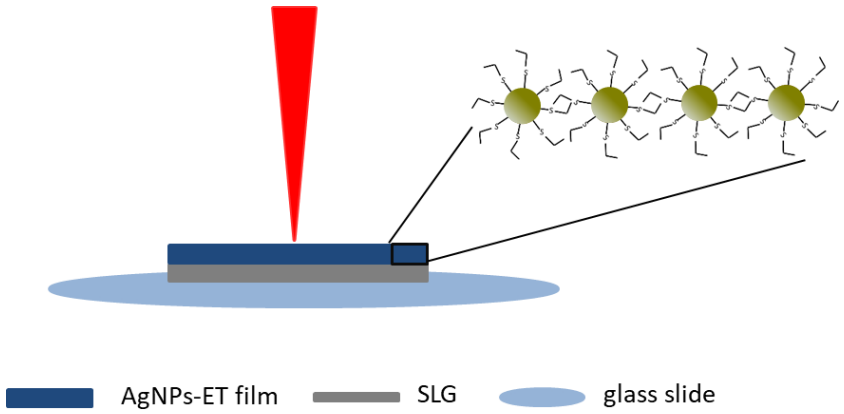

Figure 52: *Schematic depiction of glass/SLG/AgNPs-ET film hybrid system*

SERS spectra of the glass/SLG/AgNPs-ET hybrid system at four excitation wavelengths: 445, 532, 633 and 780 nm were measured and the resulting spectra are shown in Figure 53.

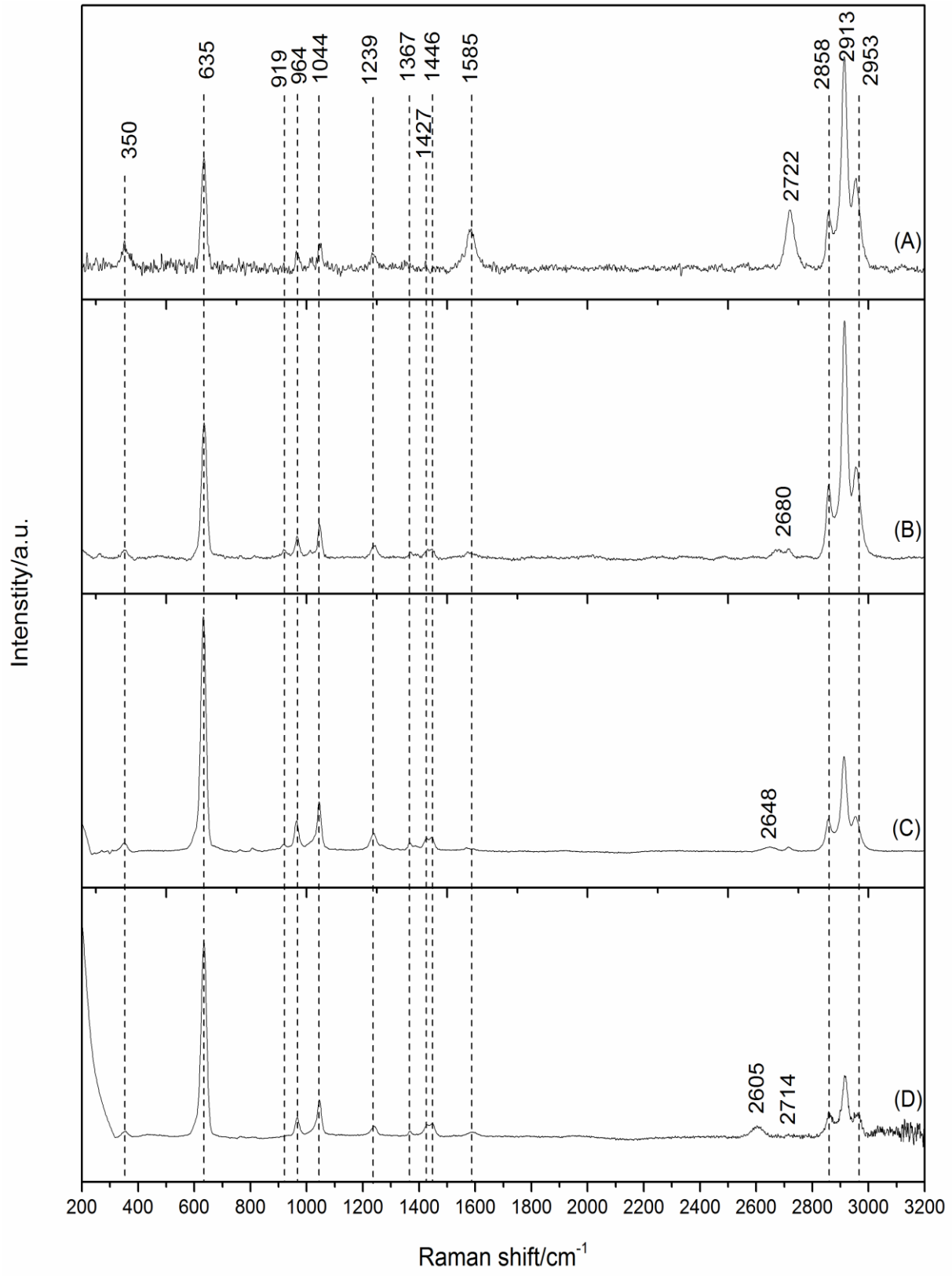

Figure 53: *SERS microRaman spectra of glass/SLG/AgNPs-ET hybrid system measured at (A) 445 (B) 532 (C) 633 and (D) 780 nm excitations.*

All spectra in Figure 53 contain the characteristic spectral bands of the Ag-ET surface species as well as those of the G and the 2D modes of SLG, as follows from their comparison with the spectra of the glass/SLG (Figure 54) and the glass/AgNPs-ET (Figure 55) reference systems.

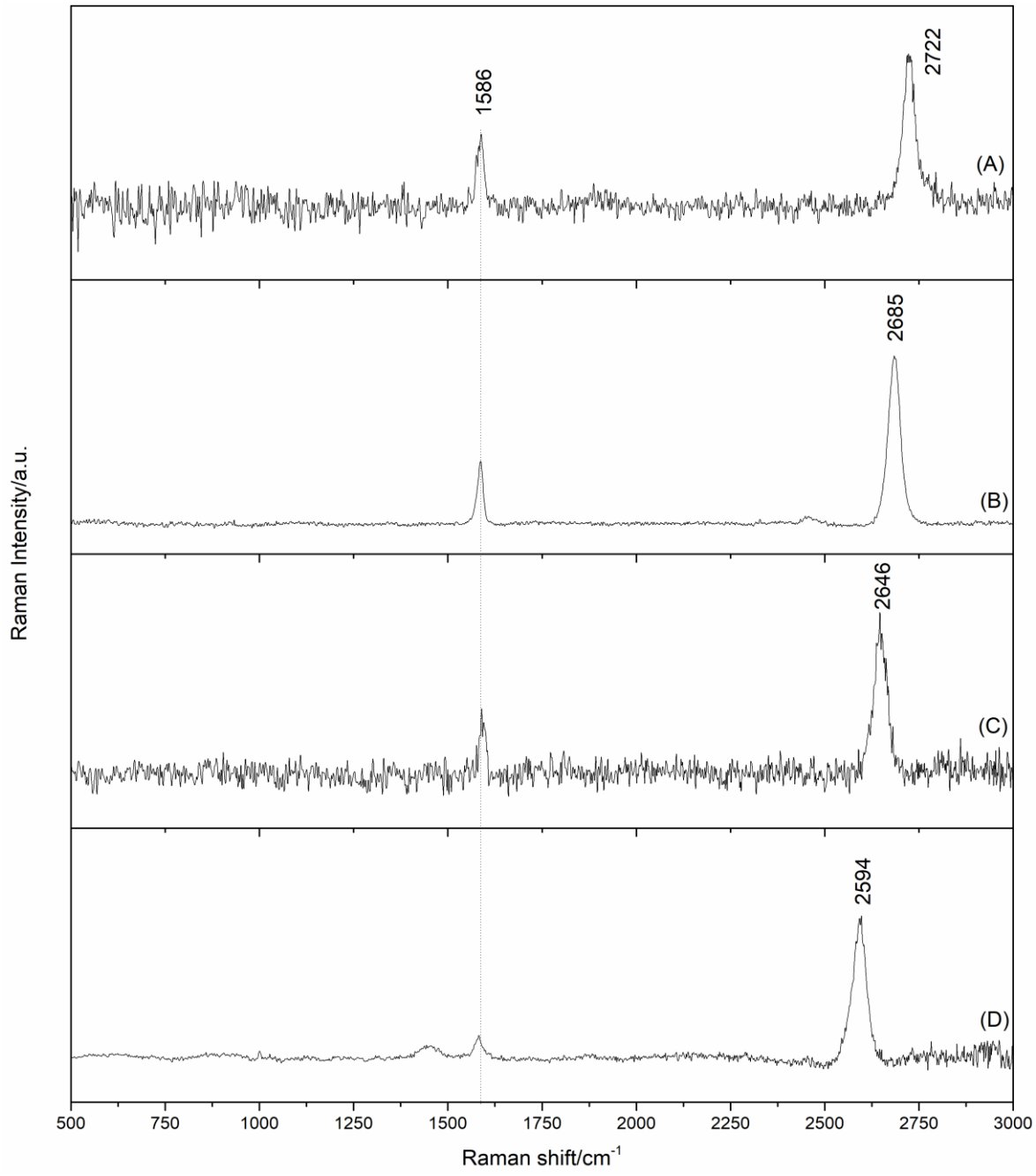

Figure 54: *SERS spectra of SLG obtained from glass/SLG reference system at (A) 445 nm (B) 532 nm (C) 633 nm (D) 780 nm excitations.*

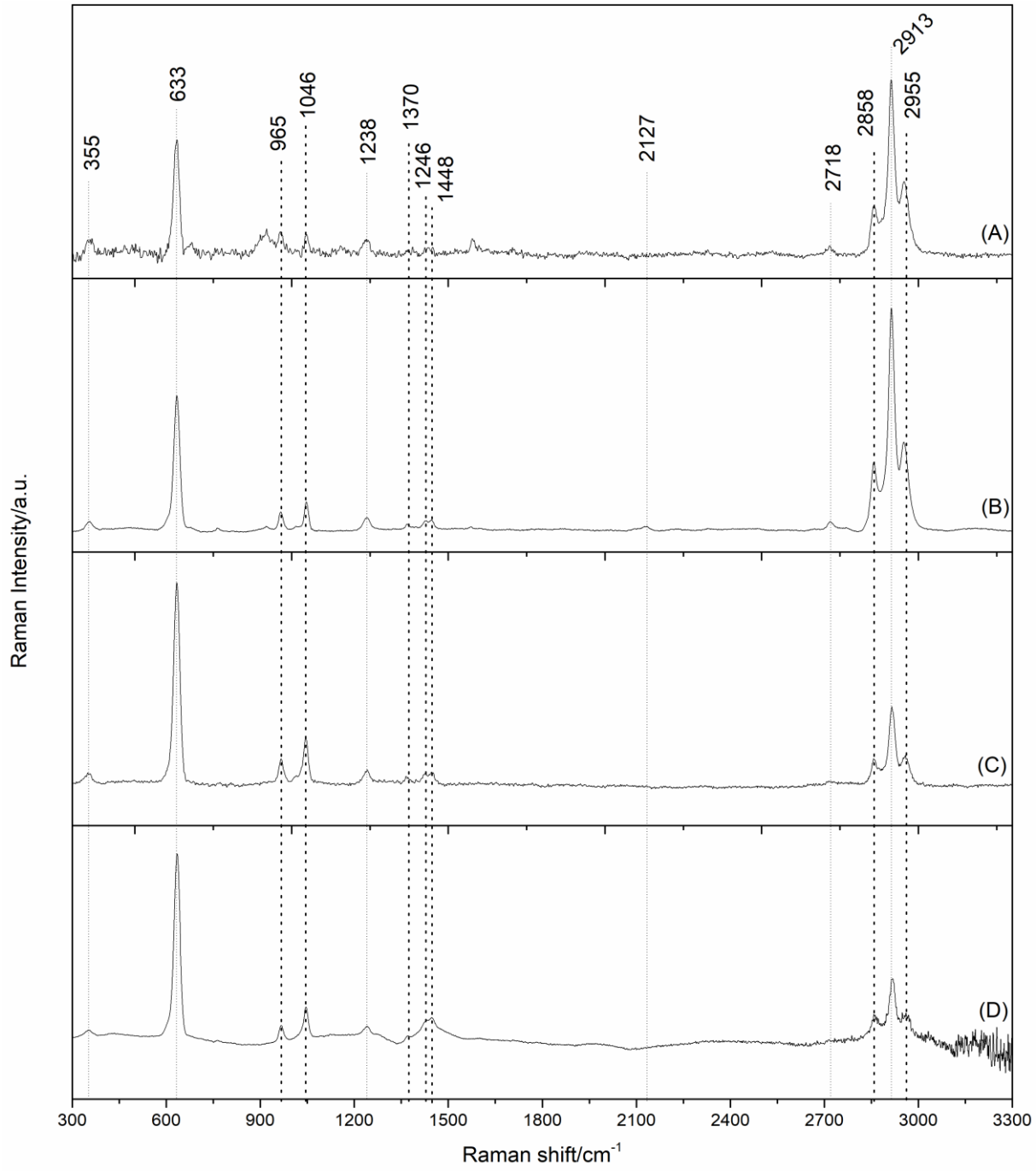

Figure 55: *SERS spectra of Ag-ethanethiolate species obtained from the glass/AgNPs-ET array reference system at (A) 445 nm (B) 532 nm (C) 633 nm (D) 780 nm excitations.*

The assignment of SERS spectral bands of Ag-ET surface species and of Raman spectral bands of free ET was done and is provided in Table 9.

Table 9: *Assignment of Raman spectral bands of ethanethiol and SERS spectral bands of Ag-ET species in Ag NPs-ET array based on refs. 21 and 95 – 97.*

Average wavenumbers/cm^{-1}		**Wavenumber Range**	**Type of vibration**
Ethanethiol	**AgNPs-ET array**		
–	350	600 – 700	-AgS
659	632	580 – 1000	C – S stretching
–	964	850 – 1000	-CH_3 rocking
1090	1045	1000 – 1150	C – C stretching
1272	1238	1200 – 1400	CH_2 rocking
–	1368	1330 – 1385	-CH_3 symmetric deformation (bending)
–	1426	1385 – 1445	CH_2 scissoring deformation (bending)
1448	1446	1400 – 1480	CH_3 antisymmetric deformation (bending)
2570	–	2520 – 2600	-SH
2737	2716	–	Overtone of 1368 cm^{-1}
–	2858	2840 – 2870	Symmetric -CH_2 stretching
2870	–	2885 – 2865	Symmetric -CH_3 stretching
2927	2913	2915 –2940	Antisymmetric -CH_2 stretching
2960	2964	2950 – 2975	Antisymmetric -CH_3 stretching

The largest differences observed between the spectra of ET and Ag-ET are the absence of the 2570 cm^{-1} band of υ (S-H) and the presence of the 350 cm^{-1} band of υ (Ag-S) in the spectrum measured from AgNPs-ET film, in contrast to the ET spectrum.

The positions of the G and 2D mode spectral bands are most clearly distinguished in the SERS spectrum of the glass/SLG/AgNPs-ET hybrid system excited at 445 nm (Figure 53, spectrum A), in which their relative intensities with respect to those of the

Ag-ET bands are the largest. The comparison of the SERS spectra of SLG in the glass/SLG/Ag-ET hybrid system and of its Raman spectra in the glass/SLG reference system obtained at the 445 nm excitation (Figure 56) show that the wavenumbers of the G mode (1585 cm^{-1} and 1586 cm^{-1}) as well as the 2D mode (2722 cm^{-1}) are the same (or virtually the same within the experimental error) in both systems.

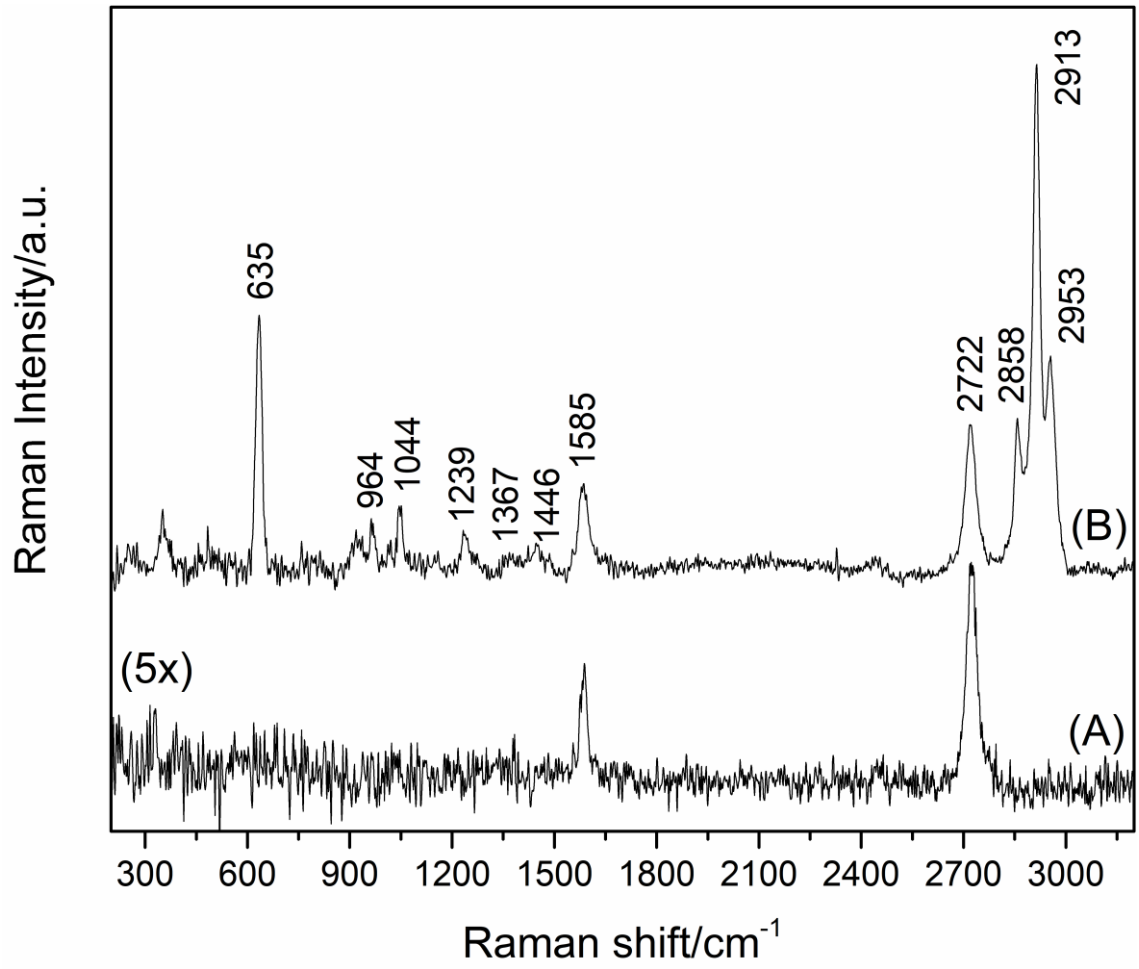

Figure 56: *Comparison of SERS spectra of (A) glass/SLG reference and (B) glass/SLG/AgNPs-ET hybrid system.*

The position of the G mode band at the 1585 cm^{-1} is close to the undoped SLG [18,19]. These results provide evidence of the presence of the unperturbed SLG in the glass/SLG/AgNPs-ET hybrid system. In contrast to that, a 5 cm^{-1} upshift of the G mode and a slight upshift of the 2D mode attributed to n-doping and compressive strain was reported for the SLG/Ag NPs hybrid system in which SLG is in the direct contact with Ag NPs [84].The Ag-ET species in the AgNPs-ET film works as a molecular spacer

which envelopes AgNPs, prevents the direct contact between SLG and AgNPs and preserves the native structure of SLG.

For the glass/SLG/AgNPs-ET hybrid system, SERS enhancement factors of the G and the 2D modes were determined as the integral intensity ratios of the spectral bands of these modes in the SERS spectra of the hybrid system and in Raman spectra of the glass/SLG reference system. Their values are listed in the first two columns of Table 10.

Table 10: *SERS enhancement factors of the SLG modes in the glass/SLG/AgNPs-ET hybrid system and the average SERS enhancement factors of the modes of the Ag-ET surface species in (I) the glass/SLG/AgNPs-ET hybrid system, and (II) the glass/Al foil/AgNPs-ET hybrid system*

λ_{exc} (nm)	SLG – G	SLG – 2D	ET – addit (I)	ET – final (I)	ET – addit (II)	ET – final (II)
445	2	2	1	5×10^5	4	2×10^6
532	9	4	4	2×10^7	12	6×10^7
633	9	6	4	8×10^6	15	8×10^8
780	2	2	1	1×10^6	1	5×10^5

The largest SERS enhancement by a factor of 9 was determined for the G mode of SLG at 532 and 633 nm excitations. This result is, in general, consistent with the shape of the SPE curve of the hybrid system (Figure 57, curve B).

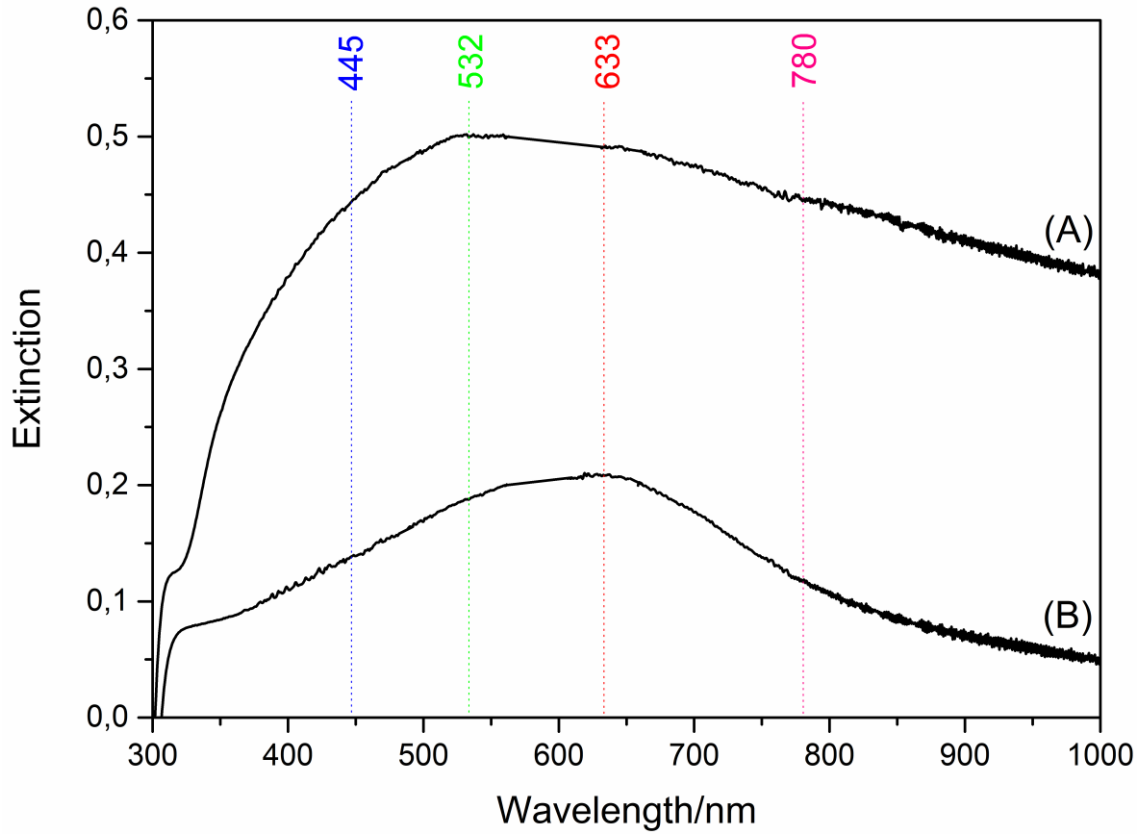

Figure 57: *SPE spectra of (A) glass/AgNPs-ET reference system and (B) glass/SLG/AgNPs-ET hybrid system with the projection of wavelengths used for SERS measurements.*

Nevertheless, in addition to the SPE shape, contributions of other factors have to be considered to explain the SERS enhancement at a particular excitation wavelength, namely: (i) an increase of the contribution of the light scattering to the overall extinction (sum of absorption and scattering) of plasmonic nanoparticle with the increasing excitation wavelength [98], and (ii) the „second part of the electromagnetic (EM) SERS enhancement“ which implies that not only the incident, but also the Raman scattered radiation is enhanced by the EM mechanism of SERS [99], i.e. by the elastic Mie scattering [7,8]. For example, the 633 nm excitation (which provides the SERS spectra with the best enhancement factors for both the G and the 2D mode, Table 10) is nearly coincident with the SPE curve maximum. The wavelength of the SPE maximum represents the wavelength at which the sum of absorption and scattering of light by the hybrid system is the largest [7,8]. On the other hand, the wavelength of the photons scattered by the G mode (at 1585 cm^{-1}) is 703 nm and that of the 2D mode (2049 cm^{-1})

photons is 761 nm, respectively, and the latter thus coincides with a lower extinction on the declining slope of the SPE band than the former (Figure 58).

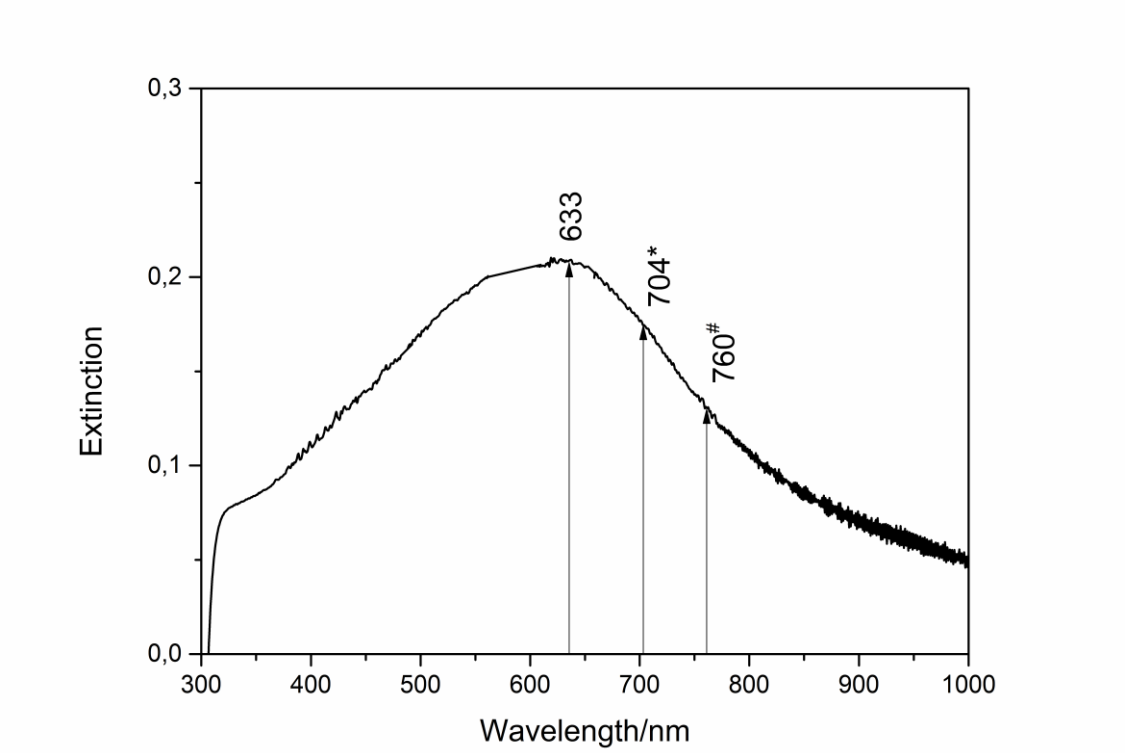

Figure 58: *Surface plasmon extinction (SPE) spectrum of glass/SLG/AgNPs-ET hybrid system in relation to (i) the 633 nm excitation wavelength (unlabelled arrow), (ii) the wavelength of photons scattered by the G mode of SLG (1581 cm^{-1}) at 633 excitation (*-labelled arrow) and (iii) wavelength of photons scattered by the 2D mode of SLG (2049 cm^{-1}) at 633 excitation ($^{\#}$-labelled arrow).*

Consequently a slightly lower SERS enhancement factor (Ef) is expected and actually observed for the 2D mode (Ef = 6) than for the G mode (Ef = 9).

Importantly, the G mode enhancement (Ef = 9) at 532 and 633 nm excitation in SERS of our hybrid system with unperturbed SLG and the hydrophobic Ag-ET spacer is actually slightly higher than that experienced by the same mode in SERS of the system with SLG underneath Ag NPs (Ef = 7) [84]. In the latter system, SLG is affected by compressive strain and n-doping, which, in turn, result from the direct contact between SLG and Ag NPs. This comparison indicates that the decrease of the SERS enhancement by the EM mechanism induced by a thin spacer [83] namely, in our case, by the hydrophobic Ag-ET spacer (terminated by the CH_3 group) of about 0.6 nm

thickness has been compensated by (i) the 2D assembling of the closely spaced, ET modified Ag NPs (*vide infra* and Figure 58 B – D), i.e. by formation of a more efficient plasmonic enhancer than the assembly of mostly isolated Ag NPs [7,8] reported in ref. 84, and, (ii) by the proper selection of excitation wavelength(s) with respect to the SPE of the AgNPs-ET assembly (Figure 57, curve B).

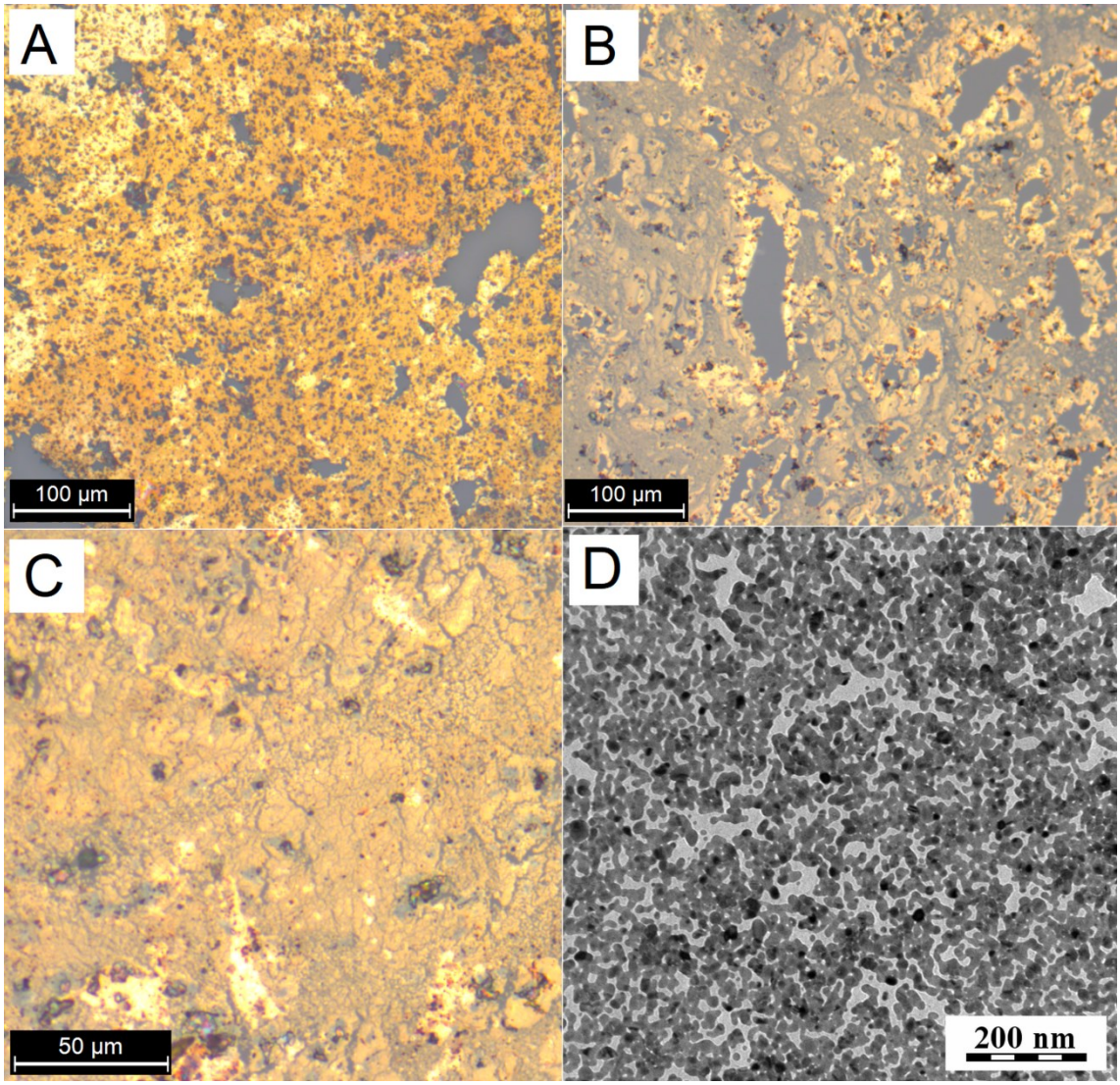

Figure 59: *Optical microscopy image of (A) glass/AgNPs-ET reference system obtained with the 20× magnification objective, (B) glass/SLG/AgNPs-ET hybrid system obtained with the 20× magnification objective, (C).glass/SLG/AgNPs-ET hybrid system obtained with the 50× magnification objective and TEM image of SLG/AgNPs-ET hybrid system deposited on carbon-coated Au grid (D)*

In accord with the morphological characterization provided above, the SPE spectrum of the glass/AgNPs-ET reference system (Figure 57, curve A) shows a markedly higher extinction than that of the glass/SLG/AgNPs-ET hybrid system (Figure 57, curve B). The observed red-shift of SPE in the latter system with respect to the former one (Figure 57) can thus originate from the efficient SLG-Ag NPs coupling [100], however, it can also be caused by the different morphologies of the Ag NPs assembly in each of these systems.

Furthermore, the average values of SERS enhancement factors of the spectral bands of the Ag-ET surface species have been determined for both the glass/SLG/AgNPs-ET hybrid and the glass/AgNPs-ET reference system from their SERS spectra measured at 445, 532, 633 and 780 nm excitation wavelengths (Table 10 and Table 11, respectively).

***Table 11**: The average SERS enhancement factors of the modes of the Ag-ET surface species in glass/ AgNPs-ET reference system*

λ_{exc}/nm	E_f
445	5×10^5
532	5×10^6
633	2×10^6
780	1×10^6

Their mutual comparison has shown that at the 532 and 633 nm excitations, the Ag-ET SERS spectral bands experience an additional enhancement by an average factor of 4 due to the presence of SLG in the hybrid system. By contrast, no such enhancement has been encountered at the 445 and 780 nm excitations (Table 10). This additional enhancement of SERS of Ag-ET has been visualised by SERS microRaman sampling experiment at 633 nm excitation in which the spectral sampling trajectory was directed over an edge of the glass-deposited SLG overdeposited by the ET-modified AgNPs array (Figure 60). The first part of the trajectory sampled ca 1.5 μm^2 areas on the glass/Ag NPs-ET part of the sample, while the second one sampled areas of the same size on the glass/SLG/AgNPs/ET part (Figure 60 – B). The increase of the Ag-ET spectral bands intensity observable after the sampling trajectory crossed the SLG edge and entered the SLG-covered part of the sample is clearly visible on the SERS spectra evolution presented in Figure 60 – A.

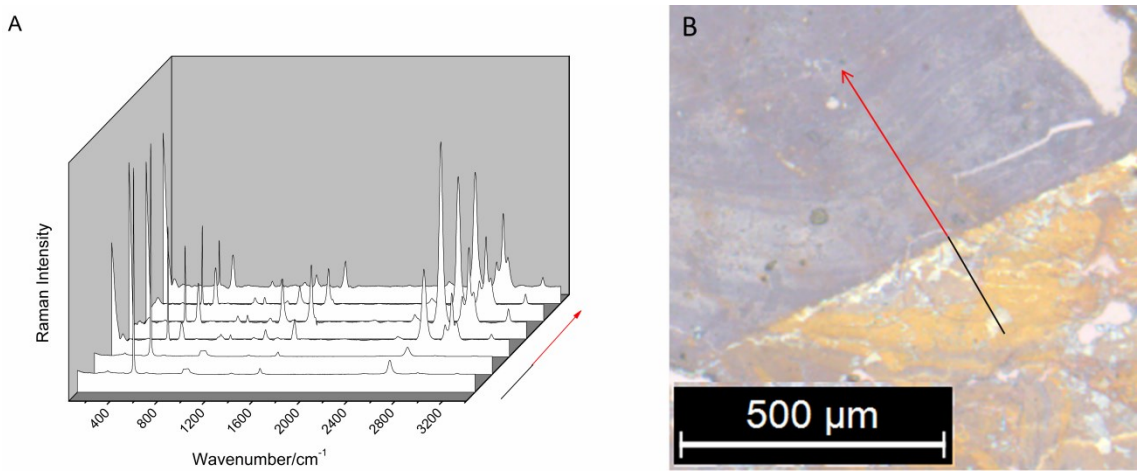

***Figure 60**: Manifestation of the additional enhancement of SERS of ET in the AgNPs-ET array induced by the presence of SLG underneath the AgNPs-ET array. A. SERS microRaman sampling carried out at 633 nm excitation along the trajectory outlined in B., i.e. in the optical image of the sample: black line: the glass/AgNPs-ET part of the sample; red line: the glass/SLG/AgNPs-ET part of the sample.*

On the basis of the results obtained in this paper as well as those published previously, several possibilities have been considered to explain this additional enhancement and its excitation wavelength dependence. First, (i) the graphene-enhanced Raman scattering (GERS) [23,25,26] and its coupling with the EM mechanism of SERS [85] has been considered. However, it has been recently concluded [25,26] that the GERS enhancement is observed only for planar aromatic molecules which is the case of neither the ET molecule, nor the Ag-ET surface species. Futhermore, (ii) the difference in the morphology (Figure. 59 A and B) and SPE spectra between the glass/AgNPs-ET (Figure 57A and B) and the glass/SLG/AgNPs-ET systems, i.e. measurements from a multilayer versus a monolayed of ET-modified Ag NPs can be also ruled out. The reason is that the SERS signal is collected predominantly from the first Ag NP-ET layer, as confirmed also by the same SERS enhancements of the Ag-ET vibrational modes in both systems (i.e. regardless the actual Ag NP layer thickness) observed at the 445 nm as well at the 780 nm excitation. Furtheron, (iii) the vibrational mode selectivity of the additional enhancement has been checked by comparison of the enhancement factors of the individual Ag-ET vibrational modes, which are shown in Table 12.

Table12: *Enhancement factors of ethanethiol bands in glass/SLG/Ag-NPs-ethanethihol film in comparison to glass/Ag-NPs-ethanethiol film*

λ_{exc} = 445 nm				λ_{exc} = 532 nm			
Position	**Intensity – with SLG**	**Intensity – with SLG**	**Ef**	**Position**	**Intensity – with SLG**	**Intensity – with SLG**	**Ef**
633	354	275	1	633	11046	40230	3
965	80	42	1	965	1518	5490	4
1047	34	34	1	1047	1813	7360	3
1238	34	37	1	1238	1576	6160	3
1426	4	4	1	1426	489	2110	4
1448	7	14	2	1448	579	1930	4
2859	187	199	1	2859	8173	27000	4
2914	799	864	1	2914	17627	97720	4
2957	251	257	1	2957	8991	30500	4
λ_{exc} = 633 nm				λ_{exc} = 780 nm			
Position	**Intensity – with SLG**	**Intensity – with SLG**	**Ef**	**Position**	**Intensity – with SLG**	**Intensity – with SLG**	**Ef**
633	12525	54052	4	633	17238	19001	1
965	1219	4936	4	965	1233	1374	1
1047	2898	8630	4	1047	2728	3137	1
1238	1021	3647	3	1238	788	864	1
1426	462	1398	3	1426	948	964	1
1448	695	2360	4	1448	1478	1524	1
2859	2022	8817	3	2859	3958	4296	1
2914	7050	29747	4	2914	7699	8661	1
2957	1994	8528	4	2957	1975	2026	1

The enhancement factors of all these modes range from 3.3 to 4.3 at 532 nm excitation and from 3.0 to 4.4 at 633 nm excitation, i.e. there is no strong preferential enhancement of a particular vibrational mode of the Ag-ET surface species.

Finally, (iv) we consider the recently reported changes of the optical characteristics of SLG localized in the optical near field resonantly excited in 2-D Ag or Au NPs arrays [101–106]. It has been demonstrated that light absorption of SLG can be manipulated by integrating SLG with a thin layer of plasmonic nanostructures (such as the 2-D Ag or Au NPs arrays with or without a dielectric spacer between SLG and the plasmonic NPs array) upon the conditions of the resonance surface plasmon excitation [101, 103–106]. In particular, the enhanced optical field thus created in the plasmonic NPs array can

effectively enhance the total absorption of SLG [101]. Considering the Fresnel equations for calculation of the reflectance R of a material from its „optical constants“, i.e. the real (*n*-real refraction index) and imaginary (*k*-index of absorption) part of its complex refraction index (*N*) [98], the increase of the index of absorption of the material leads to increase of its reflectance *R*. Therefore, we suggest that the increased absorption of SLG coupled to AgNPs results into the increase of its reflectance, and we speculate that it is actually the increased reflectance of SLG (located underneath the ET-modified Ag NPs array) which leads to the increased SERS signal intensity of the Ag-ET surface species. This speculation is consistent with the selective observation of this additional SERS enhancement at 532 and 633 nm excitations in relation to the shape of the SPE curve of the glass/SLG/AgNPs-ET hybrid which reaches maximal extinctions at the wavelengths corresponding to these excitations, but strongly drops both at 445 and 780 nm wavelengths (Figure 57, curve B). For testing the feasibility of the assumption that at 532 and 633 nm excitations, SLG in the glass/SLG/AgNPs-ET hybrid system acts actually as a reflecting surface, we have carried out the following experiment: First, a new glass/Al foil/AgNPs-ET hybrid system, in which SLG was replaced by an Al foil known as a strongly reflecting mirror, was prepared. Its SERS microRaman spectra were measured at the same excitations as those of the glass/SLG/AgNPs-ET hybrid and of the glass/AgNPs-ET reference system, and the additional average SERS enhancement experienced by the vibrational modes of the Ag-ET surface species in the hybrid system with Ag foil (with respect to the reference system without the Ag foil) has been determined, yielding a factor of 12 and 15 at 532 and 633 nm excitations, respectively (Table 10). These experiments demonstrate the possibility to increase SERS signal of molecules and/or surface complexes incorporated in 2D arrays of Ag NPs and measured by the microRaman technique by localization of the array on the strongly reflecting surface, while the 3 – 4 times higher enhancement produced by the Al foil than by SLG in the near field of Ag NPs indicates, that SLG acts as only a weakly reflecting surface under these circumstances.

4.2.2.2. SERS spectra, morphology and surface plasmon extinction of glass/AgNPs/SLG hybrid system

As the second hybrid system for SERS of SLG, the glass/AgNPs/SLG hybrid system (hybrid system II) was designed. In contrast to the glass/SLG/AgNPs-ET film hybrid

system (hybrid system I), hybrid system II promises better contact of AgNPs with SLG and thereby larger efficiency of SLG signal enhancement.

The second hybrid system was prepared by overdeposition of the parent glass/AgNPs-ET system by SLG by the procedure described in Chapter 3.4.3. SERS spectra in the straight (Figure 61 – A) and in the inverted (Figure. 61 – B) geometry of the sample were measured at 445, 532, 633 and 780 nm excitation wavelengths.

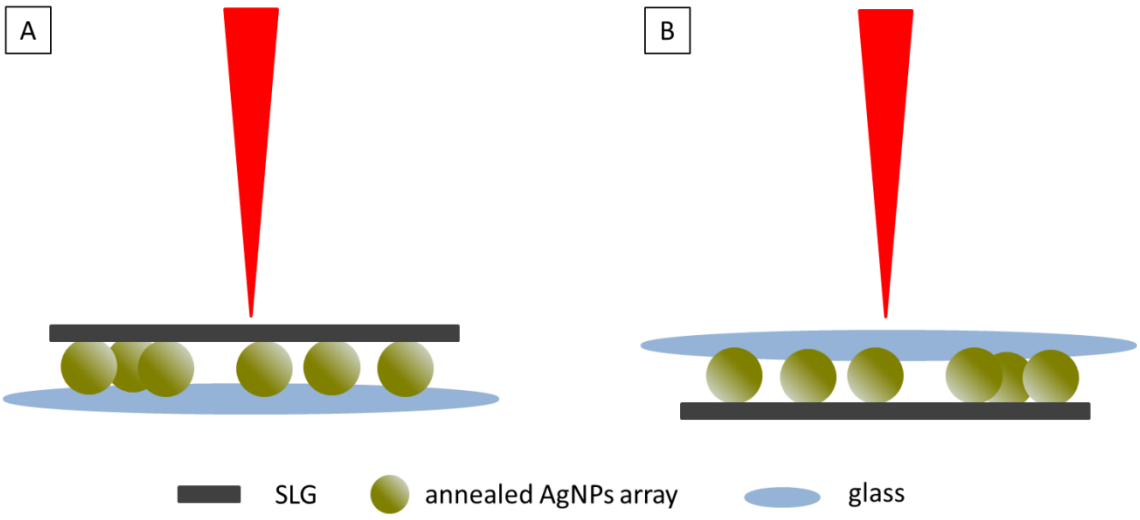

Figure 61: *Schematic depiction of glass/AgNPs/SLG hybrid system measured in (A) straight and (B) inverted geometry*

SERS spectra of the resulting system measured in the straight (i.e. as prepared) sample geometry (depicted in Figure 61 – A) and shown in Figure 62 contain none of the characteristic spectral bands of the Ag-ET species (assigned in 9 and observed in the SERS spectra of the glass/SLG/AgNPs-ET hybrid, Figure 55).

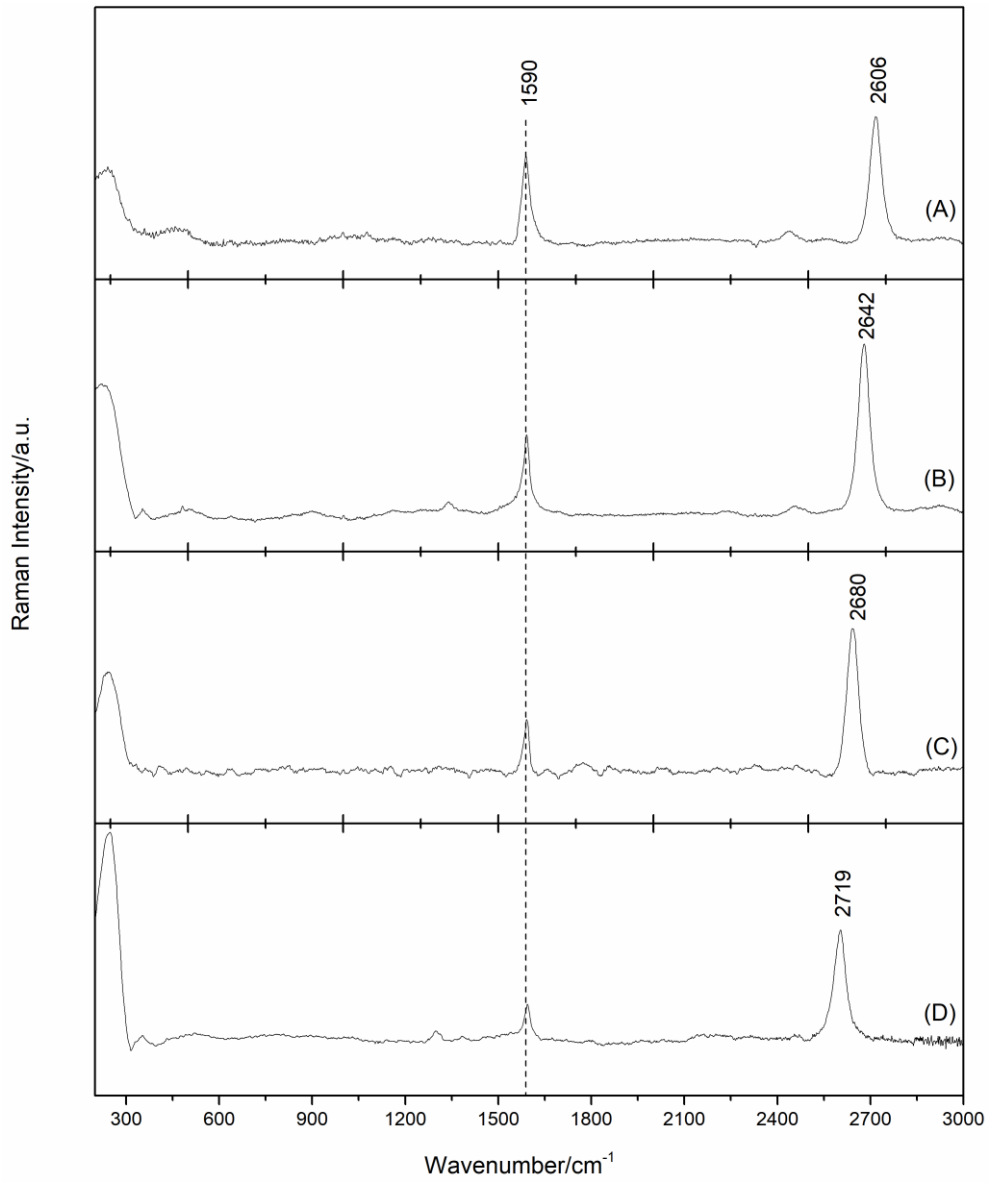

Figure 62: *SERS microRaman spectra of glass/AgNPs/SLG hybrid system measured at (A) 445, (B) 532, (C) 633 and (D) 780 nm excitation in the straight sample geometry. All spectra were baseline corrected.*

This result indicates, that ET was completely removed from the surface of the AgNPs-ET film during the SLG transfer.

The change of the hybrid system II SPE after the SLG transfer was observed by the naked eye as the colour change. The changes of morphology of the hybrid systems are captured by TEM images, as demonstrates Figure 63. In contrast with Figure 63 – A, which shows the parent AgNPs-ET film, Figure 63 – B depicts AgNPs film after the thermal heating caused by SLG transfer. The morphology changes correspond with annealing of Ag NPs (thermal and/or chemical after the ET removal from the Ag NP

surface). The quite broad particle size distribution in the AgNPs/SLG hybrid systems is quantified in Figure 63 – C. Monomers as well as dimers and trimers of Ag NPs can be distinguished in the TEM image of the AgNPs/SLG system in Figure 63 – B. The fraction of dimers and trimers has been established to ca 20% from of the circularity diagram in Figure 63 – D.

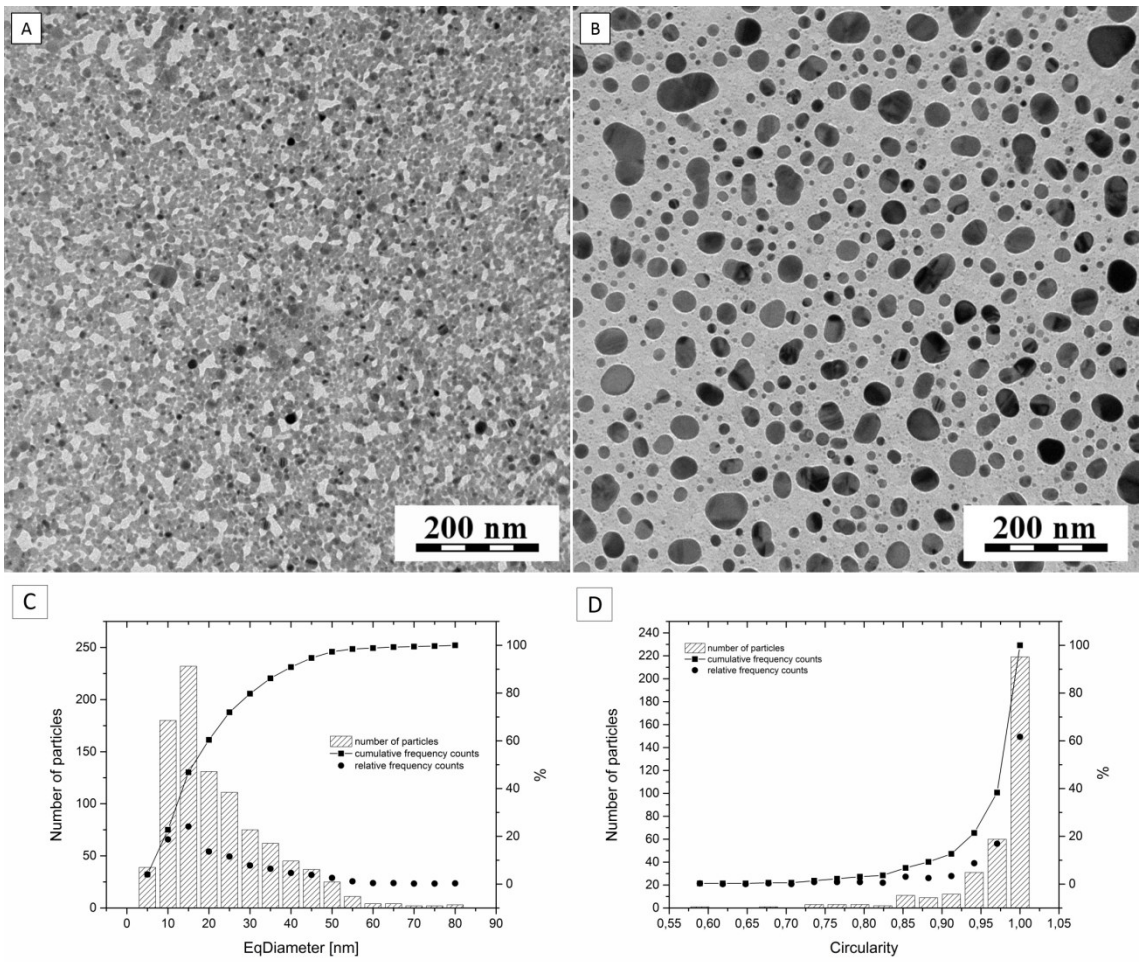

Figure 63: *(A) TEM image of the parent AgNPs/ET film deposited on a C-coated Au grid; (B). TEM image of AgNPs/SLG hybrid system deposited on a C-coated Au grid, (C) Particle size distribution in the AgNPs/SLG hybrid system.(D) Distribution of the particles circularity in the AgNPs/SLG hybrid system.*

Based on the previously published studies [107,108] we reason that both the broad particle size distribution and the presence of fused AgNPs dimers and trimers contribute to observation of the very broad and rather flat SPE curve of the Ag NPs/SLG system which spans the visible spectral region and extends itself into the near IR (Figure 64).

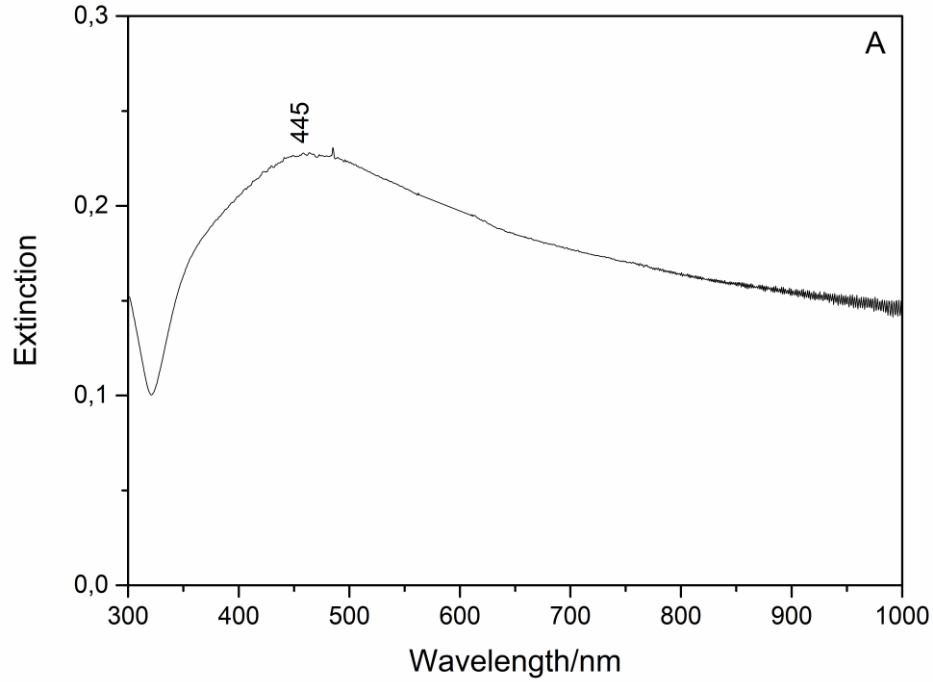

***Figure 64**: Surface plasmon extinction of the glass/AgNPs/SLG hybrid system.*

The SERS spectra of SLG measured in both geometries are shown in Figure 62 and Figure 65, respectively. Since both spectra originate from the same hybrid system, the wavenumbers of the G and 2D modes have been expected, and they are actually observed, to be virtually the same in both geometries at each of the four excitation wavelengths. In particular, the non-dispersive G mode is located at 1590 cm^{-1} in both sets of the spectra at all four excitation wavelengths. Its position is thus by 5 cm^{-1} higher than that of pristine SLG [18,19] and of SLG in the glass/SLG reference sample (Figure 54 and Figure 56, spectrum A). At 445 nm excitation, the dispersive 2D mode is located at 2719 cm^{-1} in the spectrum measured in the straight sample geometry (Figure 62) and at 2717 cm^{-1} in the spectrum obtained in the inverted geometry (Figure 65). Its position is thus by 3 and 5 cm^{-1}, respectively, lower than that of SLG in the glass/SLG reference system (Figure 56). The small upshift of the G mode wavenumber together with the small downshift of that of the 2D mode suggests a weak n-doping of SLG by Ag NPs, as reported previously [109].

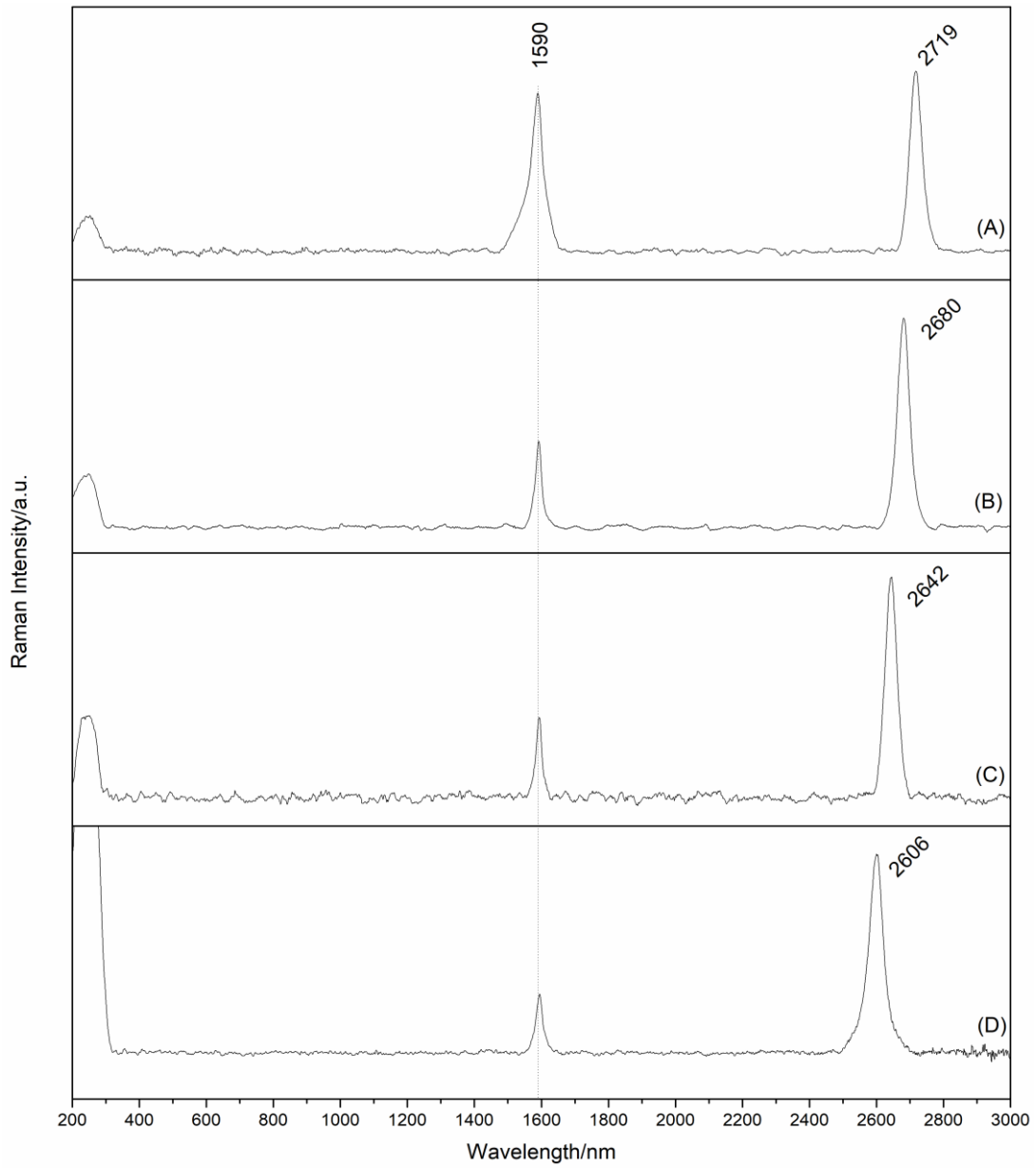

Figure 65: *SERS microRaman spectra of glass/AgNPs/SLG hybrid system measured at (A) 445, (B) 532, (C) 633 and (D) 780 nm excitation in the inverted sample geometry.*

SERS enhancement factors of the G and 2D modes of SLG determined as the intensity ratios of these modes in the SERS spectra of the glass/Ag NPs/SLG hybrid to those in Raman spectra of the glass/SLG reference system (both measured in either the straight, or the inverted sample geometry) are listed in Table 13 and depicted in Figure 66 (together with the error bars representing the standard deviations of band intensities resulting from evaluation of five spectral maps).

Table 13: *SERS enhancement factors of the SLG modes in the glass/AgNPs/SLG hybrid system*

	E_f			
	Inverted geometry		**Straight geometry**	
λ_{exc} (nm)	SLG – G	SLG – 2D	SLG – G	SLG – 2D
445	33	17	15	7
532	14	9	11	7
633	16	9	18	8
780	19	10	8	5

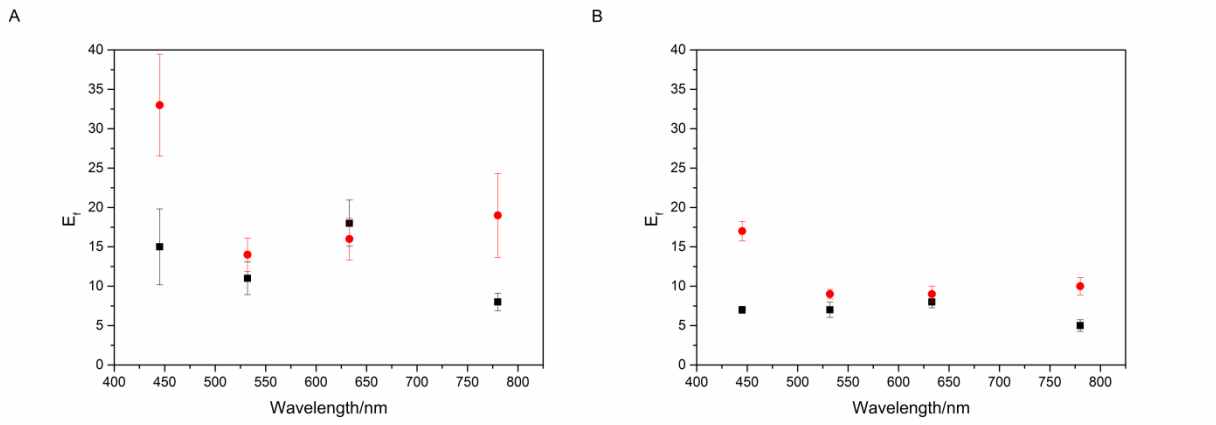

Figure 66: *Comparison of SERS enhancement factors of the G mode (A), and of the 2D mode (B) of SLG in the glass/AgNPs/SLG hybrid system plotted as a function of excitation wavelength for two sample geometries: the straight one-black squares, the inverted one-red circles.*

The SERS Efs values (Figure 66 and Table 13) demonstrate that a significant SERS enhancement is experienced by the G and the 2D mode of SLG at all excitations (445 – 780 nm) and in both sample geometries. This result is attributed to the morphology of the annealed Ag NPs array in the hybrid system, namely to the broad distribution of morphologies and sizes of Ag NPs constituting this array (Figure 63), which in turn, manifests itself by the broad SPE curve of the hybrid (Figure 64). Nevertheless, one has to keep in mind that both absorption and scattering contribute to the SPE of the Ag NPs array, while the SERS enhancement by the EM mechanism stems only from the scattering crossection. Therefore, the wavelength dependence of the scattering

crosssections of Ag NPs monomers and dimers [110] is even more appropriate for correlation with the excitation wavelength dependence of the SERS Efs of the SLG modes in the two sample geometries than the SPE curve itself.

For both the G and the 2D mode of SLG, the differences between their SERS Efs in the two samples geometries (Figures 62A and 65A) show the same excitation wavelength dependence (Figure 64 and Table 13). In particular, no significant differences in the Efs are observed at 532 and 633 nm excitations, while at 445 and 780 nm excitations, the enhancement factors are approx. 2 times larger in the inverted (Figure 65A) than in the straight (Figure 62A) sample geometry. The former observation is consistent with the presence of the same plasmonic enhancer in the hybrid system in the straight as well as inverted sample geometry (Figures 62A and 65A), while the latter one indicates that some other, excitation wavelength dependent factor(s), affect the final SERS Efs determined in each of the two sample geometries. We propose that the most important factors are (i) absorption of both the incident and the scattered light by the Ag NPs, and (ii) increased absorption and reflectance of SLG in the optical near field resonantly excited in Ag NPs. Their mutual interplay at each excitation wavelength and in each sample geometry (in which SERS spectra of SLG from the particular hybrid system have been measured) can then positively and/or negatively affect the actual values of the experimetally determined SERS Efs of the SLG modes.

In the particular case of our hybrid system constituted by SLG on the top of the Ag NPs array, the former effect (i) is expected to affect negatively the SERS spectral intensities preferentially in the inverted sample geometry (favoring thus the straight sample geometry), while the latter effect (ii) favors the inverted geometry (in which scattered light is partially reflected back into the sample) over the straigth one (in which a small fraction of the incident light is reflected from the sample surface). Since the magnitude of both effects is excitation wavelength dependent, it is understandable that the result of their interplay depends on the excitation wavelength as well.

Nevertheless, the exact values of the absorption and scattering crosssections of our particular Ag NPs array at each excitation wavelength are not available, and other factors, such as the fraction of the SLG surface located in the near field of Ag NPs at each of the excitation wavelengths also play their role. Therefore, we can only qualitatively and tentatively address the experimentally observed, excitation wavelength dependent differences between the Efs experienced by the SLG in the straight

(Figure 62A), and in the inverted (Figure 65A) sample geometry (Figure 64 and Table 13). Apparently, the two additional effects (i) and (ii) compensate each other at 532 and 633 nm excitations. By contrast, at 445 and 780 nm excitation, the measurement in the inverted geometry is favored by the twofold increase of the SERS Efs of both the G and 2D mode of SLG, hence the contribution of the effect (ii) is larger that that of the effect (i) at these wavelengths. We propose that this observation can be related to the efficient localization of SLG in the near field of Ag NPs resonantly excited at these excitation wavelengths (resulting into the increased reflectivity of SLG), in combination with the particular morphology of the annealed Ag NPs array. In particular, at 445 nm, the optical fields are resonantly excited preferentially in single Ag NPs: the optical fields in the vicinity of the single NPs are relatively weak [107,108,110], but the NPs are fairly abundant (Figure 63B, C and D), hence a relatively large fraction of SLG area is localized in these optical fields. At 780 nm excitation, stronger optical fields are excited in large Ag NPs dimers and trimers, including the very strong optical fields (hot spots) localized between the NPs in these dimers and/or trimers [107,108,110]. However, the dimers and trimers are less abundant than the single NPs (Figure 63 B and D). Therefore, at the 780 nm excitation, a smaller contact area between SLG and the optical near fields excited in Ag NPs dimers and trimers appears to be compensated by the larger optical fields strengths. The additional enhancement by a factor of approx. 2 in the inverted sample geometry is thus observed at both the 445 and 780 nm excitations (Figure 64 and Table 13).

Furthermore, standard deviations of the SERS Efs experienced by the G and the 2D mode of SLG in both sample geometries and at all excitations have been determined for each of these 16 spectral measurements from five spectral maps, and they are depicted as error bars in Figure 10 A and B. Their values are fairly low for the 2D mode at all excitations and in both sample geometries (Figure 64 B). For the G mode, low values of the error bars have been obtained at 532 and 633 nm excitations in both sample geometries and at 780 nm excitation in the straight sample geometry, while relatively large error bars have been determined at 445 nm excitation in both sample geometries and at 780 nm excitation in the straight geometry (Figure 64 A). The large standard deviations at 445 nm excitation have their origin in fluctuations of the spectral background in the 1500 – 1650 cm^{-1} region encountered at this particular excitation. At 780 nm excitation, the large signal fluctuations in the same spectral region have been observed only in the inverted sample geometry, i.e. for the measurement “through

glass“ as is shown in Figure 61B, and they are attributed to fluorescence from the glass slide [111]. In summation, these results indicate that the glass/AgNPs/SLG hybrid sample is fairly homogenous on the large scale of the SERS spectral mapping, since the large standard deviations are limited to 3 of 16 spectral mapping measurements, and they have been explained by extrinsic spectral effects unrelated to the sample morphology.

4.2.5. 2D and 3D AgNPs assemblies as substrates for SERS of SLG: their advantages and drawbacks

Overdeposition of SLG over the AgNPs aggregates (i.e. formation of glass/AgNPs aggregate/ SLG hybrid system) causes the biaxial strain in SLG (particularly in the contact areas between SLG and the Ag aggregate) which manifests itself by a downward shift (wavenumber decrease) of the G mode band (by 7 cm^{-1}) and of 2D mode band (by 13 cm^{-1}) in the SERS spectra of the sample at all 4 excitation wavelengths.

The maximum SERS enhancement of 2D modes is larger for the glass/AgNPs aggregate/SLG hybrid system than for the glass/SLG/AgNPs aggregate hybrid system at all 4 excitation wavelengths. On the other hand, the homogeneity of the SERS signal intensity distribution is, for both D and 2D modes at all 4 excitation wavelengths, substantially higher for the glass/SLG/AgNPs aggregate hybrid system measured in inverted geometry.

The inverted glass/SLG/AgNPs aggregate sample shows maximum SERS enhancement of 2D mode at 780 nm excitation ($E_f = 1\times10^2$), while the glass/AgNPs aggregate/SLG yields the maximum SERS enhancement of this mode at 532 nm excitation ($E_f = 3\times10^2$). The difference is attributed to the different sample preparation, in conjunction with the fractal morphology (D = 1.84) of the fused Ag NP aggregates and the 2D monolayer structure of SLG as the “adsorbate”.

In particular, the contact areas between SLG and AgNPs aggregate are expected to be larger for the inverted AgNPs aggregate over SLG sample (hence the largest SERS enhancement originates from the more delocalized fractal modes excited at 780 nm) than for the SLG over AgNPs aggregate sample (for which the largest SERS enhancement originates from the more localized fractal modes excited at 532 nm).

Inversion of the AgNPs aggregate over SLG hybrid system is necessary for obtaining Raman signal at all points during the linear sampling across the AgNPs aggregate. The

original glass/SLG/AgNPs aggregate hybrid systems yields SERS signal only at certain locations at the AgNPs aggregate border. The inversion of the sample geometry eliminates loses of both incident and the scattered radiation caused by the AgNPs aggregate extinction.

The inverted glass/SLG/AgNPs aggregate hybrid systems appear to be more advantageous and reliable for SLG SERS spectral probing than glass/SLG/AgNPs aggregate hybrid systems due to the absence of the effect of biaxial strain on G and 2D SLG modes and to the substantially more homogeneous distribution of SERS signal of all SLG modes. The optimal excitation wavelengths for SERS spectral probing of the former samples is 780 nm. The main disadvatages is heterogeneity of these samples. Although the 3D Ag aggregates are relatively flat, the direct contact of SLG and Ag aggregates surface is not homogeneous through whole sample. When the SLG sheet and Ag aggregate surface are in contact, SERS signal is relatively intensive. On the other hand, when the SLG sheet covers the "whole" in the Ag aggregate surface, SERS signal is less intense, or no signal of SLG is observed. These results have indicate that more flat AgNPs systems, specifically 2D assemblies AgNPs are expected to provide more suitable for SERS of SLG.

4.3. Glass/AgNPs/SLG/H_2Pc(ML) hybrid system as sample for SERS + GERS of H_2Pc

4.3.3. Characterization and spectral probing of glass/AgNPs/SLG/H_2Pc(ML) hybrid system and of the reference system.

Finally, system which connects GERS and SERS of the selected aromatic molecule, specifically the freebase phthalocyanine (H_2Pc), was developed and tested. Resulting system is depicted on Figure 67 – A. TEM image of the annealed AgNPs employed as the plasmonic enhancer in the hybrid system is presented in Figure 67 – B. The TEM image in Figure 67 – B demonstrates the presence of monomers, dimers and also trimers of this particles.

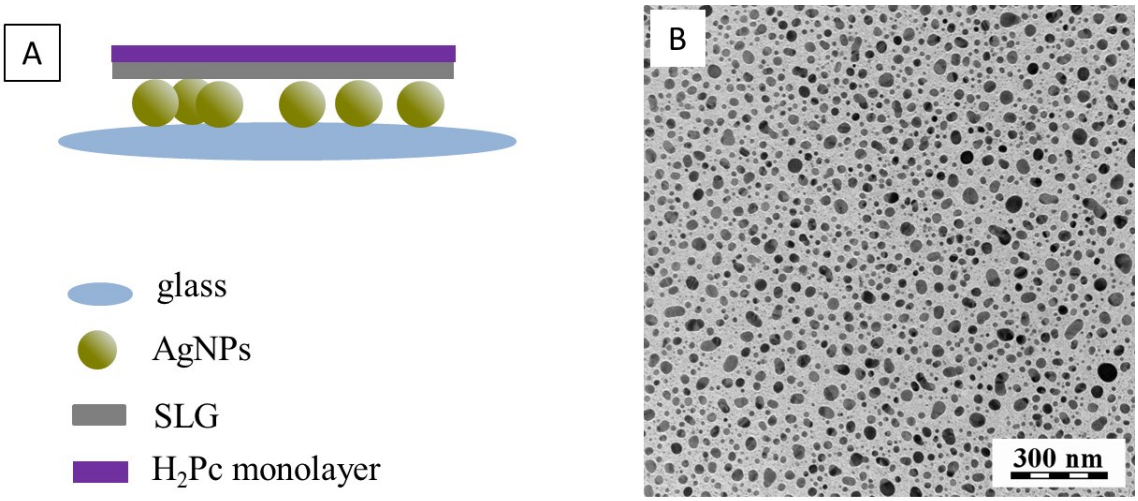

Figure 67: *(A) Schematic depiction of glass/AgNPs/SLG/H_2Pc(ML) hybrid system used for microRaman measurements of SERS+GERS of H_2P and (B) TEM image of the array of annealed AgNPs employed as the plasmonic enhancer in the glass/AgNPs/SLG/H_2Pc hybrid system.*

The SPE spectra of glass/AgNPs/SLG system before and after the deposition of H_2Pc are compared in Figure 68. Both curves reveal extension of SPE over the visible and near IR spectral region and deposition of H_2Pc onto the AgNPs hybrid system cause minimal changes in SPE spectra. The similarity of both curves provides evidence that AgNPs substrate is not perturbed by the deposition of H_2Pc monolayer and by soaking in toluene.

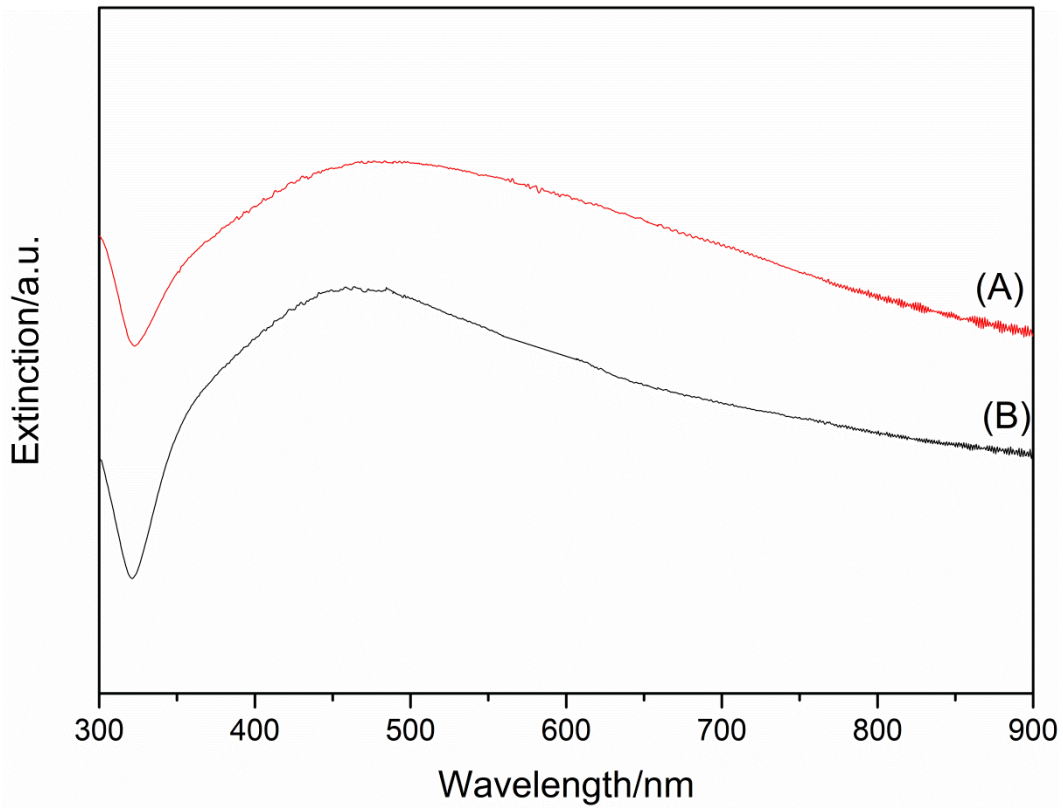

Figure 68: *SPE spectra of glass/AgNPs/SLG hybrid system: (a) before and (b) after deposition of the H_2Pc ML.*

The sample contains two types of areas: with and without Ag NPs, i.e. both the hybrid sample itself and its reference system are found on one common substrate, i.e. the special glass slide. An optical image showing the glass/AgNPs/SLG/H_2Pc(ML)-(i) and the glass/SLG/ H_2Pc(ML)-(ii) parts of the same sample and the boundary between these two parts is presented in Figure 69A. The SERS+GERS (i) and the GERS (ii) parts of the spectral map of the 683 cm^{-1} mode of H_2Pc measured at 785 nm excitation and spanning the same sample area as that in Figure 69A are shown in Figure 69B. The spectral map (Figure 69B) shows the markedly higher intensity of the Raman signal of the 683 cm^{-1} mode of H_2Pc from the glass/AgNPs/SLG/H_2Pc(ML)-(i) part of the sample than from the glass/SLG/H_2Pc-(ii) part of the sample which, in turn, provides a qualitative evidence of observation of SERS+GERS of H_2Pc in the former case, and of GERS of H_2Pc in the latter one.

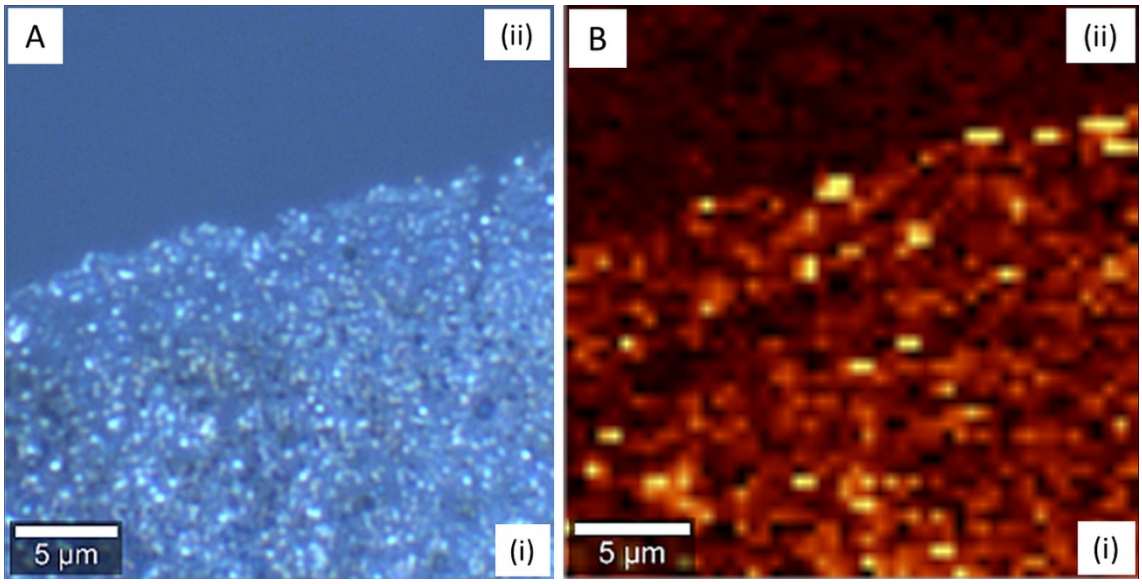

Figure 69: *(A) Optical image of the hybrid sample employed for GERS and SERS+GERS spectral measurements (mapping) of H_2Pc with the clearly distinguished boundary between the (i)-glass/AgNPs/SLG/H_2Pc part of the sample used for SERS+GERS measurements; (ii)-glass/SLG/H_2Pc part of the sample utilized for GERS measurements. (B) Spectral map of the 683 cm^{-1} band of H_2Pc acquired at 785 nm excitation from the same area of the sample as the optical image (A). The spectral map (B) shows the markedly higher intensity of the Raman signal from the (i)-glass/AgNPs/SLG/H_2Pc part of the sample (SERS+GERS) than from the (ii) glass/SLG/H_2Pc part of the sample (GERS).*

For the spectral mapping by which the average spectra were acquired at all five excitation wavelengths, the maps spanning entirely the glass/AgNPs/SLG/H_2Pc(ML) area of the sample (fully covered by a single layer of Ag NPs) were used for the SERS+GERS measurements, and those spanning the glass/SLG/H_2Pc(ML) area were employed for GERS. Figure 70 shows optical images of glass/AgNPs/SLG/H_2Pc(ML) and different SERS spectral maps at 785 nm excitation. Specifically Figure 70 – A and B shows SERS spectral maps of G and 2D modes, Figure 70 – C and D shows SERS + GERS spectral maps of 683 cm^{-1} and 1540 cm^{-1} modes of H_2Pc.

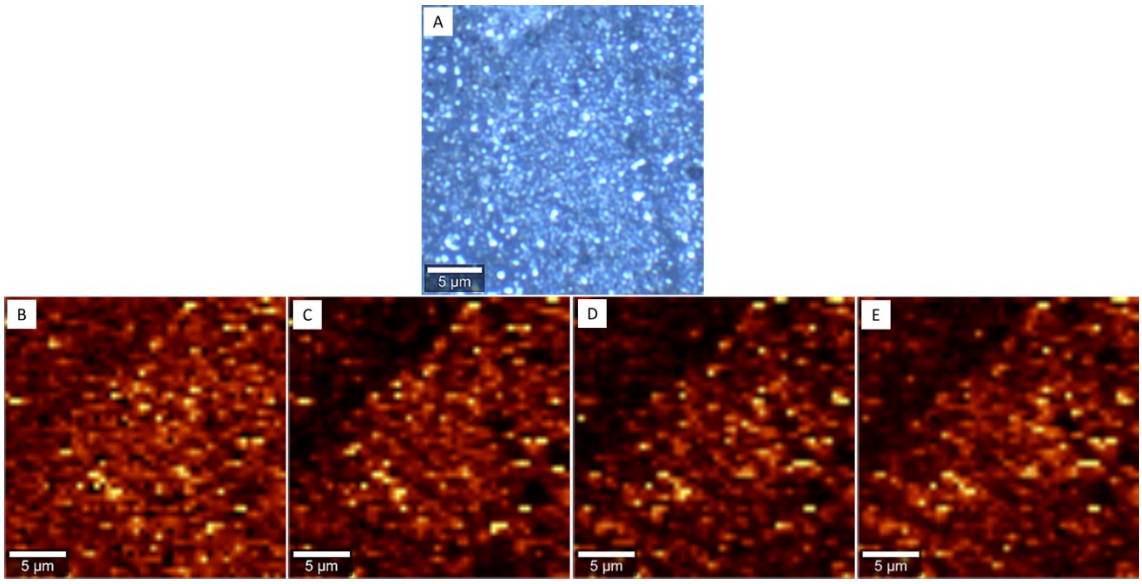

Figure 70: *(A) An optical image of the glass/AgNPs/SLG/H_2Pc(ML) area of the sample; (B) and (C) - SERS spectral maps of the G mode (1590 cm^{-1}) and 2D (2595 cm^{-1}) mode of SLG; (D) and (E) - SERS+GERS spectral maps of the 683 cm^{-1} and 1540 cm^{-1} modes of H_2Pc. The spectral maps (B)-(D) were acquired from the same area as the optical image (A) at 785 nm excitation.*

SERS spectra of SLG and SERS+GERS spectra of H_2Pc obtained from the glass/ AgNPs/SLG/H_2Pc(ML) hybrid system at 532, 633, 647, 785 and 830 nm excitations are shown in Figure 71 – A (full range spectra) and 71 – B (details in the 400-1800 cm^{-1} range). The average wavenumber of the G mode band in the spectra of the glass/AgNPs/SLG/H_2Pc is 1590 cm^{-1}. Its position is thus exactly the same as reported for the glass/AgNPs/SLG system in Chapter 4.2.2.2. This result indicates that deposition of a monolayer (ML) of H_2Pc molecules onto the glass/AgNPs/SLG platform has not caused any additional doping of SLG by H_2Pc molecules. The 1590 cm^{-1} position of the G-band is by 5 cm^{-1} higher than in the pristine SLG [18,19] and, in accord with ref. 109 indicates a weak n-doping of SLG by Ag.

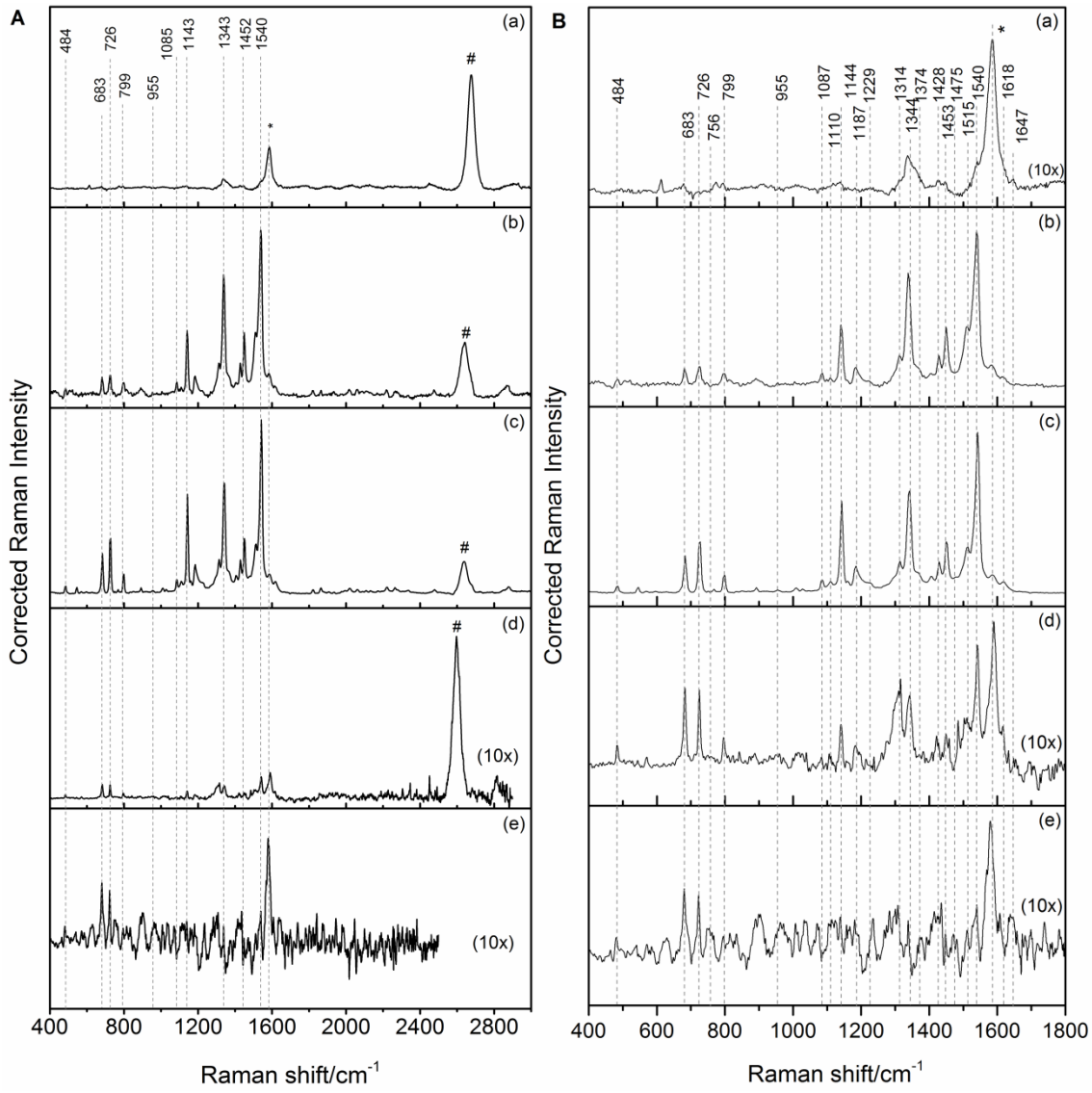

Figure 71: *(A) Full range (400 – 3000 cm^{-1})and (B) detailed (400 – 1800 cm^{-1}) SERS + GERS spectra of H_2P measured from the glass/AgNPs/SLG/H2Pc hybrid system at (a) 532, (b) 633, (c) 647, (d) 785 and (e) 830 nm excitations. The SERS spectral band of the G mode is marked by *, and the SERS spectral bands of the dispersive 2D mode are marked by #.*

Furthermore, the G-band in the Raman spectra of the glass/SLG/H_2Pc(ML) reference system is located at 1592 cm^{-1}, and its position is thus comparable (within the experimental error) with that in the glass/AgNPs/SLG/H_2Pc(ML) system. This comparison indicates, that the magnitude of the weak n-doping of SLG by glass in the former system analogous to the weak n-doping of SLG by Ag in the latter system. Consequently, the positions of the Fermi level of SLG are nearly identical in both

systems, and they were estimated to be ca -4.4 eV (i.e. upshifted by ca 0.2 eV from the Fermi level of pristine SLG at -4.6 eV [23]) on the basis of the graph in Figure 85 in ref. 18. Therefore, the fundamental conditions of operation of the mechanisms of GERS are virtually identical in the glass/AgNPs/SLG/H_2Pc(ML) hybrid system employed for SERS+GERS spectral probing and in the glass/SLG/H_2Pc(ML) system used as the reference system for GERS.

Further on, we have noticed that the position of the G-band of SLG in our glass/SLG/ H_2Pc(ML) reference system (1592 cm^{-1}) is by 7 cm^{-1} lower than that reported for the glass/SLG/H_2Pc(ML) system in ref. 90 (1599 cm^{-1}). This comparison indicates, that the n- doping by glass (in particular, by surface groups and/or water entrapped between glass and SLG) is markedly weaker than that by the glass slides used in ref. 90. Such differences in n-doping by glass have been reported previously, and they have been attributed to a different content of Na in the particular sample of glass [112]. The comparison of the positions of the Fermi level of SLG (i) at -4.4 eV in the glass/SLG/H_2Pc(ML) reference system, and (ii) at -4.3 eV in the GERS sample in ref. 90 (this system will be further referred to as the glassI/SLG/H_2Pc(ML) demonstrates the importance of doping of SLG by the substrates. On the other hand, once this important factor is properly evaluated, it can be employed for adjusting the Fermi level position of SLG.

In Table 13 are listed the average wavenumbers of the H_2Pc bands in SERS+GERS spectra of theglass/AgNPs/SLG/H_2Pc(ML) hybrid system and of the GERS spectra of the glass/SLG/H_2Pc(ML) reference system, together with their assignment based on refs [68,70]. As is shown in Table 13, the wavenumbers of SERS+GERS and the GERS spectral bands are in a good agreement (within 3 cm^{-1}).

Table 13: *The average wavenumbers of the H_2Pc bands in SERS+ GERS spectra of the glass/AgNPs/SLG/H_2Pc(ML) hybrid system and in GERS spectra of the glass/SLG/H_2Pc(ML) reference system complemented by their assignment based on refs*[24,27,42]

GERS of H_2Pc	GERS + SERS of H_2Pc	Mode symmetry	Mode description
486	484	B_{1g}	Benzene ring rocking & central ring deformation
683	683	A_g	Bridging C–N–C sym. def. and benzene ring deformation
728	726	A_g	Pyrrole deformation and C–N–C rocking
800	799	A_g	Pyrrole & benzene ring C–C str.
952	955	IR act.	C-H out-of-plane deformation
1086	1085	B_{1g}	N–H in-plane deformation
1143	1143	A_g	Benzene ring C–C str. and C–H deformation
1343	1343	A_g	Benzene ring C–C str. and pyrrole C–C stretch
1453	1452	A_g	C–H def.
1543	1540	A_g	Bridging C_α–N_m–C_α asym. str. and C_α–N_H–C_α sym. str.

4.3.4. Searching of reference system for GERS of H_2Pc

The GERS spectra of H_2PC were measured first by Tereza Uhlířová [90], however, in the hybrid system assembled on a different type of glass slide (II) than that employed in this Thesis for preparation of the glass(I)/SLG/H_2Pc reference system for SERS+GERS, and consequently, with a different position of the Fermi level of SLG, as mentioned in the previous Chapter 4.1.3. In both cases, for evaluation of GERS enhancement factors, it was necessary to find a suitable reference system. First, the highly ordered pyrolytic graphite (HOPG) and/or glass were tested for this purpose, but they were found unsuitable. HOPG was found to be partially damaged by soaking in toluene solution during H2Pc deposition [90]. As the second reference sample, glass slide was used. Unfortunately, no spontaneous adsorption of H_2Pc onto a glass substrate was detected.

Finally, a cylindrical graphite electrode for thermal evaporation of carbon was tested as substrate for the reference sample preparation. The electrode was cut in half to produce a flat surface. The surface was then rubbed and polished by abrasive papers of decreasing abrasivity, and finally polished by a filter paper. Graphite/H_2Pc monolayer (ML) sample were prepared by a similar strategy as the glass/SLG/H_2Pc (ML) sample. Nevertheless, owing to stability of this graphite substrate, the preparation protocol could be simplified by its immersion into the solution and the solvent, respectively, (rather

than only overlayed by each of them). Therefore, graphite was immersed into H_2Pc solution in toluene for 2 hours, dried by filter paper and then repeatedly immersed into pure toluene for ~24 hours.

Smoothness of the surface was checked by SEM. Though the surface looks flat and smooth, in the SEM images, two types of areas were found: The flat and smooth as shows Figure 72 – A, but also corrugated ones as demonstrates Figure 72 – B.

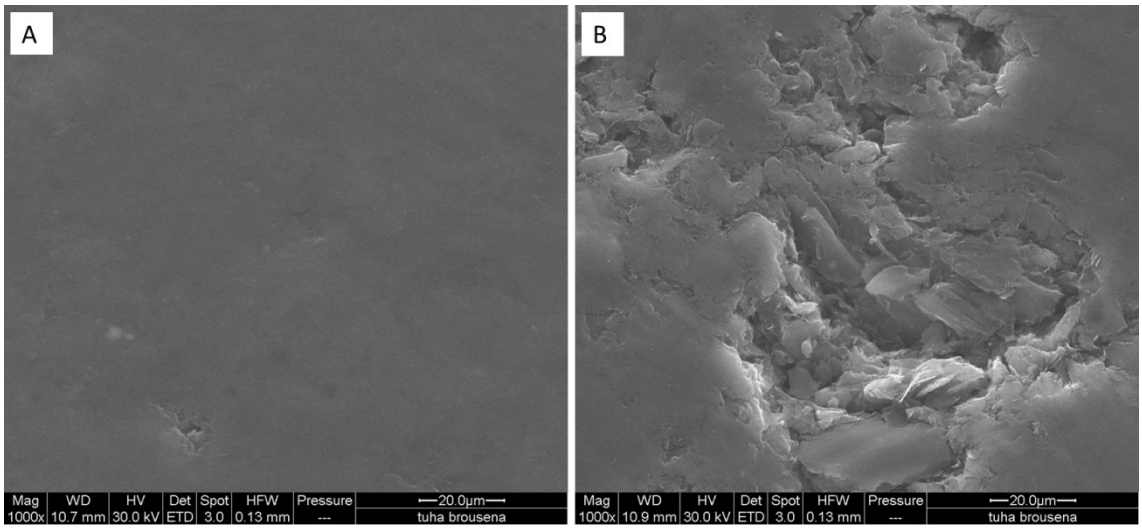

Figure 72: *SEM images of rubbed and polished graphite surface: (A) flat area, (B) corrugated area.*

For the measurement, the flat and smooth area had to be used, because of its similarity to SLG. For this reason, optical microscope of the Raman microspectrometer was used. At the optical microscope image, the flat and smooth area was found and from this area, Raman mapping was done.

In addition to the optical microscopy imaging, Raman spectral mapping can also be used for searching for the flat area. The Raman maps of the appropriate areas showed a very low intensity of the 1344 cm^{-1} graphite band, in contrast to those of the corrugated ones, in which this band was very intense.

The parameters of the spectral maps acquisitions at each of the excitation wavelengths were the same as for the glassI/SLG/H_2Pc samples. Nevertheless, owing to the above mentioned inhomogeneity of the graphite surface, it became crucial to acquire the Raman maps from exactly the same (carefully selected) flat and smooth area of the graphite surface (depicted in Figure 73) for both the graphite substrate itself, and for each of the graphite/H_2Pc samples at each of the excitation wavelengths. Fulfillment of

this condition was accomplished by construction and application of a special sample holder, and it was repeatedly controlled by the optical imaging.

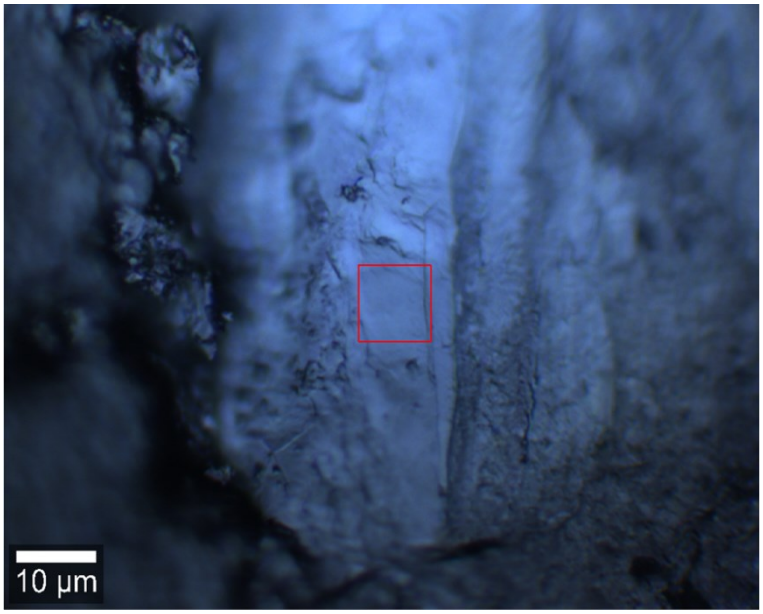

Figure 73: *Optical image of a flat and smooth location on graphite/H_2Pc surface from which Raman maps were acquired.*

4.3.5. GERS, SERS and SERS + GERS enhancement factors

From the glass/AgNPs/SLG/H2Pc hybrid system and from the glass/SLG/H_2Pc reference system combined GERS + SERS spectra and GERS spectra, respectively were measured and obtained at 5 excitation wavelengths. In contrast to them, graphite/H_2Pc, which was used as a second reference system, provided Raman (more precisely RRS) spectra only in resonance with the Q_y (0-0) electronic transition, which is at 633 and 647 excitations.

At all five excitations, SERS+GERS/GERS enhancement factors (EFs) evaluating the SERS enhancement of GERS of H_2Pc in the probed hybrid system were determined and their average values are shown in Table 14.

Table 14: *Average SERS enhancement factors (EFs) of the vibrational modes of H_2Pc at five excitation wavelengths in the 532-830 nm range. The EFs were determined as the ratios of the normalized intensities of the H_2Pc spectral bands in SERS + GERS spectra of glassI/AgNPs/SLG/H_2Pc(ML) hybrid system and in GERS spectra of glassI/SLG/H_2Pc(ML) reference system.*

Wavelength	**532**	**633**	**647**	**785**	**830**
EFs	5±2	14±5	9±3	10±3	13±4

On the other hand, GERS EFs could be numerically evaluated only at 633 and 647 nm excitations (Table 15), however, the aforementioned observation of GERS signal of H_2Pc from the glassI/SLG/H_2Pc(ML) system at all five excitation wavelengths, in contrast to the absence any of Raman signal of H_2Pc from the graphite/H_2Pc(ML) second reference system at 532, 785 and 830 nm indicates that the GERS enhancement of H_2Pc modes occurs at these wavelengths as well.

Table 15: *Average values of GERS enhancement factors (GERS versus RRS normalized band intensity ratios), SERS enhancement factors (SERS+GERS versus GERS normalized intensity ratios), SERS+GERS enhancement factors (SERS+GERS versus RRS normalized intensity ratios) and multiplications of SERS enhancement factors with GERS enhancement factors of H_2Pc vibrational modes at 633 and 647 nm excitations.*

	633 nm	**647 nm**
Average GERS EFs	3 ± 1	4 ± 1
Average SERS EFs	14 ± 5	9 ± 3
Average SERS + GERS EFs	43 ± 7	41 ± 7
Average SERS +GERS EFs (determined as SERS × GERS EFs)	42 ± 9	36 ± 7

These results confirm observation of combined SERS+GERS of H_2Pc from the glassI/AgNPs/SLG/H_2Pc(ML) hybrid system and of GERS of H_2Pc from the glassI/SLG/H_2Pc(ML) reference system. Furthermore, the average SERS+GERS EFs at 633 and 647 nm excitations (Table 15) were determined in a dual way: (i) directly from the SERS+GERS spectra (shown in Figure 71) in relation to the resonance Raman scattering (RRS) spectra of H_2Pc localized in the graphite/H_2Pc(ML) system (details for

individual bands in Table 16), and (ii) as products of the SERS and GERS EFs listed in the first and second row of Table 15.

Table 16: *SERS+GERS enhancement factors experienced by Raman modes of the H_2Pc molecule localized in the glassI/AgNPs/SLG/H_2Pc(ML) hybrid system.*

Peak position [cm^{-1}]	**EFs GERS + SERS vs RR**	
	633 nm	**647 nm**
484	26	25
683	34	25
726	14	20
798	22	28
1085	32	27
1143	46	53
1343	39	33
1452	67	72
1540	107	88

Their values (Table 15) are nearly identical at 633 nm excitation and mutually very close (within the experimental error) at 647 nm excitation. This comparison indicates that the SERS and GERS EFs are simply multiplicative, i.e. that the two enhancement mechanisms are combined without any additional enhancement or damping. It should be noted that, in our hybrid system, we can observe only the EM SERS enhancement, since H_2Pc is isolated from the Ag NPs surface by the SLG spacer. The ordering of the components in our hybrid system is thus different from the case of CuPc molecules sandwiched between a flat Au (111) surface and SLG, for which a coupling of GERS with the chemical mechanism of SERS, namely a charge transfer from Fermi level of Au to LUMO of CuPc, has been reported [113].

4.3.6. SERS +GERS excitation profiles of selected spectral bands of H_2Pc localized in the glassI/AgNPs/SLG/H_2Pc(ML) hybrid system

Excitation profiles (EPs) of the selected spectral bands of H_2Pc were constructed from the SERS + GERS spectra of the glassI/AgNPs/SLG/H_2Pc(ML) hybrid system measured at 532, 633, 647, 785 and 830 nm excitations. The complete EPs are presented in Figure 74 – A, their details in the 750-850 nm region are depicted in Figure 75 – B, and the selected SERS+GERS excitation profiles of H2Pc spectral bands with error bars are shown in Figure 75 – A.

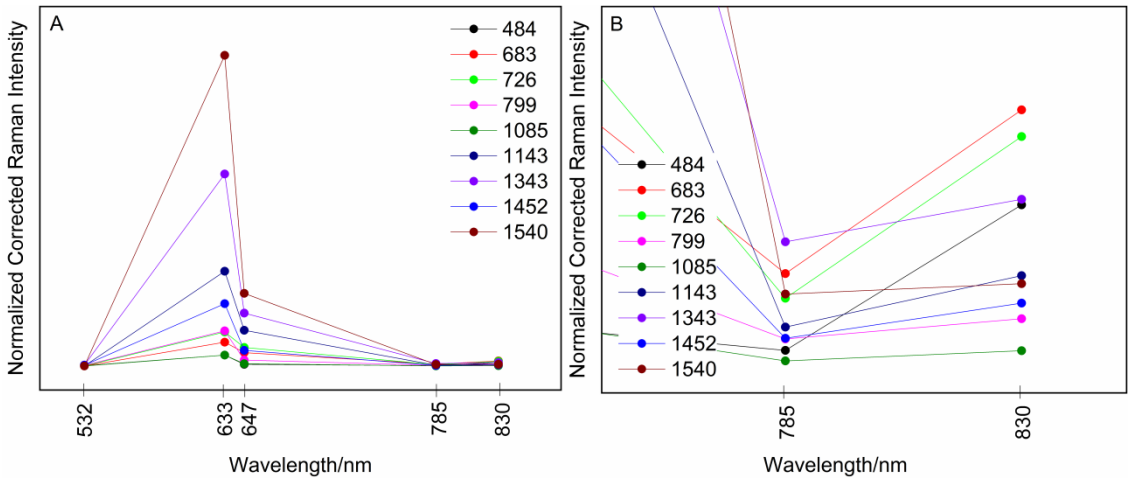

Figure 74: *SERS+GERS excitation profiles (EPs) of spectral bands of H_2Pc localized in glassI/AgNPs/SLG/H_2Pc(ML) hybrid system: (A) complete EPs in the 532 nm-830 nm range of excitation wavelengths; (B) details of the EPs in the 750-830 nm range.*

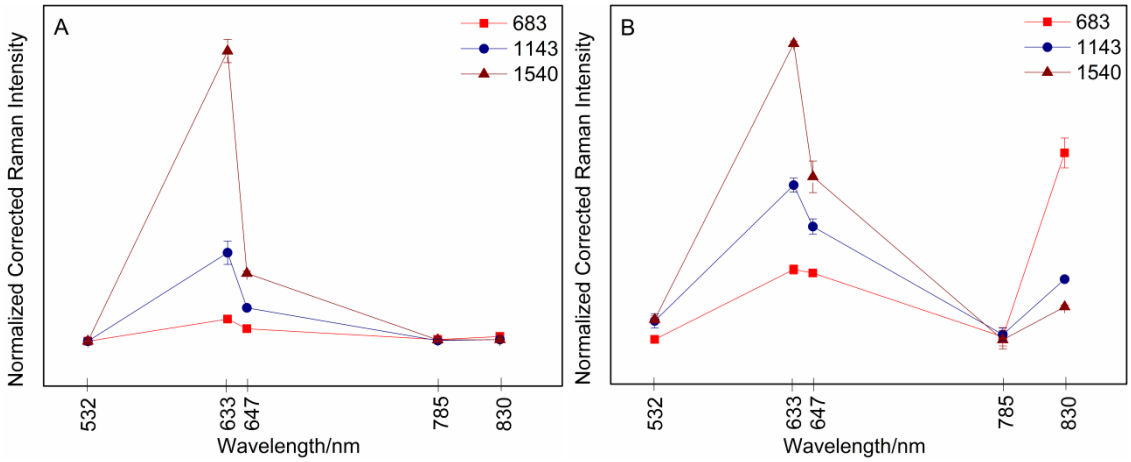

Figure 75: *(A) SERS+GERS excitation profiles of selected spectral bands of H_2Pc measured from glassI/AgNPs/SLG/H_2Pc(ML) hybrid system (B) GERS excitation profiles of the same bands of H_2Pc as in (A) measured from glassI/SLG/H_2Pc(ML) reference system. Both EPs are depicted with error bars.*

For the comparison of the GERS EPs of the selected spectral bands of H_2Pc determined from the GERS spectra of the glassI/SLG/H_2Pc(ML) reference system measured at the same five excitation wavelengths as the SERS+GERS spectra, are presented in Figure 75 – B. Both the SERS+GERS EPs (Figures 74 – A and 75 – A) and the GERS EPs (Figure 75 – B) of all H_2Pc spectral bands show a common maximum at 633 nm excitation, and a normalized band intensity increase at 830 nm. This comparison demonstrates that the shapes of the GERS EPs of all the three spectral bands, namely the two distinct resonance features at 633 and 830 nm, remain preserved upon combination of SERS with GERS of H_2Pc.

The other common features of the selected SERS+GERS EPs in Figure 75 – A and the GERS EPs in Figure 75 – B are the sequences of the normalized band intensities of the three selected H_2Pc spectral bands at 633, 647 and 830 nm excitations, in particular the 683>1143>1540 cm^{-1} sequences determined at both 633 and 647 nm excitations, and the reverse 683>1143> 1540 cm^{-1} sequence at 830 nm excitation. This result indicates that (i) each of the two resonance features (i.e. the maximum at 633 nm and the normalized intensity increase at 830 nm) observed in both the GERS EPs (Figure 75 – B) and SERS+GERS EPs (Figure 75 – A) belongs to a different resonance electronic transition, each showing a different localization within the H_2Pc molecule, and (ii) for both these resonant electronic transitions, their localization within the H_2Pc molecules remains unchanged upon combining of SERS with GERS. In summation, the only observed difference between the SERS+GERS and GERS EPs (Figure 75 – A and B) is the magnitude of the normalized intensity increase at 830 nm excitation, which is markedly higher in the latter case than in the former one. Such "smearing" of the SERS+GERS EPs shape emerges as the only consequence of the SERS enhancement contribution to the combined SERS+GERS profiles, and it can be tentatively explained by the similar values of the EM SERS mechanism enhancement of GERS of H_2Pc at 785 and at 830 nm excitation (Table 14). At this point, we find appropriate to emphasize that in both the glassI/AgNPs/SLG/ H_2Pc(ML) hybrid system used for SERS+GERS spectral measurements and construction of SERS+GERS EPs and in the glassI/SLG/H_2Pc(ML) reference system employed for GERS and GERS EPs construction, nearly the same level of doping of SLG by Ag NPs in the former system and by the glassI substrate in the latter one was established in Chapter 4.3.3. There were thus no differences in the position of Fermi level of SLG in the probed and in the

reference hybrid system which could possibly hamper the SERS+GERS and GERS EPs comparison.

4.3.7. Specification of the mechanisms of GERS and of their operation in GERS and SERS+GERS of H_2Pc in the 532-830 nm range

The next goals were (i) the assignment of two resonance electronic transitions modulating the shapes of both SERS+GERS and GERS EPs, (ii) determination of their localization within the H_2Pc molecule (on the basis of the sequences of normalized band intensities of totally symmetric vibrations and of their assignment, as reported previously for RRS [14]) and (iii) specification of the mechanisms of GERS operating in both SERS+GERS and GERS of H_2Pc in the 532-830 nm range.

First, the electronic absorption band giving rise to the 633 nm maximum on both SERS+GERS and GERS EPs of H_2Pc (Figure 74 – A, 75 – A and B) is attributed to the Q_y (0,0) electronic transition of H_2Pc on the basis of the previously reported electronic absorption spectra and EPs [66,69,70,90,115,116].

Furthermore, the same sequences of the normalized band intensities in the SERS+GERS and GERS EPs of the three selected H_2Pc bands (Figure 75 and in Chapter 4.3.6.) encountered at the 633 and at the 647 nm excitation indicate that the 647 nm excitation also falls into the contour of the Q_y (0,0) electronic absorption band.

The markedly larger normalized band intensities at 633 than at 647 nm excitation (Figure 74 – A and Figure 75), together with the ~10 nm value of the Q_y(0,0) band halfwidth determined by detailed SERRS excitation profiles of this electronic transition in Ag nanostructures/H_2Pc hybrid system [69] (as the largest reported halfwidth of this electronic transition) indicate that the maximum of this electronic transition in both the glassI/AgNPs/SLG/H_2Pc(ML) and the glassI/SLG/H_2Pc(ML) system is located between the 633 and 647 nm excitations (mutually distanced by 14 nm), but closer to the 633 nm excitation, i.e. within ca 633 – 639 nm interval. In contrast to the normalized band intensities in GERS of H_2Pc which maximize at 633 nm excitation (Figure 75A), the GERS EFs (Table 15) were determined to be larger at 647 nm (average EF=4) than at 633 nm excitation (average EF=3).

This observation is consistent with broadening and a small blue shift of this electronic absorption band in both the glassI/AgNPs/SLG/ H_2Pc(ML) hybrid and in the glassI/SLG/H_2Pc(ML) reference system, in comparison to the graphite/H_2Pc(ML) second reference system. These changes in the position and halfwidth of the Q_y (0,0)

electronic absorption band are attributed to SLG - H_2Pc(ML) interaction, and they are responsible for the GERS enhancement experienced by H_2Pc spectral modes in both the probed hybrid and the reference system at 633 and 647 nm excitations, respectively (Table 15).

Furthermore, the 1540>1143>683 cm^{-1} sequence of the normalized band intensities established in both SERS+GERS and GERS of H_2Pc at 633 and 647 nm together with the assignment of the H_2Pc vibrational modes in Table 13 and the detailed analysis of the complete GERS+SERS EPs indicate a preferential enhancement of the higher wavenumber modes, mainly the C-C stretching vibrations localized on benzene and pyrrol rings, the combined C-N-C stretch known as the cavity size marker [117] and the C-H deformation modes localized on the outer benzene rings. By contrast, this electronic transition has been reported to be localized preferencially on the tetrapyrrol macrocycle for a free H_2Pc molecule owing to the preferential enhancement of macrocycle breathing and deformation modes [67]. The change in localization of the $Q_y(0,0)$ resonant electronic transition within the H_2Pc molecule represents another manifestation of GERS in SERS+GERS of H_2Pc in the glassI/AgNPs/SLG/ H_2Pc(ML) as well as in GERS of H_2Pc in the glassI/SLG/H_2Pc(ML) reference system at 633 and 647 nm excitations, and it is also attributed to the SLG - H_2Pc(ML) interaction (Figure 76)

The second resonance which manifests itself by the relative intensity increase at 830 nm excitation was not been observed in the electronic absorption spectra of H_2Pc reported in [66,69,70,115,116]. The energy difference betwen Fermi level of SLG, which is located at -4.4 eV and LUMO of H2Pc, which is positioned at -2.87 eV [116] is 1.53 eV, i.e. 810 nm. This calculated value of the maximum of a charge transfer (CT) from Fermi level of SLG to LUMO of H_2Pc at 810 nm suggests that the 830 nm excitation is in resonance with this CT electronic transition (Figure 76). Such CT transition has been theoretically predicted as one of the four possible mechanisms of GERS [24].

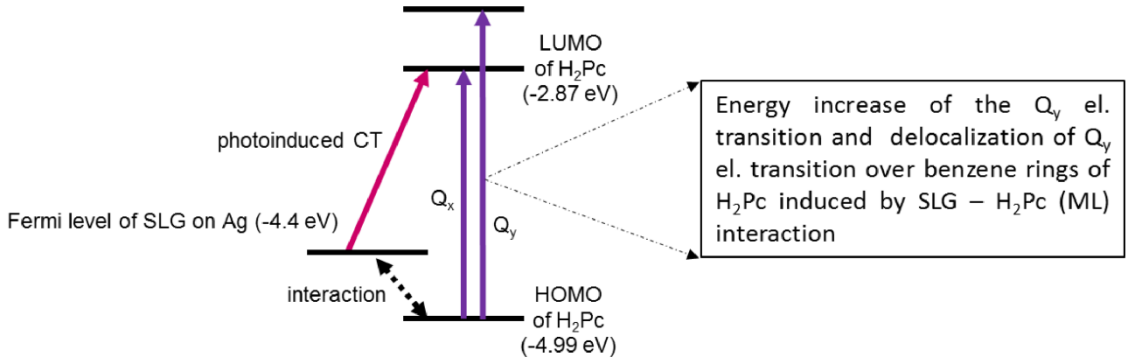

Figure 76: *Schematic depiction of two mechanisms of GERS identified in SERS +GERS of H_2Pc measured from the glassI/AgNPs/SLG/H_2Pc(ML) hybrid system as well as in GERS of H_2Pc obtained from the glassI/SLG/H_2Pc(ML) system at excitations in the 532-830 nm range. The energy of the Fermi level of SLG was determined to be ca -4.4 eV in both systems.*

4.3.8. Combined SERS + GERS of H2Pc: conditions of the additivity of two enhancement mechanisms

Evidence for a simultaneous operation of graphene-enhanced Raman scattering (GERS) and surface-enhanced Raman scattering (SERS) experienced by the free base phthalocyanine (H_2Pc) molecular monolayer (ML) localized on the top of single layer graphene (SLG) deposited over an array of annealed Ag NPs has been obtained. Preparation and characterization of the glassI/AgNPs/SLG/H_2Pc(ML) hybrid systems together with the glassI/SLG/H_2Pc(ML) and graphite/H_2Pc(ML) reference systems and their microRaman spectral mapping at five excitations in the 532-830 nm range, followed by determination of SERS, GERS and SERS+GERS enhancement factors (EFs) and construction of SERS+GERS and GERS excitation profiles (EPs) of H_2Pc vibrational modes, has emerged as an appropriate strategy for a detailed elucidation of the SERS+GERS mechanisms combination. Importantly, the same positions of Fermi level of SLG (at -4.4 eV) were obtained in the glassI/AgNPs/SLG/H_2Pc(ML) hybrid system probed for SERS+GERS and in the glassI/SLG/H_2Pc(ML) reference system probed for GERS. This was achieved by employment of the appropriate glass substrate which induces a small negative doping of SLG comparable to the doping of SLG by Ag.

GERS, SERS and GERS+ SERS EFs values have provided evidence that the combined SERS+GERS of H_2Pc is observed at all excitations in the 532-830 nm range.

This observation is attributed to a proper selection of the array of annealed Ag NPs as the plasmonic enhancer operating in the broad wavelength range. In addition to that, the mechanisms of SERS and GERS in combined SERS+GERS were found to operate additively (i.e. their enhancement factors are simply multiplicative) at 633 and 647 nm excitations. Furthermore, the comparison of SERS+GERS and GERS excitation profiles (EPs) of H_2Pc vibrational modes has revealed that the two distinct resonance features, i.e. the maximum at 633 nm and the normalized intensity increase from 785 to 830 nm excitation encountered in GERS EPs remain preserved in the SERS+GERS EPs as well. In this respect, the SERS+GERS EPs resemble the surface-enhanced resonance Raman scattering (SERRS) EPs, the shapes of which are modulated by resonance Raman scattering (RRS) of chromophoric molecules.

The particular mechanisms of GERS operating in both SERS+GERS and GERS of H_2Pc in our probed and reference hybrid systems, respectively, at different excitation wavelengths have been identified and found to be consistent with two of the four theoretically predicted mechanisms of GERS [24]. In particular, modification of localization of the resonant $Q_y(0\text{-}0)$ electronic transition (with maximum at ca 633-639 nm) within the H_2Pc molecule together with broadening and a small blue shift of its spectral band have been ascertained, and ascribed to the SLG - H_2Pc (ML) interaction. The resonance observed at 830 nm excitation is attributed to a charge transfer (CT) electronic transition from Fermi level of SLG to LUMO of H_2Pc with the calculated maximum at ca 810 nm. A slightly less pronounced (but still clearly detectable) manifestation of this CT transition in the SERS+GERS EPs in comparison to GERS EPs is the only difference between the SERS+GERS and GERS EPs of H_2Pc encountered under the conditions of our experiment, i.e. upon the same position of Fermi level of SLG in the probed and in the reference system, respectively.

In summary, observation of the combined SERS+GERS in a plasmonic NS/SLG/aromatic molecules hybrid system is conditioned by the overlap between the wavelength range of the plasmon resonance of the particular plasmonic NS and the range of wavelengths in which one of the mechanisms of GERS operates for a particular molecule. Another important aspect of SERS+GERS combination stems from the (now well established) fact that the GERS mechanism operation is, for any molecule, strongly dependent on the actual position of the Fermi level of SLG, which, in turn, is set to a particular value by doping of SLG by the plasmonic metal in the plasmonic NS/SLG/molecules hybrid system. This aspect has to be taken into account upon

designing and probing hybrid systems for SERS+GERS of aromatic molecules as well as upon selection of an appropriate substrate/SLG/molecules reference systems for evaluation of the GERS mechanism contribution to combined SERS + GERS.

5. Conclusion

Ag NPs originating from their hydrosols were demonstrated to be versatile building blocks of both 2D and 3D assemblies tailored specifically for SERS and SERRS of hydrophobic molecules, for SERS of SLG and for combined SERS+GERS of planar aromatic molecules.

In particular, incorporation of C_{60} molecules into 2D fused fractal aggregates prepared a two phase system constituted by the hydrosol of ca 27 nm sized Ag NPs modified by 0.1 M HCl and a solution of C_{60} in dichloromethane, followed by assembling of the 2D aggregates into 3D Ag nanosponge aggregates with incorporated C_{60} resulted into formation of excellent samples for SERS and SE(R)RS spectral detection of this hydrophobic adsorbate. Unperturbed (native) C_{60} molecules were detected at 445, 532, 633 and 780 nm excitation with the lowest LOD of 1×10^{-7} M at 532 nm excitation. At all four excitation wavelengths, the LODs of the Ag nanosponge aggregate samples with incorporated C_{60} were found to be one order of magnitude lower than those in the case of the reference sample prepared by overlaying of an empty Ag nanosponge aggregate with the solution of C_{60} in dichloromethane. While the latter strategy has been routinely used upon employment of Ag nanosponges as substrates for SERS, the former strategy is newly reported in this Thesis. The results of SERS spectral probing of Ag nanosponge aggregates with C_{60} demonstrates the importance of a purposeful incorporation of adsorbates into hot spots in fractal Ag NPs aggregates.

Analogous testing of the Ag nanosponge aggregates with incorporated molecules of a hydrophobic free base porphyrin H_2TPP (tetraphenylporfin) showed an interesting possibility of diprotonated H_4TPP^{2+} generation during the Ag nanosponge preparation, namely in the two phase Ag NP hydrosol +HCl/H_2TPP in dichloromethane system, in which the 2D fused fractal aggregates were produced. Diprotonation of H_2TPP in the two – phase system is catalyzed by the presence of Ag NPs, presumably by attachment of the parent H_2TPP to Ag(0) adsorption sites during assembling of Ag NPs into fused fractal aggregates at the water – dichloromethane interface. The concentration of HCl required for the H_4TPP^{2+} formation in this two phase system was at least by one order of magnitude lower than that in a control experiment performed in the absence of Ag NPs. The H_2TPP diprotonation process was found to proceed also in pores of the aggregates prepared as the "empty" aggregates in which, purposefully, the residues of the HCl – modified aqueous phase were left in the pores. By this process, the diprotonation

reaction was transferred onto nanoscale, and opens a possibility to employ the empty Ag nanosponge aggregate as a nanoreactor. On the other hand, the diprotonation of H_2TPP can be prevented by using NaCl instead of HCl as the pre-aggregating agent, as demonstrated by SERRS spectral detection of unperturbed H_2TPP.

Both 2D and 3D assemblies of AgNPs were tested as substrates for SERS of SLG (single layer graphene) in two types of hybrid samples, namely in glass/SLG/AgNPs assembly and glass/AgNPs assembly/SLG. The 2D assemblies were found to be superior to the 3D assemblies. In particular AgNPs-ET (ET= ethanethiol and/or ethanethiolate) films prepared by the previously reported procedures showed distinct advantages in each sample arrangement. In the glass/SLG/AgNPs-ET, SERS spectra of unperturbed SLG with almost no defects were obtained, and this result was attributed to the presence of adsorbed ET molecules forming a molecular spacer separating SLG from the surface of AgNPs. In the reverse hybrid sample arrangement, it was found that overdeposition of AgNPs-ET films on glass by SLG using the CVD procedure combined with NC (nitrocellulose) transfer procedure, ET molecules are removed from the surface and AgNPs are annealed. The resulting glass/AgNPs/SLG hybrid system showed SPE covering the overall visible spectral region, and thus represented an optimal platform for enhanced SERS + GERS of a planar aromatic molecule, namely H_2Pc.

For investigation of the enhanced SERS + GERS of a planar aromatic molecule, namely H_2Pc, the glass(I)/AgNPs assembly/SLG/H_2Pc(ML) (ML = monolayer) hybrid system was assembled, together with the graphite/H_2Pc(ML) reference system. The glass(I)/SLG/H_2Pc(ML) reference system was assembled on the basis of a hypothesis, that for a proper evaluation of the EM SERS enhancement factor and of the additivity of the EM mechanism of SERS and GERS, the reference GERS spectra have to be obtained from such glass(I)/SLG/H_2Pc(ML) reference system in which doping of SLG by glass(I) will be the same as the weak negative doping of SLG by Ag metal (NPs) in the glass(I)/AgNPs assembly/SLG/H_2Pc hybrid system. Fulfillment of this condition was accomplished by using a special microcopy glass slide, and verified by determination of position of the Fermi level of SLG, which, in both cases was estimated to be -4.4. eV. Under these conditions, the SERS + GERS and GERS excitation profiles are of the same shape, and the SERS and GERS enhancement factors were found to be additive.

Finally, operation of two of the four theoretically predicted mechanisms of GERS has been established both in SERS + GERS of the hybrid system, and in GERS of the reference system. The first mechanism is described as modification of the position (a small blue shift) of the Q_y electronic transition (with maximum at 633 – 639 nm) and of the localization of this electronic transition, namely its delocalization over the benzene rings of the H_2Pc molecule. The second mechanism is attributed to a CT (charge transfer) transition from Fermi level of SLG to the LUMO of H_2Pc (with maximum at ca 810 nm).

6. References

[1] Ron, R.; Haleva, E.; Salomon, A. Nanoporous Metallic Networks: Fabrication, Optical Properties, and Applications. *Adv. Mater.* **2018**, *30*, 1706755

[2] Procházka M., Surface-Enhanced Raman Spectroscopy, Bioanalytical, Biomolecular and Medical Applications, Springer International Publishing: Switzerland, **2016**.

[3] Matějka, P.; Vlčková, B.; Bednárová, L.; Maloň, P.: Advances and Challenges in Optical Molecular Spectroscopy Including Surface Plasmon Resonance-Based Methods for Bioanalysis, in *Natural Products Analysis: Instrumentation, Methods and Applications,* John Wiley and Sons, Hoboken, New Yersey, USA, **2014.**

[4] Cialla, D.; Marz, A.; Bohme, R.; Theil, F.; Weber, K.; Schmitt, M.; Popp, J. Surface-enhanced Raman spectroscopy (SERS): progress and trends. *Anal. Bioanal. Chem.* **2012,** *403*, 27 – 54.

[5] Schlücker, S., Ed. *Surface Enhanced Raman Spectroscopy. Analytical, Biophysical and Life Science Applications*, Wiley-VCH: Weinheim, Germany, 2011.

[6] McNay, G.; Eustace, D.; Smith, W.E.; Faulds, K.; Graham, D. Surface-Enhanced Raman Scattering (SERS) and Surface-Enhanced Resonance Raman Scattering (SERRS): A Review Applications. *Appl. Spectros.* **2011**, *65*, 825 – 837.

[7] Le Ru, E.C.; Etchegoin, P.G. *Principles of Surface-enhanced Raman Spectroscopy and Related Plasmonic Effects*, Elsevier, Elsevier: Amsterdam, The Netherlands, **2009**.

[8] Maier, S.A. Plasmonics: Fundamentals and Applications, Springer International Publishing, **2017.**

[9] Aroca, R. *Surface-Enhanced Vibrational Spectroscopy,* John Wiley & Sons, Ltd.:, Chichester, U.K., **2006**.

[10] Kneipp, K.; Moskovits, M.; a Kneipp, H. *Surface-Enhanced Raman Scattering. Physics and Applications.*, Topics in Applied Physics, *103,* Springer-Verlag: Berlin, Heidelberg, **2006**.

[11] Cotton, T.M.; Spectroscopy of Surfaces in *Advances in Spectroscopy, vol. 16*, John Wiley & Sons Ltd.: Chicester, U.K., **1988**; pp. 91-153.

[12] Moskovits, M. Surface-ehnanced Spectroscopy. *Rev. Mod. Phys*. **1985**, *57*, 783 – 826.

[13] Stockman, M.I.; Shalaev, V.M.; Moskovits, M.; Botet, R.; Georgie, T.F. Enhanced Raman scattering by fractal clusters: Scale-invariant theroy. *Phys. Rev. B* **1992**, 46, 2821 – 2830.

[14] Zhang, P.; Haslett, T.L.; Douketis, C.; Moskovits, M. Model in self-affine fractal interfaces observed by near-field microscopy. *Phys. Rev. B.* **1998**, *57*, 15513 – 15518.

[15] Johansson, P.; Xu, H; Kall, M. Raman spectroscopic studies of terthiophenes for molecular electronics. *Phys. Rev. B* **2006**, *72*, 035427-1-035427-16.

[16] Xu, H.; Aizpurua, J.; Kall, M.; Apell, P. Electromagnetic contributions to single-molecule sensitivity in surface-enhanced Raman scattering. *Phys. Rev. E* **2000**, *62*, 4318 – 4324.

[17] Vlčková, B; Moskovits, M.; Pavel, I.; Šišková, K.; Sládková, M.; Šlouf, M. Single-molecule surface-enhanced Raman spectroscopy from a molecular-bridged silver nanoparticle dimer. *Chem. Phys. Lett*. **2008**, *455*, 131-134.

[18] Jorio, A.; Saito, R.; Dresselhaus, G.; Dresselhaus, M.S. *Raman Spectroscopy in Graphene Related Systems*, Wiley-VCH Verlag GmbH&Co.KgaA:Weinheim, Germany, **2011**.

[19] Ferrari, A. C.; Basko, D. M. Raman Spectroscopy as a Versatile Tool for Studying the Properties of Graphene. *Nat. Nanotechnol.* **2013**, *8*, 235 – 245.

[20] Vlčková, B.; Matějka, P.; Šimonová, J.; Čermáková, K.; Pančoška, P.; Baumruk, V. Surface-Enhanced Resonance Raman-Spectra of Free-Base 5,10,15,20-Tetrakis(4-Carboxyphenyl)porphyrin and Its Silver Complex in Systems with Silver Colloid: Direct Adsorption in Comparison to Adsorption via Molecular Spacer. *J. Phys. Chem.* **1993**, *97*, 9719 – 9729.

[21] Michl, M.; Vlčková, B.; Mojzeš, P. Colloid-1-alkanethiol Films: Spacer-modified Substrates for SERRS Spectroscopy of Chromophoric Molecules. *Vibr. Spectros.* **1999**, *19*, 239 – 242.

[22] Vlčková, B.; Šmejkal, P.; Michl, M.; Procházka, M.; Mojzeš, P.; Lednický, F.; Pfleger, Surface-enhanced resonance Raman spectroscopy of porphyrin and metalloporphyrin species in systems with Ag nanoparticles and their assemblies. *J. Inorg. Biochem.* **2000**, *79*, 295 – 300.

[23] Ling, X.; Xie, L.; Fang, Y.; Xu, H.; Zhang, H.; Kong, J.; Dresselhaus, M. S.; Thang, J.; Liu, Z. Can Graphene Be Used as a Substrate for Raman Enhancement? *Nano Lett.* **2010**, *10*, 553–561.

[24] Barros, E. B.; Dresselhaus, M. S. Theory of Raman Enhancement by Two-Dimensional materials: Applications for Graphene-Enhanced Raman Spectroscopy. *Phys. Rev. B* **2014**, *90*, 90035443.

[25] Ling, X.; Huang, S.; Mao, N.; Kong, J.; Dresselhaus, M. S.; Zhang, J. Lighting Up the Raman Signal of Molecules in the Vicinity of Graphene Related Materials. *Accounts Chem. Res.* **2015**, *48*, 1862–1870.

[26] Huang, S.; Ling, X.; Liang, L.; Song, Y.; Fang, W.; Zhang, J.; Kong, J.; Meunier, V.; Dresselhaus, M. S. Molecular Selectivity of Graphene-Enhanced Raman Scattering. *Nano Lett.* **2015**, *15*, 2892–2901.

[27] Fleischmann, M; Hendra, P.J.; McQuillan, A.J. Raman spectra of pyridine adsorbed at a silver electrode. *Chem. Phys. Lett.* **1974**, *26*, 163 – 166.

[28] Jeanmaire, D.L.; van Duyne, R. Surface raman spectrochemistry: Part I. Heterocyclic, aromatic, and aliphatic amines adsorbed on the anodized silver electrode. *J. Electroanal. Chem.* **1977**, *84*, 1 – 20.

[29] Creighton, J.A.; Blatchford, C.G.; Albrecht, M.G. Plasma resonance enhanced Raman scattering by pyridine adsorbed on silver or gold sol particles of size comparable to the excitation wavelength. *J. Chem. Soc. 2, Faraday Trans.* **1979**, *75*, 790 – 798.

[30] Moskovits, M. Surface roughness and the enhanced intensity of Raman scattering by molecules adsorbed on metals. *J. Chem. Phys.* **1978**, *69*, 4159 – 4161.

[31] Weitz, D.A.; Garoff, S.: The Enhancement of Raman Scattering, Resonance Raman Scattering, and Fluorescence from Molecules Adsorbed on a Rough Silver Surface. *J. Phys. Chem*. **1983**, *78*, 5324-5338.

[32] Campion, A.; Kambhampati, P. Surface-enhanced Raman scattering. *Chem. Soc. Rev.* **1998**, *27*, 241 – 250.

[33] Kneipp, K.; Kneipp, H.; Itzkan, I.; Ramachandra, D.R.; Feld, M.S. Ultrasensitive chemical analysis by Raman spectroscopy. *Chem. Rev*., **1999**, *99*, 2957 – 2962.

[34] Moskovits, M. Surface-enhanced Raman spectroscopy: a brief retrospective. *J. Raman. Spectrosc.* **2005**, *36*, 485 – 496.

[35] Lombardi, J.R.; Birke, R.L. A Unified View of Surface-Enhanced Raman Scattering. *Acc. Chem. Res.* **2009**, *42*, 734 – 742.

[36] Ahern, A.A.; Garrell, R.L. In situ photoreduced silver nitrate as a substrate for surface-enhanced Raman spectroscopy. *Anal. Chem* **1987**, *59*, 2813 – 2816.

[37] Leopold, N.; Lendl, B. A. A new method for fast preparation of highly surface-enhanced Raman scattering (SERS) active silver colloids at room temperature by reduction of silver nitrate with hydroxylamine hydrochloride. *J. Phys. Chem. B* **2003**, *107*, 5273 – 5727.

[38] Larmour, I.A.; Faulds, K.; Graham, D. SERS aktivity and stability of the most frequently used silver colloids. *J. Raman Spectrosc.* **2012**, *43*, 202 – 206.

[39] Lee, P.C.; Meisel D. Adsorption and surface-enhanced Raman of dyes on silver and gold sols. *J. Phys. Chem* **1982**, *86*, 3391 – 3395.

[40] Fojtik, A.; Henglein, A. Laser Ablation of Films and Suspended Particles in a Solvent – Formation of Clusters and Colloid Solutions. *Ber. Bunsenges. Phys. Chem*. **1993**, *97*, 252 – 254.

[41] Neddersen, J.; Chumanov, G.; Cotton, T.M. Laser Ablation of Metals: A New Method for Preparing SERS Active Colloids. *Applied Spectroscopy* **1993**, *97*, 1959 – 1964.

[42] Procházka, M.; Mojzeš, P.; Štěpánek, J.; Vlčková, B.; Turpin, P.Y. Probing applications of laser ablated Ag colloids in SERS spectroscopy: Improvement of ablation procedure and SERS spectral testing. *Anal. Chem*. **1997**, *69*, 5103 – 5108.

[43] Šišková, K.; Vlčková, B.; Turpin, P.Y.; Thorel, A.; Procházka, M. Laser Ablation of Silver in Aqueous Solutions of Organic Species: Probing Ag Nanoparticle-Adsorbate Systems Evolution by Surface-Enhanced Raman and Surface Plasmon Extinction Spectra. *J. Phys. Chem. C.* **2011**, *115*, 5404 – 5412.

[44] Solecká-Čermáková, K.; Vlčková, B.; Lednický, F. Structural characteristic of Ag colloid-adsorbate films determined from transmission electron microscopic images: Fractal dimensions, particle size and spacing distributions, and their relationship to formation and optical responses of the films. *J. Phys. Chem*. **1996**, *100*, 4954 – 4960.

[45] Michl, M.; Vlčková, B.; Šloufová, I.; Mojzeš, P. SERS and SERRS Spectra of Unperturbed Hydrophobic Molecular and Biomolecular Species Embedded in Sulphuric Acid – modified Silver Nanoparticle Films. *Can. J. Anal. Sci. Spectros.* **2003**, *48*, 46 – 54.

[46] Tang, S.; Vongehr, S.; Wang, Y.; Cui, J.; Wang, X.; Meng, X. Versatile synthesis of high surface area multi-metallic nanosponges allowing control over nanostructure and alloying for catalysis and SERS detection. *J. Mater. Chem. A* **2014**, *2*, 3648 – 3660.

[47] Marques, P.A.A.P.; Nogueira, I.S.H.; Pinto, J.B.R.; Neto, P.C.; Trindade, T. Silver-bacterial cellulosic sponges as active SERS substrates. *J. Raman. Spec.* **2008**, *39*, 439 – 443.

[48] Carrión-Carrillo, C.; Simonet, B.M.; Valcárcel, M.; Lendl, B. Determination of pesticides by capillary chromatography and SERS detection using a novel Silver-Quantum dots "spongge" nanocomposite. *J. Chromatography A* **2012**, *1225*, 55 – 61.

[49] Ron, R.; Gachet, D.; Rechav, K.; Salomon, A. Direct Fabrication of 3D Metallic Networks and Their Performance. *Adv. Mater.* **2017**, *29*, 1604018.

[50] Sutrová, V. Bachelor Thesis, 2013, Charles University, Prague

[51] Sutrová V. Diploma Thesis, 2015, Charles University, Prague

[52] Sutrová, V.; Šloufová, I.; Nevoralová, M.; Vlčková, B. SERS microRaman spectral probing of adsorbate-containing, liquid-overlayed nanosponge Ag aggregates assembled from fractal aggregates. *J. Raman. Spec.* **2015**, *46*, 559 – 565.

[53] Kroto, H.W.; Heath, J.R.; O´Brien, S.C.; Curl, R.F.; Smalley, R.E. C_{60}: Buckminsterfullerene. *Nature*, **1985**, *318*, 162 – 163.

[54] Diederich, F.; Rubin, Y. Synthetic Approaches toward Molecular and Polymeric Carbon Allotropes. *Angew. Chem. Int.* **1992**, *31*, 1101 – 1123.

[55] Bethnune, D.S.; Meijer, G.; Wade, C.T.; Rosen, H.J..; Golden, W. G.; Seki, H.; Brown, Ch.A.; de Vries, M.S. Vibrational Raman and infrared spectra of chromatographically separated C_{60} and C_{70} fullerene clusters. *Chem. Phys. Lett.* **1991**, *179*, 181 – 186.

[56] Schettino, V.; Pagliai, M.; Ciabini, L.; Cardini, G. The vibrational Spectrum of Fullerene C_{60}. *J. Phys. Chem. A* **2001**, *105*, 11192 – 11196.

[57] Akers, K.L.; Cousins, L.M.; Moskovits, M. Surface-enhanced vibrational Raman spectroscopy of C_{60} and C_{70} on rough silver surfaces. *Chem. Phys. Lett.* **1992**, *190*, 614 – 620.

[58] Rosenberg, A.; DiLella, D.P.n Anomalously enhanced Raman scattering from C_{60} on Ag surfces. *Chem. Phys. Lett.* **1994**, *223*, 76 – 81.

[59] Dolphin, D. *The Porphyrins*, vols. 1 – 7, Academic Press, New York, **1978**.

[60] *The Porphyrin Handbook, Volume 16: Applicatons: Past, Present and Future*; Kadish, K., Guilard, R., Smith, K. M., Eds.; Academic Press, **2003**

[61] Saini, G.S.S. Resonance Raman study of free-base tetraphenylporphine and its dication. *Spectrochim. Acta A* **2006**, *64*, 981 – 986.

[62] Xu, L.C.; Li, Z.Y.; Tan, W.; He, T.J.; Liu, F.Ch.; Chen, D.M. Density functional theory studies on Raman and IR spectra of *meso*-tetraphenylporphyrin diacid. *Spectrochim. Acta A* **2005**, *62*, 850 – 862.

[63] Hajduková, N.; Procházka, M.; Molnár, P.; Štěpánek, J. SERRS of free-base porphyrins on immobilized metal gold and silver nanoparticles. *Vib. Spectros*. **2008**, *48*, 142 – 147.

[64] Munoz, Z.; Cohen, A.S.; Nguyen, L.M.; McIntosh, T.A., Hoggard, P.E. Photocatalysis by tetraphenylporphyrin of the decomposition of chloroform. *Photochem. Photobiol. Sci.* **2008**, *7*, 337 – 343.

[65] *The Porphyrin Handbook, Volume 17: Phthalocyanines*: *Properties and Materials*; Kadish, K., Guilard, R., Smith, K. M., Eds.; Academic Press, **2003**

[66] Menaa, B.; Takahashi, M.; Tokuda, Y.; Yoko, T. Dispersion and Photoluminescence of Free-Metal Phtalocyanine Doped in Sol-Gel Polyphenylsiloxane Glass Film. *J. Photochem. Photobiol. A* **2007**, *194,* 362 – 366.

[67] Heutz, S.; Salvan, G.; Silaghi, S.D.; Jones, T.S.; Zahn, D.R.T. Raman Scattering as a Probe of Crystallinity in PTCDA and H2Pc Single-Layer and Double-Layer Thin Film Heterostructures. *J. Phys. Chem. B* **2003**, *107*, 3782 – 3788.

[68] Murray, C.; Dozova, N.; McCaffrey, J.G.; Fitzgerald, S. Infra-red and Raman spectroscopy of free-base and zinc phthalocyanines isolated in matrices. *Phys. Chem. Chem. Phys.* **2010**, *12*, 10406 – 10422.

[69] Brotman, A.; Burstein, E. Raman Scattering-Excitation Profiles of Molecules Adsorbed on Metal Surfaces: Free-Base Phthalocyanine on Silver. *Phys. Scripta* **1985**, *32*, 385–390.

[70] Murray, C.; Dozova, N.; McCaffrey, J. G.; Shafizadeh, N.; Chin, W.; Broquier, M.; Crépin, C. Visible Luminescence Spectroscopy of Free-Base and Zinc Phthalocyanines Isolated in Cryogenic Matrices. *Phys. Chem. Chem. Phys.* **2011**, *13*, 17543–17554.

[71] Aroca, R.; Loutfy, R.O. Enhanced Raman scattering from molecular-dye films on silver. *J. Ram. Spec.* **1982**, *12*, 262 – 265.

[72] Bonaccorso, F.; Sun, Z.; Hasan, T.; Ferrari, A.C.; Graphene photonics and optoelectronics. *Nat. Photonics* **2010**, *4*, 611-622.

[73] Novoselov, K.S.; Geim, A.K.; Morozov, S:V.; Jiang, D.; Zhang, Y.; Dubonos, S.V.; Grigorieva, I.V.; Firsov, A.A. Electric Field Effect in Atomically Thin Carbon Films. Science, 2004, 306, 666 – 669.

[74] Kalbáč, M.; Frank, O.; Kavan, L. The Control of Graphene Double-Layer Formation in Copper-Catalyzed Chemical Vapor Deposition. *Carbon* **2012**, *50*, 3682–3687.

[75] Hallam, T.; Berner, N. C.; Yim, C.; Duesberg G. S. Strain, Bubbles, Dirt, and Folds: A Study of Graphene Polymer-Assisted Transfer. *Adv. Mater. Interfaces* **2014,** *1*, 1400115.

[76] Schedin, F.; Lidorikis, E.; Lombardo, A.; Kravets, V.G..; Geim, A.K.; Grigorenko, A.N.; Novoselov, S.K.; Ferrari, C.A. Surface-enhanced Raman Spectroscopy of Graphene. *ACS Nano* **2010**, *4*, 5617-5626.

[77] Fu, X.; Bei, F.; Wang, X.; O´Brien, S.; Lombardi R.J. Excitation profile of surface-enhanced Raman scattering in graphene-metal nanoparticle based derivatives, *Nanoscale* **2010**, *2*, 1461-1466.

[78] Heeg, S.; Fernandez-Garcia, R.; Oikonomou, A.; Schedin, F.; Narula, R.; Maier, A.S.; Vijayaraghavan, A.; Reich, S. Polarized Plasmonic Enhancement by Au Nanostructures Probed through Raman Scattering of Suspended Graphene. *Nano Lett*. **2013**, *13*, 301-308

[79] Kravets, V. G.; Schedin, F.; Jalil, R.; Britnell, L.; Novoselov, K. S.; Grigorenko, A. N., Surface Hydrogenation and Optics of a Graphene Sheet Transferred onto a Plasmonic Nanoarray. *J Phys Chem C* **2012**, *116*, 3882-3887.

[80] Xu, W. G.; Mao, N. N.; Zhang, J., Graphene: A Platform for Surface-Enhanced Raman Spectroscopy. *Small* **2013**, *9*, 1206-1224.

[81] Kalbáč, M.; Valeš, V.; Vejpravová, J., The Effect of a Thin Gold Layer on Graphene: A Raman Spectroscopy Study. *RSC Adv* **2014** *4*, 60929-60935.

[82] Zhao, Y.; Zhu, Y. W., Graphene-Based Hybrid Films for Plasmonic Sensing. *Nanoscale* **2015**, *7*, 14561-14576.

[83] Weiss, J.E.; Costa, S.; Frank, O.; Fridrichová, M.; Vlčková, B.; Vejpravová, J.; Kalbac, M. SERS of Isotopicallly Labeled 12C/13C Graphene Bilayer–Gold Nanostructured Film Hybrids: Graphene Layer as Spacer and SERS Probe. *J. Phys. Chem. C* **2017**, *121*, 11680-11686.

[84] Gong, T.; Zhan, J.; Zhu, Y.; Wang, W.; Zhang, X. Optical properties and surface-enhanced Raman scattering of hybrid structures with Ag nanoparticles and graphene. *Carbon* **2016**, *102*, 245-254.

[85] Hao, Q.; Wang, B.; Bossard, J.A.; Kiraly, B.; Zeng, Y.; Chiang, I-K.; Jensen, L.;Werner, D.H.; Huang, T.J. Surface-Enhanced Raman Scattering Study on Graphene-Coated Metallic Nanostructure Substrates. *J. Phys. Chem. C* **2012**, *116*, 7249-7254.

[86] Kang, L.; Chu, J.; Zhao, H.; Xu, P.; Sun, M. Recent Progress in the Applications of Graphene in Surface-Enhanced Raman Scattering and Plasmon-Induced Catalytic Reactions. *J. Mater. Chem*. **2015**, *3*, 9024-9037.

[87] Xu, S.; Man, B.; Jiang, S.; Wang, J.; Wei, J.; Xu, S.; Liu, H.; Gao, S.; Liu, H.; Li, Z.; Li, H.; Qiu, H. Graphene/Cu Nanoparticle Hybrids Fabricated by Chemical Vapor Deposition as Surface-Enhanced Raman Scattering Substrate for Label-Free Detection of Adenosine. *Appl. Mater. Interfaces* **2015**, *7*, 10977-10987.

[88] Gopal, J.; Abdelhamid, H.N.; Huang, J.-H.; Wu, H.-F Nondestructive Detection of the Freshness of Fruits and Vegetables Using Gold and Silver Mediated Graphene Enhanced Raman Spectroscopy. *Sens. Actuators B* **2016**, *224*, 413-424.

[89] Xu, S.; Jiang, S.; Wang, J.; Wei, J.; Yue, W.; Ma, Y. Graphene Isolated Au Nanoparticle Arrays with High Reproducibility for High-Performance Surface-Enhanced Raman Scattering. *Sens. Actuators B* **2016**, *222*, 1175-1183.

[90] Uhlířová, T. Excitation Wavelenght-Dependent Raman Spectra of Single-Layer Graphene-Phthalocyanine Hybrid Systems. **2016**, Bachelor Thesis, Charles University, Prague.

[91] Schettino, V.; Salvi, P.R.; Bini, R.; Cardini, G. On the vibrational assignment of fullerene C_{60}. *J. Chem. Phys.* **1994**, *101*, 11079 – 11081.

[92] Dědic, R.; Molnár, A.; Svoboda, A.; Hála, J. Light-induced TPP photoproduct formation in chloroform and protective role of lipids. *J. Porphyr. Phtalocyanines* **2010**, *14*, 962 – 967.

[93] Hore, D.K.; Walker, D.S.; MacKinnon, L.; Richmond, G.L. Molecular Structure of the Chloroform – Water and Dichloromethane – Water Interfaces. *J. Phys. Chem. C* **2007**, *111*, 8832 – 8842 .

[94] Metzger, C.; Rémi, S.; Liu, M; Kusminskiy, S.V.; Castro Neto, A.H.; Swan, A.K.; Goldberg, B.B. Biaxial Strain in Graphene Adhered to Shallow Depressions. *Nano Lett*. **2010**, *10*, 6 – 10.

[95] Bensebaa, F.; Zhou, Y.; Brolo, A.G.; Irish, D.E.; Deslandes, Y.; Kruus, E.; Ellis, T.H. Raman characterization of metal-alkanethiolates, *Spectrochim. Acta A*, **1999**, *55*, 1229-1236.

[96] Kudelski, A. Characterization of thiolate-based mono- and bilayers by vibrational spectroscopy: A review. *Vibrational Spectrosc* **2005**, *39,* 200-213.

[97] Socrates, G. *Infrared and Raman Characteristic Group Frequencies*, John Wiley & Sons, LTD, England, 2001.

[98] Bohren, C.F. and Huffman, D.R. *Absorption and Scattering of Light by Small Particles*, WILEY-VCH Verlag GmbH & Co. KGaA, Weinheim, **2004.**

[99] Cialla, D.; Petschulat, J.; Hübner, U.; Schneidewing, H.; Zeisberger, M.; Mattheis, R.; Pertsch, T.; Schmitt, M.; Möller, R. Investigation on the Second Part of the electromagnetic SERS Enhancement and Resulting Fabrication Strategies of Anisotropic Plasmonic Arrays, *Chem. Phys. Chem.*, **2010**, *11*, 1918-1924.

[100] Niu, J.; Shin, J.Y.; Son, J.; Lee, Y.; Ahn, J.H.; Yang, H. Shifting of surface plasmon resonance dute to electromagnetic coupling between graphene and Au nanoparticles, *Optics Express*, **2010**, *20*, 19690

[101] Liu, Y.; Cheng, R.; Zhou, H.; Bai, J.; Liu, G.; Liu, L; Huang, Y.; Duan, X.; Plasmon resonance enhanced multicolour photodetection by graphene. *Nat. Commun*., **2011**, *2*, 579.

[102] Niu, J.; Shin, J.Y.; Son, J.; Lee, Y.; Ahn, J.H.; Yang, H. Shifting of surface plasmon resonance dute to electromagnetic coupling between graphene and Au nanoparticles, *Optics Express*, **2010**, *20*, 19690

[103] Zhu, J.; Liu, Q.H.; Lin, T. Manipulating light absorption of graphene using plasmonic nanoparticles, *Nanoscale*, **2015**, *5*, 7785 – 7789

[104] Du, Y.; Zhao, Y.; Qu, Y.; Chen, Ch.-H.; Chen, Ch.-M.; Chuang Ch.-H.; Zhu, Y.; Enhanced light-matter interaction of graphene-gold nanoparticle hybrid films for high-performance SERS detection, *J. Mater. Chem. C*, **2014**, *2*, 4683 – 4691.

[105] Lee, S.; Kim, J. Desing of optical metamaterial mirror with metallic nanoparticles for floating-gate graphene optoelectronic devices, *Optic Express*, **2015**, *23*, 21809.

[106] Teridi, M.A.M.; Sookhakian, M.; Basirun, W.J.; Zakaria, r.; Schneider, F.K.; Silva, W.J.; Kim, J.; Lee, S.J.; Kim, H.P.; Yusoff, A.R.M.; Jang, J. Plasmon enhanced organic devices utilizing highly ordered nanoimprinted gold nanodisk and nitrogen doped graphene, *Nanoscale*, **2015**,*7*,7091 – 7100.

[107] Gunnarsson, L.; Rindzevicius, T.; Prikulis, J.; Kasemo, B.; Käll, M.; Zou, S.; Schatz. G.C. Confined Plasmon in Nanofabricated Single Silver Particle Pairs: Experimental

Observation of Strong Interparticle Interactions, *J. Phys. Chem. B*, **2005**, *109*, 1079 – 1087.

[108] Feng, X.; Ruan, F.; Hong, R.; Ye, J.; Hu, J.; Hu., G.; Yang, Z. Synthetically Directed Self-Assembly and Enhanced Surface-Enhanced Raman Scattering Property of Twinned Crystalline Ag/Ag Homojunction Nanoparticles. *Langmuir*, **2011**, *27*, 2204 – 2210.

[109] Giovannetti, G.; Khomyakov, P.A.; Karpan, V.M.; Brink, J.; Kelly, P.J. Doping graphene with metal contacts, *Phys. Rev. Lett.,* 2008, *101*, 026803.

[110] Tamaru, H.; Kuwata, H.; Miyazaki, H.T.; Miyano, K. Resonant light scattering from individual Ag nanoparticles and particle pairs. *Applied Phys. Lett*., **2002**, *80*, 1826 – 1828.

[111] Tuschel, D. Selecting an Excitation Wavelength for Raman Spectroscopy, *Spectroscopy*, **2016***, 31,* 14-23.

[112] Dissanayake, D. M. N. M.; Ashraf, A.; Dwyer, D.; Kisslinger, K.; Zhang, L.; Pang, Y.; Efstathiadis, H.; Eisman, M. D. Spontaneous and Strong multilayer Graphene n-doping on Soda-Lime Glass and its Applications in Graphene-Semiconductor Junctions. *Sci. Reports* **2016**, *6*, 21070.

[113] Lin, W.I.; Gholami, M.F.; Beyer, P.; Severin, N.; Shao, F.; Zenobi, R.; Rabe, J. Strongly Enhanced Raman Scattering of Cu-Phthalocyanine Sandwiched between Graphene and Au(111). *Chem. Commun*. **2017**, *53*, 724 – 727.

[114] Clark, R. J. H.; Dines, T. J. Resonance Raman Spectroscopy, and its Applications to Inorganic Chemistry. *Angew. Chem. Int. Ed. Engl.* **1986,** *25*, 131-158.

[115] Cook, M.; Chambrier, I. In *The Porphyrin Handbook, Volume 17: Phthalocyanines*: *Properties and Materials*; Kadish, K., Guilard, R., Smith, K. M., Eds.; Academic Press, **2003**; Chapter Phthalocyanine Thin Films: Deposition and Structural Studies, pp 37–128.

[116] Nilson, K.; Ahlund, J.; Brena, B.; Göthelid, E.; Schiessling, J.; Martensson, N.; Puglia, C. Scanning Tunneling Microscopy Study of Metal-Free Phthalocyanine Monolayer Structure on Graphite. *J. Chem. Phys.* **2007**, *127* 114702.

[117] Tackley, D. R.; Dent, G.; Smith, W. E. Phthalocyanines: Structure and Vibrations. *Phys. Chem. Chem. Phys.* **2001**, *3*, 1419–1426.

7. List of abbreviation

NS/NSs	Nanostructure/Nanostructures
NP/ NPs	Nanoparticle/ Nanoparticles
SERS	Surface-enhanced Raman scattering
SER(R)S	Surface-enhanced (resonance) Raman scattering
SERRS	Surface-enhancement resonance Raman scattering
EM	Electromagnetic mechanism
MR	Molecular resonance
SLG	Single layer graphene
GERS	Graphene-enhanced Raman scattering
SPE	Surface plasmon extinction
UV/VIS	Ultra-violet/Visible
LOD/LODs	Limit of detection/ Limits of detection
PA	Pre-aggregating agent
ET	Ethanethiol and/or Ethanethiolate
H_2TPP	5,10,15,20-tetraphenyl-21H,23H-porphine
H_4TPP^{2+}	Diprotonated (diacid) form of 5,10,15,20-tetraphenyl-21H,23H-porphine
H_2Pc	29H,31H-Phthalocyanine
BH1 hydrosol	AgNPs hydrosol prepared by reduction of 2.2×10^{-3}M $AgNO_3$ by 1.2×10^{-3} M $NaBH_4$
BH2 hydrosol	AgNPs hydrosol prepared by reduction of 4.6×10^{-3}M $AgNO_3$ by 1.2×10^{-3} M $NaBH_4$
HA-AgNPs hydrosol	AgNPs hydrosol prepared by reduction of 1.2×10^{-2} M $AgNO_3$ by 1.6×10^{-3}M $NH_2OH\cdot HCl$
CT	Charge transfer
NCA	Normal coordinate analysis
EP	Excitation profile
EF	Enhancement factor

8. Supplement

8.1. Publication I: Raman excitation profiles of hybrid systems constituted by single-layer graphene and free base phthalocyanine: Manifestation of two mechanisms of graphene-enhanced Raman scattering

Tereza Uhlířová[a], Peter Mojzeš[b], Zuzana Melniková[c] Martin Kalbáč[c], Veronika Sutrová[a,d], Ivana Šloufová[a], Blanka Vlčková[a*]

[a] Charles University, Faculty of Science, Department of Physical and Macromolecular Chemistry, Hlavova 8, Prague 2, 128 40, Czech Republic, vlc@natur.cuni.cz

[b] Charles University, Faculty of Mathematics and Physics, Institute of Physics, Ke Karlovu 5, Prague 2, 121 16, Czech Republic

[c] J. Heyrovsky Institute of Physical Chemistry of the ASCR, v.v.i, Dolejškova 3, 182 21 Prague 8, Czech Republic

[d] Institute of Macromolecular Chemistry AS CR, Heyrovsky Sq. 2, 162 06 Prague 6, Czech Republic

My contribution:

Reference sample preparation, SEM imaging, participation on MS preparation.

Research article

Journal of RAMAN SPECTROSCOPY

Received: 9 March 2017 Revised: 14 June 2017 Accepted: 14 June 2017 Published online in Wiley Online Library: 26 July 2017

(wileyonlinelibrary.com) DOI 10.1002/jrs.5206

Raman excitation profiles of hybrid systems constituted by single-layer graphene and free base phthalocyanine: Manifestations of two mechanisms of graphene-enhanced Raman scattering

Tereza Uhlířová,[a] Peter Mojzeš,[b] Zuzana Melniková,[c] Martin Kalbáč,[c] Veronika Sutrová,[a,d] Ivana Šloufová[a] and Blanka Vlčková[a]*

The ability of single-layer graphene (SLG) to enhance Raman scattering of planar aromatic molecules denoted graphene-enhanced Raman scattering (GERS) is currently the subject of focused interest. We report on manifestations of two mechanisms of GERS in Raman spectra of glass/SLG/free base phthalocyanine (H_2Pc) monolayer (ML) hybrid systems: (i) photoinduced charge transfer from SLG Fermi level to LUMO of H_2Pc excited at onset of the near IR region, and (ii) modification of resonance Raman scattering of H_2Pc in the visible region by SLG–H_2Pc interaction resulting into delocalization of the electronic transition over the benzene rings of H_2Pc. Glass/SLG/H_2Pc hybrid systems with either a bilayer or a monolayer of H_2Pc molecules and a graphite/H_2Pc (ML) reference system were prepared by a spectrally controlled adsorption–desorption of H_2Pc from solution, followed by Raman mapping of samples at excitation wavelengths in the 532–830 nm range, construction of excitation profiles for H_2Pc Raman bands of the glass/SLG/H_2Pc samples and determination of GERS enhancement factors for the glass/SLG/H_2Pc (ML) sample *versus* the graphite/H_2Pc (ML) reference sample (3–24 at 633 nm and 3–19 at 647 nm excitations). Selectivity of the excitation profiles and of the GERS enhancement factors with respect to localization of the vibrational modes within the H_2Pc molecule demonstrates involvement of a different resonant electronic transition in each of the two mechanisms of GERS. Copyright © 2017 John Wiley & Sons, Ltd.

Keywords: graphene-enhanced Raman scattering; single-layer graphene; free base phthalocyanine; Raman excitation profiles; photoinduced charge transfer

Introduction

Raman spectroscopy is currently one of the principal tools used for characterization of graphene, a planar sheet of sp^2-bonded carbon atoms forming a hexagonal honeycomb crystal lattice.[1,2]

The ability of graphene to enhance Raman scattering of molecules located on graphene surfaces in hybrid systems was first reported in 2010 and denoted graphene-enhanced Raman scattering (GERS).[3] Recently, the six years of activity in this research field have been reviewed.[4,5] The magnitude of the GERS enhancement has been found to depend on several factors, such as the structure and symmetry of a molecule, energy of its highest occupied molecular orbital (HOMO) and lowest unoccupied molecular orbital (LUMO), molecule–graphene distance, graphene sample thickness, graphene Fermi level energy and laser excitation wavelength. About 30 different molecules have already been probed for GERS, and the best results have been obtained for planar aromatic molecules and single-layer graphene (SLG).[4,5] The average GERS enhancement factor values were found to be in the 2–15 range (for planar molecules on SLG surface), while the largest GERS enhancement factor of 47 was achieved for CuPc (Pc = phthalocyanine) at 633-nm excitation.[4,5]

These experimental results have been rationalized by the theoretical treatment of the GERS effect reported in 2014.[6] The origin of GERS has been attributed to a charge transfer between Fermi level of graphene and HOMO or LUMO of an aromatic molecule of D_{nh} symmetry, or to a mutual interaction between close lying Fermi level of graphene and HOMO or LUMO of the molecule,

* Correspondence to: Blanka Vlčková, Charles University, Faculty of Science, Department of Physical and Macromolecular Chemistry, Hlavova 8, Prague 2 128 40, Czech Republic.
E-mail: vlc@natur.cuni.cz

a Faculty of Science, Department of Physical and Macromolecular Chemistry, Charles University, Hlavova 8, Prague 2 128 40, Czech Republic

b Faculty of Mathematics and Physics, Institute of Physics, Charles University, Ke Karlovu 5, Prague 2 121 16, Czech Republic

c J. Heyrovsky Institute of Physical Chemistry of the ASCR, v.v.i, Dolejškova 3, 182 21, Prague 8, Czech Republic

d Institute of Macromolecular Chemistry AS CR, Heyrovsky Sq. 2, 162 06, Prague 6, Czech Republic

and the resonance conditions for the largest GERS enhancements have been formulated.[5,6]

Free base phthalocyanine (H_2Pc), a planar aromatic molecule of D_{2h} symmetry (Fig. 1, inset), has been a subject of numerous spectroscopic studies motivated by its interesting electronic structure[7–11] as well as by its potential applications in molecular photonics and optoelectronics,[12,13] in gas sensor development[14] and as a sensitizer in the photodynamic therapy of cancer.[15] Owing to its D_{2h} symmetry which distinguishes between the x and y directions of the electronic transition moment (Fig. 1, inset), the Q electronic absorption band of H_2Pc in the visible spectral region is split into Q_x and Q_y branch (Fig. 1), the actual positions and maxima of which are strongly dependent on the molecular environment [7–11] Both Raman and resonance Raman (RR) spectra of H_2Pc thin films (α, β and *x* phase) have been investigated,[16–20] while the RR measurements of H_2Pc molecules in KBr discs and in isolation matrices have been hampered by a strong luminescence.[8,21] By contrast, quenching of the luminescence of H_2Pc molecules upon their adsorption onto Ag island films allowed for obtaining both SERS and SERRS/SE(R)RS = surface-enhanced (resonance) Raman scattering/ spectra of H_2Pc.[7,22]

H_2Pc has also been among the very first molecules probed for GERS in 2010.[3] Raman spectra of $Si/SiO_2/SLG/H_2Pc$ hybrid samples prepared by H_2Pc sputtering onto the SLG surface were measured at 488.0, 514.5 and 633-nm wavelength, and quenching of the H_2Pc luminescence has been demonstrated. Graphene-enhanced Raman scattering enhancement of H_2Pc spectral bands by factors 5–15 has been determined in relation to the $Si/SiO_2/H_2Pc$ reference sample at 633-nm excitation. On the other hand, the actual mechanism of GERS enhancement has not been established, and the LUMO and HOMO energies considered in this paper were not appropriate, because the value of their difference corresponded with the B (Soret) electronic transition (in the UV spectral region) rather than with the Q_x electronic transition corresponding with the actual HOMO − LUMO difference.

In this paper, we focus on identification of the resonance conditions for GERS and on manifestations of its mechanisms for H_2Pc in hybrid systems with SLG by Raman spectral measurements in a broad range (532–830 nm) of excitation wavelengths, and by construction and analysis of Raman (GERS) excitation profiles of the Raman spectral bands of H_2Pc. The importance of the excitation profiles in GERS has already been demonstrated; however, up to now, this tool has been employed for investigation of the mechanism of GERS only once, and in a markedly more narrow range of excitation wavelengths.[23] On the other hand, the excitation profiles have been frequently employed in RR and SERS and SERRS spectral studies.[24–28] In our analysis of the GERS excitation profiles and GERS enhancement factors, we have focused particularly on their selectivity with respect to (i) wavenumbers of scattered photons, (ii) symmetry of vibrational modes and/or (iii) their localization within the H_2Pc molecule. Preparation of both the glass/SLG/H_2Pc samples and of the selected reference samples has been, in our case, based on a spontaneous adsorption of H_2Pc molecules onto the particular substrate from its toluene solution (followed by the removal of excess molecules). Therefore, we have selected graphite/H_2Pc as a reference sample in which the adsorption ability of the graphite substrate is similar to that of SLG, but for which no GERS enhancement has been observed.[3] We have focused particularly on achievement of a monolayer coverage of both the glass/SLG and the graphite substrate by H_2Pc molecules. Concerning the assignment of vibrational modes, we found greatly helpful the recently reported DFT calculations.[8,21] Furthermore, concerning the HOMO and LUMO energies of H_2Pc, we rely on the results of two DFT calculations [10,29] which show a reasonable mutual agreement of their values. We also take advantage of the recently published theoretical treatment of GERS and of the formulation of the conditions for GERS.[6] In the case of H_2Pc, these conditions and the actual LUMO and HOMO energy values [10,28] indicate that it is worthwhile to extend Raman spectral measurements into the region of excitation wavelengths above 633 nm in which the HOMO H_2Pc → Fermi level of SLG and/or Fermi level SLG → LUMO H_2Pc CT transition(s) could possibly take place. As a result of this effort, we propose that two mechanisms of GERS manifest themselves in the Raman spectra of glass/SLG/H_2Pc hybrid system, each in the different range of excitation wavelengths and with a different localization of the most enhanced vibrational modes within the H_2Pc molecule.

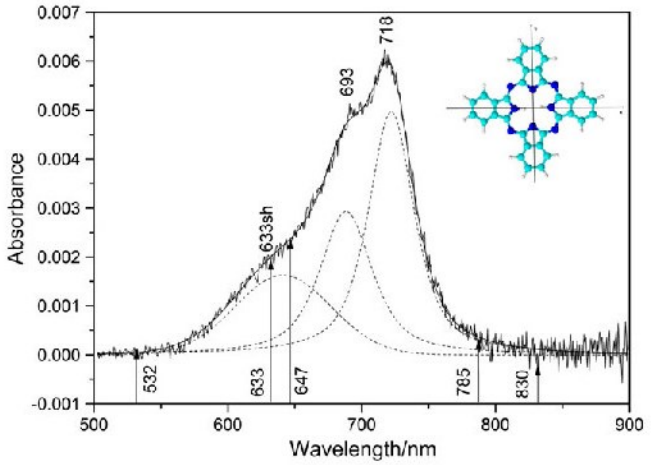

Figure 1. Electronic absorption spectrum of glass/SLG/H_2Pc (BL)-I system: Electronic absorption bands maxima: Q_x – 718 nm, Q_y – 693 nm; shoulder – 633 nm. Final results of spectral bands separation: three bands presented as dashed curves (details in Fig. S3 in SI). Excitation wavelengths used for Raman measurements are marked by arrows. Inset: Schematic depiction of H_2Pc molecule structure (D_{2h} symmetry) with the directions of the electronic transition dipoles[39] marked by arrows. [Colour figure can be viewed at wileyonlinelibrary.com]

Experimental

Materials

29,31H-Phthalocyanine, H_2Pc (β-form, 98%), 29,31H-phthalocyanine-C,C,C,C-tetrasulfonate hydrate, H_2PcTS and cellulose nitrate were purchased from Sigma-Aldrich. Toluene for spectroscopy (Merck, Uvasol) and/or distilled deionized water were used as solvents.

Preparation procedures

Glass/single-layer graphene hybrid system

Single-layer graphene was prepared by the previously reported CVD procedure.[30] The as-grown graphene was transferred to the glass substrate using cellulose nitrate (NC).[31] The majority of the NC layer was removed by methanol drops at room temperature. Then, the glass/SLG sample was annealed at 160 °C for 30 min in order to remove the NC residuals from the SLG surface.

Glass/single-layer graphene/phthalocyanine hybrid systems

All samples were prepared by using the same first step: The parent glass/SLG hybrid systems were overlayed by a thin layer of a saturated ($<5 \times 10^{-5}$ M) solution of H_2Pc in toluene (which was filtered by the 1-μm filter prior to use). Subsequently, they were kept in the toluene-saturated atmosphere in a sealed weighting bottle for 24 h to accomplish adsorption of H_2Pc onto the SLG surface. The sample was then extracted from the weighting bottle, and the solution layer was removed by soaking into a slip of filter paper. The second step aimed at the removal of excess H_2Pc molecules was performed by overlaying the as-prepared glass/SLG/H_2Pc sample by a thin layer of pure toluene and by keeping it in the same setup as described above for 10 min. The solvent layer was then removed by the filter paper. The particular samples mutually differed by the multiplicity of the second step applications, and this multiplicity has been employed for the sample notation throughout this paper. In particular, the samples soaked in pure toluene only once are denoted as glass/SLG/H_2Pc-I system, those soaked 6× as -VI system and those soaked 10× as -X system.

Graphite/H_2Pc hybrid systems were prepared by the procedure similar to that described above for the glass/SLG/H_2Pc hybrid systems. Nevertheless, the procedure was preceded by the graphite substrate preparation and followed by the specifically developed strategy of Raman spectral mapping. The detailed description of these procedures is provided in Supporting information (SI), Text S1, and documented by Figs S1 and S2 in SI.

Instrumentation

Raman spectra as well as optical images of all hybrid samples and reference hybrid samples were obtained using WITec alpha300 Raman micro-spectrometer. An objective (Zeiss) with 100× magnification was used for all the above mentioned Raman spectral measurements performed at 532, 633, 647, 785 and 830-nm excitations. For measurements on WITec alpha300, two spectrographs equipped with charge-coupled device (CCD) detectors optimized for the blue–green and for the red-NIR (near infrared) spectral ranges have been used, the first one for collection of spectra at 532-nm excitation and the second one for the other four excitation wavelengths, i.e. 633, 647, 785 and 830 nm. Excitation was provided by the following lasers at the respective wavelengths and laser power values (at the sample): SHG Nd:YVO_4, 532 nm (2.3 mW); He–Ne, 633 nm (2.5 mW); Kr^+ ion, 647 nm (5.0 mW), diode, 785 nm (50.0 mW), diode, 830 nm (11.0 mW). Raman spectral mapping was performed by using the 25 μm × 25 μm area scans with 50 × 50 points. Defect-free areas of samples were selected for spectral mapping by the previously established relationship between optical images and Raman spectra of glass/SLG samples.

UV–Vis electronic absorption spectra of glass/SLG/H_2Pc(BL)-I hybrid system were measured with a home-assembled microspectrometer system consisting of a 20-W Oriel tungsten-halogen lamp coupled to a modified Nicolet Nicplan microscope which in turn passed through an Acton spectrograph (resolution of approximately 1.7 nm), and the light was finally detected by a Princeton Instruments Si diode-array detector. The measured area was 350 μm × 260 μm.[32] The very low absorbance A = 0.006 of this sample (Fig. 1) documents the impossibility to obtain meaningful absorption spectra for samples VI and X containing a monolayer of H_2Pc molecules.

Raman and UV/vis spectral measurements of solutions are described in Text S2 in SI.

Calibrations related to Raman spectral measurements with the WITec alpha300 apparatus and spectral data processing are described in Text 2 in SI and supported by ref. [33].

Raman excitation profiles of glass/single-layer graphene/phthalocyanine hybrid samples

Excitation profiles (EP) were constructed for each Raman spectral band of H_2Pc, and they represent plots of their normalized band intensity as a function of the excitation wavelength in the 532–830 nm region. The EPs were constructed from the excitation wavelength-dependent Raman spectra of glass/SLG/H_2Pc-I, glass/SLG/H_2Pc-VI and glass/SLG/H_2Pc-X hybrid systems collected at the 532, 633, 647, 785 and 830 nm excitations. Raman spectra of polystyrene acquired under the very same experimental conditions as those of the samples were employed as the external intensity standards. At each excitation wavelength, intensities of the H_2Pc Raman bands (in terms of the band areas) in the spectrum of each of the hybrid samples were normalized to the intensity of the 1005 cm^{-1} polystyrene Raman band.

Graphene-enhanced Raman scattering enhancement factors

Graphene-enhanced Raman scattering enhancement factors were determined as the intensity ratios (in terms of the integrated band areas) of the corresponding Raman bands in the spectra of the glass/SLG/H_2Pc (ML)-X sample and the graphite/H_2Pc (ML) reference sample. The spectra were baseline-corrected by the third-order polynomial function which was found to be optimal for the subsequent determination of the integrated band areas. The actual values of the GERS enhancement factors of the H_2Pc spectral bands are affected by an experimental error estimated to be about ±10%. The major contribution of this error stems from the fact that neither the glass/SLG nor the graphite surface of our sample and reference sample are perfectly flat, and their surface area/projected area ratio has been only roughly estimated to 1.1–1.3.[34] On the other hand, we suppose that this uncertainty does not affect the vibrational mode selectivity of the GERS enhancement factors with respect to their localization within the H_2Pc molecule.

Results and discussion

A. Characterization of glass/single-layer graphene/phthalocyanine samples I, VI and X and determination of single-layer graphene surface coverage by phthalocyanine

Electronic absorption spectrum of glass/SLG/H_2Pc-I system (baseline corrected) is shown in Fig. 1. The two distinct maxima at 718 and 693 nm are attributed to the Q_x (0–0) and Q_y (0–0) bands, respectively. The shoulder at 633 nm is attributed to the vibronic sideband of the Q_y band, i.e. to Q_y (0–1) vibronic transition. The presence of three spectral bands is confirmed by the peak fitting procedure the results of which are shown in Fig. 1 (details in Fig. S3 in SI). The maxima of both Q (0–0) bands (Fig. 1) are markedly red-shifted in comparison to those of H_2Pc in chloronaphtalene[13] and toluene (Fig. S4 in SI) solutions, in isolation matrices[8] and in polysiloxane films.[13] In particular, the Q_x bands are located in the 670–702 nm range and the Q_y bands in the 627–666 nm range in the systems reported previously[8,13] and/or shown in Fig. S4 in SI. In addition to that, SERRS excitation profiles of H_2Pc molecules adsorbed on Ag island films show maxima at 692 (Q_x) and

Journal of RAMAN SPECTROSCOPY

674 nm (Q_y), respectively.[7] The red shift of both Q-bands in the electronic absorption spectrum of the glass/SLG/H_2Pc-I system thus indicates the presence of J-type dimers (or very small aggregates) of H_2Pc molecules on SLG.[10,35,36]

For further characterization of the glass/SLG/H_2Pc hybrid system I as well as of the hybrid systems VI and X, we compared the number of scattering molecules in all these three systems. For this purpose, we performed Raman spectral mapping of the same areas (25 × 25 μm) of the three samples under the same measurement conditions, namely at 532-nm excitation, which appears to be out-of-resonance for both isolated H_2Pc molecules (Fig. S4 in SI and refs. [8,13]) as well as for those in the glass/SLG/H_2Pc-I system (Fig. 1). Because at a non-resonant excitation, the intensity of Raman scattering is directly proportional to the number of scattering molecules,[37] the mutual comparison of the relative average band intensities of the same selected spectral bands (determined from the spectra shown in Fig. S5 in SI and set to 1.00 for the system I) provided us with the comparison of the relative numbers of scattering molecules in the three systems (Fig. S6 in SI). This comparison demonstrates that the additional soaking in pure toluene/performed 5 more times for the sample VI (6×) than for the sample I (1×) reduced the number of scattering molecules to less than a half of the original value, namely to 0.41. By contrast, a further additional soaking in pure toluene performed 4 more times for the sample X (10×) than for the sample (6×) has not further reduced the number of scattering molecules, because the values of 0.41 and 0.44, respectively, can be considered as comparable regarding the precision of the experiment. We thus attribute the sample I to the glass/SLG/~ a bilayer (BL) of H_2Pc hybrid system, and the samples VI and X to the glass/SLG/~ a monolayer (ML) of H_2Pc hybrid systems.

B. Assignment of Raman spectral bands of phthalocyanine and single-layer graphene in glass/phthalocyanine/single-layer graphene hybrid systems and their comparison with those of the reference systems

Raman spectral bands of both SLG and H_2Pc were observed for all three glass/SLG/H_2Pc hybrid systems, i.e. (BL)-I, (ML)-VI and (ML)-X, at all five excitation wavelengths, i.e. at 532, 633, 647, 785 and 830 nm (Figs 2–4). Full range Raman spectra of these samples at 633 and 647-nm excitations are compared in Figs S7 and S8 (SI). By contrast, the Raman spectral bands of H_2Pc were observed only at 633 and 647-nm excitations for the graphite/H_2Pc (ML) reference sample. Raman spectra of the glass/SLG/H_2Pc (ML)-X sample and of the graphite/H_2Pc (ML) reference sample at 633 and 647-nm excitations are mutually compared in Figs 5 and 6. The average values of the H_2Pc Raman band wavenumbers of all three glass/SLG/H_2Pc samples and of the graphite/H_2Pc reference sample are listed in Table 1.

Table 1 demonstrates the large extent of similarities in the spectral band wavenumbers of H_2Pc for all three samples as well as for the reference one. On the other hand, one can notice minor, but very important differences in the H_2Pc Raman spectra between the glass/SLG/H_2Pc (BL)-I sample and the (ML) samples -VI and -X, as well as between the glass/SLG/H_2Pc (ML) samples and the graphite/H_2Pc (ML) reference sample. The former differences are represented by the appearance of a new 1533 cm^{-1} band and by the shift of the 951 cm^{-1} band to 958 cm^{-1} upon reduction of the H_2Pc coverage in the glass/SLG/H_2Pc hybrid samples from ~a bilayer to a monolayer. The latter differences manifest themselves by the presence of new spectral bands, namely those at 1533, 1218, 958 and 750 cm^{-1}, for the glass/SLG/H_2Pc (ML) samples as compared to the graphite/H_2Pc reference sample, and their appearance can be attributed to the differences between the strength of the SLG–H_2Pc (ML) and the graphite–H_2Pc (ML) interaction (details in Text S4 in SI).

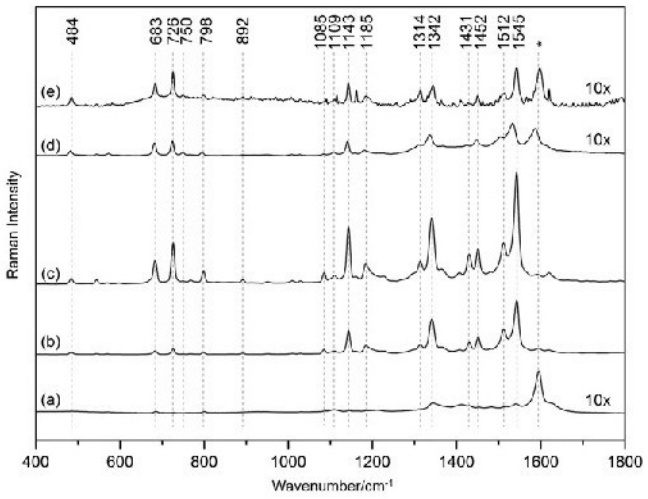

Figure 2. Raman spectra of glass/SLG/H_2Pc (BL)-I system measured at (a) 532-nm, (b) 633-nm, (c) 647-nm, (d) 785-nm and (e) 830-nm excitation wavelengths. The G band of SLG is marked by an asterisk. The bands in the 1500–1600 cm^{-1} range at 785-nm excitation are slightly downshifted by a sample-specific effect.

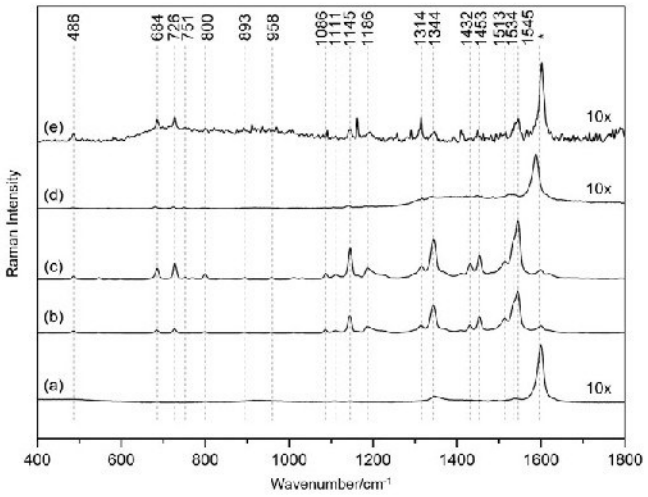

Figure 3. Raman spectra of glass/SLG/H_2Pc (ML)-VI system measured at (a) 532-nm, (b) 633-nm, (c) 647-nm, (d) 785-nm and (e) 830-nm excitation wavelengths. The G band of SLG is marked by an asterisk. The bands in the 1500–1600 cm^{-1} range at 785-nm excitation are slightly downshifted by a sample-specific effect.

For a proper understanding of the above mentioned spectral differences as well as for interpretation of Raman (GERS) excitation profiles and GERS enhancement factors *(vide infra)*, the assignment of H_2Pc spectral bands to vibrational modes of the particular symmetry species and localization within the molecule is of key importance. A detailed description of additional experiments and arguments for both types of band assignment presented in Table 1 (i.e. the symmetry and the localization of the Raman active vibrational modes) is provided in Text 3 in SI and related to refs. [38–41]. Briefly, the assignment of the spectral bands to Raman active

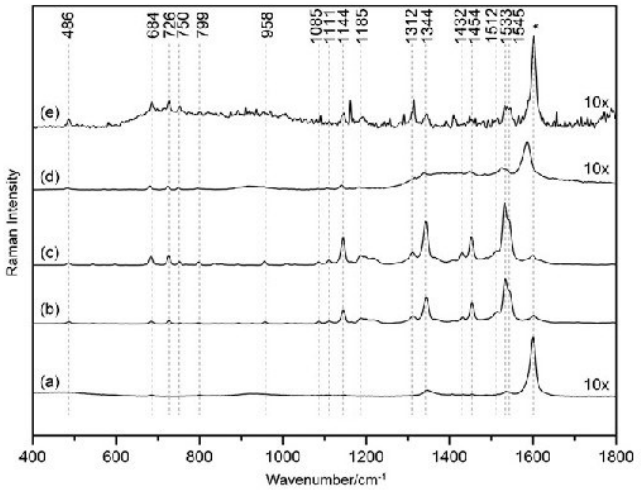

Figure 4. Raman spectra of glass/SLG/H_2Pc (ML)- X system measured at (a) 532-nm, (b) 633-nm, (c) 647-nm, (d) 785-nm and (e) 830-nm excitation wavelengths. The G band of SLG is marked by an asterisk. The bands in the 1500–1600 cm^{-1} range at 785-nm excitation are slightly downshifted by a sample-specific effect.

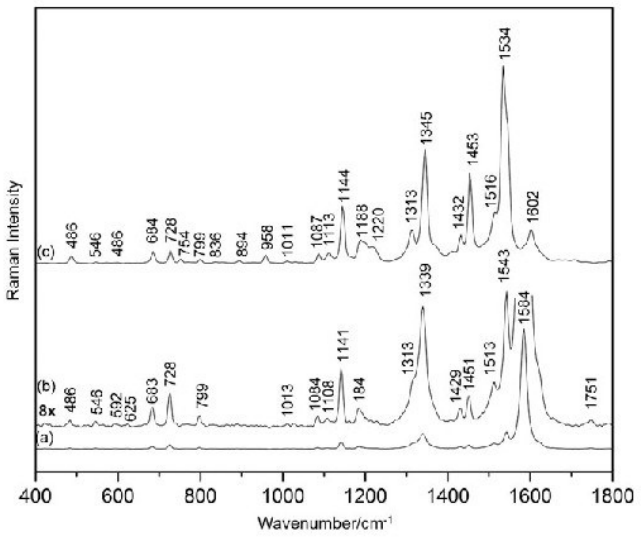

Figure 5. Comparison of Raman spectra of (a) graphite/H_2Pc reference system, (b) the same spectrum expanded 8× and (c) glass/SLG/H_2Pc (ML)-X system at 633-nm excitation. Spectra (a) and (c) are shown in scales respecting the intensity ratio of their absolute Raman signals.

modes of the isolated H_2Pc molecule of a particular symmetry and localization based on DFT calculations [8,21] has been adopted for assignment of the corresponding modes of H_2Pc in the hybrid systems (Table 1).

In addition to the H_2Pc fundamentals (Table 1), overtone and combination bands of the totally symmetric A_g fundamentals have been observed in Raman spectra of all three glass/SLG/H_2Pc hybrid samples as well as in those of the graphite/H_2Pc reference sample at both 633 and 647-nm excitation (Table S2, and Figs S7 and S8 in SI). Nevertheless, their number as well as relative intensities is markedly lower for the reference sample than for the three hybrid samples. No overtones of the SLG Raman modes[42] were observed in the spectra of the hybrid systems with SLG.

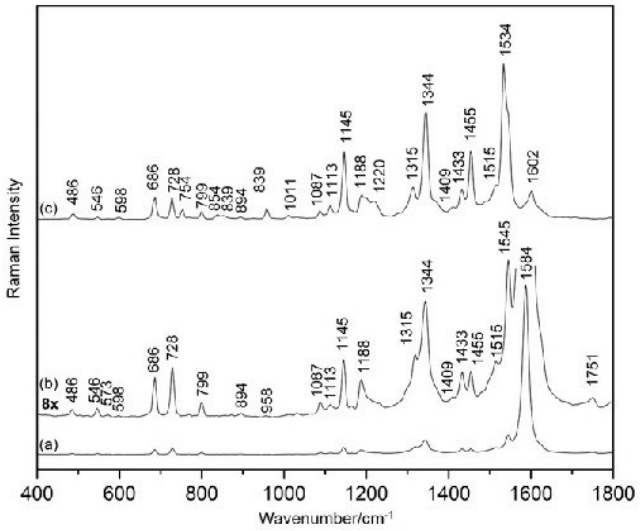

Figure 6. Comparison of Raman spectra of (a) graphite/H_2Pc reference system, (b) the same spectrum expanded 8× and (c) glass/SLG/H_2Pc (ML)-X system at 647-nm excitation. Spectra (a) and (c) are shown in scales respecting the intensity ratio of their absolute Raman signals.

Finally, we turn our attention to the assignment of SLG mode bands in the Raman spectra of the hybrid systems and to their comparison with those of the glass/SLG reference system. The bands of the SLG modes in the Raman spectra of the glass/SLG/H_2Pc hybrid systems are most clearly observed at 532-nm excitation, at which the spectral bands of the H_2Pc fundamentals are weak and those of overtones are absent (Fig. S7, SI). The only exception is the ~1344 cm^{-1} band of the D mode which overlaps with the 1343 cm^{-1} band of H_2Pc. The G bands of the hybrid systems are found at 1595 cm^{-1} (sample BL-I) and 1600 cm^{-1} (samples ML-VI and ML-X), while the same band of the parent glass/SLG system is located at 1598 cm^{-1}. The G-band of SLG was observed for all three hybrid samples as well as for the parent glass/SLG sample at all five excitation wavelengths, yielding the average values of 1595 cm^{-1} for sample BL-I, 1599 cm^{-1} for samples ML-VI and ML-X, and 1598 cm^{-1} for the parent glass/SLG system. The position of the G band is, for all these systems, higher than that of the pristine SLG which is found at 1585 cm^{-1}.[1,2] This discrepancy can most probably be explained by n-doping of SLG by the Na-containing glass substrate, as described in the recently published paper.[43] On the basis of the above mentioned wavenumber difference of the G mode position, the level of n-doping of SLG on glass samples was estimated to induce a ca 0.3-eV upshift of the Fermi level of pristine SLG (from −4.6 eV^3 to −4.3 eV) on the basis of the graph in Fig. 8.5, ref. [2]. Furthermore, the wavenumbers of the spectral bands of the dispersive 2D mode (Table S3 in SI) of samples BL-I, ML-VI, ML-X and of the parent glass/SLG samples show a reasonably good mutual agreement (analogously to the case of the G band). These observations indicate that deposition of H_2Pc onto the glass/SLG system has not induced any detectable effect of an additional doping or strain in SLG.

C. Excitation profiles of selected Raman bands of glass/single-layer graphene/phthalocyanine hybrid systems

Excitation profiles (EPs) of H_2Pc Raman spectral bands were constructed from Raman spectra of glass/SLG/H_2Pc (BL)-I, glass/SLG/H_2Pc (ML)-VI and glass/SLG/H_2Pc (ML)-X hybrid systems collected

Table 1. Average wavenumbers (in cm^{-1}) of H_2Pc spectral bands in Raman spectra of the hybrid systems investigated and their assignment to vibrational modes of H_2Pc

SLG/H_2Pc-I BL	SLG/H_2PcVI ML	SLG/H_2PcX ML	Graphite/H_2Pc ML	Mode symmetry	Mode description
484	486	486	485	B_{1g}	Benzene ring rocking and central ring deformation
545	546	545	546	A_g	—
571	571	571	573	A_g	Benzene ring deformation/central ring breathing
683	684	684	685	A_g	Bridging C—N—C sym. def. and benzene ring deformation
726	726	726	728	A_g	Pyrrole deformation and C—N—C rocking
750	751	750	—	IR act.	N—H out-of-plane deformation
768	771	770	768	A_g	—
798	800	799	799	A_g	Pyrrole and benzene ring C—C str.
892	893	893	894	B_{1g}	—
951	958	958	—	IR act.	C—H out-of-plane deformation
1009	1010	1010	1013	A_g	Sym. benzene ring C—H def
1028	1030	1030	1030	B_{1g}	—
1085	1086	1085	1086	B_{1g}	N—H in-plane deformation
1109	1111	1111	1111	A_g	—
1143	1145	1144	1144	A_g	Benzene ring C—C str. and C—H deformation
1162	1163	1163	1163	A_g	—
1184	1186	1185	1186	A_g	C—H def. on benzene ring
1220	1222	1218	—	B_{1g}	C—H def, benzene ring def. and N—H in-plane deformation
1314	1314	1312	1316	B_{1g}	—
1342	1344	1344	1343	A_g	Benzene ring C—C str. and pyrrole C—C stretch
1408	1408	1409	1409	A_g	—
1431	1432	1432	1431	B_{1g}	—
1452	1453	1454	1453	A_g	C—H def.
1512	1513	1512	1514	A_g	—
—	1534	1533	—	A_g	Bridging C_α–N_m–C_α asym. str. and C_α–N_H–C_α sym. str.
1543	1545	1545	1544	A_g	Bridging C_α–N_m–C_α asym. str. and C_α–N_H–C_α sym. str.
1620	1621	1619	Not observable	B_{1g}	Benzene ring deformation

at the 532, 633, 647, 785 and 830-nm excitation wavelengths (Figs 2–4 and details in Experimental). The EPs are presented in Figs 7 and 8, profiles A-C. Shown in Fig. 7(A–C) are the overviews of EPs of all selected H_2Pc spectral bands of all three samples, while the corresponding details of the close-lying EPs of the less enhanced bands are shown in Fig. S10, profiles A–C (SI). The details of the EPs in the high excitation wavelengths region (785 and 830 nm) of all three samples are presented in Fig. 8, profiles A–C.

In case of all three samples, the EPs of the selected spectral bands exhibit a maximum for the 647-nm excitation. Furthermore, while the EP of glass/SLG/H_2Pc (BL)-I sample appears to be rather flat at higher excitation wavelengths (with some of the bands slightly declining and some slightly increasing, Figs 7 and 8, profiles A), the EPs of glass/SLG/H_2Pc (ML)-VI and glass/SLG/H_2Pc (ML)-X hybrid systems show a pronounced normalized intensity increase from 785 to 830 nm for at least half of the spectral bands (Figs 7 and 8, profiles B and C). Importantly, the EPs of the glass/SLG/H_2Pc (BL)-I Raman spectral bands (profiles A in Figs 7 and 8, and in Fig. S10 in SI) can be related to the electronic absorption spectrum of this hybrid system (Fig. 1). The particular EPs were analyzed in the following manner. The sequences of relative intensities of the individual spectral bands were determined for all three hybrid systems at 633 and 647-nm excitations, for glass/SLG/H_2Pc (BL)-I also at 785 nm and for glass/SLG/H_2Pc (ML)-VI and glass/SLG/H_2Pc (ML)-X systems also at 830-nm excitations. The series were analyzed in terms of the symmetries of the corresponding normal vibrations and their localizations within the H_2Pc molecule. For the totally symmetric vibrations, the sequence of the decreasing normalized band intensities in the resonance Raman spectra excited at a particular excitation wavelength corresponds to the decreasing magnitude of changes of their normal coordinates upon the electronic transition which is in resonance with the particular excitation wavelength. The largest changes of the normal coordinates of the totally symmetric A_g modes thus determine localization of the resonant electronic transition within the H_2Pc molecule.[24] An analogous approach has been already successfully employed, e.g. for the SERRS EPs analysis.[27]

Excitation profiles of Raman bands of glass/single-layer graphene/phthalocyanine (BL)-I hybrid system

The sequence of the most intense bands of H_2Pc at 647-nm excitation (Figs 7, 8 and Fig. S10 in SI, profiles A) was ascertained as follows: 1543 (A_g) > 1341 (A_g) > 1143 (A_g) > 726 (A_g) > 1451 (A_g) > 683 (A_g) ~ 1184 (A_g) ~ 1314 (B_{1g}) > 1367 > 798 (A_g) > 1110 (B_{1g}) > 1085 (B_{1g}) > 484 (B_{1g}) > 544 (A_g) > 768 (A_g) > 1009 (B_{1g}) >1162 (A_g) > 1029 (B_{1g}) > 750. The most enhanced modes belong to A_g symmetry and comprise both stretching and deformation (bending) vibrations of the macrocycle (Table 1). The B_{1g} modes, the A_g vibrations localized also (or preferentially) on the benzene ring, as well as C—H deformation modes are to be found among the less enhanced ones. This enhancement pattern is consistent with the expected behavior upon excitation into Q_x (or Q_y) purely electronic (0–0) transition which was found previously to be localized predominantly on the tetrapyrrole macrocycle in the samples constituted entirely by H_2Pc molecules.[17]

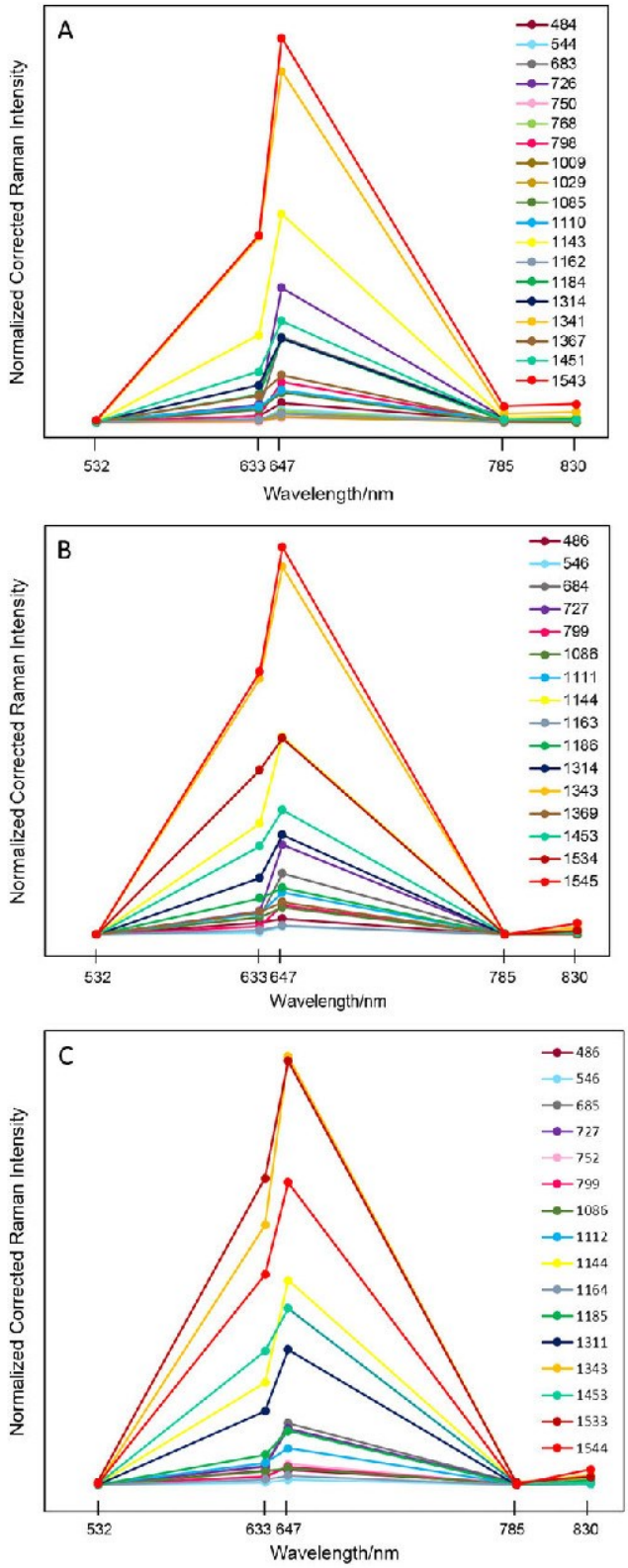

Figure 7. Excitation profiles of H_2Pc Raman spectral bands in (A) glass/SLG/H_2Pc (BL)-I system, (B) glass/SLG/H_2Pc (ML)- VI system and (C) glass/SLG/H_2Pc (ML)-X system in the 532–830 nm range. Details of the EPs of the less enhanced bands are provided in Fig. S10 in SI.

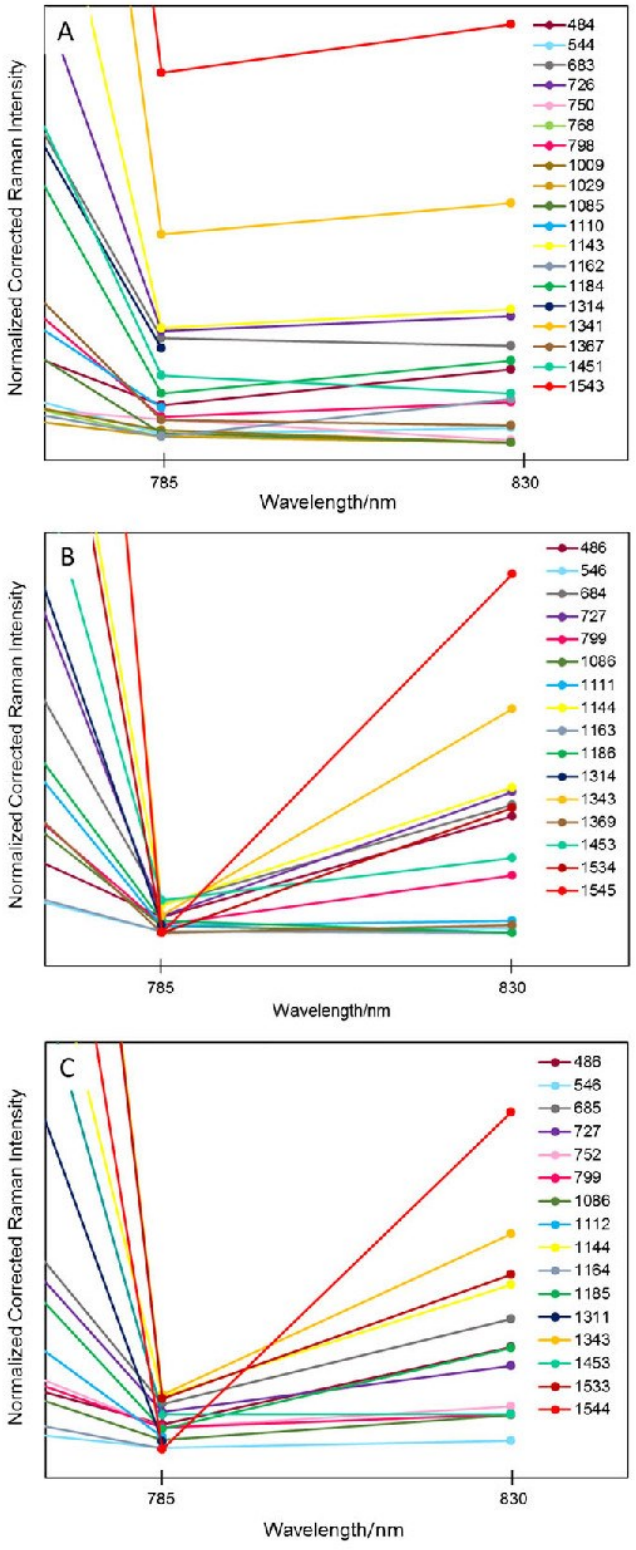

Figure 8. Details of excitation profiles of H_2Pc Raman spectral bands in (A) glass/SLG/H_2Pc (BL)-I system, (B) glass/SLG/H_2Pc (ML)-VI system and (C) glass/SLG/H_2Pc (ML)-X system at 785 and 830-nm excitations.

The series at 633-nm excitation (Figs 7, 8 and Fig. S10 in SI, profiles A) was found to be: 1543 (A_g) > 1341 (A_g) > 1143 (A_g) > 1451 (A_g) > 1314 (B_{1g}) > 1184 (A_g) ~ 1367 > 726 (A_g) > 1110 (B_{1g}) > 1085 (B_{1g}) > 683 (A_g) > 484 (B_{1g}) > 798 (A_g) > 1162 (Ag) ~ 1009 (B_{1g}) ~ 1029 (B_{1g}) ~ 768 (A_g) > 544 (A_g) > 750. Although the relative intensities of the three most enhanced bands (1543, 1344 and 1144 cm^{-1}) are comparable at the 647 and 633-nm excitations, there is a substantial difference in case of the 685 and 726 cm^{-1} bands belonging to the modes localized on the H_2Pc macrocycle. While they are among the more enhanced bands at 647 nm, they fall into the category of weakly enhanced ones for the 633-nm excitation.

This difference can be tentatively explained by considering the electronic absorption spectrum of the glass/SLG/H_2Pc-(BL)-I hybrid system (Fig. 1). While the 647-nm excitation falls within the main electronic absorption band belonging to Q_y (0–0) transition, the 633-nm excitation appears to coincide with the shoulder located at about the same wavelength. This shoulder (giving rise to a separate band in peak fitting in Fig. 1) has been attributed to the vibronic Q_y (0–1) side band of the Q_y (0–0) electronic absorption band arising from the coupling of the Q_x and Q_y excited electronic states by B_{1g} vibrations. [17] The difference between the position of the vibronic side band (633 nm) and the band maximum of the Q_y (0–0) electronic transition is ~1368 cm^{-1}, i.e. it falls into the higher wavenumber region. This rationalizes the observed stronger enhancement of some of the high wavenumber B_{1g} modes than that of the low wavenumber A_g modes of the tetrapyrrole macrocycle at 633-nm excitation.

The coincidence of the 647-nm excitation with the Q_y (0–0) electronic transition band is further corroborated by evaluation of the sequence of the most enhanced bands at 785 nm (Figs 7, 8 and Fig. S10 in SI, profiles A). Electronic absorption spectrum of the hybrid system (Fig. 1) shows that this particular excitation wavelength falls into the very onset of the Q_x band with its maximum appearing at 718 nm. This implies that the enhancement of Raman spectral bands at 785-nm excitation most probably originates from resonance (or preresonance) with the Q_x (0–0) electronic transition. The following sequence of normalized band intensities was determined: 1543 (A_g) > 1341 (A_g) > 1143 (A_g) ~ 726 (A_g) > 683 (A_g) > 1314 (B_{1g}) > 1451 (A_g) > 1184 (A_g) > 484 (B_{1g}) ~ 1110 (B_{1g}) > 798 (A_g) ~ 750 ~ 1367 > 1009 (B_{1g}) ~ 1085 (B_{1g}) ~ 544 (A_g) ~ 1162 (A_g) ~ 1029 (B_{1g}) ~ 768 (A_g). The sequence resembles to that at 647-nm excitation particularly by the appearance of the bands at 684 and 726 cm^{-1} (belonging to the macrocycle modes) among the most enhanced ones.

Excitation profiles of Raman bands of glass/single-layer graphene/phthalocyanine (ML)-VI hybrid system

The normalized intensity sequence of the H_2Pc Raman bands for the glass/SLG/H_2Pc (ML)-VI system at 647-nm excitation (Figs 7, 8 and Fig. S10 in SI, profiles B) has been determined as: 1545 (A_g) > 1343 (A_g) > 1534 ~ 1144 (A_g) > 1453 (A_g) > 1314 (B_{1g}) > 727 (A_g) > 684 (A_g) > 1186 (A_g) > 1111 (B_{1g}) > 1369 > 799 (A_g) > 1086 (B_{1g}) > 486 (B_{1g}) > 1163 (A_g) > 546 (A_g). For the 633-nm excitation, the band order is the following (Figs 7, 8 and Fig. S10 in SI, profiles B): 1545 (A_g) > 1343 (A_g) > 1534 ~ 1144 (A_g) > 1453 (Ag) > 1314 (B_{1g}) > 1186 (A_g) > 727 (A_g) ~ 1369 > 1111 (B_{1g}) ~ 684 (A_g) > 1086 (B_{1g}) > 486 (B_{1g}) > 799 (A_g) > 1163 (A_g) > 546 (A_g). The sequences of normalized band intensities are thus quite similar at both excitations. In particular, the sequences of the first five bands are virtually the same (involving also the newly appearing 1534 cm^{-1} band), while the 684 and 727 cm^{-1} macrocycle bands are among the less intense ones.

Excitation profiles of Raman bands of glass/single-layer graphene/phthalocyanine (ML)-X hybrid system

The normalized intensity sequence for glass/SLG/H_2Pc (ML)-X spectral bands at 647 nm was ascertained to be (Figs 7, 8 and Fig. S10 in SI, profiles C): 1343 (A_g) ~ 1533 > 1544 (A_g) > 1144 (A_g) > 1453 (A_g) > 1311 (B_{1g}) > 685 (A_g) > 727 (A_g) > 1185 (A_g) > 1112 (B_{1g}) > 752 ~ 799 (A_g) > 1086 (B_{1g}) > 486 (B_{1g}) > 1164 (A_g) > 546 (A_g). At 633 nm excitation, this sequence was determined as: (Figs 7, 8 and Fig. S10 in SI, profiles C): 1533 > 1343 (A_g) > 1544 (A_g) > 1453 (A_g) > 1144 (A_g) > 1311 (B_{1g}) > 1185 (A_g) > 1112 (B_{1g}) > 727 (A_g) ~685 (A_g) > 486 (B_{1g}) ~ 1086 (B_{1g}) ~ 799 (A_g) > 752 ~ 1164 (A_g) > 546 (A_g). The sequences of the normalized band intensities show a pronounced mutual analogy, and they are also quite similar to those encountered for the glass/SLG/H_2Pc (ML)-VI hybrid system, particularly in observing the low wavenumber macrocycle bands among the less intense ones. The only apparent difference between the samples (ML)-VI and (ML)-X is thus a pronounced intensity gain of the 1533 cm^{-1} band, which, in the latter case, becomes the most intense band at 647 nm (together with the 1343 cm^{-1} band) as well as at 633 nm excitation. This difference is explained in Text S4 in SI.

Comparison of excitation profiles of glass/single-layer graphene/phthalocyanine (BL)-I, glass/single-layer graphene/phthalocyanine (ML)-VI and glass/single-layer graphene/phthalocyanine (ML)-X hybrid systems in the visible region

The sequences of the normalized band intensities at 633 and 647-nm excitations were found to be largely similar for both hybrid systems containing a monolayer of H_2Pc molecules, i.e. (ML)-VI) and (ML)- X. By contrast, distinct differences between both systems with the H_2Pc monolayer on one hand, and that with the H_2Pc bilayer, i.e. (BL)-I on the other hand have been found in this respect. We propose that two factors contribute to the observed differences: (i) the electronic absorption bands of H_2Pc blue-shifts upon diminishing the SLG coverage by H_2Pc from a BL (formed by J-type dimers with the electronic absorption bands strongly red shifted with respect to those of the H_2Pc monomers, as established in sub-Chapter A), to a ML, and (ii) the SLG–H_2Pc interaction is stronger for the SLG–H_2Pc (ML) hybrids than for the SLG–H_2Pc (BL) one (as established in Text S4 in SI). The former factor appears to be the reason why, (i) for the glass/SLG/H_2Pc (BL)-I hybrid, the 633-nm excitation falls into the vibronic Q_y(0–1) sideband of the Q_y(0–0) electronic absorption band and the 647-nm excitation into the Q_y (0–0) absorption band (giving rise to the different sequences of the relative band intensities at 633 and 647-nm excitations, respectively), while, (ii) for the glass/SLG/H_2Pc (ML)-VI and glass/SLG/H_2Pc (ML)-X hybrids, both excitation wavelengths coincide with the Q_y (0–0) electronic transition, giving rise to mutually analogous sequences of the relative band intensities at both excitations. The latter factor is proposed to be responsible for the observed differences in the sequences of relative band intensities at 647 nm, i.e. upon excitation into the Q_y (0–0) electronic transition, between both systems with the H_2Pc monolayer (i.e. ML-VI and ML-X) on one hand, and that with the H_2Pc bilayer (i.e. BL-I) on the other hand. In particular, we propose that the above mentioned differences originate from the differences in the localization of the Q_y (0–0) electronic transitions induced by the SLG–H_2Pc interaction which is stronger in the SLG–H_2Pc (ML) hybrids than in the SLG–

H_2Pc (BL) one (as established in Text S4 in SI). This tentative explanation is consistent with the vibrational mode selectivity of GERS enhancement factors determined and presented in sub-Chapter D *(vide infra)*.

Excitation profiles of Raman bands of glass/single-layer graphene/phthalocyanine hybrid systems in the high wavelengths region

For the glass/SLG/H_2Pc (ML)-VI and glass/SLG/H_2Pc (ML)-X samples (both with a monolayer coverage of SLG by H_2Pc), the normalized intensities of all spectral bands strikingly drop at 785-nm excitation, while, for the majority of spectral bands, they exhibit a pronounced increase at 830-nm excitation (Fig. 8, profiles B and C). By contrast, for the glass/SLG/H_2Pc (BL)-I system, the normalized band intensities show no such distinctive intensity drop and rise at 785 and 830-nm excitations, respectively (Fig. 8, profile A). Therefore, this feature appears selectively in excitation profiles of samples VI and X containing ~ a monolayer of H_2Pc molecules, and it can thus be attributed to a manifestation of the SLG–H_2Pc (ML) interaction.

The sequence of the normalized band intensities for glass/SLG/H_2Pc (ML)-VI system at 830-nm excitation (Fig. 8(B)) was determined as: 1545 (A_g) > 1343 (A_g) > 1144 (A_g) ~ 727 (A_g) ~ 684 (A_g) ~ 1534 (A_g) ~ 486 (B_{1g}) > 1453 (A_g) > 799 (A_g) > 1111 (B_{1g}) > 1369 > 546 (A_g). In case of the glass/SLG/H_2Pc (ML)-X sample (Fig. 8(C)), the following sequence of band intensities was found: 1544 (A_g) > 1343 (A_g) > 1533 (A_g) ~ 1144 (A_g) > 685 (A_g) > 486 (B_{1g}) ~ 1185 (A_g) > 727 (A_g) > 752 > 1453 (A_g) ~ 799 (Ag) ~ 1086 (B_{1g}) > 546 (A_g). Common features of the two series include the largest enhancement of the 1545 and 1343 cm^{-1} bands, as well as the inclusion of the 684 and 727 cm^{-1} bands of the A_g modes, together with the 486 cm^{-1} band of the B_{1g} mode, among the strongly enhanced ones. All the latter bands belong to the modes localized on the macrocycle. On the other hand, the two above mentioned series of bands differ particularly in the relative intensity increase of the band at 1533 cm^{-1} for sample (ML)-X with respect to sample (ML)-VI. This difference between the glass/SLG/H_2Pc-(ML)-VI and the glass/SLG/H_2Pc (ML)-X hybrid systems has been encountered also at excitations in the visible spectral region, and it is attributed to reorganization of H_2Pc molecules constituting a monolayer on SLG upon the repetitive soaking of the sample in toluene (explained in Text S4 in SI and supported by ref. [44]).

D. Determination of graphene-enhanced Raman scattering enhancement factors of phthalocyanine modes in the Raman spectra of glass/single-layer graphene/phthalocyanine (ML)-X system at 633 and 647-nm excitations.

In contrast to all three glass/SLG/H_2Pc hybrid systems, the signal of H_2Pc is observed only at 633 and 647-nm excitations for the graphite/H_2Pc (ML) reference system. This observation indicates that the H_2Pc molecules arranged in a monolayer on graphite surface experience a strong resonance enhancement of their Raman scattering only at 633 and 647-nm wavelengths. The comparison of Raman spectra of the glass/H_2Pc/SLG (ML)-X and of the graphite/H_2Pc (ML) systems in Figs 5 and 6 shows that this resonance enhancement experiences an additional intensity increase as well as relative band intensity changes, together with the appearance of the additional spectral bands when the graphite substrate is replaced by SLG on glass. The assignment and the origin of the additional bands is addressed in the Text S4 in SI. The GERS enhancement has been quantitatively evaluated in terms of GERS enhancement factors (Table 2) which, in turn, have been determined as the intensity ratios of the corresponding H_2Pc Raman spectral bands in the spectra of the glass/SLG/H_2Pc (ML)-X and of the graphite/H_2Pc (ML) system, respectively (details in Experimental).

The GERS enhancement factors (EFs) listed in Table 2 are in the range from 3 to 24 at 633 nm and from 3 to 19 at 647-nm excitation, and the average values of GERS enhancement factors are 9.3 and 8.4, respectively. The maximum as well as the average GERS enhancement is thus slightly higher at 633-nm than at 647-nm excitation. Furthermore, the selectivity of GERS enhancement factors at both the 633-nm and the 647-nm excitations (Table 2) with respect to the symmetry of the vibrational modes (A_g or B_{1g}), wavenumbers of the vibrational modes (probed on the basis of their significance

Table 2. GERS enhancement factors calculated from the intensity ratios of the H_2Pc Raman spectral bands in the spectra of glass/SLG/H_2Pc (ML)-X system and of the graphite/H_2Pc (ML) reference system, respectively

Band wavenumber [cm^{-1}]	GERS enhancement factors at 633-nm excitation	GERS enhancement factors at 647-nm excitation	H_2Pc mode symmetry	H_2Pc mode assignment
487	**9**	**8**	B_{1g}	b.r. rock + c.r. def
685	**5**	**5**	A_g	CNC + b.r. def
727	**3**	**3**	A_g	pyr + CNC def
751	On SLG only	On SLG only	IR act	oopδN—H
799	**3**	**3**	A_g	νC=C (b.r. + pyr)
958	On SLG only	On SLG only	IR act	oopδC—H
1087	**8**	**5**	B_{1g}	ipδN—H
1114	**12**	**16**	A_g	—
1144	**8**	**10**	A_g	b.r.(νCC + δCH)
1220	On SLG only	On SLG only	B_{1g}	b.r. def + δCH+ ipδN—H
1315	**11**	**12**	B_{1g}	—
1345	**12**	**11**	A_g	νC=C (b.r. + pyr)
1432	**8**	**6**	B_{1g}	—
1453	**24**	**19**	A_g	b.r. δCH
1516	**7**	**5**	A_g	—
1534	On SLG only	On SLG only	A_g	νCNC c.r.
1543	**11**	**6**	A_g	νCNC c.r.

in the theoretical treatment of GERS[5,6]) and localization of the vibrational modes within the H_2Pc molecule (assignment of bands to normal modes) has been probed. Because the ranges of GERS EFs experienced by A_g and B_{1g} modes (namely 3–24 for A_g and 8–11 for B_{1g} modes at 633-nm excitation as well as 3–19 for A_g and 5–12 for B_{1g} modes at 647-nm excitation) mutually overlap, and the average values of GERS EFs of A_g and B_{1g} modes are similar at both excitations (namely 9.4 for A_g modes and 9.0 for B_{1g} modes at 633-nm excitation, and 8.6 for A_g and 7.8 for B_{1g} modes at 647-nm excitation), no generalization concerning the dependence of the GERS EFs on the symmetry of vibrational modes can be done. In addition to that, there is no systematic dependence of GERS EFs on the wavenumbers of the vibrational modes bands, because the maximal enhancement is obtained for the 1453 cm^{-1} band at both 633 and 647-nm excitations while the EF values decrease for the bands of both lower and higher wavenumbers. Localization of vibrational modes within the H_2Pc molecule thus emerges as the most important factor which governs their GERS enhancement. In particular, the largest enhancement (EF values 24 and 19 at 633 and 647-nm excitation, respectively) is observed for the 1453 cm^{-1} band assigned to the A_g vibrational mode with a strong contribution of C—H deformation on the benzene ring. A large GERS enhancement is experienced also by the 1218 cm^{-1} mode (B_{1g}) involving C—H and N—H in-plane deformations and benzene ring deformation (Table 2), the band of which is extremely weak in the Raman spectra of graphite–H_2Pc sample, and hence its GERS enhancement factor could not be exactly determined. In fact, nearly all strongly and/or moderately enhanced bands belong to modes localized on the benzene rings of H_2Pc. On the other hand, the modes delocalized over the tetrapyrrole macrocycle are among the least enhanced ones (Table 2).

E. Evidence for two mechanism of graphene-enhanced Raman scattering in glass/single-layer graphene/phthalocyanine (ML) hybrid systems

Enhancement of Raman scattering with a distinct selectivity towards localization of individual vibrational modes within the H_2Pc molecule has been observed for H_2Pc molecules in the glass/SLG/H_2Pc (ML) hybrid systems upon excitations falling into (i) the visible (633 and 647 nm) and (ii) the onset of near IR (830 nm) spectral regions. In this sub-Chapter, we inspect the origin of each of these two enhancement effects.

(i) Both the 633 and 647-nm excitations fall into the electronic absorption band of a Q_y (0–0) electronic transition of H_2Pc molecules monolayer (more precisely, into its lower wavelengths side), as established by the analysis of EPs of the glass/SLG/H_2Pc (ML) hybrids (Fig. 7(B), (C) and Fig. S10(B), (C) in SI) presented in sub-Chapter C. Both excitation wavelengths thus obey the resonance condition for GERS formulated by the first part of Eqn 15 (i) in ref. [6] which is defined as excitation into the electronic absorption band related to the HOMO–LUMO transition within a planar aromatic molecule.[5,6] Furthermore, the enhancement of Raman spectral bands of individual vibrational modes of H_2Pc in glass/SLG/H_2Pc (ML)-X system with respect to those of the graphite–H_2Pc (ML) reference system has been quantified in terms of their mutual intensity ratios, i.e. the GERS EFs (sub-Chapter D). The fact that at least some GERS enhancement of the Raman signal has been determined for all spectral bands of H_2Pc indicates a small change in the position, the intensity and/or the half-width of the electronic absorption band of the Q_y (0–0) electronic transition for the H_2Pc monolayer in the glass/SLG/H_2Pc (ML)-X hybrid system with respect to the graphite/H_2Pc reference hybrid system. Because the electronic absorption spectra of none of these two systems could be obtained (details in Experimental), we cannot precisely determine the difference between them. On the other hand, the GERS enhancement factors are slightly higher at 633-nm than at 647-nm excitation (sub-Chapter D and Table 2), while the EPs of the Raman bands of the glass/SLG/H_2Pc (ML)-X hybrid system (Fig. 7 and Fig. S10 in SI) show a normalized intensity increase for all Raman bands at 647-nm excitation with respect to the 633-nm excitation. Therefore, it is the broadening of the Q_y (0–0) electronic absorption band of the monolayer of H_2Pc molecules in the system with SLG in comparison to that with graphite which is most consistent with the above mentioned observations. Is should also be noted that the broadening of both the Q_y (0–0) and Q_x (0–0) electronic absorption bands of H_2Pc molecules upon their adsorption on Ag islands has been determined on the basis of detailed EPs spanning these electronic transitions, and it was attributed to bonding of H_2Pc molecules to Ag by lone pairs of N atoms[7]. The nature of the relatively strong H_2Pc–SLG interaction (determined in Text S4 in SI) is different from the Ag–H_2Pc one, because it is ascribed to $\pi - \pi$ interaction and/or van der Waals forces[3,8]. Nevertheless, its effect on the electronic absorption spectrum of H_2Pc can be similar.

Furthermore, the vibrational mode selectivity of the GERS enhancement, namely the preferential GERS enhancement of the vibrational modes fully or partially localized on the benzene rings of H_2Pc (established in sub-Chapter D) indicates (in accord with the theory of RRS[24]) the difference in localization of the resonant Q_y (0–0) electronic transition within the H_2Pc molecule between the glass/SLG/H_2Pc system and the graphite–H_2Pc reference system, in particular, delocalization of this electronic transition over the benzene rings of H_2Pc in the former system, i.e. for H_2Pc on SLG. It should be noted that both Q_y (0–0) and Q_x (0–0) electronic transitions were found to be localized preferentially on the H_2Pc macrocycle for samples involving only the H_2Pc molecules,[17] as confirmed also by the results of the ab-initio calculations of the localization of HOMO, LUMO and LUMO + 1 for the isolated H_2Pc molecule.[45] The difference in the localization of the Q_y (0–0) electronic transition between glass/SLG/H_2Pc system and the graphite–H_2Pc reference system can thus be tentatively attributed to delocalization of HOMO of H_2Pc over the benzene rings H_2Pc in the latter system. This situation, in turn, could originate from the relatively strong SLG–H_2Pc interaction and short SLG–H_2Pc distance (established in Text S4 in SI), in which the $\pi - \pi$ interaction between the benzene rings of H_2Pc and the conjugated benzene rings of SLG can be expected to play an important role.

In summation, the mechanism of GERS enhancement observed for the glass/SLG/H_2Pc (ML)-X hybrid system with respect to the graphite–H_2Pc reference system at 633 and 647-nm excitations can be attributed to RRS of H_2Pc modified by a relatively strong SLG–H_2Pc (ML) interaction. The modifications manifest themselves by minor changes in the half-width of the electronic absorption band and by pronounced changes in localization of this resonant Q_y (0–0) electronic transition within the H_2Pc molecule (Fig. 9).

(ii) Upon excitations at the onset of near IR spectral region (namely those at 785 and 830 nm), the vibrational-mode specific normalized intensity increase of the majority of Raman bands of H_2Pc from 785-nm to 830-nm excitation has been encountered selectively in Raman excitation profiles of the glass/SLG/H_2Pc (ML)-VI and the glass/SLG/H_2Pc (ML)-X hybrid systems, i.e. for samples constituted by SLG and a monolayer of H_2Pc molecules (sub-Chapter C and Fig. 8(B), (C)). The absence of the Raman signal of H_2Pc at both these excitations for the graphite/H_2Pc (ML) reference sample

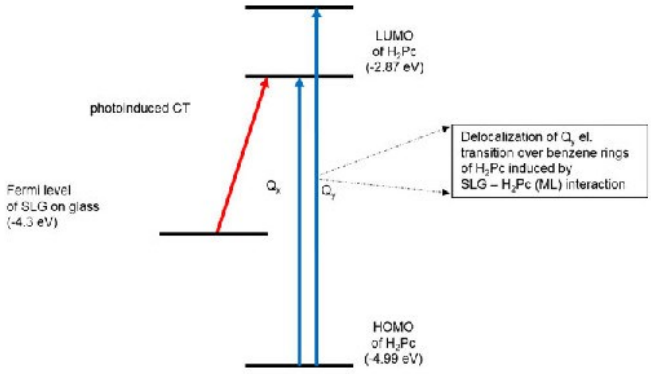

Figure 9. Schematic depiction of the two mechanisms of GERS operating in the glass/SLG/H_2Pc (ML) system. The SLG Fermi level energy of pristine SLG (−4.6 eV)[3] has been corrected for the established n-doping of SLG by glass. HOMO and LUMO energies of H_2Pc have been adopted from ref [10]. [Colour figure can be viewed at wileyonlinelibrary.com]

hampers determination of the GERS enhancement factors values. On the other hand, it indicates a substantial enhancement of Raman scattering of the above mentioned samples with respect to the reference sample at the 830-nm excitation. Furthermore, the sequence of the normalized band intensities at 830-nm excitations shows a distinct selectivity with respect to localization of the corresponding vibrational modes within the H_2Pc molecule which, in turn, is largely similar for both the glass/SLG/H_2Pc (ML) samples (i.e. VI and X). Importantly, for both samples, the sequence of the relative band intensities at 830 nm (sub-Chapter C and Fig. 8(B), (C)) differs from that encountered at 633-nm and 647-nm excitations which coincide with a Q_y (0–0) electronic absorption band (sub-Chapter C, Fig. 7(B), (C) and Fig. S10(B), (C) in SI). For example, the 684 and 726 cm^{-1} A_g bands localized on the macrocycle are among the more enhanced modes in the former case, while they are among the less enhanced ones in the latter case. This difference in localization of the most enhanced bands within the H_2Pc molecule indicates that at 830-nm excitation, the LUMO of H_2Pc has been populated by a new electronic transition different (in its localization within the H_2Pc molecule) from the two Q (0–0) electronic transitions (Fig. 9). Comparison of the SLG Fermi level energy (the position of which was corrected for doping of SLG by the glass substrate evaluated in sub-Chapter B) with the HOMO and LUMO energies of H_2Pc[10] demonstrated by the scheme presented in Fig. 9 indicates fulfillment of the energy condition for a photo-induced charge transfer (CT) between Fermi level of SLG and LUMO of H_2Pc at 830-nm excitation. This explanation also agrees with one of the four theoretically predicted resonance conditions for the GERS enhancement observation[5,6], namely with that defined by Eqn 15 (iv) in ref. [6]:

$$h\nu_0 = E_L - E_F \quad \text{or} \quad h\nu_0 = E_L - E_F - h\nu_q,$$

where $h\nu_0$ is the energy of excitation, E_F and E_L are the energies of Fermi level of SLG and of LUMO of H_2Pc, respectively, and $h\nu_q$ is the phonon (i.e. the vibrational mode) energy. Because the sequence of the most enhanced bands does not systematically follow the phonon energy (i.e. the vibrational mode wavenumber) sequence, we reason that it is the first of the two resonance conditions in the abovementioned equation which is actually fulfilled at 867 nm, which is the wavelength equivalent of the 1.43-eV energy difference between E_L and E_F (Fig. 9). We can thus speculate that the 830-nm excitation falls into the lower wavelength slope of the electronic absorption band of the abovementioned photoinduced CT transition with a maximum close to 867 nm.

Furthermore, the absence of such pronounced normalized intensity increase of Raman bands in excitation profiles of the glass/SLG/H_2Pc (BL)-I hybrid system indicates that observation of the photoinduced CT transition is conditioned by the stronger SLG–H_2Pc interaction in the case of the monolayer coverage of SLG by H_2Pc than in the case of the bilayer one (established in Text S4 in SI).

Finally, we notice some analogy between this particular mechanism of GERS and the chemical mechanism of SERS (particularly when the latter one operates in the absence of the electromagnetic mechanism of SERS on flat metal surfaces[46]). The common feature of the two mechanisms is a photoinduced CT transition from the Fermi level of the metal or SLG to LUMO of a molecule conditioned by a relatively strong surface–molecule interaction. On the other hand, it has to be noted that the chemisorption which is the necessary condition for operation of the chemical mechanism of SERS [25,26,46] is different in its nature and strength from the π–π interaction involved in SLG-aromatic molecule (e.g. H_2Pc) monolayer systems; hence, different types of molecules can obey the necessary condition for this photoinduced CT mechanism in GERS and in SERS, respectively.

Conclusions

The glass/SLG/free-base phthalocyanine (H_2Pc) hybrid systems with monolayer (ML) coverages of SLG by H_2Pc molecules were prepared by a spectrally controlled adsorption–desorption of H_2Pc molecules from solution. The graphite/H_2Pc (ML) and the glass/SLG/H_2Pc (BL) hybrids were prepared as well and employed as the reference systems. Raman spectra of all hybrid systems were measured as a function of excitation wavelengths in the 532–830 nm range. Assignment of the specific Raman spectral features allowed to establish the relative strength of interaction between the single carbon atom layer and H_2Pc molecules: graphite–H_2Pc (ML) < SLG–H_2Pc (BL) < SLG–H_2Pc (ML). Excitation profiles of H_2Pc Raman bands of the SLG containing hybrids were constructed, and the sequences of the normalized band intensities at each wavelength were analyzed for the vibrational mode specificity.

Raman excitation profiles of glass/SLG/H_2Pc (ML) hybrid systems in the 532–830 nm region have revealed two types of resonance mechanisms conditioned specifically by the relatively strong interaction between SLG and a monolayer of H_2Pc molecules. Both of them manifest themselves by an additional enhancement of Raman modes of H_2Pc (denoted as the GERS enhancement[3–6]); however, for each of them, a different energy as well as localization of the resonance electronic transition within the H_2Pc molecule has been established. The different energies of the two resonant electronic transitions also indicate that each of them obeys a different resonance condition theoretically predicted for GERS.[6] In particular, at the 633 and 647-nm excitations falling into the low wavelength side of the Q_y (0–0) electronic absorption band of H_2Pc, the GERS enhancement of the Raman modes of H_2Pc in the glass/SLG/ H_2Pc (ML) hybrid system is attributed to RRS of H_2Pc modified by a relatively strong SLG–H_2Pc (ML) interaction. The most pronounced modification is delocalization of the resonant Q_y (0–0) electronic transition over the outer benzene rings of H_2Pc. Furthermore, the GERS enhancement at 830-nm excitation is ascribed to the proximity of this excitation to the energy of a photoinduced charge transfer transition from Fermi level of SLG on glass to LUMO of H_2Pc. The energy of this photoinduced CT transition was

calculated as the difference between the energy of the Fermi level of SLG on glass (−4.3 eV) and the previously reported energy of LUMO of H_2Pc[10]. To the best of our knowledge, this experimental evidence for the theoretically predicted GERS enhancement by the photoinduced CT mechanism[6] is reported here for the first time.

Finally, we propose that the approach presented in this paper for the SLG- H_2Pc (ML) can be applied also to other hybrid systems constituted by SLG and a monolayer of planar aromatic molecules, provided that their specificity, namely their various E_L and E_H values, are taken into account. The merit of such studies is not only the observation of the GERS enhancement, but also specification of its excitation wavelength dependence and of the mechanism of its origin for a particular SLG–aromatic molecule hybrid and excitation wavelength. Another benefit is obtaining information about the Raman spectral and electronic effects of SLG–aromatic molecule interaction in such hybrid systems.

Acknowledgments

The authors thank Prof. George R. Rossman and Prof. Antonin Vlcek for acquisition of the UV–Vis electronic absorption spectra of glass/SLG/H_2Pc-(BL)-I hybrid system on the special UV/Vis spectrometer assembled by Prof. G.R. Rossman at the California Institute of Technology, Division of Geological and Planetary Sciences. Financial support by the 15-01953S grant awarded by the Czech Science Foundation (Grantová Agentura České Republiky) is gratefully acknowledged.

References

[1] A. Jorio, R. Saito, G. Dresselhaus, M. S. Dresselhaus, *Raman Spectroscopy in Graphene Related Systems*, Wiley-VCH Verlag GmbH & Co. KGaA, Weinheim, Germany, **2011**.
[2] A. C. Ferrari, D. M. Basko, *Nat. Nanotechnol.* **2013**, *8*, 235.
[3] X. Ling, L. Xie, Y. Fang, H. Xu, H. Zhang, J. Kong, M. S. Dresselhaus, J. Thang, Z. Liu, *Nano Lett.* **2010**, *10*, 553.
[4] X. Ling, S. Huang, N. Mao, J. Kong, M. S. Dresselhaus, J. Zhang, *Accounts Chem. Res.* **2015**, *48*, 1862.
[5] S. Huang, X. Ling, L. Liang, Y. Song, W. Fang, J. Zhang, J. Kong, V. Meunier, M. S. Dresselhaus, *Nano Lett.* **2015**, *15*, 2892.
[6] E. B. Barros, M. S. Dresselhaus, *Phys. Rev. B* **2014**, *90*, 90035443.
[7] A. Brotman, E. Burstein, *Phys. Scripta* **1985**, *32*, 385.
[8] C. Murray, N. Dozova, J. G. McCaffrey, N. Shafizadeh, W. Chin, M. Broquier, C. Crépin, *Phys. Chem. Chem. Phys.* **2011**, *13*, 17543.
[9] M. Cook, I. Chambrier, in *The Porphyrin Handbook, Volume 17: Phthalocyanines: Properties and Materials* (Eds: K. Kadish, R. Guilard, K. M. Smith), Academic Press, San Diego, **2003**, pp. 37–128.
[10] K. Nilson, J. Ahlund, B. Brena, E. Göthelid, J. Schiessling, N. Martensson, *J. Chem. Phys.* **2007**, *127*, 114702.
[11] B. J. C. Cabral, V. W. D. Cruzeiro, K. Coutinho, S. Canuto, *Chem. Phys. Lett.* **2014**, *595–596*, 97.
[12] M. V. Martínez-Díaz, G. de la Torre, T. Torres, *Chem. Commun.* **2010**, *46*, 7090.
[13] B. Menaa, M. Takahashi, Y. Tokuda, T. Yoko, *J. Photochem. Photobiol. A* **2007**, *194*, 362.
[14] E. N. Kaya, T. Basova, M. Polyakov, M. Durmus, B. Kadem, A. Hassan, *RCS Advances* **2015**, *5*, 91855.
[15] M. Ochsner, *J. Photochem. Photobiol. B: Biology* **1996**, *39*, 1.
[16] R. Aroca, D. P. DiLella, *J. Phys. Chem. Solid* **1982**, *43*, 707.
[17] S. Heutz, G. Salvan, S. D. Silaghi, T. S. Jones, D. R. T. Zahn, *J. Phys. Chem. B* **2003**, *107*, 3782.
[18] J. Marshell, *Mat. Sci. Res. Ind.* **2010**, *7*, 221.
[19] R. O. Loutfy, *Can. J. Chem.* **1981**, *59*, 549.
[20] S. M. Bayliss, S. Heutz, T. S. Jones, *Phys. Chem. Chem. Phys.* **1999**, *1*, 3673.
[21] C. Murray, N. Dozova, J. G. McCaffrey, S. FitzGerald, *Phys. Chem. Chem. Phys.* **2010**, *12*, 10406.
[22] R. Aroca, R. O. Loutfy, *J. Raman Spectrosc.* **1982**, *12*, 262.
[23] X. Ling, L. G. Moura, M. A. Pimenta, J. Zhang, *J. Phys. Chem. C* **2012**, *116*, 25112.
[24] R. J. H. Clark, T. J. Dines, *Angew. Chem. Int. Ed. Engl.* **1986**, *25*, 131.
[25] R. Aroca, *Surface-Enhanced Vibrational Spectroscopy*, John Wiley and Sons, Ltd., Chichester, UK, **2006**.
[26] M. Procházka, *Surface-Enhanced Raman Spectroscopy-Bioanalytical, Biomolecular and Medical Applications*, Springer International Publishing, Switzerland, **2016**.
[27] I. Srnová-Šloufová, B. Vlčková, T. L. Snoeck, D. J. Stufkens, P. Matějka, *Inorg. Chem.* **2000**, *39*, 3551.
[28] I. Šloufová, B. Vlčková, M. Procházka, J. Svoboda, J. Vohlídal, *J. Raman Spectrosc.* **2014**, *45*, 338.
[29] S. Zheng-Lin, Z. Fu-Shi, C. Xi-Qiao, Z. Fu-Qun, *Acta Phys.-Chim. Sin.* **2003**, *19*, 130.
[30] M. Kalbáč, O. Frank, L. Kavan, *L. Carbon* **2012**, *50*, 3682.
[31] T. Hallam, N. C. Berner, C. Yim, G. S. Duesberg, *Adv. Mater. Interfaces* **2014**, *1*, 1400115.
[32] M. N. Taran, G. R. Rossman, *Am. Mineral.* **2001**, *86*, 973.
[33] S. J. Choquette, E. S. Etz, W. S. Hurst, D. H. Blackburn, S. D. Leigh, *Appl. Spectrosc.* **2007**, *61*, 117.
[34] L. Henke, N. Nagy, U. Krull, *J. Biosensors and Bioelectronics* **2002**, *17*, 547.
[35] C. A. Hunter, J. K. M. Sanders, *J. Am. Chem. Soc.* **1990**, *112*, 5525.
[36] B. J. Prince, B. E. Williamson, R. J. Reeves, *JOL* **2001**, *93*, 293.
[37] K. Nakamoto, *Infrared and Raman Spectra of Inorganic and Coordination Compounds*, 4th ed., John Wiley & Sons, Inc., New York, **1986**.
[38] C. A. Melendres, V. A. Maroni, *J. Raman Spectrosc.* **1984**, *15*, 319.
[39] X. Zhang, Y. Zhang, J. Jiang, *Vib. Spectrosc.* **2003**, *33*, 153.
[40] H. F. Shurvell, L. Pinzuti, *Can. J. Chem.* **1966**, *44*, 125.
[41] D. R. Tackley, G. Dent, W. E. Smith, *Phys. Chem. Chem. Phys.* **2001**, *3*, 1419.
[42] C. Cong, T. Yu, G. F. Dresselhaus, M. S. Dresselhaus, *ACS Nano* **2011**, *5*, 1600.
[43] D. M. N. M. Dissanayake, A. Ashraf, D. Dwyer, K. Kisslinger, L. Zhang, Y. Pang, H. Efstathiadis, M. D. Eisman, *Sci. Reports* **2016**, *6*, 21070.
[44] T. Komeda, H. Isshiki, J. Liu, *Sci. Technol. Adv. Mater* **2010**, *11*, 054602.
[45] K. Toyota, J. Hasegawa, H. Takatsuji, *J. Phys. Chem. A* **1997**, *101*, 446.
[46] A. Campion, P. Kambhampati, *Chem. Soc. Rev.* **1998**, *27*, 241.

Supporting information

Additional Supporting Information may be found online in the supporting information tab for this article.

Supporting Information

Excitation wavelength dependence of Raman spectra of single layer graphene-free base phthalocyanine hybrid systems: GERS excitation profiles, mechanisms and enhancement factors

Tereza Uhlířova[a], Peter Mojzeš[b], Zuzana Melniková[c] Martin Kalbáč[c], Veronika Sutrová[a,d], Ivana Šloufová[a], Blanka Vlčková[a]*

[a] Charles University, Faculty of Science, Department of Physical and Macromolecular Chemistry, Hlavova 8, Prague 2, 128 40, Czech Republic

[b] Charles University, Faculty of Mathematics and Physics, Institute of Physics, Ke Karlovu 5, Prague 2, 121 16, Czech Republic

[c] J. Heyrovsky Institute of Physical Chemistry of the ASCR, v.v.i, Dolejškova 3, 182 21 Prague 8, Czech Republic

[d] Institute of Macromolecular Chemistry AS CR, Heyrovsky Sq. 2, 162 06 Prague 6, Czech Republic

* Corresponding author's e-mail: vlc@natur.cuni.cz

Supporting Information Text 1: Preparation and Raman spectral mapping of graphite/H_2Pc (ML) reference sample

A cylindrical graphite electrode for thermal evaporation of carbon was cut in half to produce a flat surface. The surface was then rubbed and polished by abrasive papers of decreasing abrasivity, and finally polished by a filter paper. The surface appeared to be flat and smooth, however, its SEM imaging revealed the presence both of the flat and smooth areas (Fig. S1, image A) and of the corrugated ones (Fig.S1, image B). Imaging with the optical microscope of the Raman microspectrometer revealed that the flat and smooth areas can be found also on the optical images (Fig. S2), and used for the subsequent Raman mapping. Moreover, the areas suitable for mapping of the graphite/H_2Pc reference samples could be identified also by the Raman spectra resulting from mapping of the parent graphite surface. The Raman maps of the appropriate areas showed a very low intensity of the 1344 cm-1 graphite band, in contrast to those of the corrugated ones, in which this band was very intense.

Graphite/H_2Pc monolayer (ML) samples were prepared by a similar strategy as those of glass/SLG/H_2Pc, i.e. first by soaking in H_2Pc solution in toluene and by a subsequent repeated soaking in pure toluene. Nevertheless, owing to stability of the graphite substrate, the preparation protocol could be simplified by its immersion into the solution and the solvent, respectively, (rather than only overlayed by each of them). Therefore, graphite was immersed into H_2Pc solution in toluene for 2 hours, dried by filter paper and then repeatedly immersed into pure toluene for ~24 hours. Achievement of a ~ monolayer coverage was established in a similar manner as in the case of glass/SLG/H_2Pc sample.

The parameters of the spectral maps acquisitions at each of the excitation wavelengths were the same as for the glass/SLG/H_2Pc samples. Nevertheless, owing to the above mentioned inhomogeneity of the graphite surface, it became crucial to acquire the Raman maps from exactly the same (carefully selected) flat and smooth area of the graphite surface (depicted in Fig S2) for both the graphite substrate itself, and for each of the graphite/H_2Pc samples at each of the excitation wavelengths. Fulfillment of this condition was accomplished by construction and application of a special sample holder, and it was repeatedly controlled by the optical imaging.

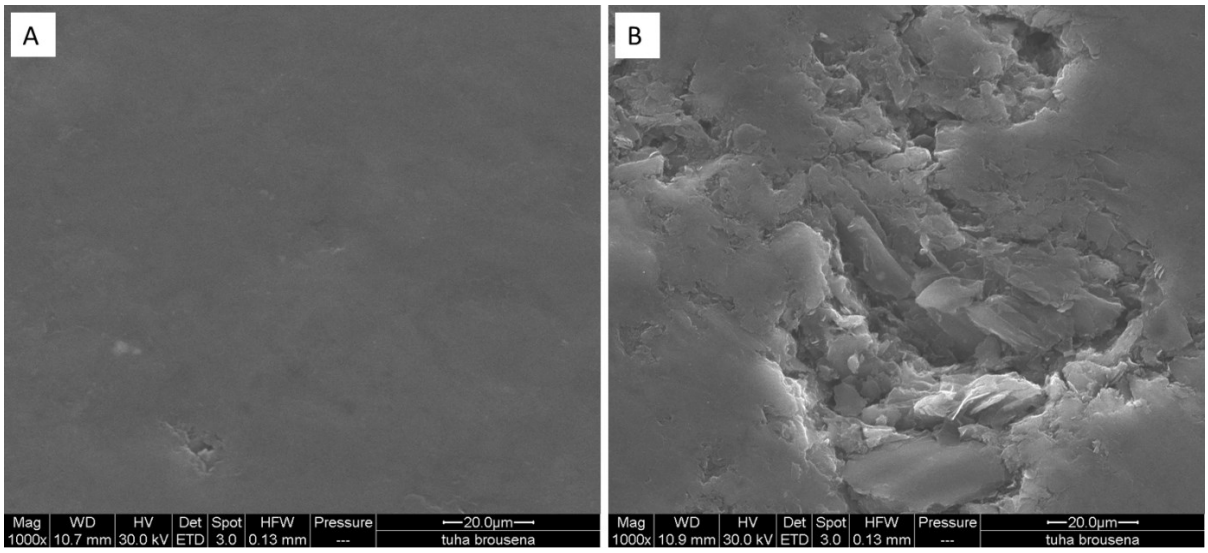

Fig. S1 SEM images of rubbed and polished graphite surface: (A) flat area, (B) corrugated area.

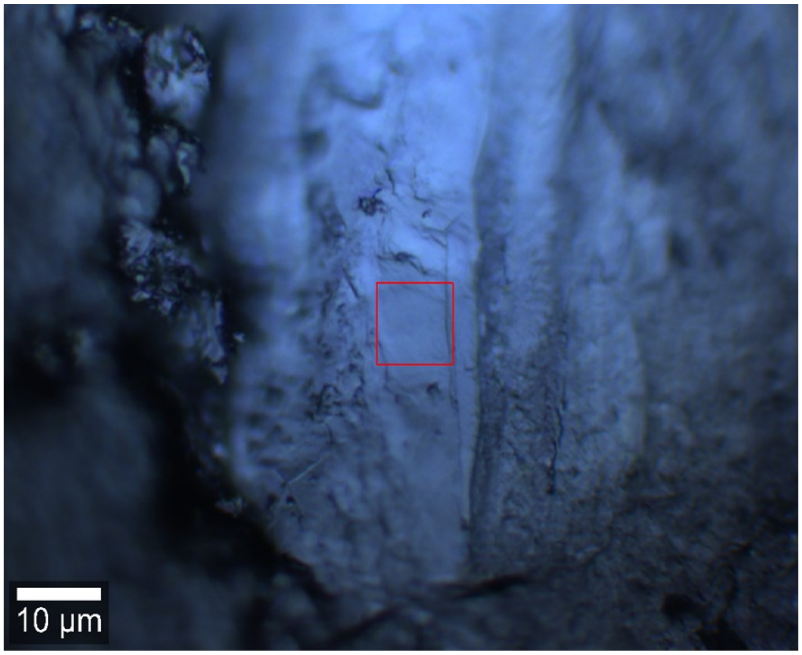

Fig. S2 Optical image of a flat and smooth location on graphite/H_2Pc surface from which Raman maps were acquired.

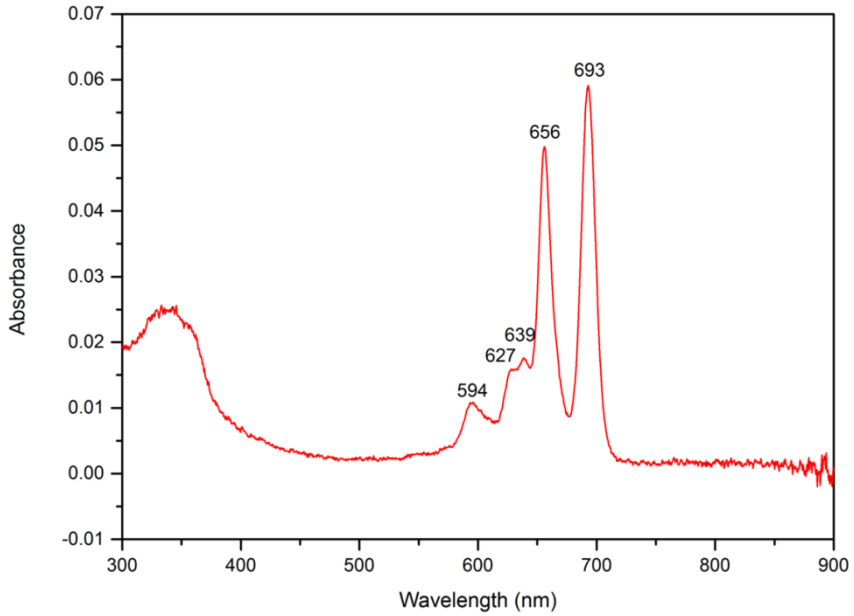

Fig. S3 Electronic absorption spectrum of a filtered saturated (<5x10^{-5} M) solution of H_2Pc in toluene.

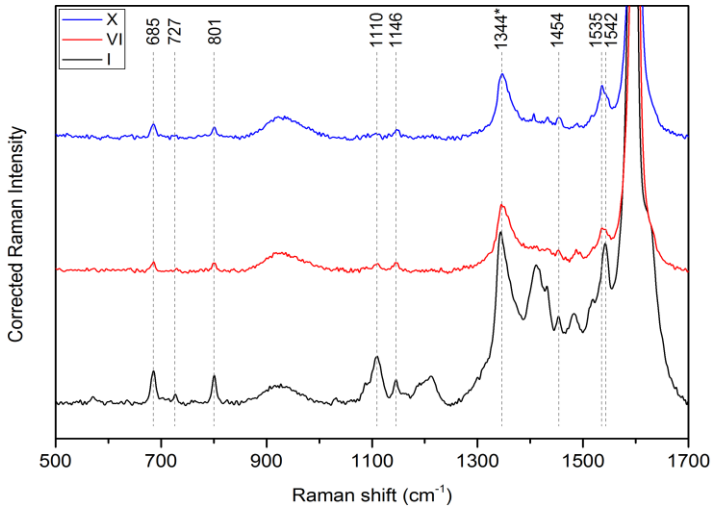

Fig. S4 Raman spectra (500-1700 cm-1) of glass/SLG/H_2Pc (BL)-I (black), glass/SLG/H_2Pc (ML)-VI (red) and glass/SLG/H_2Pc (ML)-X (blue) systems at 532 nm excitation.

Supporting Information Text 2: Details of the assignment of the H_2Pc Raman spectral bands in the hybrid systems.

Since the vast majority of spectral bands observed in the spectra of all hybrid samples can be related to their analogues in the previously reported Raman spectra of H_2Pc in thin films [16,17,20] and in a KBr pellet [8,21], the previously published assignments of Raman spectral bands can, in principle, be used. A normal coordinate analysis (NCA) has not been reported for H_2Pc. Nevertheless, the NCA performed for FePc metallophthalocyanine indicates a strong vibrational coupling of the individual (characteristic) modes and, consequently, a strong vibrational delocalization of normal modes over the Pc macrocycle.[39] Consequently, the assignment of H_2Pc vibrations based on the DFT (density functional theory) calculations [8,21] appears to be more comprehensive than the previously published empirical one.[16] The former assignment has thus been adopted into Table 1.

Raman active vibrations of H_2Pc molecule belong to A_g, B_{1g}, B_{2g} and B_{3g} symmetry species. Nevertheless, only the bands of A_g and B_{1g} in plane vibrations are usually observed in Raman spectra of H_2Pc.[8] It should be noted that both the A_g and B_{1g} Raman active vibrations experience a resonance enhancement upon excitations overlapping with the Q-band spectral region. Excitations at the wavelengths matching those of the purely electronic Q_x (0-0) and Q_y(0-0) transitions lead to the resonace enhancement of totally symmetric A_g modes by the Franck-Condon mechanism. In addition to that, the B_{1g} modes are enhanced by the Herzberg-Teller mechanism originating from coupling of the close lying Q_x and Q_y excited electronic states by vibrations of B_{1g} symmetry. Furthermore, excitations falling into the vibronic side-band of the Q_y band (originating from coupling of the B, i.e. the Soret, and the Q electronic transitions) also lead to the resonance enhancement of both A_g and B_{1g} vibrations. [16,17] Assignment of the Raman spectral bands of H_2Pc in the KBr pellet to A_g and B_{1g} symmetry species based on the DFT calculation has been performed.[8] For the experimental verification of this assignment, we attempted to determine the depolarization ratios of Raman spectral bands at an off-resonance excitation (to avoid observation of anomalously polarized bands). Since solubility of H_2Pc in toluene was not sufficient for this purpose, depolarization ratios of Raman spectral bands were obtained from Raman spectral polarization measurements of an aqueous solution of the water soluble derivative of H_2Pc, namely H_2Pc-TS (TS= tetrasulphonatophenyl), at 532 nm, i.e. by the strategy previously employed for FePc [39]. Comparison of the polarization characteristics (p-

polarized, dp-depolarized) of the H_2PcTS Raman spectral bands with the symmetry species (A_g or B_{1g}) assigned to the corresponding bands of the H_2Pc vibrations in the glass/SLG/H_2Pc (ML)-X system on the basis of the results of the DFT calculation for H2Pc is shown in Table S1, and the results have been incorporated into Table 1. The match between the DFT-calculated and the experimentally determined symmetry properties of vibrations derived from the depolarization ratios of their spectra bands (p-A_{1g}, dp-B_{1g}) has been obtained for all the Raman bands with a clearcut correspondence between the H_2Pc and H_2Pc-TS spectral bands. (Table S1).

The wavenumbers of Raman spectral bands observed for the glass/SLG/H_2Pc(BL)-I hybrid system at 633 nm (Fig. 2, spectrum b), in comparison to those in the previously reported Raman (GERS) spectra of the Si/SiO_2/SLG/H_2Pc hybrid system of about 0.2 nm thickness measured at this particular excitation wavelength,[3] show a good mutual agreement. In addition to those reported previously,[3] we report the spectral bands in the 400-600 cm^{-1} region, namely those at 484, 544 and 569 cm^{-1}as well as two new spectral bands at 750 and 951 cm^{-1}. All the spectral bands in the spectra of glass/SLG/H_2Pc (BL)-I at 633 nm excitation have their analogues in the newly reported spectra at the 647 nm excitation (and most of them are observed also at 785, 830 and 532 nm excitations) (Fig. 2 and Table 1). At both 633 and 647 nm excitations, we observe also analogues of the 766, 1159 and 1407 cm^{-1} bands (namely at 768,1162 and 1406 cm^{-1}) which, in ref. 3, were assigned to the SLG activated IR (infrared) modes. Nevertheless, in the meantime, analogues of these bands (765, 1155, 1407 cm^{-1}) have been observed in the Raman spectra of H_2Pc in a KBr pellet excited at 532 nm and assigned to Raman active A_g modes on the basis of the DFT calculations.[21] On the other hand, the newly observed spectral bands at 750 and 951 cm^{-1} do not have analogues in the previously published Raman (and/or GERS) spectra of H_2Pc. [3,16,21] Since these bands belong neither to Raman bands of toluene (used as solvent for H_2Pc deposition by adsorption) nor to those of impurities originating from the SLG deposition (they are absent in Raman spectra of the parent glass/SLG system, Fig.S7 spectrum d), their origin deserves a more thorough discussion provided below.

The 750, 958, 1218 and 1533 cm^{-1} Raman bands of H_2Pc are the spectral features related to the SLG-H_2Pc interaction in glass/SLG/H_2Pc hybrids. Of these, the 1533 cm^{-1} band occurs specifically upon SLG-H_2Pc (ML) interaction. We note that the 750 and 958 cm^{-1} bands (which do not have any previously reported Raman analogues) do have their counterparts in the IR spectra of H_2Pc, namely the 752 and 952 cm^{-1} bands

assigned to the out of plane N-H and out of plane C-H deformation modes, respectively.[21,40,41] Their Raman spectral activation by the SLG-H_2Pc interaction could presumably be related to a decrease of the effective symmetry of H_2Pc molecule ($D_{2h} \rightarrow D_{2d}$) by its axial interaction with SLG. It should also be noted that the graphite-SLG interaction is not strong enough to induce such effect, since the two above mentioned bands are virtually absent in the Raman spectra of graphite-H_2Pc (ML) system. A probable reason for the graphite –H_2Pc interaction being weaker that SLG-H_2Pc one is the fact that in the graphite-H_2Pc system, the top graphene layer of graphite interacts with both H2Pc and with the other graphene layers in graphite.

A similar argument, i.e. the relatively strong SLG-H_2Pc interaction, can be used for explanation of the appearance of the 1218 cm^{-1} Raman band (belonging to B_{1g} symmetry mode), as well as of the 1533 cm^{-1} in the spectra of glass/SLG/H_2Pc hybrids. Nevertheless, the origin of the latter band requires a closer inspection for the following reasons. First, its observation is limited to the glass/SLG/H_2Pc/ (ML) samples VI and X, however, its actual relative intensity is different for the sample VI and X, and, for the sample X, it becomes the most intense Raman spectral band of H_2Pc. Secondly, in the spectra of both samples VI and X, this band is observed as the part of a doublet with a close-lying band at 1545 cm^{-1} which decreases in its relative intensity for the sample X with respect to the sample VI. The latter Raman spectral band is, in turn, typical for the spectra of both glass/SLG/H_2Pc(BL)-I and graphite/H_2Pc (ML) hybrids.

This single Raman band observed at 1543 cm^{-1} for glass/SLG/H_2Pc(BL)-I and at 1544 cm^{-1} for graphite/H_2Pc (ML) corresponds with the 1540 cm^{-1} band of H_2Pc in the KBr pellet assigned to the C-Nm-C asymmetric stretching and C-N_H-C symmetric stretching, i.e. to the overall motion of 16 C-N bonds of A_g symmetry. [8,21] This band has also been denoted as the cavity size marker on the basis of the spectra of various metallophthalocyanines [42]. In the case of H_2Pc Raman spectra, this band has also been observed in the 1534-1539 cm^{-1} range for various samples of the α -H_2Pc polymorph films [16,17,20] and as a 1539 and 1525 cm^{-1} doublet for the β -H_2Pc polymorph films. In the latter case, observation of a doublet can be attributed to the presence of two non-equivalent H_2Pc molecules in the unit cell. [9]

In search for a possible explanation of observations of the 1545, 1533 cm^{-1} doublet in Raman spectra of hybrid systems constituted by SLG and a monolayer of H_2Pc molecules, we speculate that there can actually be two types of adsorption sites for H_2Pc on SLG, and that at one of them, the SLG-H_2Pc interaction is stronger than on the other.

This, in turn, could result into observation of two C-N-C mode bands. Furthermore, the additional soaking of the sample VI in toluene could lead to reorganization of molecules within the adsorbed H_2Pc monolayer resulting into a higher population of the sites with a stronger H_2Pc -SLG interaction in sample X . This, in turn, can lead to the the gain of the 1533 cm^{-1} band intensity on the expenses of that of the 1545 cm^{-1} band. Importantly, the exchange of relative band intensities of the two above mentioned bands projects itself into the wavenumbers of the corresponding overtone bands, which are observed at 3080 cm^{-1} for sample VI and at 3060 cm^{-1} for sample X (Table 2 and Figs.S5 and S6). In particular, observation of the 1533 cm^{-1} band overtone at 3060 cm^{-1} indicates, that the corresponding fundamental is of A_g symmetry and can thus be attributed the combined C-N-C vibrational mode. This assignment has been incorporated into Table 1. Note: the references correspond to those listed in the paper.

Table S1: Wavenumbers of H_2PcTS Raman spectral bands (in an aqueous solution) and their polarization (p = polarized, dp = depolarized), wavenumbers of H_2Pc Raman spectral bands in glass/SLG/H_2Pc-X hybrid system and the symmetry of corresponding modes from DFT calculations by Murray et al. [21]. The 1276 cm^{-1} band (marked *) belongs to sulfonate group[39]

Band wavenumbers of H_2PcTS (cm^{-1})	Polarization	Band wavenumbers of H_2Pc (cm^{-1})	Symmetry
576	p	545	A_g
588	p	597	A_g
688	p	684	A_g
727	p	726	A_g
805	p	798	A_g
		1010	A_g
1020	dp		
1035	dp	1029	B_{1g}
1071	dp	1085	B_{1g}
1103	dp	1111	B_{1g}
1128	dp		
		1145	A_g
1180	p	1185	A_g
1190	dp	1197	B_{1g}
1228	dp	1219	B_{1g}
1276	*	–	
1312	dp	1311	B_{1g}
1337	p	1343	A_g
1394	p	1408	A_g
1431	dp	1431	B_{1g}
1463	p	1453	A_g
1518	p	1512	A_g
1535	dp	1532	–
	p	1544	A_g
1578	P	–	
1614	dp	1620	B_{1g}

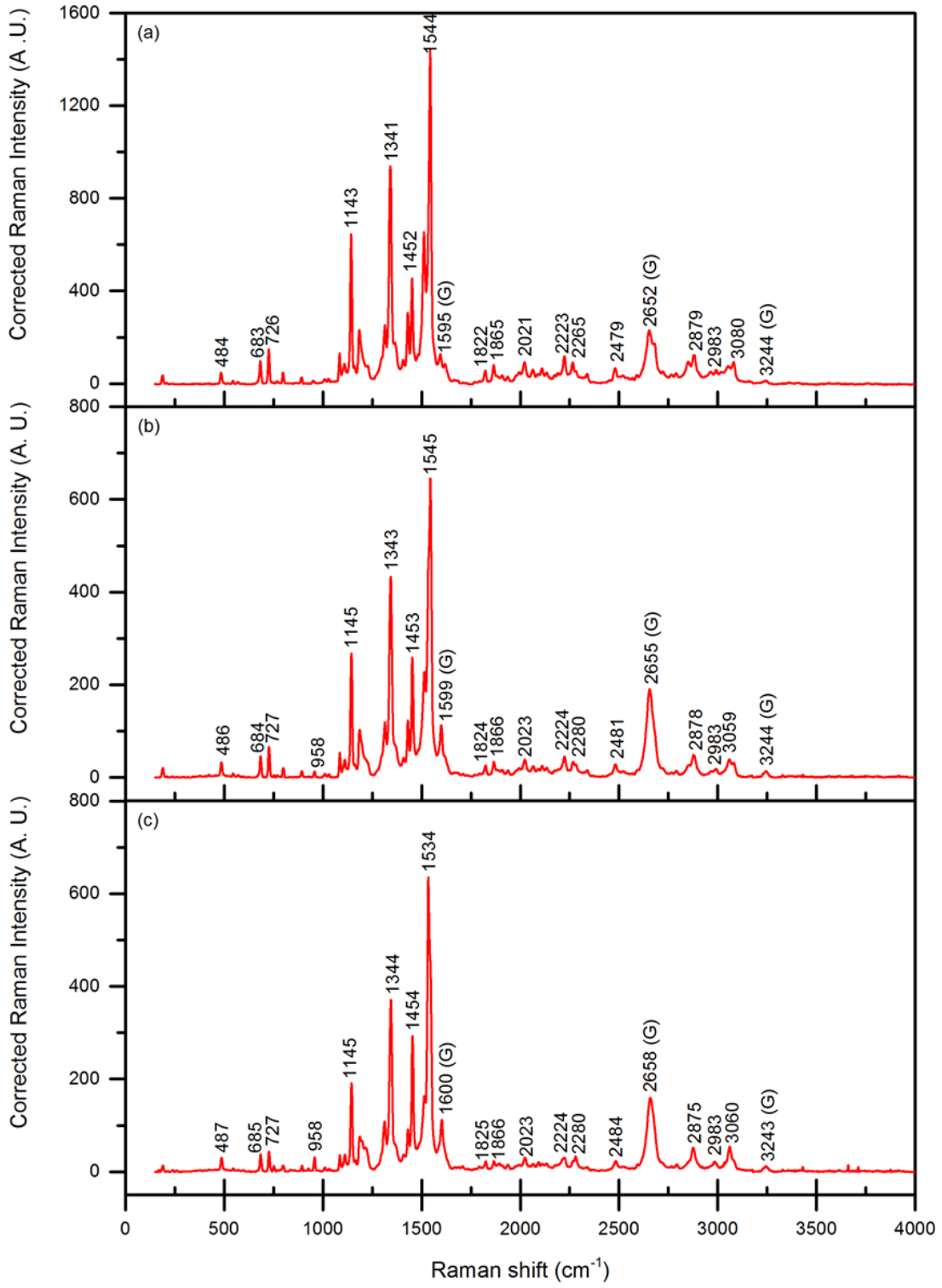

Fig. S5 Full range (400-4000 cm-1) Raman spectra of (a) glass/SLG/H_2Pc (BL)-I, (b) glass/SLG/H_2Pc (ML)-VI and (c) glass/SLG/H_2Pc (ML)-X systems at 633 nm excitation.

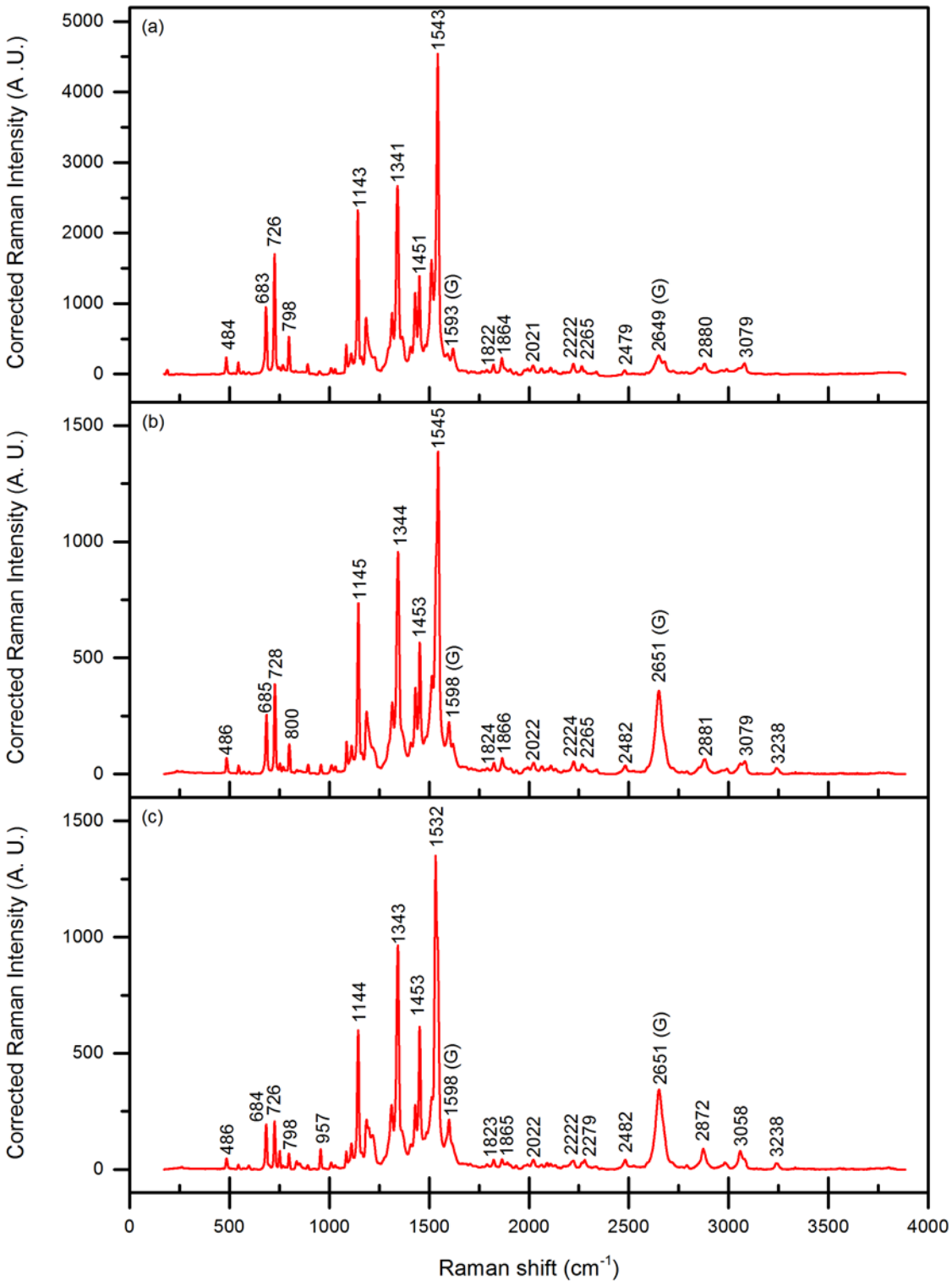

Fig. S6 Full range (400-4000 cm-1) Raman spectra of (a) glass/SLG/H_2Pc (BL)-I, (b) glass/SLG/H_2Pc (ML)-VI and (c) glass/SLG/H_2Pc (ML)-X systems at 647 nm excitation.

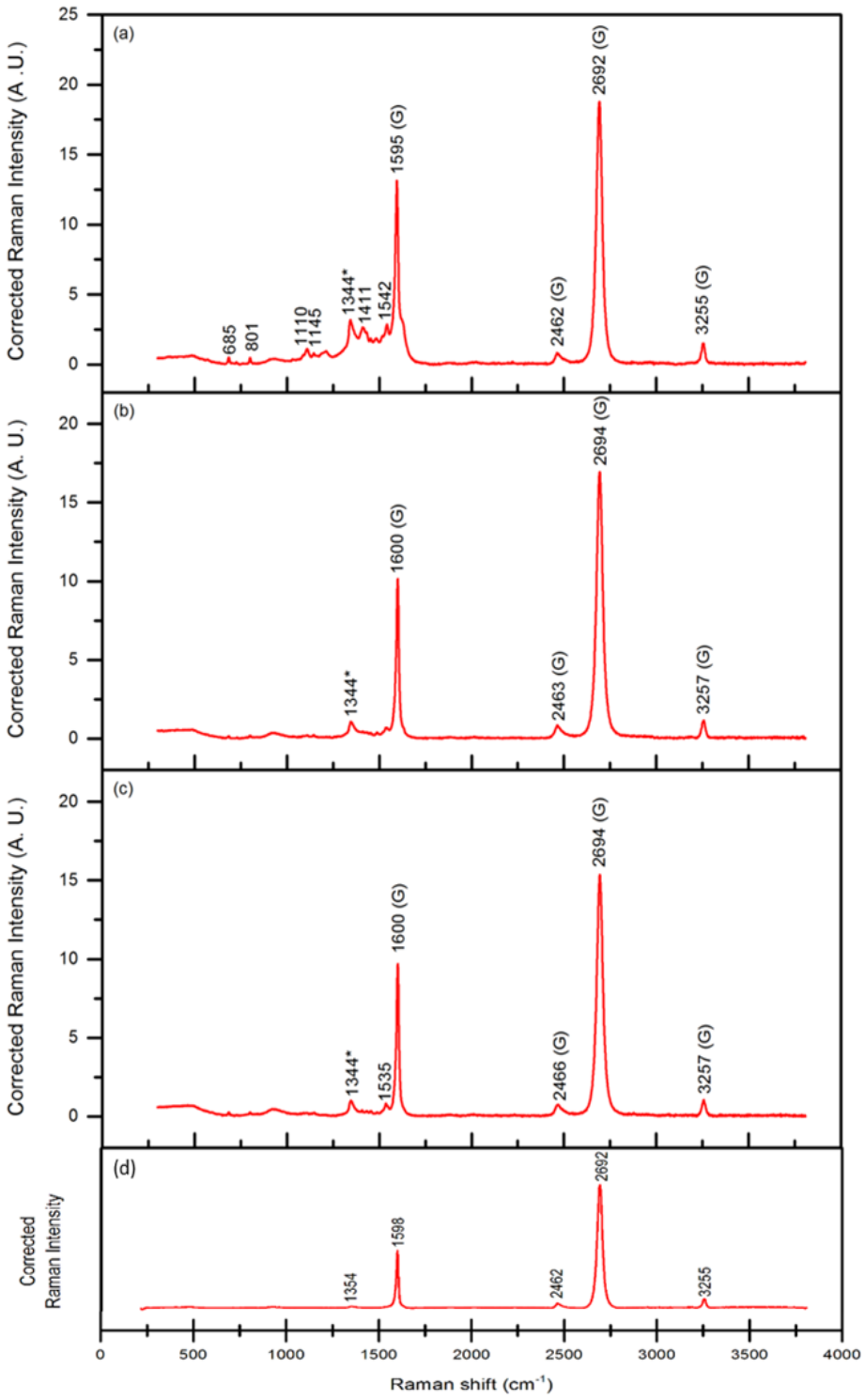

Fig. S7 Comparison of the full range Raman spectra of glass/SLG/H_2Pc systems (a) (BL)-I, (b) (ML)-VI, (c) (ML)-X and of (d) glass/SLG reference system at 532 nm excitation.

Table S2: The 2D mode dispersion in the parent glass/SLG system and in the hybrid system with H_2Pc

Excitation wavelength [nm]	glass/SLG/H_2Pc – I	glass/SLG/H_2Pc – VI	glass/SLG/H_2Pc – X	glass/SLG
532	2692	2694	2694	2692
633	2652	2655	2658	2655
647	2649	2651	2651	2647
785	2597	2596	2595	2600

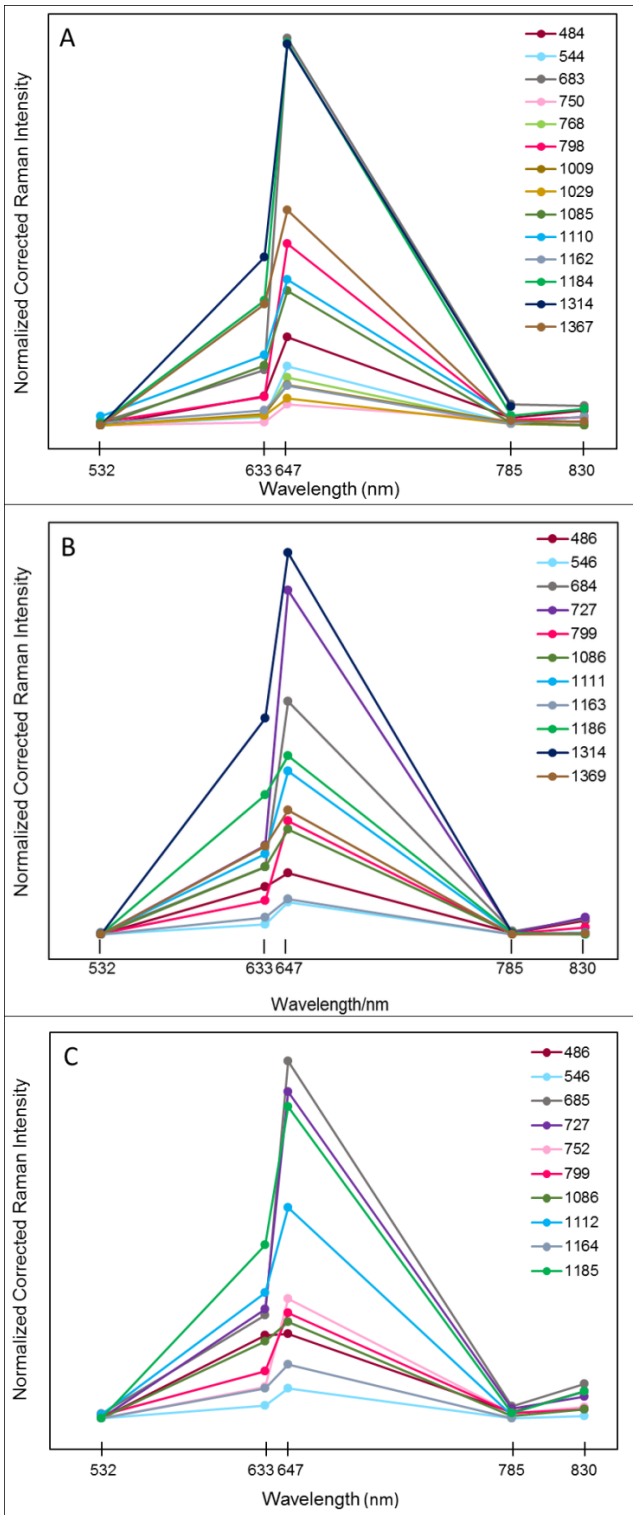

Fig. S8 Details of Raman spectral bands excitation profiles of (A) glass/SLG/H_2Pc (BL)-I system, (B) glass/SLG/H_2Pc (ML)-VI system, (C) glass/SLG/H_2Pc (ML)-X system in the 532-830 nm range (with the focus on the less enhanced bands).

8.2. Publication II: Effect of ethanethiolate spacer presence and/or removal on morphology and optical responses of hybrid systems constituted by single layer graphene and Ag nanoparticle arrays

Veronika Sutrová[a,c], Ivana Šloufová[a], Zuzana Melniková[b], Martin Kalbáč[b], Ewa Pavlova[c], Blanka Vlčková[a]*

[a] Charles University, Faculty of Science, Department of Physical and Macromolecular Chemistry, Hlavova 8, Prague 2, 128 40, Czech Republic, vlc@natur.cuni.cz

[b] J. Heyrovsky Institute of Physical Chemistry of the ASCR, v.v.i, Dolejškova 3, 182 21 Prague 8, Czech Republic

[c] Institute of Macromolecular Chemistry AS CR, Heyrovsky Sq. 2, 162 06 Prague 6, Czech Republic

My contribution:

All experimental work: i.e. samples preparations, SERS spectral testing, TEM + SEM imaging, except of SLG sample preparation, data evaluation and principal participation in MS preparation.

LANGMUIR Article
Cite This: Langmuir 2017, 33, 14414−14424 pubs.acs.org/Langmuir

Effect of Ethanethiolate Spacer on Morphology and Optical Responses of Ag Nanoparticle Array−Single Layer Graphene Hybrid Systems

Veronika Sutrová,[†,§] Ivana Šloufová,[†] Zuzana Melníková,[‡] Martin Kalbáč,[‡] Ewa Pavlova,[§] and Blanka Vlčková*[,†]

[†]Faculty of Science, Department of Physical and Macromolecular Chemistry, Charles University, Hlavova 8, Prague 2, 128 40, Czech Republic

[‡]J. Heyrovsky Institute of Physical Chemistry of the ASCR, v.v.i, Dolejškova 3, 182 21 Prague 8, Czech Republic

[§]Institute of Macromolecular Chemistry AS CR, Heyrovsky Square 2, 162 06 Prague 6, Czech Republic

Supporting Information

ABSTRACT: Single layer graphene (SLG) and two-dimensional (2-D) plasmonic Ag nanoparticle arrays assembled by chemisorption of ethanethiol (ET) molecules (AgNPs-ET) were employed as components of two types of hybrid systems designed for surface-enhanced Raman scattering (SERS) spectral probing of SLG localized in the vicinity of plasmonic NPs. Both hybrids were characterized by optical microscopy, transmission electron microscopy (TEM), surface plasmon extinction (SPE), and SERS microRaman spectral measurements at four excitation wavelengths spanning the 445−780 nm range. SERS spectral probing of the glass/SLG/AgNPs-ET hybrid prepared by overdeposition of SLG on glass by the array of ET-modified Ag NPs has shown that the chemisorbed ET acts as an efficient molecular spacer between SLG and Ag NPs surface which, in turn, enabled to obtain SERS spectra of SLG unperturbed by doping or strain. TEM imaging and SERS spectral probing of the second hybrid prepared by overdeposition of AgNPs-ET array on glass by SLG revealed removal of the adsorbed ET molecules and annealing of Ag NPs during the SLG deposition. The characteristics of the resulting glass/AgNPs/SLG hybrid system, namely (i) broad distribution of the annealed Ag NPs sizes and shapes, (ii) SPE curve covering the overall visible spectral region, (iii) absence of the ET spectral bands in SERS spectra, and (iv) fairly uniform SERS enhancement of the G and 2D mode of SLG in the 532−780 nm range in the straight sample geometry indicate that this hybrid can provide a suitable platform for investigation of the excitation wavelength dependence of combined SERS/GERS (graphene-enhanced Raman scattering) enhancement experienced by various molecular species brought into contact with SLG in this hybrid. Finally, weak optical effects attributed to increased reflectivity of SLG in the near field of Ag NPs arrays have been observed in the excitation wavelength dependence of the SERS spectra of both types of hybrid systems.

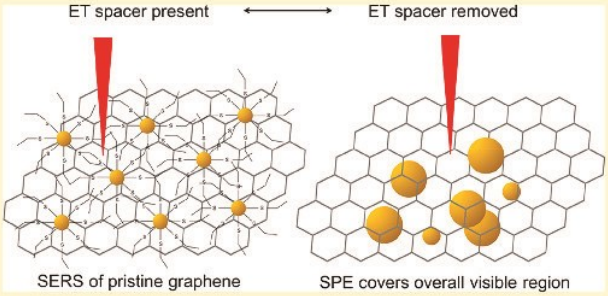

INTRODUCTION

Hybrid systems constituted by plasmonic metal nanoparticles (NPs) and graphene are currently the subject of considerable interest stemming from the specific properties of the components as well as new effects resulting from integrating of these components. In particular, the ability of plasmonic NPs to confine visible light into subwavelength dimensions by resonance excitations of dipolar (localized) surface plasmons is widely used in plasmonics, optoelectronics, and in surface-enhanced Raman spectroscopy.[1−3] Graphene, and particularly single-layer graphene (SLG), is a highly desirable material for optoelectronics due to its unique properties, such as a ultrathin (atomic) thickness, high carrier mobility, and mechanical flexibility.[4] For example, the potential of SLG as a material for construction of fast photodetectors has been been considered, but found to be hampered by its very low quantum efficiency and an absence of the spectral selectivity. Nevertheless, these limitations have been overcome by integration of graphene with a thin layer of plasmonic nanostructures. In such systems, the plasmonic nanostructures act as nanoantennas that enhance the photoresponse selectively at their plasmon resonance wavelength(s), and thus enable construction of graphene-based photodetectors with the desired light wavelength (color) selectivity.[5] Subsequently, the wavelength-dependent absorption induced by localization of SLG into the near field optically excited in the vicinity of two-dimensional (2-D) arrays of Ag and/or Au NPs has been explored both by model calculations and experiments.[6−10]

Received: October 6, 2017
Revised: November 24, 2017
Published: November 27, 2017

DOI: 10.1021/acs.langmuir.7b03462
Langmuir 2017, 33, 14414−14424

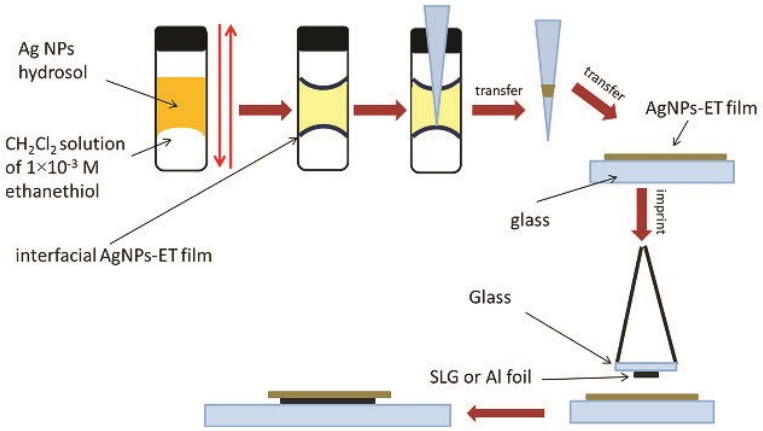

Figure 1. Preparation of arrays of ethanethiolate-modified Ag NPs, their deposition onto glass slides, and their transfer onto glass/SLG and/or glass/Al foil supporting surfaces.

Furthermore, the effect of coupling of SLG with plasmonic metal nanostructures, e.g., Ag or Au NPs arrays, on doping and/or strain experienced by SLG in the plasmonic metal NPs/SLG hybrid systems, has been successfully explored by surface enhanced Raman scattering (SERS) spectroscopy.[11−19] Interpretation of the SERS studies of such hybrid systems takes advantage of the previously published Raman spectral studies of SLG under various, but well-defined conditions.[20,21] Furthermore, the SERS enhancement experienced by the SLG modes has been attributed to the electromagnetic (i.e., the localized plasmon resonance) mechanism of SERS.[14] SERS spectra of SLG were obtained from hybrid systems constituted by SLG and the overdeposited plasmonic NPs as well as from the assemblies of plasmonic NPs overlaid by SLG.[11−18] A comparison of SERS of SLG from these two types of hybrid systems has been addressed,[19] however, a mutual comparison of the SERS enhancement factors experienced by the SLG modes in each of these two hybrid systems was somewhat hampered by different morphology of the Ag NPs and of their assembly in each of them. In addition to that, the hybrid systems constituted by graphene and plasmonic NPs were employed as platforms for SERS of graphene,[22] SERS spectral sensing platforms for molecules,[15,17,18,23,24] as well as for SERS spectral monitoring of plasmon-driven reactions[25] and of specific sensor−analyte interactions.[26]

In this work, we investigate the effect of ethanethiolate spacer presence and/or removal on morphology and optical responses of hybrid systems constituted by SLG and Ag nanoparticle arrays. First, we explore the effect of a thin molecular spacer separating SLG from a 2-D array of Ag NPs, on the SERS spectra of SLG. Our aim is to reveal whether the presence of the thin molecular spacer can eliminate the strain and/or doping induced by a direct interaction between SLG and Ag NPs. Our effort is targeted on (i) preservation of pristine SLG structure, and (ii) obtaining at least some SERS enhancement of Raman modes of SLG. This approach has been partially motivated by previous SERS spectral studies carried out by us and others,[3,27−30] in which SERS and/or SERRS spectra of structurally unperturbed molecular species have been obtained on substrates constituted by Ag NPs modified by molecular spacers tailored specifically for the particular types of molecular species investigated. For SERS of SLG on spacer-modified plasmonic NPs, we selected Ag NPs modified by adsorption of ethanethiol (ET) upon formation of Ag-ET surface species, as reported previously.[28] ET that is chemisorbed on Ag NPs at the interface between the aqueous and the dichloromethane phase has been shown to play a dual role: (i) a hydrophobic spacer enveloping the Ag NPs and (ii) a mediator of the 2-D assembling of ET-modified Ag NPs at the interface.[28,29]

In the first part of this paper, we report on assembling of glass/SLG/AgNPs-ET hybrid system (constituted by SLG deposited on a glass substrate and overdeposited by a 2-D array of ET-modified Ag NPs) and on the results of its SERS spectral probing at four excitation wavelengths in the 445−780 nm range. As the reference systems for evaluation of the SLG and the Ag-ET spectral bands positions and intensities, we employ the glass/SLG and the glass/AgNPs-ET system, respectively. Furthermore, we compare the morphology and surface plasmon extinction (SPE) spectra of the hybrid system and of the second reference system as a part of our effort to explain the observed additional SERS enhancement experienced by the Ag-ET surface species in the hybrid system with SLG.

In the second part of this paper, we provide SERS spectral evidence of the complete removal of the ET spacer upon deposition of SLG onto the glass-deposited 2-D array of ET-modified Ag NPs by the chemical vapor deposition (CVD) procedure,[31] namely, by the nitrocellulose (NC) method. This method of SLG transfer involves a solvent exposure as well as a moderate heating of the as prepared hybrid system.[32] We explore the effect of this procedure on the morphology and SPE of Ag NPs in the resulting glass/AgNPs/SLG hybrid system as well as on the SERS spectra of SLG. In particular, we employ a novel strategy of SERS microRaman spectral measurements of the glass/AgNPs/SLG hybrid system samples in two different orientations with respect to the incident laser excitation (further denoted as the straight and the inverted sample geometry). Comparison of the SERS enhancement experienced by the SLG spectral modes in each of the two sample geometries allows us to address the question of whether localization of the same plasmonic enhancer (i.e., a 2-D array of Ag NPs) above or underneath SLG does actually affect the experimentally determined SERS enhancement factors of the SLG spectral modes.

■ EXPERIMENTAL SECTION

Materials. Analytical-grade $AgNO_3$ and sodium borohydride as well as spectral grade dichloromethane (UVASOL) were purchased from Merck, and 1-ethanethiol (97%) from Sigma-Aldrich. Al foil was

DOI: 10.1021/acs.langmuir.7b03462
Langmuir 2017, 33, 14414−14424

obtained from Scienceware. Distilled deionized water was used for all sample preparations.

Preparation of Glass/SLG Hybrid System. SLG was prepared by the previously reported CVD procedure.[31] The as-grown graphene was transferred to the glass substrate using cellulose nitrate (NC).[32] The majority of the NC layer was removed by methanol drops at room temperature. The glass/SLG sample was then annealed at 160 °C for 30 min in order to remove the NC residuals from the SLG surface. Raman spectral mapping of the sample showed no spectral features of the NC residuals.

Preparation of Ag NP Hydrosol. Ag NP hydrosol was prepared by reduction of silver nitrate by sodium borohydride according to the previously published procedure.[28] A transmission electron microscopy (TEM) image of the dried drop of the hydrosol deposited on a carbon-coated grid for TEM and the distribution of the Ag NPs sizes are shown in Figure S1 in the Supporting Information (SI). The average value of Ag NPs size is 7.5 nm.

Preparation and Deposition of Arrays of Ethanethiolate-Modified Ag NPs. Arrays of Ag NPs modified by chemisorbed ethanethiol (further denoted as AgNPs-ET arrays) were prepared according to the procedure reported by Michl et al.[28] Briefly, a two-phase system constituted by 2 mL of Ag NPs hydrosol and 2 mL of a 1×10^{-3} M solution of ethanethiol in dichloromethane was vigorously shaken until a lustrous nanoparticulate film appeared at the interface between the aqueous and the organic phase (photographically depicted in Figure S2). The interfacial film was then transferred by a pipet onto a glass slide (scheme in Figure 1), and it was either directly used for preparation of hybrid system I, of glass/Al foil/AgNPs-ET reference system and/or samples for TEM by imprinting on the particular supporting surface (glass/SLG, glass/Al foil, C-coated grid for TEM or SLG covered, C-coated TEM grid, respectively, Figure 1 and Figure S2 in the SI), or allowed to dry in air and employed as the reference system for SERS spectral measurements and/or as the component of the hybrid system II. By differential electronic absorption and/or SPE spectral measurements, the efficiency of the ET incorporation into interfacial films was established to be ca. 2%, and the Ag NPs assembling efficiency was found to be ca. 83%.

Preparation of Hybrid System I. The hybrid system constituted by SLG overdeposited by the Ag NPs-ET array was prepared by transfer of the Ag NPs-ET array from a glass slide by its imprinting onto SLG deposited on a glass slide (Figure 1 and Figure S2 in the SI).

Preparation of Hybrid System II. The hybrid system II was prepared by overdeposition of the glass-deposited AgNPs-ET array by SLG using the CVD procedure,[31] in particular the NC method[32] of the as prepared SLG transfer onto the Ag NPs-ET array on glass. The majority of the NC layer from the resulting glass/AgNPs-ET/SLG/NC hybrid was removed by methanol drops at room temperature. Then the glass/AgNPs-ET/SLG sample was annealed at 160 °C for 30 min in order to remove the NC residuals from the SLG surface. SERS spectral mapping of the sample (*vide infra*) showed no spectral features of the NC residuals, which, in turn, demonstrates that an advantage of this particular preparation procedure is obtaining of the spectrally pure glass/AgNPs/SLG samples.

Preparation of Glass/Al Foil/AgNPs-ET Reference System. This reference system was prepared by transfer of the AgNPs-ET array from a glass slide by its imprinting onto an Al foil attached to a glass slide (Figure 1).

Instrumentation. Raman and surface-enhanced Raman (SERS) spectra were recorded on a DXR Raman spectrometer (Thermo Scientific) interfaced to an Olympus microscope. An objective with 50× magnification was employed. The following excitation lines were used: 445 nm (diode laser), 532 nm (diode-pumped solid-state laser), 633 nm (He−Ne laser), and 780 nm (diode laser). The laser power ranged from 0.1 to 2 mW, and a full-range grating was used for all measurements. Raman and/or SERS spectra mapping was performed by measuring maps of 6 points × 6 points spanning the 60 μm × 60 μm sample area.

Surface plasmon extinction (SPE) spectra were measured on a Shimadzu UV-2401 spectrometer. Transmission electron microscopy images were obtained with a Tecnai G2 (FEI) transmission electron microscope with the acceleration voltage 120 keV. Optical microscopy images were obtained with a Leica DM6000 M (Leica Microsystems) optical microscope.

RESULTS AND DISCUSSION

SERS Spectra, Morphology, and Surface Plasmon Extinction of Glass/SLG/AgNPs-ET Hybrid System: The Effects of the ET Spacer Presence. The glass/SLG/AgNPs-ET hybrid system as a sample for SERS microRaman spectral measurements is schematically depicted in Figure 2A. SERS spectra obtained from this hybrid system at 445, 532, 633, and 780 nm excitations are shown in Figure 2B, spectra a−d. All spectra in Figure 2B contain the characteristic spectral bands of the Ag-ET surface species as well as those of the G and the 2D modes of SLG, as follows from their comparison with the spectra of the glass/SLG (Figure S3) and the glass/AgNPs-ET

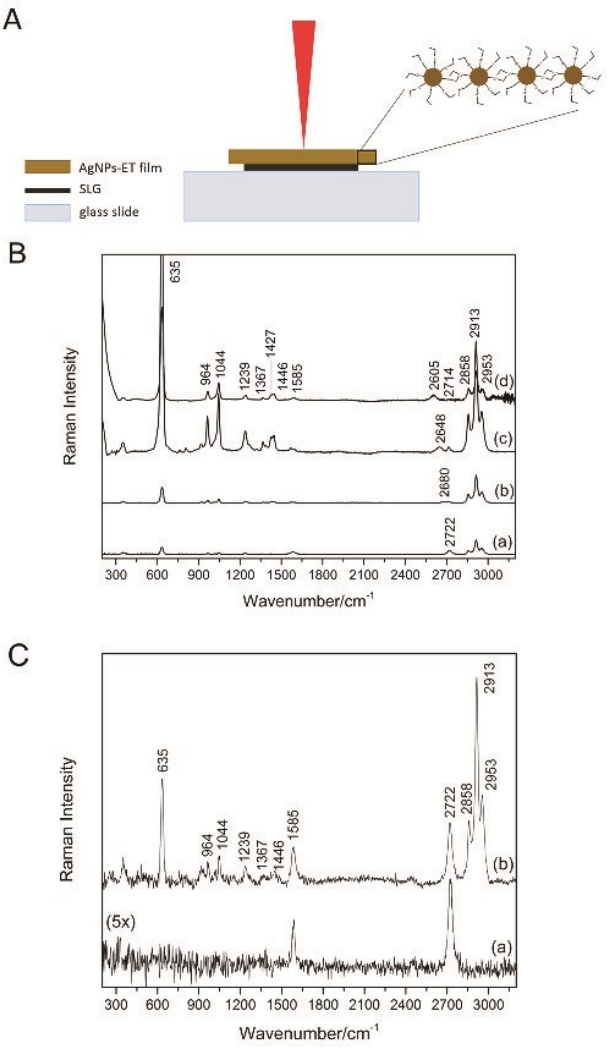

Figure 2. (A) Schematic depiction of glass/SLG/AgNPs-ET hybrid system as a sample for SERS microRaman measurement. (B) SERS microRaman spectra of glass/SLG/AgNPs-ET hybrid system measured at (a) 445, (b) 532, (c) 633, and (d) 780 nm excitation. (C) Comparison of SERS microRaman spectra of glass/SLG reference (a) and of glass/SLG/AgNPs-ET hybrid (b) systems at 445 nm excitation. Spectrum (a) was multiplied by a factor of 5.

DOI: 10.1021/acs.langmuir.7b03462
Langmuir 2017, 33, 14414−14424

(Figure S4) reference systems. The assignment of the SERS spectral bands of Ag-ET surface species as well as of Raman spectral bands of the free ET is provided in Table S1. The most pronounced differences between the spectra of ET and Ag-ET is the absence of the 2570 cm^{-1} band of υ(S−H) and the presence of the 350 cm^{-1} band of υ(Ag−S) in the latter spectrum, in contrast to the former one.

The positions of the G and 2D mode spectral bands are most clearly distinguished in the SERS spectrum of the glass/SLG/Ag NPs-ET hybrid system excited at 445 nm (Figure 2B, spectrum a), in which their relative intensities with respect to those of the Ag-ET bands are the largest. The comparison of the SERS spectra of SLG in the glass/SLG/Ag-ET hybrid and of its Raman spectra in the glass/SLG reference system obtained at the 445 nm excitation (Figure 2C, spectra a and b) show that the wavenumbers of the G mode (1585 and 1586 cm^{-1}) as well as of the 2D mode (2722 cm^{-1}) are the same (or virtually the same within the experimental error) in both systems. Moreover, the position of the G mode band at 1585 cm^{-1} is close to that of the undoped SLG.[20,21] These results provide evidence of the presence of the unperturbed SLG in the glass/SLG/AgNPs-ET hybrid system. In contrast to that, a 5 cm^{-1} upshift of the G mode and a slight upshift of the 2D mode attributed to n-doping and compressive strain was reported for the SLG/Ag NPs hybrid system in which SLG is in direct contact with Ag NPs.[19] Preservation of the native structure of SLG is thus ascribed to the Ag-ET molecular spacer enveloping Ag NPs and preventing the direct SLG-Ag NPs contact.

SERS enhancement factors of the G and the 2D modes of SLG in the glass/SLG/Ag-ET hybrid at each of the four excitation wavelengths were determined as the integral intensity ratios of the spectral bands of these modes in the SERS spectra of the hybrid system and in Raman spectra of the glass/SLG reference system. Their values are listed in the first two columns of Table 1. The largest SERS enhancement by a factor

Table 1. SERS Enhancement Factors of the SLG Modes in the Glass/SLG/AgNPs-ET Hybrid System and the Average SERS Enhancement Factors of the Modes of the Ag-ET Surface Species in (I) the Glass/SLG/AgNPs-ET Hybrid System and (II) the Glass/Al Foil/AgNPs-ET Hybrid System

λ_{exc} (nm)	SLG-G	SLG-2D	ET-addit (I)	ET-final (I)	ET-addit (II)	ET-final (II)
445	2	2	1	5×10^5	4	2×10^6
532	9	4	4	2×10^7	12	6×10^7
633	9	6	4	8×10^6	15	8×10^8
780	2	2	1	1×10^6	1	5×10^5

of 9 was determined for the G mode of SLG at 532 and 633 nm excitations. This result is, in general, consistent with the shape of the SPE curve of the hybrid system (Figure 3, curve b). Nevertheless, in addition to the SPE shape, contributions of other factors have to be considered to explain the SERS enhancement at a particular excitation wavelength, namely: (i) an increase of the contribution of the light scattering to the overall extinction (sum of absorption and scattering) of a plasmonic nanoparticle array with the increasing excitation wavelength,[33] and (ii) the "second part of the electromagnetic (EM) SERS enhancement", which implies that not only the incident, but also the Raman scattered radiation is enhanced by the EM mechanism of SERS,[34] i.e., by the elastic Mie

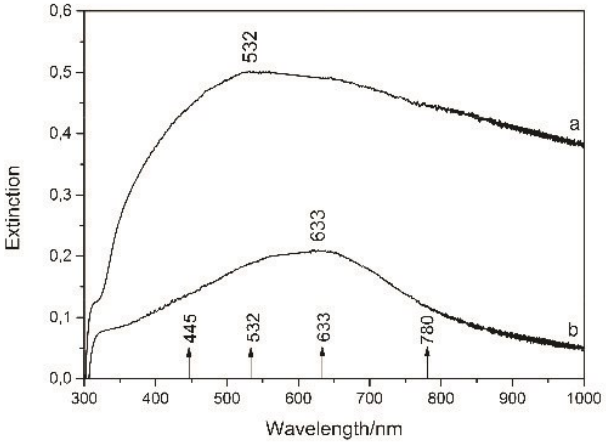

Figure 3. Surface plasmon extinction spectra of (a) glass/AgNPs-ET reference system, (b) glass/SLG/AgNPs-ET hybrid system, together with the projections of SERS excitation wavelengths.

scattering.[1,2] For example, the 633 nm excitation (which provides the SERS spectra with the best enhancement factors for both the G and the 2D mode, Table 1) is nearly coincident with the SPE curve maximum. The wavelength of the SPE maximum represents the wavelength at which the sum of absorption and scattering of light by the hybrid system is the largest.[1,2] On the other hand, the wavelength of the photons scattered by the G mode (at 1585 cm^{-1}) is 704 nm and that of the 2D mode (2648 cm^{-1}) photons is 760 nm, respectively, and the latter thus coincides with a lower extinction on the declining slope of the SPE band than the former (Figure S5 in the SI). Consequently, a slightly lower SERS enhancement factor (Ef) is expected and actually observed for the 2D mode (Ef = 6) than for the G mode (Ef = 9).

Importantly, the G mode enhancement (Ef = 9) at 532 and 633 nm excitation in SERS of our hybrid system with unperturbed SLG and the hydrophobic Ag-ET spacer is actually slightly higher than that experienced by the same mode in SERS of the system with SLG underneath Ag NPs (Ef = 7).[19] In the latter system, SLG is affected by compressive strain and n-doping, which, in turn, result from the direct contact between SLG and Ag NPs. This comparison indicates that the decrease of the SERS enhancement by the EM mechanism induced by a thin spacer[18] namely, in our case, by the hydrophobic Ag-ET spacer (terminated by the CH_3 group) of about 0.6 nm thickness has been compensated by (i) the 2-D assembling of the closely spaced, ET modified Ag NPs (*vide infra* and Figure 4B−D), i.e., by formation of a more efficient plasmonic enhancer than the assembly of mostly isolated Ag NPs[1,2] reported in ref 19, and, (ii) by the proper selection of excitation wavelength(s) with respect to the SPE of the AgNPs-ET assembly (Figure 3b).

In summation, the results of our SERS study provide evidence that employment of the thin hydrophobic spacer enables an efficient localization of SLG unperturbed by strain (affecting its mechanical properties[4,20,21]) and/or doping (affecting its electronic properties[4,20,21]) into the near field resonantly optically excited in the spacer-modified Ag NPs assembly.

In addition to that, a comparison of the optical images of the glass/AgNPs-ET reference system (Figure 4A) and of the glass/SLG/AgNPs-ET hybrid system (Figure 4B) obtained in

DOI: 10.1021/acs.langmuir.7b03462
Langmuir 2017, 33, 14414−14424

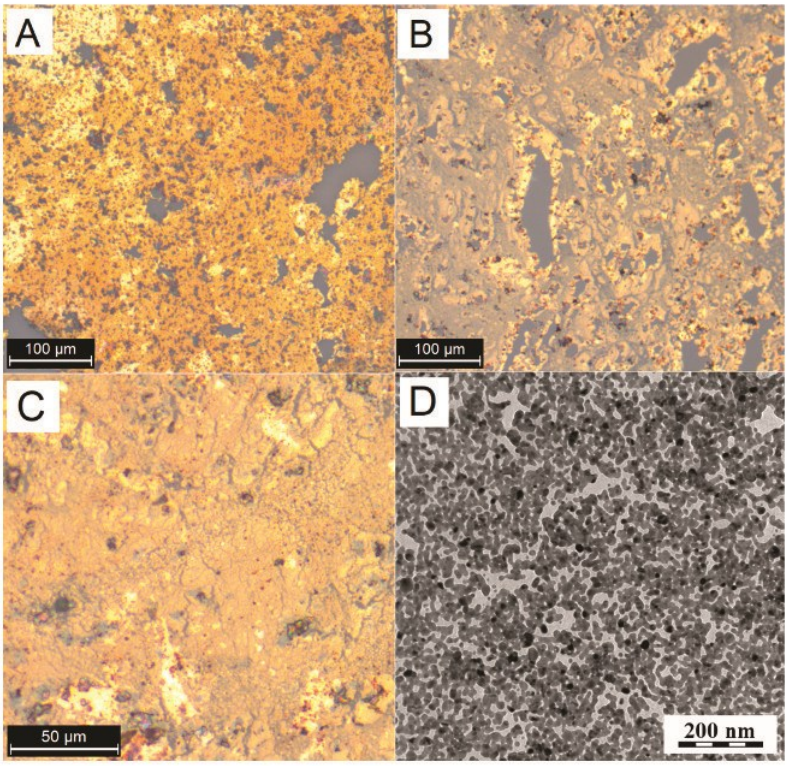

Figure 4. (A) Optical microscopy image of glass/AgNPs-ET reference system obtained with the 20x magnification objective. (B) Optical microscopy image of glass/SLG/AgNPs-ET hybrid system obtained with the 20x magnification objective. (C) Optical microscopy image of glass/SLG/AgNPs-ET hybrid system obtained with the 50x magnification objective. (D) TEM image of SLG/AgNPs-ET hybrid system deposited on carbon-coated Au grid.

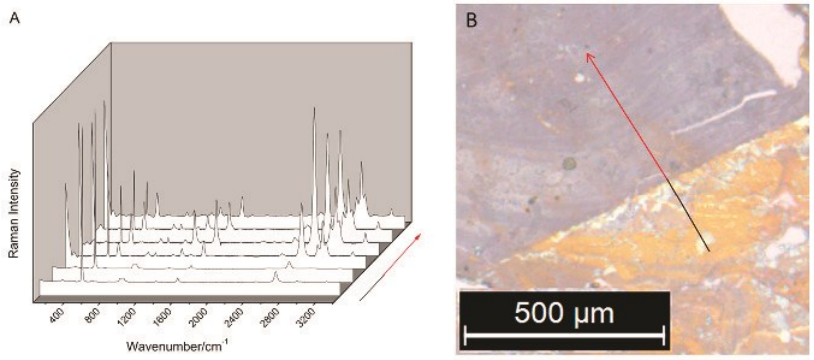

Figure 5. Manifestation of the additional enhancement of SERS of ET in the AgNPs-ET array induced by the presence of SLG underneath the AgNPs-ET array. (A) SERS microRaman sampling carried out at 633 nm excitation along the trajectory outlined in panel B, i.e., in the optical image of the sample; black line: the glass/AgNPs-ET part of the sample; red line: the glass/SLG/AgNPs-ET part of the sample.

the same magnification indicates that, while the hydrophobic ET-modified Ag NPs in the former system tend to form multilayers on the glass substrate (Figure 4A), the presence of SLG in the latter system has promoted the 2-D assembling of these hydrophobic Ag NPs (Figure 4B). The last mentioned observation is further corroborated by the optical images of the hybrid system in a higher magnification (Figure 4C) and by the TEM image the assembly of ET-modified Ag NPs on a SLG-covered, carbon-coated Au grid for TEM (Figure 4D).

In accord with the morphological characterization provided above, the SPE spectrum of the glass/AgNPs-ET reference system (Figure 3, curve a) shows a markedly higher extinction than that of the glass/SLG/AgNPs-ET hybrid system (Figure 3, curve b). The observed red-shift of SPE in the latter system with respect to the former one (Figure 3, curves a and b) can thus originate from the efficient SLG-Ag NPs coupling,[6] however, it can also be caused by the different morphologies of the Ag NPs assembly in each of these systems.

Furthermore, the average values of SERS enhancement factors of the spectral bands of the Ag-ET surface species have been determined for both the glass/SLG/AgNPs-ET hybrid and the glass/AgNPs-ET reference system from their SERS spectra measured at 445, 532, 633, and 780 nm excitation wavelengths (Table 1 and Table S2 in SI, respectively). Their

DOI: 10.1021/acs.langmuir.7b03462
Langmuir 2017, 33, 14414−14424

mutual comparison has shown that at the 532 and 633 nm excitations, the Ag-ET SERS spectral bands experience an additional enhancement by an average factor of 4 due to the presence of SLG in the hybrid system. By contrast, no such enhancement has been encountered at the 445 and 780 nm excitations (Table 1). This additional enhancement of SERS of Ag-ET has been visualized by SERS microRaman sampling experiment at 633 nm excitation in which the spectral sampling trajectory was directed over an edge of the glass-deposited SLG overdeposited by the ET-modified AgNPs array (Figure 5). The first part of the trajectory sampled ca. 1.5 μm^2 areas on the glass/Ag NPs-ET part of the sample, while the second one sampled areas of the same size on the glass/SLG/AgNPs/ET part (Figure 5B). The increase of the Ag-ET spectral bands intensity observable after the sampling trajectory crossed the SLG edge and entered the SLG-covered part of the sample is clearly visible on the SERS spectra evolution presented in Figure 5A.

On the basis of the results obtained in this paper as well as those published previously, several possibilities have been considered to explain this additional enhancement and its excitation wavelength dependence. First, (i) the graphene-enhanced Raman scattering (GERS)[35−37] and its coupling with the EM mechanism of SERS[38] has been considered. However, it has been recently concluded[36,37] that the GERS enhancement is observed only for planar aromatic molecules which is the case of neither the ET molecule, nor the Ag-ET surface species. Futhermore, (ii) the difference in the morphology (Figure 4A,B) and SPE spectra between the glass/AgNPs-ET (Figure 3A,B) and the glass/SLG/AgNPs-ET systems, i.e., measurements from a multilayer versus a monolayed of ET-modified Ag NPs can be also ruled out. The reason is that the SERS signal is collected predominantly from the first Ag NP-ET layer, as confirmed also by the same SERS enhancements of the Ag-ET vibrational modes in both systems (i.e., regardless the actual Ag NP layer thickness) observed at the 445 nm as well as at the 780 nm excitation. Furthermore, (iii) the vibrational mode selectivity of the additional enhancement has been checked by comparison of the enhancement factors of the individual Ag-ET vibrational modes (Table S3 in the SI). The enhancement factors of all these modes range from 3.3 to 4.3 at 532 nm excitation and from 3.0 to 4.4 at 633 nm excitation, i.e., there is no strong preferential enhancement of a particular vibrational mode of the Ag-ET surface species.

Finally, (iv) we consider the recently reported changes of the optical characteristics of SLG localized in the optical near field resonantly excited in 2-D Ag or Au NPs arrays.[5−10] It has been demonstrated that light absorption of SLG can be manipulated by integrating SLG with a thin layer of plasmonic nanostructures (such as the 2-D Ag or Au NPs arrays with or without a dielectric spacer between SLG and the plasmonic NPs array) upon the conditions of the resonance surface plasmon excitation.[5,7−10] In particular, the enhanced optical field thus created in the plasmonic NPs array can effectively enhance the total absorption of SLG.[5] Considering the Fresnel equations for calculation of the reflectance R of a material from its "optical constants", i.e., the real (n-real refraction index) and imaginary (k-index of absorption) part of its complex refraction index (N),[33] the increase of the index of absorption of the material leads to increase of its reflectance R. Therefore, we suggest that the increased absorption of SLG coupled to AgNPs results in the increase of its reflectance, and we speculate that it is actually the increased reflectance of SLG (located underneath the ET-modified Ag NPs array) that leads to the increased SERS signal intensity of the Ag-ET surface species. This speculation is consistent with the selective observation of this additional SERS enhancement at 532 and 633 nm excitations in relation to the shape of the SPE curve of the glass/SLG/AgNPs-ET hybrid, which reaches maximal extinctions at the wavelengths corresponding to these excitations, but strongly drops both at 445 and 780 nm wavelengths (Figure 3, curve b). For testing the feasibility of the assumption that, at 532 and 633 nm excitations, SLG in the glass/SLG/AgNPs-ET hybrid system actually acts as a reflecting surface, we have carried out the following experiment: First, a new glass/Al foil/AgNPs-ET hybrid system, in which SLG was replaced by an Al foil known as a strongly reflecting mirror, was prepared. Its SERS microRaman spectra were measured at the same excitations as those of the glass/SLG/AgNPs-ET hybrid and of the glass/AgNPs-ET reference system, and the additional average SERS enhancement experienced by the vibrational modes of the Ag-ET surface species in the hybrid system with Ag foil (with respect to the reference system without the Ag foil) has been determined, yielding a factor of 12 and 15 at 532 and 633 nm excitations, respectively (Table 1). These experiments demonstrate the possibility to increase SERS signal of molecules and/or surface complexes incorporated in 2-D arrays of Ag NPs and measured by the microRaman technique by localization of the array on the strongly reflecting surface, while the 3−4 times higher enhancement produced by the Al foil than by SLG in the near field of Ag NPs indicates that SLG acts as only a weakly reflecting surface under these circumstances.

SERS Spectra, Morphology, and Surface Plasmon Extinction of Glass/AgNPs/SLG Hybrid System Originating from the Parent Glass/AgNPs-ET System: The Effects of the ET Spacer Removal during SLG Deposition. The second hybrid system investigated in this paper was prepared by overdeposition of the parent glass/AgNPs-ET system by SLG. SERS spectra of the resulting system measured at 445, 532, 633, and 780 nm wavelengths in the straight (i.e., as prepared) sample geometry (depicted in Figure 6A) and shown in Figure 6B contain none of the characteristic spectral bands of the Ag-ET species (assigned in Table S1 and observed in the SERS spectra of the glass/SLG/AgNPs-ET hybrid, Figure 2B).

This result indicates that ET was completely removed from the surface of the ET-modified Ag NPs during their overdeposition by SLG using the NC method of SLG transfer[31,32] (details in the Experimental Section). The hybrid system is thus denoted as glass/AgNPs/SLG (Figure 6A).

The changes in the morphology of Ag NPs caused by the moderate heating (160 °C) and the ET removal during deposition of SLG have been inspected by comparison of the TEM images of the parent AgNPs-ET array (deposited on the TEM grid prior to the SLG deposition, Figure 7A) and of the resulting AgNPs-SLG hybrid system (Figure 7B) obtained at the same magnification. The morphology changes correspond with annealing of Ag NPs (thermal and/or chemical after the ET removal from the Ag NP surface). Furthermore, the fairly uniform coverage of the glass surface by the annealed Ag NPs at a longer range 4 μm × 4 μm scale is depicted in Figure S6 in the SI, and the quite broad particle size distribution is quantified in Figure 7C. Monomers as well as dimers and trimers of Ag NPs can be distinguished in the TEM image of the Ag NPs-SLG system in Figure 7B. The fraction of dimers and trimers has been established to ca. 20% from of the circularity diagram in Figure 7D.

DOI: 10.1021/acs.langmuir.7b03462
Langmuir 2017, 33, 14414−14424

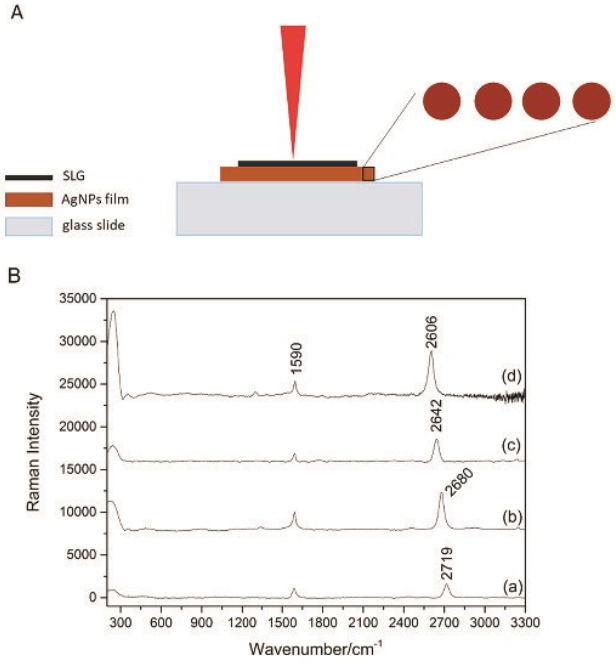

Figure 6. (A) Schematic depiction of glass/AgNPs/SLG hybrid system as a sample for SERS microRaman measurement in the straight geometry. (B) SERS microRaman spectra of glass/AgNPs/SLG hybrid system measured at (a) 445, (b) 532, (c) 633, (d) 780 nm excitation in the straight sample geometry.

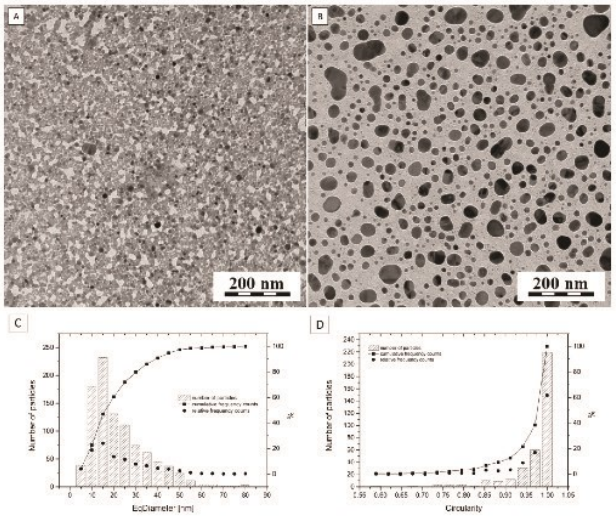

Figure 7. (A) TEM image of the parent Ag NPs-ET film deposited on a C-coated Au grid. (B) TEM image of AgNPs/SLG hybrid system deposited on a C-coated Au grid. (C) Particle size distribution in the AgNPs/SLG hybrid system. (D) Distribution of the particles circularity in the AgNPs/SLG hybrid system.

On the basis of the previously published studies,[39,40] we reason that both the broad particle size distribution and the presence of fused Ag NPs dimers and trimers contribute to observation of the very broad and rather flat SPE curve of the Ag NPs-SLG system, which spans the visible spectral region and extends itself into the near IR (Figure 8).

The glass/AgNPs/SLG hybrid system thus differs from the glass/SLG/AgNPs-ET hybrid addressed in the first part of this

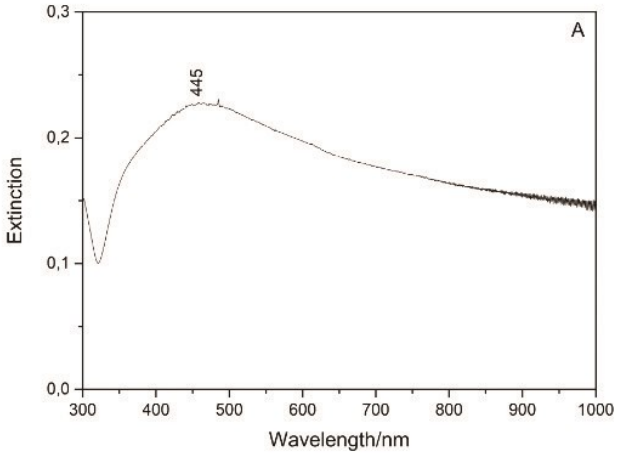

Figure 8. Surface plasmon extinction of the glass/AgNPs/SLG hybrid system.

paper not only by the reverse order of the components assembling, but also by the morphology and SPE of the 2-D Ag NPs array and by the Ag NPs-SLG distance (due to the ET spacer removal). Consequently, a mutual comparison of SERS enhancement factors of the G and 2D modes of SLG in these two hybrid systems is not particularly meaningful, since three different factors simultaneously contribute to their mutual difference. On the other hand, we have reasoned that SERS microRaman sample setup can offer a possibility to measure the same hybrid system in two different orientations with respect to the laser beam excitation: the straight one (Figure 6A) and the inverted one (Figure 9A). In that case, the SERS enhancement will be affected only by the different mutual positions of the same plasmonic enhancer (i.e., the Ag NPs array) and SLG (Figures 6A and 9A).

SERS spectra of the glass/AgNPs/SLG hybrid were measured at 445, 532, 633, and 780 nm excitations in both the straight (Figure 6A) and the inverted (Figure 9A) sample geometry. The SERS spectra of SLG obtained from each of them are shown in Figure 6B and Figure 9B, respectively. Since both spectra originate from the same hybrid system, the wavenumbers of the G and 2D modes have been expected, and they are actually observed to be virtually the same in both geometries at each of the four excitation wavelengths. In particular, the nondispersive G mode is located at 1590 cm^{-1} in both sets of the spectra at all four excitation wavelengths. Its position is thus by 5 cm^{-1} higher than that of pristine SLG[20,21] and of SLG in the glass/SLG reference sample (Figure 2C, spectrum a, and Figure S3 in the SI). At 445 nm excitation, the dispersive 2D mode is located at 2719 cm^{-1} in the spectrum measured in the straight sample geometry (Figure 6B) and at 2717 cm^{-1} in the spectrum obtained in the inverted geometry (Figure 9B). Its position is thus by 3 and 5 cm^{-1}, respectively, lower than that of SLG in the glass/SLG reference system (Figure 2C). The small upshift of the G mode wavenumber together with the small downshift of that of the 2D mode suggests a weak n-doping of SLG by Ag NPs, as reported previously.[41] SERS enhancement factors of the G and 2D modes of SLG determined as the intensity ratios of these modes in the SERS spectra of the glass/Ag NPs/SLG hybrid to those in the Raman spectra of the glass/SLG reference system (both measured in either the straight or the inverted sample geometry) are listed in Table 2 and depicted in Figure 10

DOI: 10.1021/acs.langmuir.7b03462
Langmuir 2017, 33, 14414−14424

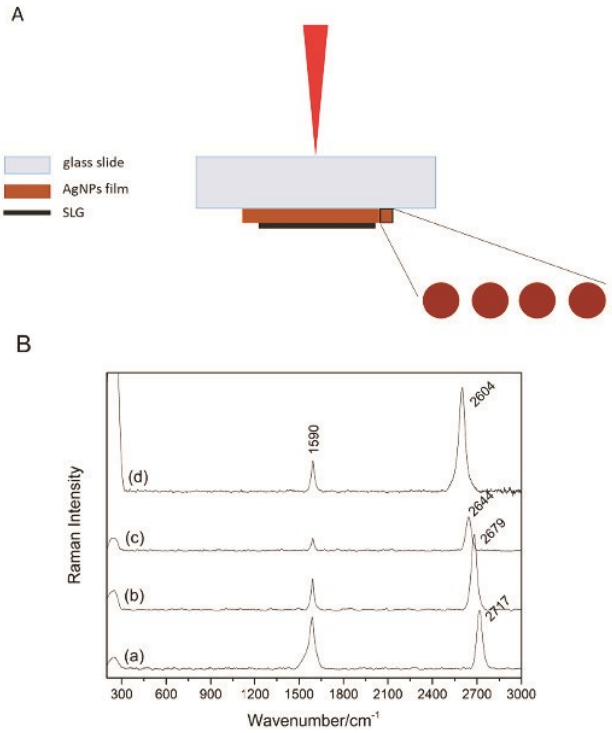

Figure 9. (A) Schematic depiction of glass/AgNPs/SLG hybrid system as a sample for SERS microRaman measurement in the inverted geometry. (B) SERS microRaman spectra of glass/AgNPs/SLG hybrid system measured at (a) 445, (b) 532, (c) 633, (d) 780 nm excitation in the inverted sample geometry.

(together with the error bars representing the standard deviations of band intensities resulting from evaluation of five spectral maps).

Table 2. SERS Enhancement Factors of the SLG Modes in the Glass/AgNPs/SLG Hybrid System

	Ef			
	inverted geometry		straight geometry	
λ_{exc} (nm)	SLG - G	SLG – 2D	SLG - G	SLG – 2D
445	33	17	15	7
532	14	9	11	7
633	16	9	18	8
780	19	10	8	5

The SERS Ef values (Figure 10 and Table 2) demonstrate that a significant SERS enhancement is experienced by the G and the 2D mode of SLG at all excitations (445–780 nm) and in both sample geometries. This result is attributed to the morphology of the annealed Ag NPs array in the hybrid system, namely, to the broad distribution of morphologies and sizes of Ag NPs constituting this array (Figure 7), which in turn, manifests itself by the broad SPE curve of the hybrid (Figure 8). Nevertheless, one has to keep in mind that both absorption and scattering contribute to the SPE of the Ag NPs array, while the SERS enhancement by the EM mechanism stems only from the scattering crossection. Therefore, the wavelength dependence of the scattering crosssections of Ag NPs monomers and dimers[42] is even more appropriate for correlation with the excitation wavelength dependence of the SERS Efs of the SLG modes in the two sample geometries than the SPE curve itself.

For both the G and the 2D mode of SLG, the differences between their SERS Ef's in the two samples geometries (Figures 6A and 9A) show the same excitation wavelength dependence (Figure 10 and Table 2). In particular, no significant differences in the Efs are observed at 532 and 633 nm excitations, while at 445 and 780 nm excitations, the enhancement factors are approximately 2 times larger in the inverted (Figure 9A) than in the straight (Figure 6A) sample geometry. The former observation is consistent with the presence of the same plasmonic enhancer in the hybrid system in the straight as well as inverted sample geometry (Figures 6A and 9A), while the latter one indicates that some other, excitation wavelength-dependent factor(s), affect the final SERS Efs determined in each of the two sample geometries. We propose that the most important factors are (i) absorption of both the incident and the scattered light by the Ag NPs, and (ii) increased absorption and reflectance of SLG in the optical near field resonantly excited in Ag NPs. Their mutual interplay at each excitation wavelength and in each sample geometry (in which SERS spectra of SLG from the particular hybrid system have been measured) can then positively and/or negatively affect the actual values of the experimetally determined SERS Efs of the SLG modes.

In the particular case of our hybrid system constituted by SLG on the top of the Ag NPs array, the former effect (i) is expected to affect negatively the SERS spectral intensities preferentially in the inverted sample geometry (favoring thus the straight sample geometry), while the latter effect (ii) favors the inverted geometry (in which scattered light is partially reflected back into the sample) over the straight one (in which a small fraction of the incident light is reflected from the sample surface). Since the magnitude of both effects is excitation wavelength dependent, it is understandable that the result of their interplay depends on the excitation wavelength as well.

Nevertheless, the exact values of the absorption and scattering crosssections of our particular Ag NPs array at each excitation wavelength are not available, and other factors, such as the fraction of the SLG surface located in the near field of Ag NPs at each of the excitation wavelengths, also play their role. Therefore, we can only qualitatively and tentatively address the experimentally observed excitation wavelength-dependent differences between the Efs experienced by the SLG in the straight (Figure 6A) and in the inverted (Figure 9A) sample geometry (Figure 10 and Table 2). Apparently, the two additional effects (i) and (ii) compensate each other at 532 and 633 nm excitations. By contrast, at 445 and 780 nm excitation, the measurement in the inverted geometry is favored by the 2-fold increase of the SERS Efs of both the G and 2D mode of SLG, hence the contribution of the effect (ii) is larger that that of the effect (i) at these wavelengths. We propose that this observation can be related to the efficient localization of SLG in the near field of Ag NPs resonantly excited at these excitation wavelengths (resulting into the increased reflectivity of SLG), in combination with the particular morphology of the annealed Ag NPs array. In particular, at 445 nm, the optical fields are resonantly excited preferentially in single Ag NPs: the optical fields in the vicinity of the single NPs are relatively weak,[39,40,42] but the NPs are fairly abundant (Figure 7B,C,D), hence a relatively large fraction of SLG area is localized in these optical fields. At 780 nm excitation, stronger optical fields are excited in large Ag NPs dimers and trimers, including the very strong

DOI: 10.1021/acs.langmuir.7b03462
Langmuir 2017, 33, 14414–14424

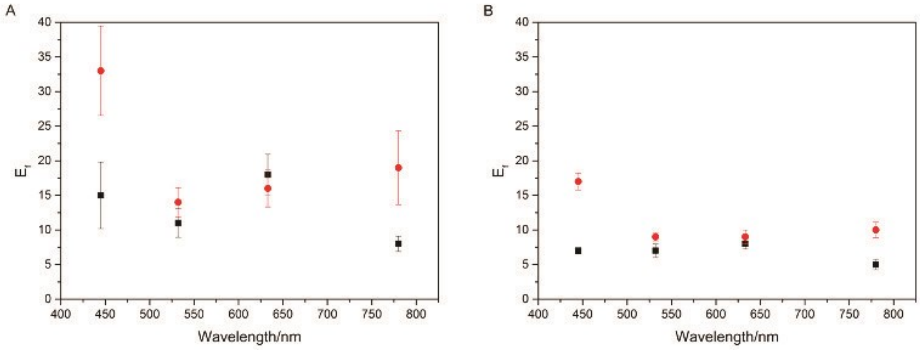

Figure 10. Comparison of SERS enhancement factors of the G mode (A) and of the 2D mode (B) of SLG in the glass/AgNPs/SLG hybrid system plotted as a function of excitation wavelength for two sample geometries: the straight one - black squares, the inverted one - red circles.

optical fields (hot spots) localized between the NPs in these dimers and/or trimers.[39,40,42] However, the dimers and trimers are less abundant than the single NPs (Figure 7 B and D). Therefore, at the 780 nm excitation, a smaller contact area between SLG and the optical near fields excited in Ag NPs dimers and trimers appears to be compensated by the larger optical fields strength. The additional enhancement by a factor of approximately 2 in the inverted sample geometry is thus observed at both the 445 and 780 nm excitations (Figure 10 and Table 2).

Furthermore, standard deviations of the SERS Efs experienced by the G and the 2D mode of SLG in both sample geometries and at all excitations have been determined for each of these 16 spectral measurements from five spectral maps, and they are depicted as error bars in Figure 10A,B. Their values are fairly low for the 2D mode at all excitations and in both sample geometries (Figure 10 B). For the G mode, low values of the error bars have been obtained at 532 and 633 nm excitations in both sample geometries and at 780 nm excitation in the straight sample geometry, while relatively large error bars have been determined at 445 nm excitation in both sample geometries and at 780 nm excitation in the straight geometry (Figure 10A). The large standard deviations at 445 nm excitation have their origin in fluctuations of the spectral background in the 1500–1650 cm^{-1} region encountered at this particular excitation. At 780 nm excitation, the large signal fluctuations in the same spectral region have been observed only in the inverted sample geometry (i.e., for the measurement "through glass", Figure 9A), and they are attributed to fluorescence from the glass slide.[43] In summation, these results indicate that the glass/AgNPs/SLG hybrid sample is fairly homogenoues on the large scale of the SERS spectral mapping, since the large standard deviations are limited to 3 of 16 spectral mapping measurements, and they have been explained by extrinsic spectral effects unrelated to the sample morphology.

■ CONCLUSIONS

Two approaches to coassembling of SLG and 2D-arrays of ethanethiol (ET) modified Ag NPs were adopted, and each of them resulted into a different hybrid SERS active system: (i) with and (ii) without ET chemisorbed to Ag NPs, i.e., with and without the molecular spacer between the Ag NPs surface and SLG. Comparison of their morphological, structural and optical characteristics enabled us to address the specific advantages of the spacer presence and/or removal.

The system with the ET spacer resulted from overlaying SLG on a glass slide by ET-modified, hydrophobic Ag NPs, which assembled on the hydrophobic SLG surface into a 2-D array. The efficiency of the ET molecular spacer was proved by observation of the SERS spectral bands of the G and 2D mode of SLG unaffected by doping and/or strain. Preservation of the native structure of SLG, the consistence of the excitation wavelength dependence of the SERS enhancement of the G and 2D mode of SLG at excitations in the 445–780 nm range with the SPE of the AgNPs-ET array as well as the manifestations of the second part of the EM SERS enhancement experienced by the G and the 2D modes of SLG, respectively, have provided evidence of the EM mechanism origin of the SERS enhancement of the SLG modes in this hybrid system. Overlaying of SLG by the ET-modified Ag NPs can thus be viewed as a prospective pathway to SERS spectral probing of "real life" SLG samples deposited on various substrates and exposed to various conditions that induce doping and/or strain.

Furthermore, the excitation wavelength selective additional enhancement of SERS of the Ag-ET modes observed at 633 and 532 nm excitations (falling into the region of the largest SPE of the hybrid) by a factor of 4 has been tentatively attributed to the increased reflectance of SLG in the near field resonantly excited in the Ag NPs-ET array. This explanation is in accord with the earlier observations that optical properties of SLG can be modified by the near field of Ag NPs array even in the case when SLG is distanced from the AgNPs surface by a spacer.

Preparation of the second hybrid system by deposition of the components in the reverse order, i.e., by overdeposition of the Ag NPs-ET array on glass by SLG, resulted in the removal of the chemisorbed ET and annealing of Ag NPs, i.e., into formation of the glass/AgNPs/SLG hybrid. The direct contact between the Ag NPs and SLG manifests itself in the SERS spectra of SLG by the wavenumber positions of the G mode and the 2D mode consistent with a weak n-doping of SLG by Ag NPs. Annealing of the Ag NPs causes their merging into larger monomers with a broad distribution of sizes as well as into dimers and trimers of fused NPs, and results in a very broad SPE curve of the hybrid, which extends over the overall visible spectral region.

Exploration of the effect of localization of the same plasmonic enhancer (namely of the array of the annealed Ag NPs) on the top and/or underneath SLG by SERS spectral mapping of the glass/Ag NPs/SLG in two different sample orientations with respect to the exciting laser beam, i.e., in the straight and in the inverted sample geometry, respectively, (at four excitations in the 445–780 nm range) revealed that for

DOI: 10.1021/acs.langmuir.7b03462
Langmuir 2017, 33, 14414–14424

both SLG modes, the Efs are the same at 532 and 633 nm excitations, and by a factor of 2 higher in the inverted sample geometry than in the straight one at 445 and 780 nm. These excitation wavelength dependent differences have been tentatively explained by the interplay of two factors: absorption of both the incident and the scattered light by the Ag NPs, and increased absorption and reflectance of SLG in the optical near field resonantly excited in Ag NPs, in relation to our hybrid system preparation (SLG on the top of Ag NPs array) and the actual morphology of the Ag NPs array in the hybrid. We propose that, owing to its morphological characteristics and optical properties, this particular glass/annealed-AgNPs-array/SLG hybrid system could provide a suitable platform for GERS/SERS of aromatic molecules. In more general terms, we have found that localization of the same plasmonic enhancer underneath or above SLG can affect the optical properties of the hybrid system; however, the magnitude and the excitation wavelength dependence of this effect will depend on the actual morphology of the plasmonic enhancer.

■ ASSOCIATED CONTENT

Supporting Information

The Supporting Information is available free of charge on the ACS Publications website at DOI: 10.1021/acs.langmuir.7b03462.

Figures S1−S6: TEM image and PSD of parent Ag NP hydrosol, photographic depiction of Ag NPs-ET film preparation and transfer, SERS spectrum of glass/Ag NPs-ET system, Raman spectrum of glass/SLG system, SPE spectrum of glass/SLG/AgNPs-ET system in relation to its SERS spectrum at 633 nm, TEM image of Ag NPs/SLG system; Tables S1−S3: assignment of ET and Ag-ET spectral bands, SERS enhancement factors of Ag-ET spectral bands in glass/AgNPs-ET and glass/SLG/AgNPs-ET hybrids (PDF)

■ AUTHOR INFORMATION

Corresponding Author

*E-mail: vlc@natur.cuni.cz.

ORCID

Veronika Sutrová: 0000-0001-8320-2078
Ivana Šloufová: 0000-0002-4757-6029
Martin Kalbáč: 0000-0001-9574-4368
Blanka Vlčková: 0000-0003-0553-3722

Notes

The authors declare no competing financial interest.

■ ACKNOWLEDGMENTS

Financial support by the 15-01953S grant awarded by the Czech Science Foundation is gratefully acknowledged. We also acknowledge assistance provided by the Research Infrastructure NanoEnviCz, supported by the Ministry of Education, Youth and Sports of the Czech Republic under Project No. LM2015073 and Project No. CZ.02.1.01/0.0/0.0/16_013/0001821. V.S. acknowledges financial support by the 892217 students grant awarded by Grant Agency of Charles University.

■ REFERENCES

(1) Le Ru, E. C.; Etchegoin, P. G. *Principles of Surface-enhanced Raman Spectroscopy and Related Plasmonic Effects*; Elsevier: Amsterdam, 2009.

(2) Maier, S. A. *Plasmonics, Fundamentals and Applications*; Springer Science+Business Media LLC: New York, 2007.

(3) Procházka, M. *Surface-Enhanced Raman Spectroscopy-Bioanalytical, Biomolecular and Medical Applications*; Springer International Publishing: Cham, Switzerland, 2016.

(4) Bonaccorso, F.; Sun, Z.; Hasan, T.; Ferrari, A. C. Graphene photonics and optoelectronics. *Nat. Photonics* **2010**, *4*, 611−622.

(5) Liu, Y.; Cheng, R.; Zhou, H.; Bai, J.; Liu, G.; Liu, L.; Huang, Y.; Duan, X. Plasmon resonance enhanced multicolour photodetection by graphene. *Nat. Commun.* **2011**, *2*, 579.

(6) Niu, J.; Shin, J. Y.; Son, J.; Lee, Y.; Ahn, J. H.; Yang, H. Shifting of surface plasmon resonance dute to electromagnetic coupling between graphene and Au nanoparticles. *Opt. Express* **2012**, *20*, 19690.

(7) Zhu, J.; Liu, Q. H.; Lin, T. Manipulating light absorption of graphene using plasmonic nanoparticles. *Nanoscale* **2013**, *5*, 7785−7789.

(8) Du, Y.; Zhao, Y.; Qu, Y.; Chen, Ch.-H.; Chen, Ch.-M.; Chuang, Ch.-H.; Zhu, Y. Enhanced light-matter interaction of graphene-gold nanoparticle hybrid films for high-performance SERS detection. *J. Mater. Chem. C* **2014**, *2*, 4683−4691.

(9) Lee, S.; Kim, J. Desing of optical metamaterial mirror with metallic nanoparticles for floating-gate graphene optoelectronic devices. *Opt. Express* **2015**, *23*, 21809.

(10) Mat Teridi, M. A.; Sookhakian, M.; Basirun, W. J.; Zakaria, R.; Schneider, F. K.; da Silva, W. J.; Kim, J.; Lee, S. J.; Kim, H. P.; Mohd Yusoff, A. R.; Jang, J. Plasmon enhanced organic devices utilizing highly ordered nanoimprinted gold nanodisk and nitrogen doped graphene. *Nanoscale* **2015**, *7*, 7091−7100.

(11) Schedin, F.; Lidorikis, E.; Lombardo, A.; Kravets, V.G.; Geim, A. K.; Grigorenko, A. N.; Novoselov, S. K.; Ferrari, C. A. Surface-enhanced Raman Spectroscopy of Graphene. *ACS Nano* **2010**, *4*, 5617−5626.

(12) Fu, X.; Bei, F.; Wang, X.; O'Brien, S.; Lombardi, R. J. Excitation profile of surface-enhanced Raman scattering in graphene-metal nanoparticle based derivatives. *Nanoscale* **2010**, *2*, 1461−1466.

(13) Heeg, S.; Fernandez-Garcia, R.; Oikonomou, A.; Schedin, F.; Narula, R.; Maier, A. S.; Vijayaraghavan, A.; Reich, S. Polarized Plasmonic Enhancement by Au Nanostructures Probed through Raman Scattering of Suspended Graphene. *Nano Lett.* **2013**, *13*, 301−308.

(14) Kravets, V. G.; Schedin, F.; Jalil, R.; Britnell, L.; Novoselov, K. S.; Grigorenko, A. N. Surface Hydrogenation and Optics of a Graphene Sheet Transferred onto a Plasmonic Nanoarray. *J. Phys. Chem. C* **2012**, *116*, 3882−3887.

(15) Xu, W. G.; Mao, N. N.; Zhang, J. Graphene: A Platform for Surface-Enhanced Raman Spectroscopy. *Small* **2013**, *9*, 1206−1224.

(16) Kalbáč, M.; Valeš, V.; Vejpravová, J. The Effect of a Thin Gold Layer on Graphene: A Raman Spectroscopy Study. *RSC Adv.* **2014**, *4*, 60929−60935.

(17) Zhao, Y.; Zhu, Y. W. Graphene-Based Hybrid Films for Plasmonic Sensing. *Nanoscale* **2015**, *7*, 14561−14576.

(18) Ek Weiss, J.; Costa, S.; Frank, O.; Fridrichová, M.; Vlčková, B.; Vejpravová, J.; Kalbac, M. SERS of Isotopicallly Labeled 12C/13C Graphene Bilayer−Gold Nanostructured Film Hybrids: Graphene Layer as Spacer and SERS Probe. *J. Phys. Chem. C* **2017**, *121*, 11680−11686.

(19) Gong, T.; Zhang, J.; Zhu, Y.; Wang, W.; Zhang, X.; Zhang, J. Optical properties and surface-enhanced Raman scattering of hybrid structures with Ag nanoparticles and graphene. *Carbon* **2016**, *102*, 245−254.

(20) Jorio, A.; Saito, R.; Dresselhaus, G.; Dresselhaus, M. S. *Raman Spectroscopy in Graphene Related Systems*; Wiley-VCH Verlag GmbH & Co. KGaA: Weinheim, Germany, 2011.

(21) Ferrari, A. C.; Basko, D. M. Raman spectroscopy as a versatile tool for studying the properties of graphene. *Nat. Nanotechnol.* **2013**, *8*, 235−245.

(22) Zaretski, A. V.; Marin, B. C.; Moetazedi, H.; Dill, T. J.; Jibril, L.; Kong, C.; Tao, A. R.; Lipomi, D. J. Using the Thickness of Graphene

DOI: 10.1021/acs.langmuir.7b03462
Langmuir 2017, 33, 14414−14424

to Template Lateral Subnanometer Gaps between Gold Nanostructures. *Nano Lett.* **2015**, *15*, 635−640.
(23) Xu, S.; Jiang, S.; Wang, J.; Wei, J.; Yue, W.; Ma, Y. Graphene isolated Au nanoparticle arrays with high reproducibility for high-performance surface-enhanced Raman scattering. *Sens. Actuators, B* **2016**, *222*, 1175−1183.
(24) Xu, S.; Man, B.; Jiang, S.; Wang, J.; Wei, J.; Xu, S.; Liu, H.; Gao, S.; Liu, H.; Li, Z.; Li, H.; Qiu, H. Graphene/Cu Nanoparticle Hybrids Fabricated by Chemical Vapor Deposition As Surface-Enhanced Raman Scattering Substrate for Label-Free Detection of Adenosine. *ACS Appl. Mater. Interfaces* **2015**, *7*, 10977−10987.
(25) Dai, Z.; Xiao, X.; Wu, W.; Zhang, Y.; Liao, L.; Guo, S.; Ying, J.; Shan, Ch.; Sun, M.; Jiang, Ch Plasmon-driven reaction controlled by the number of graphene layers and localized surface plasmon distribution during optical excitation. *Light: Sci. Appl.* **2015**, *4*, e342.
(26) Zhang, X.; Dai, Z.; Si, S.; Zhang, X.; Wu, W.; Deng, H.; Wang, F.; Xiao, X.; Jiang, C. Ultrasensitive SERS substrate integrated with uniform subnanometer scale "hot spots" created by a graphene spacer for the detection of mercury ions. *Small* **2017**, *13*, 1603347.
(27) Vlčková, B.; Matějka, P.; Šimonová, J.; Pančoška, P.; Čermáková, K.; Baumruk, V. Surface Enhanced (Resonance) Raman Spectra of Free Base 5,10,15,20−Tetrakis (4-carboxyphenyl)-Porphyrin and Its Silver Complex In Systems With Silver Colloid: Direct Adsorption versus Adsorption via Molecular Spacer. *J. Phys. Chem.* **1993**, *97*, 9719−9729.
(28) Michl, M.; Vlčková, B.; Mojzeš, P. Ag Colloid-1-alkanethiol Films: Spacer-modified Substrates for SERRS Spectroscopy of Chromophoric Molecules. *Vib. Spectrosc.* **1999**, *19*, 239−242.
(29) Vlčková, B.; Šmejkal, P.; Michl, M.; Procházka, M.; Mojzeš, P.; Lednický, F.; Pfleger, J. Surface-enhanced Resonance Raman Spectroscopy of Porphyrin and Metalloporphyrin Species in Systems with Ag Nanoparticles and Their Assemblies. *J. Inorg. Biochem.* **2000**, *79*, 295−300.
(30) Corra, S.; Lewandowska, U.; Benetti, E. M.; Wennemers, H. Size-Controlled Formation of Noble-Metal Nanoparticles in Aqueous Solution with a Thiol-Free Tripeptide. *Angew. Chem., Int. Ed.* **2016**, *55*, 8542−8245.
(31) Kalbáč, M.; Frank, O.; Kavan, L. The control of graphene double-layer formation in copper-catalyzed chemical vapor deposition. *Carbon* **2012**, *50*, 3682−3687.
(32) Hallam, T.; Berner, N. C.; Yim, C.; Duesberg, G. S. Strain, Bubbles, Dirt, and Folds: A Study of Graphene Polymer-Assisted Transfer. *Adv. Mater. Interfaces* **2014**, *1*, 1400115.
(33) Bohren, C. F.; Huffman, D. R. *Absorption and Scattering of Light by Small Particles*; WILEY-VCH Verlag GmbH & Co. KGaA: Weinheim, Germany, 2004.
(34) Cialla, D.; Petschulat, J.; Hübner, U.; Schneidewind, H.; Zeisberger, M.; Mattheis, R.; Pertsch, T.; Schmitt, M.; Möller, R.; Popp, J. Investigation on the Second Part of the electromagnetic SERS Enhancement and Resulting Fabrication Strategies of Anisotropic Plasmonic Arrays. *ChemPhysChem* **2010**, *11*, 1918−1924.
(35) Ling, X.; Xie, L.; Fang, Y.; Xu, H.; Zhang, H.; Kong, J.; Dresselhaus, M. S.; Zhang, J.; Liu, Z. Can graphene be used as a Substrate for Raman Enhancement? *Nano Lett.* **2010**, *10*, 553−561.
(36) Ling, X.; Huang, S.; Mao, N.; Kong, J.; Dresselhaus, M. S.; Zhang, J. Lighting Up the Raman Signal of Molecules in the Vicinity of Graphene Related Materials. *Acc. Chem. Res.* **2015**, *48*, 1862−1870.
(37) Huang, S.; Ling, X.; Liang, L.; Song, Y.; Fang, W.; Zhang, J.; Kong, J.; Meunier, V.; Dresselhaus, M. S. Molecular Selectivity of Graphene-Enhanced Raman Scattering. *Nano Lett.* **2015**, *15*, 2892−2901.
(38) Hao, Q.; Wang, B.; Bossard, J. A.; Kiraly, B.; Zeng, Y.; Chiang, I.-K.; Jensen, L.; W erner, D. H.; Huang, T. J. Surface-Enhanced Raman Scattering Study on Graphene-Coated Metallic Nanostructure Substrates. *J. Phys. Chem. C* **2012**, *116*, 7249−7254.
(39) Gunnarsson, L.; Rindzevicius, T.; Prikulis, J.; Kasemo, B.; Käll, M.; Zou, S.; Schatz, G. C. Confined Plasmon in Nanofabricated Single Silver Particle Pairs: Experimental Observation of Strong Interparticle Interactions. *J. Phys. Chem. B* **2005**, *109*, 1079−1087.
(40) Feng, X.; Ruan, F.; Hong, R.; Ye, J.; Hu, J.; Hu, G.; Yang, Z. Synthetically Directed Self-Assembly and Enhanced Surface-Enhanced Raman Scattering Property of Twinned Crystalline Ag/Ag Homojunction Nanoparticles. *Langmuir* **2011**, *27*, 2204−2210.
(41) Giovannetti, G.; Khomyakov, P. A.; Karpan, V. M.; van den Brink, J.; Kelly, P. J. Doping graphene with metal contacts. *Phys. Rev. Lett.* **2008**, *101*, 026803.
(42) Tamaru, H.; Kuwata, H.; Miyazaki, H. T.; Miyano, K. Resonant light scattering from individual Ag nanoparticles and particle pairs. *Appl. Phys. Lett.* **2002**, *80*, 1826−1828.
(43) Tuschel, D. Selecting an Excitation Wavelength for Raman Spectroscopy. *Spectroscopy* **2016**, *31*, 14−23.

DOI: 10.1021/acs.langmuir.7b03462
Langmuir 2017, 33, 14414−14424

Supporting information

Effect of ethanethiolate spacer on morphology and optical responses of Ag nanoparticle array - single layer graphene hybrid systems

Veronika Sutrová[a,c], Ivana Šloufová[a], Zuzana Melniková[b], Martin Kalbáč[b], Ewa Pavlova[c], Blanka Vlčková[a]*

[a] Charles University, Faculty of Science, Department of Physical and Macromolecular Chemistry, Hlavova 8, Prague 2, 128 40, Czech Republic, vlc@natur.cuni.cz

[b] J. Heyrovsky Institute of Physical Chemistry of the ASCR, v.v.i, Dolejškova 3, 182 21 Prague 8, Czech Republic

[c] Institute of Macromolecular Chemistry AS CR, Heyrovsky Sq. 2, 162 06 Prague 6, Czech Republic

* Corresponding author E-mail: vlc@natur.cuni.cz

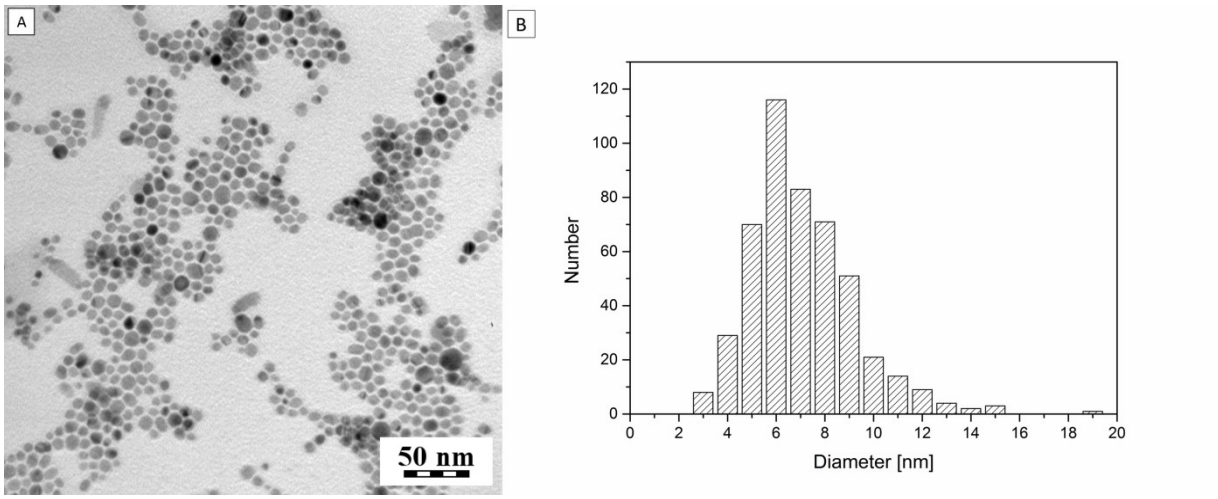

Fig S1: Left: TEM image of a dried drop of parent Ag NP hydrosol prepared according to the ref. S1 (identical with the ref. 23 in the main paper). Right: Particle size distribution determined from the TEM image of the depositd Ag NPs hydrosol.

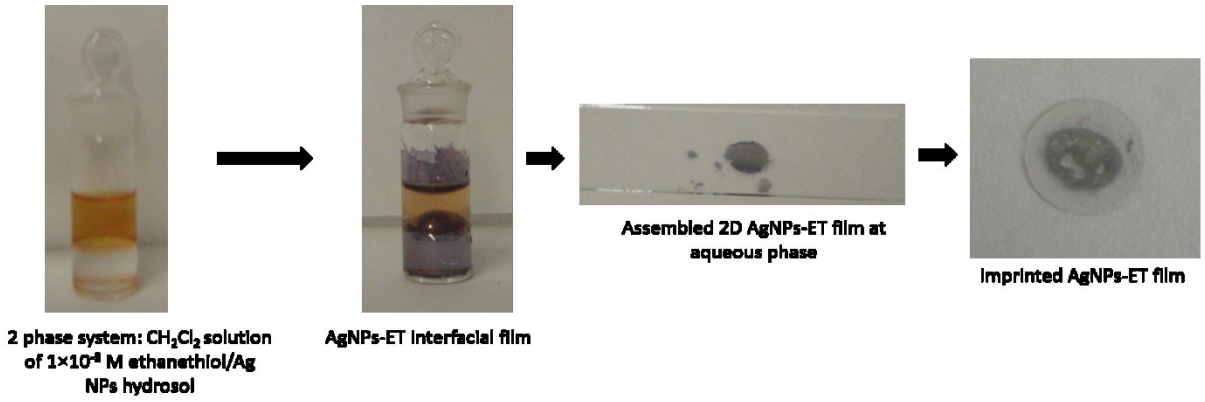

Fig S2: Photographic depiction of the Ag NPs-ET interfacial nanoparticulate film preparation and of its transfer on a glass slide by imprinting.

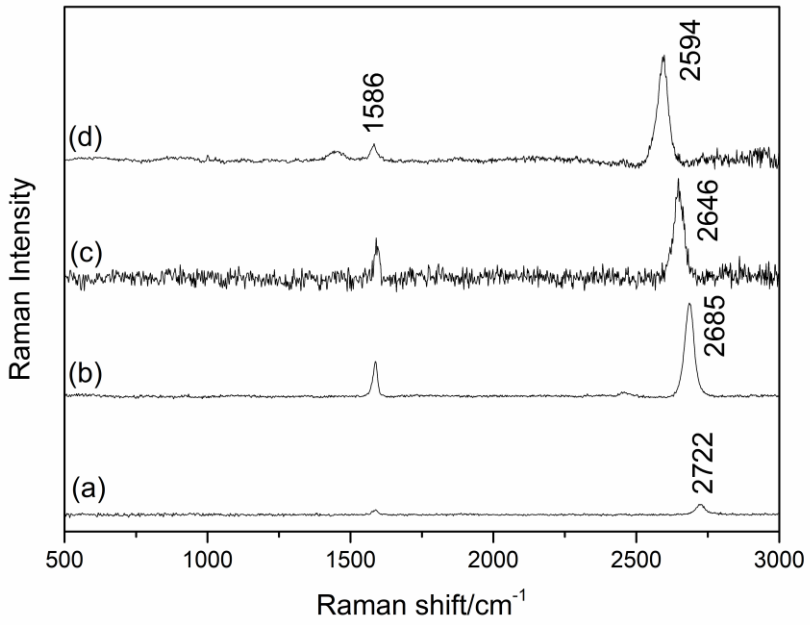

Fig S3: SERS spectra of SLG obtained from glass/SLG reference system at (a) 445 nm (b) 532 nm (c) 633 nm (d) 780 nm excitations.

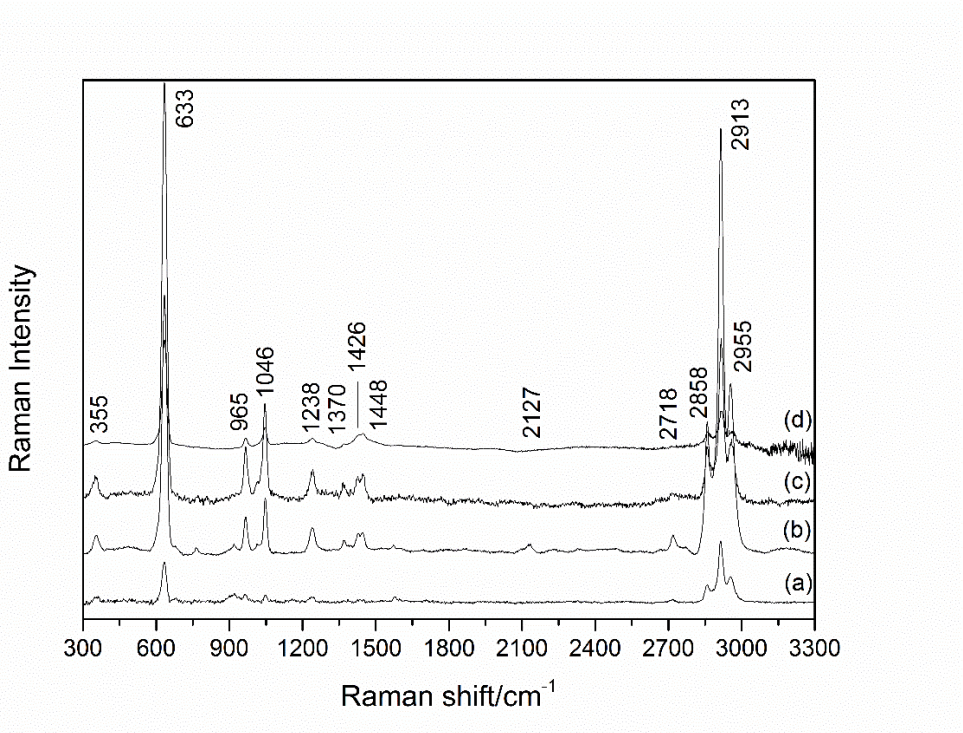

Fig S4: SERS spectra of Ag-ethanethiolate species obtained from the glass/AgNPs-ET array reference system at (a) 445 nm (b) 532 nm (c) 633 nm (d) 780 nm excitations.

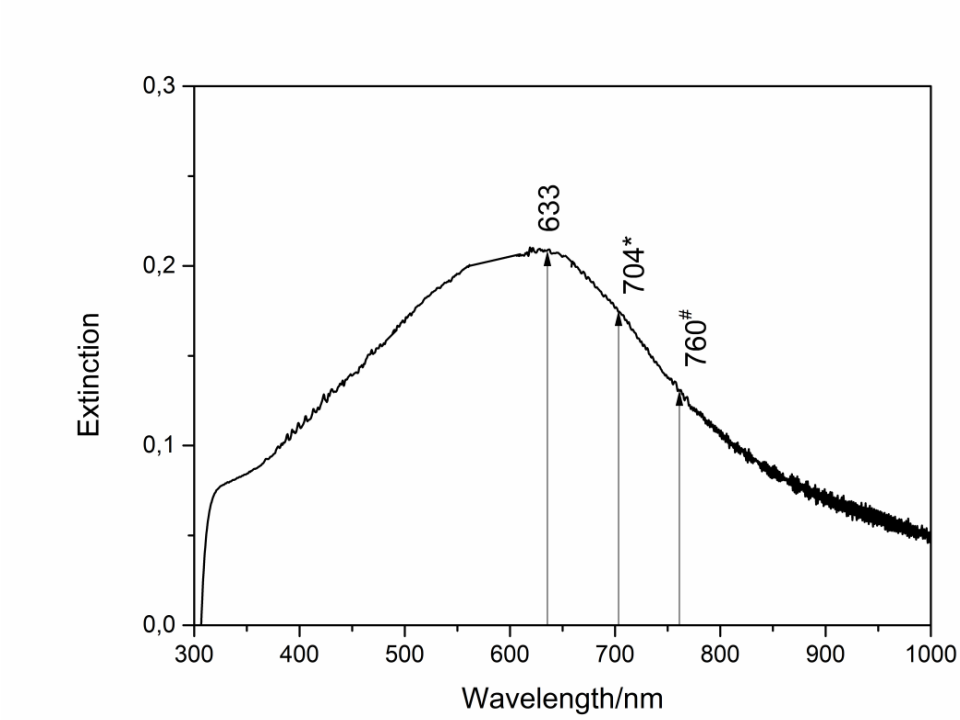

Fig S5: Surface plasmon extinction (SPE) spectrum of glass/SLG/AgNPs-ET hybrid system in relation to (i) the 633 nm excitation wavelength (unlabelled arrow), (ii) the wavelength of photons scattered by the G mode of SLG (1585 cm^{-1}) at 633 excitation (*-labelled arrow) and (iii) wavelength of photons scattered by the 2D mode of SLG (2648 cm^{-1}) at 633 excitation ($^{\#}$-labelled arrow).

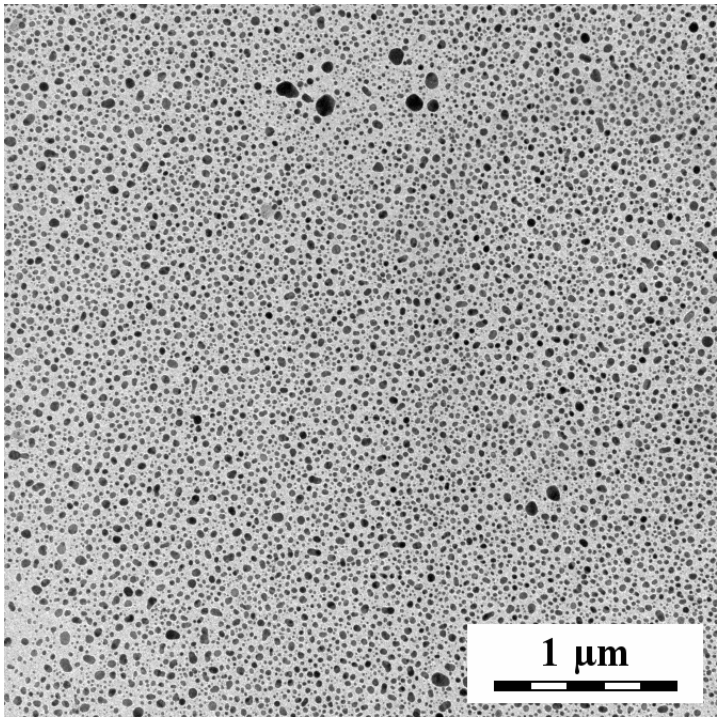

Fig S6: TEM image of the glass/annealed AgNPs array/SLG at low magnification

Table S1: Assignment of Raman spectral bands of ethanethiol and SERS spectral bands of Ag-ET species in Ag NPs-ET array based on refs S1-S4.

Average wavenumbers/cm^{-1}		**Wavenumber range**	**Type of vibration**
Ethanethiol	AgNPs-ET array		
–	350	600 – 700	-AgS
659	632	580 – 1000	C – S stretching
–	964	850 – 1000	-CH_3 rocking
1090	1045	1000 – 1150	C – C stretching
1272	1238	1200 – 1400	CH_2 rocking
–	1368	1330 – 1385	-CH_3 symmetric deformation (bending)
–	1426	1385 – 1445	CH_2 scissoring deformation (bending)
1448	1446	1400 – 1480	CH_3 antisymmetric deformation (bending)
2570	–	2520 – 2600	-SH
2737	2716	–	Overtone of 1368 cm^{-1}
–	2858	2840 – 2870	Symmetric -CH_2 stretching
2870	–	2885 – 2865	Symmetric -CH_3 stretching
2927	2913	2915 – 2940	Antisymmetric -CH_2 stretching
2960	2964	2950 – 2975	Antisymmetric -CH_3 stretching

Table S2: The average SERS enhancement factors of the modes of the Ag-ET surface species in glass/ AgNPs-ET reference system

λ_{exc}/nm	**E_f**
445	5×10^5
532	5×10^6
633	2×10^6
780	1×10^6

Table S3: Enhancement factors of ethanethiol bands in glass/SLG/Ag-NPs-ethanethihol film in comparison to glass/Ag-NPs-ethanethiol film

λ_{exc} = 445 nm				**λ_{exc} = 532 nm**			
Position	Intensity	Intensity with	Ef	Position	Intensity	Intensity with	Ef
633	354	275	λ_{exc} =	633	11046	40230	3
965	80	42	1	965	1518	5490	4
1047	34	34	1	1047	1813	7360	3
1238	34	37	1	1238	1576	6160	3
1426	4	4	1	1426	489	2110	4
1448	7	14	2	1448	579	1930	4
2859	187	199	1	2859	8173	27000	4
2914	799	864	1	2914	17627	97720	4
2957	251	257	1	2957	8991	30500	4
λ_{exc} = 633 nm				**λ_{exc} = 780 nm**			
Position	Intensity	Intensity with	Ef	Position	Intensity	Intensity with	Ef
633	12525	54052	4	633	17238	19001	1
965	1219	4936	4	965	1233	1374	1
1047	2898	8630	4	1047	2728	3137	1
1238	1021	3647	3	1238	788	864	1
1426	462	1398	3	1426	948	964	1
1448	695	2360	4	1448	1478	1524	1
2859	2022	8817	3	2859	3958	4296	1
2914	7050	29747	4	2914	7699	8661	1
2957	1994	8528	4	2957	1975	2026	1

References to Supporting Info:

[S1] Michl, M.; Vlčková, B.; Mojzeš, P. Ag Colloid-1-alkanethiol Films: Spacer-modified Substrates for SERRS Spectroscopy of Chromophoric Molecules.*Vibrational Spectrosc.* **1999,** *19,* 239-242.

[S2] Bensebaa, F.; Zhou, Y.; Brolo, A.G.; Irish, D.E.; Deslandes, Y.; Kruus, E.; Ellis, T.H. Raman characterization of metal-alkanethiolates, *Spectrochim. Acta A*, **1999**, *55*, 1229-1236.

[S3] Kudelski, A. Characterization of thiolate-based mono- and bilayers by vibrational spectroscopy: A review. *Vibrational Spectrosc* **2005**, *39,* 200-213.

[S4] Socrates, G. *Infrared and Raman Characteristic Group Frequencies*, John Wiley & Sons, LTD, England, 2001.

8.3. Publication III: Excitation wavelength dependence of combined surface- and graphene-enhanced Raman scattering experienced by free-base phthalocyanine localized on single layer graphene-covered Ag nanoparticle array

Veronika Sutrová[a,d] Ivana Šloufová[a] Peter Mojzeš[b], Zuzana Melniková[c] Martin Kalbáč[c], Blanka Vlčková[a*]

[a] Charles University, Faculty of Science, Department of Physical and Macromolecular Chemistry, Hlavova 8, Prague 2, 128 40, Czech Republic, vlc@natur.cuni.cz

[b] Charles University, Faculty of Mathematics and Physics, Institute of Physics, Ke Karlovu 5, Prague 2, 121 16, Czech Republic

[c] J. Heyrovsky Institute of Physical Chemistry of the ASCR, v.v.i, Dolejškova 3, 182 21 Prague 8, Czech Republic

[d] Institute of Macromolecular Chemistry AS CR, Heyrovsky Sq. 2, 162 06 Prague 6, Czech Republic

My contribution:

All experimental work: i.e. samples preparations, SERS, GERS and SERS + GERS spectral testing, TEM imaging, except of SLG sample preparation, data evaluation, construction of excitation profiles, calculation of enhancement factors and principal participation in MS preparation.

THE JOURNAL OF PHYSICAL CHEMISTRY C

Article

Cite This: J. Phys. Chem. C 2018, 122, 20850−20860

pubs.acs.org/JPCC

Excitation Wavelength Dependence of Combined Surface- and Graphene-Enhanced Raman Scattering Experienced by Free-Base Phthalocyanine Localized on Single-Layer Graphene-Covered Ag Nanoparticle Arrays

Veronika Sutrová,[†,∥] Ivana Šloufová,[†] Peter Mojzeš,[‡] Zuzana Melníková,[§] Martin Kalbáč,[§] and Blanka Vlčková*[,†]

[†]Faculty of Science, Department of Physical and Macromolecular Chemistry, Charles University, Hlavova 8, Prague 2 128 40, Czech Republic

[‡]Faculty of Mathematics and Physics, Institute of Physics, Charles University, Ke Karlovu 5, Prague 2 121 16, Czech Republic

[§]J. Heyrovsky Institute of Physical Chemistry of the ASCR, v.v.i, Dolejškova 3, 182 21 Prague 8, Czech Republic

[∥]Institute of Macromolecular Chemistry AS CR, Heyrovsky Sq. 2, 162 06 Prague 6, Czech Republic

Supporting Information

ABSTRACT: Hybrid systems constituted by plasmonic nanostructures and single-layer graphene (SLG) as well as their employment as platforms for surface-enhanced Raman scattering (SERS) of the molecular species have recently become a subject of interest. By contrast, only a few studies were targeted specifically on the combination of SERS with graphene-enhanced Raman scattering (GERS) of aromatic molecules. In this paper, we have investigated the mechanisms of combined SERS + GERS by micro-Raman spectral mapping of the hybrid system constituted by annealed Ag nanoparticles (NPs) on the glass substrate overdeposited first by SLG and, subsequently, by a monolayer (ML) of free-base phthalocyanine (H_2Pc) molecules, as well as of glass/SLG/H_2Pc(ML) and of graphite/H_2Pc(ML) reference systems. Raman mapping was performed at multiple excitation wavelengths spanning the 532−830 nm range and was complemented by surface plasmon extinction and transmission electron microscopy images of the Ag NP platform. Observation of SERS + GERS in the aforementioned hybrid system was established by the determination of GERS, SERS, and SERS + GERS enhancement factors. By construction and the mutual comparison of GERS + SERS and GERS excitation profiles of H_2Pc vibrational modes, operation of two mechanisms of GERS additively with the electromagnetic SERS enhancement in SERS + GERS of H_2Pc in the glass/Ag NPs/SLG/H_2Pc(ML) hybrid system has been ascertained. Finally, achievement of the same level of the weak negative doping of SLG by Ag NPs in the probed hybrid system and by glass in the reference system has been established as a necessary condition for the proper evaluation of mechanisms of combined SERS and GERS, and evidence for the fulfillment of this condition in the hybrid systems reported here was provided.

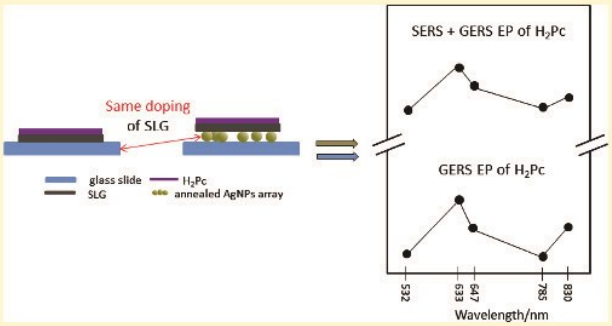

1. INTRODUCTION

One of the primary as well as persistent stimuli for design, preparation, and applications of hybrid systems constituted by plasmonic metal nanostructures (NSs) and chromophoric molecules is a possibility to combine the molecular resonance enhancement of Raman scattering of the chromophores with the enhancement of both the incident and the Raman scattered radiation by the resonance excitation of surface plasmons localized on the NSs, followed by the resulting dipole emission, that is, with the electromagnetic (EM) mechanism of surface-enhanced Raman scattering (SERS), giving rise to surface-enhanced resonance Raman scattering (SERRS).[1−7] The design of such hybrid systems has been targeted on the most efficient coupling of the two enhancement mechanisms upon preservation of the native structure of the chromophores, which, in some cases, can be perturbed by the direct chromophore−metal NS interaction.[5,7] It has been demonstrated that separation of the chromophore from the metal NS by insertion of a thin molecular spacer into the hybrid system can lead to the fulfillment of both goals: preservation of the native structure of the chromophore without a loss in the overall SERRS enhancement by a molecular resonance damping.[3−7]

Received: June 29, 2018
Revised: August 15, 2018
Published: August 16, 2018

DOI: 10.1021/acs.jpcc.8b06218
J. Phys. Chem. C 2018, 122, 20850−20860

Single-layer graphene (SLG), an ultrathin (0.3 nm) array of hexagonally packed carbon atoms, was proposed as a prospective alternative to molecular spacers.[8−19] In particular, it has been demonstrated that the EM mechanism enhancement experienced by the second layer of isotopically labeled SLG deposited over the first layer of SLG (mimicking thus localization of planar aromatic molecules on a SLG spacer) is lower only by a factor of 0.7 than that in the first SLG layer.[14] In addition to that, the SLG spacer was shown to induce, under appropriate resonance conditions, an additional enhancement of Raman scattering of planar aromatic molecules, denoted as graphene-enhanced Raman scattering (GERS).[20] Four mechanisms of GERS have been theoretically predicted,[21] and the factors affecting the observation of GERS and the magnitude of GERS enhancement factors (EFs) were reviewed and summarized.[22,23] Recently, we have reported on the evidence for the operation of two mechanisms of GERS in the spectra of the glass/SLG/H_2Pc monolayer (ML) hybrid system (H_2Pc = free-base phthalocyanine) measured at excitations in the 532−830 nm range: (i) broadening of the Q_y(0−0) absorption band of H_2Pc accompanied by a modification of localization of this resonant electronic transition within the H_2Pc molecule induced by the SLG−H_2Pc interaction and (ii) a charge transfer (CT) from the Fermi level of SLG to the lowest unoccupied molecular orbital (LUMO) of H_2Pc.[24]

The idea of combining the GERS and the EM SERS enhancement of Raman or RRS of a particular molecular species leads to design, preparation, and probing of several types of hybrid systems constituted by plasmonic NSs, SLG, and planar aromatic molecules.[15−19] In particular, regular Au NSs constituted by Au nanoparticles (NPs) and/or nanohole arrays were employed for a comparison of SERS + GERS spectra of methylene blue (MB) dye obtained from the Au NS/SLG/MB hybrid system with its SERS spectra from the Au NS/MB hybrid at 647 nm excitation.[15] A threefold and/or ninefold additional average GERS enhancement of MB vibrational modes was established in the former system with the nanoholes and the NPs, respectively.[15]

In this work, we employ a strategy alternative to that employed previously in ref 15 and more elaborated owing to the employment of multiple excitation wavelengths covering the 532−830 nm range for comparison of the GERS and the EM SERS + GERS spectra of a particular molecular species. Our first goal has been obtaining the evidence of the GERS enhancement as well as of an additional enhancement of GERS of an aromatic molecule, namely, the free-base phthalocyanine (H_2Pc), by the EM mechanism of SERS induced by the localization of a plasmonic enhancer platform underneath the SLG/H_2Pc hybrid system. We demonstrate that both types of enhancement have been encountered for our plasmonic enhancer/SLG/H_2Pc hybrid system at all excitation wavelengths in the 532−830 nm range (vide infra), hence observation of combined SERS + GERS has been unequivocally confirmed, and employment of this term throughout this paper is fully justified. Our second goal, and in fact the most important aim, is to establish whether the mechanisms of GERS and the resonance conditions of their operation remain preserved upon combination of GERS with SERS for this particular aromatic molecule. In addition to that, we attempt to ascertain whether the EM SERS and the GERS enhancements experienced by H_2Pc in the above-mentioned hybrid system are simply additive, that is, whether their combined EFs are simply multiplicative.

For fulfillment of these goals, we have designed, prepared, and probed spectrally the appropriate testing as well as reference hybrid systems. In particular, we considered that the selected plasmonic enhancer in the plasmonic enhancer/SLG/molecule hybrid system has to provide the EM SERS enhancement throughout the overall range of excitation wavelengths, that is, 532−830 nm. The array of Ag NPs annealed upon SLG deposition and recently reported by us[25] was expected and found to be suitable for the fulfillment of this condition. Furthermore, the selection of H_2Pc as the appropriate molecular species was motivated by the results of our aforementioned study of GERS of H_2Pc,[24] as well as by the interesting electronic structure of this molecule,[26−32] leading to its prospective applications in molecular photonics and optoelectronics,[30] in gas sensor development,[31] and as a sensitizer in the photodynamic therapy of cancer.[32] In particular, H_2Pc is a chromophoric aromatic molecule of D_{2h} symmetry, showing the Q_x and the Q_y electronic absorption bands in the visible spectral region, namely, in the 620−720 nm range. The actual positions of these bands' maxima were found to be strongly dependent on the molecular environment (e.g., a solvent and/or inert matrix element employed for the isolation matrix preparation).[26−29] As an example, the electronic absorption spectrum of a saturated solution of H_2Pc in toluene is provided in Figure S1 of the Supporting Information. In the case of the SLG/H_2Pc hybrid system, the positions of the Q_x and the Q_y electronic absorption bands depend on the bilayer and/or ML coverage of SLG by H_2Pc molecules, as revealed by GERS excitation profiles (EPs).[24]

In addition to that, on the basis of the previously reported dependence of the GERS mechanism operation on the actual position of the Fermi level of SLG,[33,34] we have speculated that the difference in doping of SLG by Ag in the Ag NPs/SLG/H_2Pc hybrid system and by a substrate in the substrate/SLG/H_2Pc reference hybrid system could actually induce differences in the operation of GERS in each of the two hybrids, which would not be related specifically to the SERS + GERS combination. We address this issue in the first part (section 3.1) of Results and Discussion, and we have used these results for selection of the appropriate glass substrate (denoted as glassI) for assembling the glassI/SLG/H_2Pc reference system newly reported and employed in this paper. Finally, as tools for achievement of our goals, we employ the determination of GERS, SERS, and SERS + GERS EFs of selected Raman active modes of H_2Pc (section 3.2) as well as the construction of SERS + GERS and GERS EPs of Raman spectral bands of H_2Pc from the excitation wavelength-dependent spectra of the tested and the reference hybrid systems, respectively (section 3.3). Finally, we specify the two mechanisms of GERS, which operate in the SERS + GERS of the glassI/Ag NPs/SLG/H_2Pc hybrid system and their resonance conditions (section 3.4).

2. EXPERIMENTAL SECTION

2.1. Materials. 29,31*H*-Phthalocyanine, H_2Pc (β-form, 98%), 1-ethanethiol (97%), and cellulose nitrate were purchased from Sigma-Aldrich. Analytical grade $AgNO_3$ and sodium borohydride as well as spectral grade dichloromethane and toluene (UVASOL) were purchased from Merck. Distilled deionized water was also used as a solvent where appropriate. Special glass slides different from those employed in ref 24, namely, the microscope glass cover slides (Glaswarenfabrik Karl Hecht GmbH & Co KG), were employed as substrates, and they are denoted as glassI throughout this paper.

DOI: 10.1021/acs.jpcc.8b06218
J. Phys. Chem. C 2018, 122, 20850−20860

2.2. Preparation Procedures. *2.2.1. Ag NP Hydrosol.* Ag NP hydrosol was prepared by reduction of $AgNO_3$ by sodium borohydride according to the previously published procedure.[35]

2.2.2. GlassI/AgNPs/SLG and GlassI/SLG Systems. First, the arrays of Ag NPs modified by chemisorbed ethanethiol (Ag-ET NPs) were prepared according to the procedure reported by Michl et al.[35] Briefly, a two-phase system constituted by 2 mL of Ag NP hydrosol and 2 mL of a 1×10^{-3} M solution of ethanethiol in dichloromethane was vigorously shaken until a lustrous nanoparticulate film appeared at the interface between the aqueous and the organic phase. The interfacial film was then transferred by a pipette into the central part of a special glass slide for optical microscopy and was let to dry in air. Both the central part of the slide containing the array of the Ag-ET NPs and the exteriors of the Ag NPs-free glass slide were then over-deposited by SLG prepared by using the chemical vapor deposition procedure,[36] in particular, the nitrocellulose (NC) method[37] of the as-prepared SLG transfer. The majority of the NC layer from the resulting glassI/Ag NPs-ET/SLG/NC hybrid was removed by methanol drops at room temperature. The sample was then annealed at 160 °C for 30 min in order to remove the NC residuals from the SLG surface. SERS spectral evidence of removal of not only the NC residuals but also of the adsorbed ET from the Ag NP surfaces has been provided, and morphological characterization of the sample showed annealing of Ag NPs.[25]

2.2.3. GlassI/Ag NPs/SLG/H_2Pc(ML) and GlassI/SLG/H_2Pc(ML) Hybrid Systems. The hybrid systems were prepared by adapting the procedure employed for the preparation of the glass/SLG/H_2Pc(ML-*X*) systems.[24] The adapted procedure is graphically depicted in Figure S2 in the Supporting Information. Briefly, the parent glassI/Ag NPs/SLG hybrid system (in which the areas not covered by Ag NPs were distinguished by optical microscopy) was overlaid by a thin layer of a saturated ($<5 \times 10^{-5}$ M) solution of H_2Pc in toluene (which was filtered by the 1 μm filter prior to use), and it was kept in the toluene-saturated atmosphere in a sealed weighing bottle for 24 h to accomplish the adsorption of H_2Pc onto the SLG surface. The sample was then extracted from the weighing bottle, and the solution layer was removed by soaking into a slip of filter paper. In the second step, the excess H_2Pc molecules were removed by overlaying the as-prepared sample by a thin layer of pure toluene and by keeping it in the same setup as described above for 10 min. The solvent layer was then removed by the filter paper, and the overall second step procedure was repeated 10 times.

2.2.4. Graphite/H_2Pc(ML) Reference System. The graphite/H_2Pc(ML) reference system was prepared by the procedure analogous to that described above for the hybrid systems. The graphite substrate preparation and the specifically developed strategy of Raman spectral mapping of the graphite/H_2Pc(ML) system were adopted from ref 24.

2.3. Instrumentation. Raman (RRS, GERS, and GERS + SERS) spectra as well as optical images of all hybrid samples and reference hybrid samples were obtained using a WITec alpha300 Raman micro-spectrometer. An objective (Zeiss) with 100× magnification was used for all the above-mentioned Raman spectral measurements performed at 532, 633, 647, 785, and 830 nm excitations. For measurements on WITec alpha300, two spectrographs equipped with charge-coupled device detectors optimized for the blue-green and the red-NIR (near-infrared) spectral ranges have been used, the first one for the collection of spectra at 532 nm excitation and the second one for the other four excitation wavelengths, that is, 633, 647, 785, and 830 nm. The following lasers, excitation wavelengths, and laser power values (at the sample) were employed: SHG Nd:YVO_4, 532 nm (2.3 mW); He−Ne, 633 nm (2.5 mW); Kr^+ ion, 647 nm (5.0 mW), diode, 785 nm (50.0 mW), diode, 830 nm (11.0 mW). Raman spectral mapping was performed by using the 25 μm × 25 μm area scans with 50 × 50 points. Two types of the areas were selected for the Raman spectral mapping of the combined glassI/AgNPs/SLG/H_2Pc(ML) and glassI/SLG/H_2Pc(ML) samples: (i) the areas of the sample showing the presence of both SLG and Ag NPs on the optical images corresponding to the glassI/AgNPs/SLG/H_2Pc(ML) hybrids probed for GERS + SERS and (ii) the areas with SLG, but without Ag NPs, representing the glassI/SLG/H_2Pc(ML) reference system (probed for GERS). The graphite/H_2Pc(ML) hybrid was employed as the second reference system for Raman and resonance Raman spectral probing of a ML of H_2Pc. Surface plasmon extinction (SPE) (UV/vis) spectra were measured on a Shimadzu UV-2401 spectrometer. Transmission electron microscopy (TEM) images were obtained with a Tecnai G2 (FEI) transmission electron microscope with an acceleration voltage of 120 keV.

2.4. GERS, SERS, and SERS + GERS EFs. GERS EFs of selected H_2Pc modes were determined as the intensity ratios of the corresponding Raman bands in the average spectra of the glassI/SLG/H_2Pc(ML) area of the hybrid sample and in those of the graphite/H_2Pc(ML) reference sample. SERS EFs of GERS of H_2Pc were ascertained as the intensity ratios of the corresponding Raman bands in the average spectra of the glassI/AgNPs/SLG/H_2Pc(ML) area of the hybrid sample and in those of the glassI/SLG/H_2Pc(ML) area of the reference sample. SERS + GERS EFs represent the intensity ratios of the corresponding Raman bands in the average spectra of the glassI/AgNPs/SLG/H_2Pc(ML) area of the hybrid sample and in those of the graphite/H_2Pc(ML) reference sample. While the SERS enhancement of GERS of H_2Pc has been evaluated at all five excitation wavelengths, the GERS and the SERS + GERS EFs could be exactly determined only at 633 and 647 nm excitations, at which the resonance Raman spectra of H_2Pc have been obtained from the graphite/H_2Pc(ML) reference sample. All the intensity ratios were determined in terms of the integrated band areas, and all spectra were baseline-corrected. The procedure of determination of the standard deviations of the EFs is described in Text S1 in the Supporting Information.

2.5. SERS + GERS and GERS EPs. EPs of the H_2Pc bands in the SERS + GERS spectra obtained from the glassI/AgNPs/SLG/H_2Pc hybrid samples at 532, 633, 647, 785, and 830 nm excitations as well as GERS EPs of H_2Pc bands in the glassI/SLG/H_2Pc(ML) reference system were constructed as plots of their normalized band intensities as a function of the excitation wavelength. Raman spectra of polystyrene acquired under the very same experimental conditions as those of the samples were employed as the external intensity standards. At each excitation wavelength, the intensities of the H_2Pc Raman bands (in terms of the integrated band areas) in the spectrum of the hybrid and/or the reference sample were normalized to the intensity of the 1004 cm^{-1} Raman band of polystyrene. The procedure of determination of the standard deviations of the normalized band intensities is described in Text S1 in the Supporting Information. The same procedures of the wave-

DOI: 10.1021/acs.jpcc.8b06218
J. Phys. Chem. C 2018, 122, 20850−20860

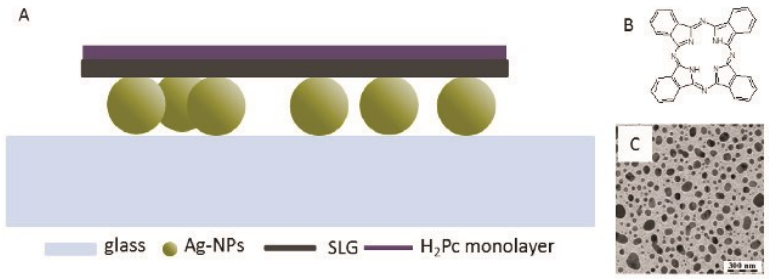

Figure 1. (A) Schematic depiction of the glassI/AgNPs/SLG/H_2Pc(ML) hybrid system used for micro-Raman measurements of SERS + GERS of the H_2Pc (B) molecular structure of H_2Pc; (C) TEM image of the array of annealed Ag NPs employed as the plasmonic enhancer in the glassI/Ag NPs/SLG/H_2Pc hybrid system.

number and intensity calibration of the Raman microspectrometer as those described in ref 24 have been employed.

3. RESULTS AND DISCUSSION

3.1. Characterization and Spectral Probing of the Glass(I)/AgNPs/SLG/H_2Pc(ML) Hybrid System and of the Reference System. The glassI/AgNPs/SLG/H_2Pc(ML) hybrid system used for SERS + GERS micro-Raman spectral probing is schematically depicted in Figure 1A. The molecular structure of H_2Pc is shown in Figure 1B, and the TEM image of the annealed Ag NPs employed as the plasmonic enhancer in the hybrid system (Figure 1A) is presented in Figure 1C. A closer inspection of the TEM image in Figure 1C reveals the presence of monomers as well as dimers and trimers of annealed Ag NPs. The rather broad range of Ag NP shapes and sizes is expected (in accord with ref 25) to cause extension of the SPE of this plasmonic enhancer over the visible and the onset of the NIR spectral region.

The SPE spectra of the glassI/AgNPs/SLG system before and after deposition of H_2Pc are compared in Figure 2. The

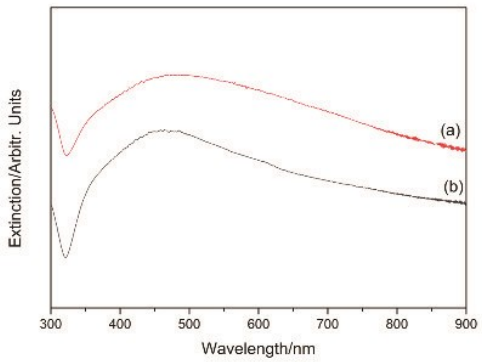

Figure 2. SPE spectra of the glass/Ag NPs/SLG hybrid system: before (a) and after (b) deposition of the H_2Pc ML.

major feature, that is, the extension of SPE over the visible and NIR spectral region, remains preserved upon the H_2Pc deposition, and the differences between the two SPE curves (Figure 2, spectra a and b) are evaluated as minor.

An optical image showing (i) the glassI/AgNPs/SLG/H_2Pc(ML) and (ii) the glassI/SLG/H_2Pc(ML) parts of the same sample and the boundary between these two parts is presented in Figure 3A. The SERS + GERS and the GERS parts of the spectral map of the 683 cm^{-1} mode of H_2Pc measured at 785 nm excitation and spanning the same sample area as that in Figure 3A are shown in Figure 3B. The spectral

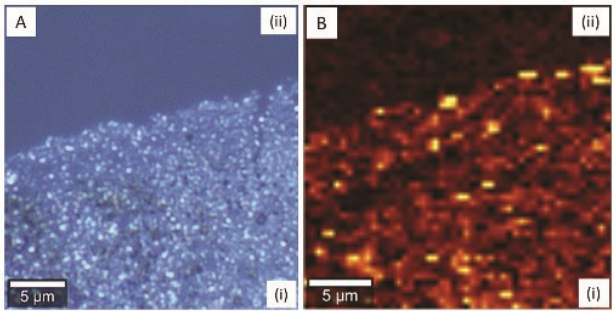

Figure 3. (A) Optical image of the hybrid sample employed for GERS and SERS + GERS spectral measurements (mapping) of H_2Pc with the clearly distinguished boundary between the (i) glass/AgNPs/SLG/H_2Pc part of the sample used for SERS + GERS measurements and (ii) glass/SLG/H_2Pc part of the sample utilized for GERS measurements. (B) Spectral map of the 683 cm^{-1} band of H_2Pc acquired at 785 nm excitation from the same area of the sample as the optical image (A). The spectral map (B) shows the markedly higher intensity of the Raman signal from the (i) glass/AgNPs/SLG/H_2Pc part of the sample (SERS + GERS) than from the (ii) glass/SLG/H_2Pc part of the sample (GERS).

map (Figure 3B) shows the markedly higher intensity of the Raman signal of the 683 cm^{-1} mode of H_2Pc from the (i) glassI/AgNPs/SLG/H_2Pc(ML) part of the sample than from the (ii) glassI/SLG/H_2Pc part of the sample, which, in turn, provides a qualitative evidence of observation of SERS + GERS of H_2Pc in the former case and of GERS of H_2Pc in the latter one.

For the actual spectral mapping by which the average spectra were acquired at all five excitation wavelengths, the maps spanning entirely the glassI/AgNPs/SLG/H_2Pc(ML) area of the sample (fully covered by a single layer of Ag NPs) were used for the SERS + GERS measurements, and those spanning the glassI/SLG/H_2Pc(ML) area were employed for GERS. As an example, an optical image of the glassI/AgNPs/SLG/H_2Pc(ML) area of the sample and the SERS spectral maps of the G mode (1590 cm^{-1}) and 2D (2595 cm^{-1}) mode of SLG as well as the SERS + GERS spectral maps of the 683 and 1540 cm^{-1} modes of H_2Pc acquired from this area at 785 nm excitation are shown in Figure S3A–E, respectively, in the Supporting Information.

SERS spectra of SLG and SERS + GERS spectra of H_2Pc obtained from the glassI/Ag NPs/SLG/H_2Pc(ML) hybrid system at 532, 633, 647, 785, and 830 nm excitations are shown in Figure 4A (full range spectra) and Figure 4B (details in the 400–1800 cm^{-1} range). The average wavenumber of the G mode band in the spectra of the glassI/AgNPs/SLG/H_2Pc is

DOI: 10.1021/acs.jpcc.8b06218
J. Phys. Chem. C 2018, 122, 20850–20860

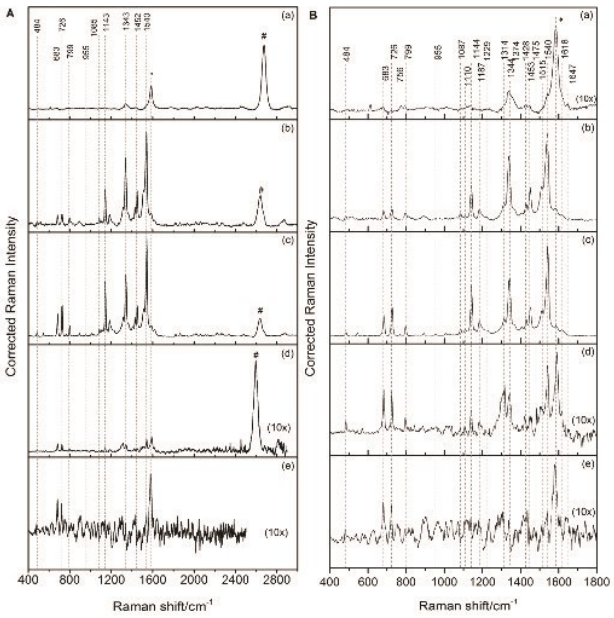

Figure 4. (A) Full range (400−3000 cm^{-1}) and (B) detailed (400−1800 cm^{-1}) SERS + GERS spectra of H_2Pc measured from the glassI/AgNPs/SLG/H_2Pc(ML) hybrid system at (a) 532, (b) 633, (c) 647, (d) 785, and (e) 830 nm excitations. The SERS spectral band of the G mode is marked by *, and the SERS spectral bands of the dispersive 2D mode are marked by #.

1590 cm^{-1}, that is, exactly the same as reported for the glass/Ag NPs/SLG system.[25] This result indicates that deposition of a ML of H_2Pc molecules onto the glassI/Ag NPs/SLG platform has not caused any additional doping of SLG by H_2Pc molecules. The 1590 cm^{-1} position of the G band is 5 cm^{-1} higher than in the pristine SLG[39,40] and, in accord with refs 25 and 38, indicates a weak n-doping of SLG by Ag.

Furthermore, the G band in the Raman spectra of the glassI/SLG/H_2Pc(ML) reference system is located at 1592 cm^{-1}, and its position is thus comparable (within the experimental error) with that in the glassI/AgNPs/SLG/H_2Pc(ML) system. This comparison indicates that the magnitude of the weak n-doping of SLG by glass in the former system is analogous to the weak n-doping of SLG by Ag in the latter system. Consequently, the positions of the Fermi level of SLG are nearly identical in both systems, and they were estimated to be ca. −4.4 eV (i.e., upshifted by ca. 0.2 eV from the Fermi level of pristine SLG at −4.6 eV[20]) on the basis of the graph in Figure 8.5 in ref 39. Therefore, the fundamental conditions of operation of the mechanisms of GERS are virtually identical in the glassI/AgNPs/SLG/H_2Pc(ML) hybrid system employed for SERS + GERS spectral probing and in the glassI/SLG/H_2Pc(ML) system used as the reference system for GERS in this paper.

Furthermore, we have noticed that the position of the G band of SLG in our glassI/SLG/H_2Pc(ML) reference system (1592 cm^{-1}) is lower by 7 cm^{-1} than that reported for the glass/SLG/H_2Pc(ML) system in ref 24 (1599 cm^{-1}). This comparison indicates that the n-doping by glass (in particular, by surface groups and/or water entrapped between glass and SLG) is markedly weaker than that by the glass slides used in ref 24. Such differences in n-doping by glass have been reported previously, and they have been attributed to a different content of Na in the particular sample of glass.[41] The comparison of the positions of the Fermi level of SLG (i) at −4.4. eV in the glassI/SLG/H_2Pc(ML) reference system and (ii) at −4.3 eV in the GERS sample in ref 24 (further referred to as the glassII/SLG/H_2Pc(ML) system in this paper) demonstrates the importance of doping of SLG by the substrates. On the other hand, once this important factor is properly evaluated, it can be employed for adjusting the Fermi level position of SLG.

The average wavenumbers of the H_2Pc bands in SERS + GERS spectra of the glassI/AgNPs/SLG/H_2Pc(ML) hybrid system as well as in the GERS spectra of the glassI/SLG/H_2Pc(ML) reference system, together with their assignment based on refs 27 and 42, are listed in Table 1. The wavenumbers of SERS + GERS and the GERS spectral bands show a reasonably good mutual agreement (within 3 cm^{-1}).

Table 1. Average Wavenumbers of the H_2Pc Bands in SERS + GERS Spectra of the GlassI/AgNPs/SLG/H_2Pc(ML) Hybrid System and in GERS Spectra of the GlassI/SLG/H_2Pc(ML) Reference System Complemented by Their Assignment Based on Refs 24, 27, 42

GERS of H_2Pc	GERS + SERS of H_2Pc	mode symmetry	mode description
486	484	B_{1g}	benzene ring rocking & central ring deformation
683	683	A_g	bridging C−N−C sym. def. and benzene ring deformation
728	726	A_g	pyrrole deformation and C−N−C rocking
800	799	A_g	pyrrole and benzene ring C−C str.
952	955	IR act	C−H out-of-plane deformation
1086	1085	B_{1g}	N−H in-plane deformation
1143	1143	A_g	benzene ring C−C str. and C−H deformation
1343	1343	A_g	benzene ring C−C str. and pyrrole C−C stretch
1453	1452	A_g	C−H def.
1543	1540	A_g	bridging C_α−N_m−C_α asym. str. and C_α−N_H−C_α sym. str.

3.2. GERS, SERS, and SERS + GERS EFs of Selected Spectral Bands of H_2Pc Localized in the GlassI/SLG/H_2Pc Reference Hybrid System and in the GlassI/AgNPs/SLG/H_2Pc Hybrid System, Respectively. Raman spectra of H_2Pc were obtained from the glassI/AgNPs/SLG/H_2Pc(ML) probed hybrid system (Figure 4) as well as from the glassI/SLG/H_2Pc(ML) reference system at all five excitation wavelengths. By contrast, the graphite/H_2Pc second reference system yielded Raman spectra of H_2Pc only upon resonance with the $Q_y(0-0)$ electronic transition, that is, at 633 and 647 nm excitations, in accord with ref 24. Therefore, the EFs evaluating the SERS enhancement of GERS of H_2Pc in the probed hybrid system (denoted as SERS + GERS/GERS EFs and abbreviated as SERS EFs) could be determined at all five excitation wavelengths (details in section 2.4 of the Experimental Section), and their average values as a function of excitation wavelength are listed in Table 2. The average EFs are of comparable values in the 633−830 nm range. The slightly larger EFs at 633 and 830 nm are attributed to plasmon resonances with the more abundant large spherical or slightly ellipsoidal Ag NPs and with less abundant dimers or trimers of Ag NPs upon generation of strong optical fields, respectively.

On the other hand, GERS EFs (details in section 2.4) could be numerically evaluated only at 633 and 647 nm excitations

DOI: 10.1021/acs.jpcc.8b06218
J. Phys. Chem. C 2018, 122, 20850−20860

Table 2. Average SERS EFs of the Vibrational Modes of H_2Pc at Five Excitation Wavelengths in the 532−830 nm Range[a]

wavelength	532	633	647	785	830
EFs	5 ± 2	14 ± 5	9 ± 3	10 ± 3	13 ± 4

[a]The EFs were determined as the ratios of the normalized intensities of the H_2Pc spectral bands in SERS + GERS spectra of the glassI/AgNPs/SLG/H_2Pc(ML) hybrid system and in GERS spectra of the glassI/SLG/H_2Pc(ML) reference system.

(Table 3); however, the aforementioned observation of the GERS signal of H_2Pc from the glassI/SLG/H_2Pc(ML) system at all five excitation wavelengths, in contrast to the absence of any Raman signal of H_2Pc from the graphite/H_2Pc(ML) second reference system at 532, 785, and 830 nm, indicates that the GERS enhancement of H_2Pc modes occurs at these wavelengths as well.

Table 3. Average Values of GERS EFs (GERS vs RRS Normalized Band Intensity Ratios), SERS EFs (SERS + GERS vs GERS Normalized Intensity Ratios), SERS + GERS EFs (SERS + GERS vs RRS Normalized Intensity Ratios) and Multiplications of SERS EFs with GERS EFs of H_2Pc Vibrational Modes at 633 and 647 nm Excitations

	633 nm	647 nm
average GERS EFs	3 ± 1	4 ± 1
average SERS EFs	14 ± 5	9 ± 3
average SERS + GERS EFs	43 ± 7	41 ± 7
average SERS + GERS EFs (determined as SERS × GERS EFs)	42 ± 9	36 ± 7

These results confirm the observation of combined SERS + GERS of H_2Pc from the glassI/AgNPs/SLG/H_2Pc(ML) hybrid system and of GERS of H_2Pc from the glassI/SLG/H_2Pc(ML) reference system. Furthermore, the average SERS + GERS EFs at 633 and 647 nm excitations (Table 3) were determined in a dual way: (i) directly from the SERS + GERS spectra (shown in Figure 4) in relation to the RRS spectra of H_2Pc localized in the graphite/H_2Pc(ML) system (details for individual bands in Table S1 in the Supporting Information) and (ii) as products of the SERS and GERS EFs listed in the first and second row of Table 3. Their values (Table 3) are nearly identical at 633 nm excitation and mutually very close (within the experimental error) at 647 nm excitation. This comparison indicates that the SERS and GERS EFs are simply multiplicative, that is, that the two enhancement mechanisms are combined without any additional enhancement or damping. It should be noted that in our hybrid system, we can observe only the EM SERS enhancement because H_2Pc is isolated from the Ag NP surface by the SLG spacer. The ordering of the components in our hybrid system is thus different from the case of CuPc molecules sandwiched between a flat Au(111) surface and SLG, for which a coupling of GERS with the chemical mechanism of SERS, namely, a CT from the Fermi level of Au to the LUMO of CuPc, has been reported.[43]

3.3. SERS + GERS EPs of Selected Spectral Bands of H_2Pc Localized in the GlassI/AgNPs/SLG/H_2Pc(ML) Hybrid System. EPs of the selected spectral bands of H_2Pc were constructed from the SERS + GERS spectra of the glassI/Ag NPs/SLG/H_2Pc(ML) hybrid system measured at 532, 633, 647, 785, and 830 nm excitations by the procedure described in section 2.5. The complete EPs are presented in Figure 5A, their details in the 750−850 nm region are depicted in Figure 5B, and the selected profiles with error bars are shown in Figure 6A. For the sake of comparison, the GERS EPs of the selected spectral bands of H_2Pc determined from the GERS spectra of the glassI/SLG/H_2Pc(ML) reference system measured at the same five excitation wavelengths as the SERS + GERS spectra are presented in Figure 6B. Both the SERS + GERS EPs (Figures 5A and 6A) and the GERS EPs (Figure 6B) of all H_2Pc spectral bands maximize at 633 nm excitation. Furthermore, the average value of the normalized intensities of the H_2Pc spectral bands (depicted in Figure 5), and its average standard deviation at 633 nm excitation (EPs maximum) have been determined by the procedure described in Text S1 in the Supporting Information, yielding a value of 4 ± 0.3.

For a mutual comparison of SERS + GERS EPs and GERS EPs in Figure 6, the profiles of the 683,1143, and 1540 cm^{-1} totally symmetric (A_g) vibrational modes of H_2Pc (assigned in Table 1) have been selected from the complete set of SERS + GERS EPs in Figure 5A and complemented by error bars depicting the experimental error of the spectral mapping (Figure 6A). The GERS EPs of the same bands have been constructed from the GERS spectra of the glassI/SLG/H_2Pc(ML) reference system measured at the same five excitations and complemented by error bars (Figure 6B). Both the SERS + GERS EPs (Figure 6A) and the GERS EPs (Figure 6B) show a common maximum at 633 nm excitation

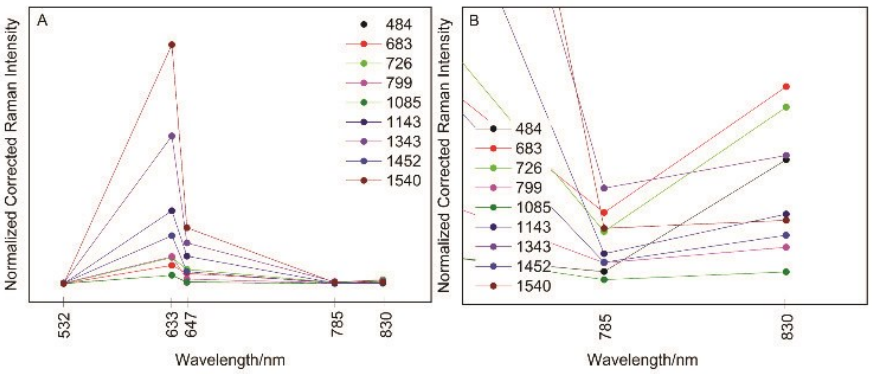

Figure 5. SERS + GERS EPs of spectral bands of H_2Pc localized in the glassI/AgNPs/SLG/H_2Pc(ML) hybrid system: (A) complete EPs in the 532−830 nm range of excitation wavelengths and (B) details of the EPs in the 750−830 nm range.

DOI: 10.1021/acs.jpcc.8b06218
J. Phys. Chem. C 2018, 122, 20850−20860

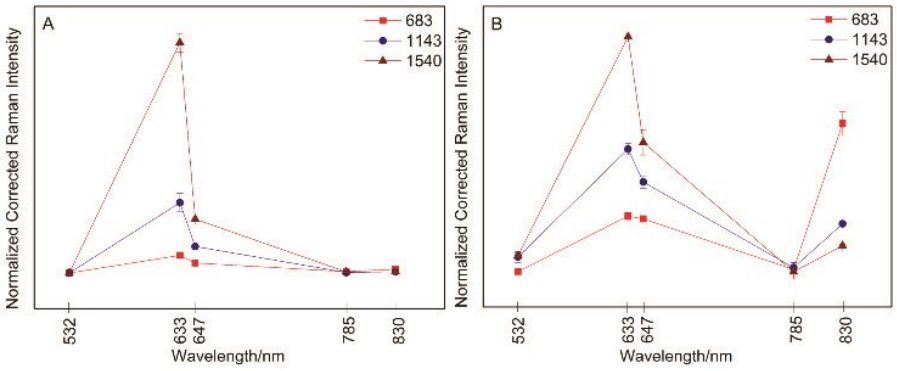

Figure 6. (A) SERS + GERS EPs of selected spectral bands of H_2Pc measured from the glassI/AgNPs/SLG/H_2Pc(ML) hybrid system. (B) GERS EPs of the same bands of H_2Pc as in (A) measured from the glassI/SLG/H_2Pc(ML) reference system. Both EPs are depicted with error bars.

and a normalized band intensity increase at 830 nm. This comparison demonstrates that the shapes of the GERS EPs of all the three spectral bands, namely, the two distinct resonance features at 633 and 830 nm, remain preserved upon the combination of SERS with GERS of H_2Pc.

The other common features of the selected SERS + GERS EPs in Figure 6A and the GERS EPs in Figure 6B are the sequences of the normalized band intensities of the three selected H_2Pc spectral bands at 633, 647, and 830 nm excitations, in particular, the 683 > 1143 > 1540 cm^{-1} sequences determined at both 633 and 647 nm excitations and the reverse 683 > 1143 > 1540 cm^{-1} sequence at 830 nm excitation. This result indicates that (i) each of the two resonance features (i.e., the maximum at 633 nm and the normalized intensity increase at 830 nm) observed in both the GERS EPs (Figure 6B) and SERS + GERS EPs (Figure 6A) belongs to a different resonance electronic transition, each showing a different localization within the H_2Pc molecule, and (ii) for both these resonant electronic transitions, their localization within the H_2Pc molecules remains unchanged upon the combination of SERS with GERS. In summation, the only observed difference between the SERS + GERS and GERS EPs (Figure 6A,B) is the magnitude of the normalized intensity increase at 830 nm excitation, which is markedly higher in the latter case than in the former one. Such "smearing" of the SERS + GERS EP shape emerges as the only consequence of the SERS enhancement contribution to the combined SERS + GERS profiles, and it can be tentatively explained by the similar values of the EM SERS mechanism enhancement of GERS of H_2Pc at 785 and 830 nm excitation (Table 2). At this point, we find appropriate to emphasize that both in the glassI/AgNPs/SLG/H_2Pc(ML) hybrid system used for SERS + GERS spectral measurements and construction of SERS + GERS EPs and in the glassI/SLG/H_2Pc(ML) reference system employed for GERS and GERS EPs construction, nearly the same level of doping of SLG by Ag NPs in the former system and by the glassI substrate in the latter one was established (section 3.1). There were thus no differences in the position of the Fermi level of SLG in the probed system and in the reference hybrid system, which could possibly hamper the comparison of SERS + GERS and GERS EPs.

3.4. Specification of the Mechanisms of GERS and of Their Operation in GERS and SERS + GERS of H_2Pc in the 532−830 nm Range. In this section, we focus on the assignment of two resonance electronic transitions modulating the shapes of both SERS + GERS and GERS EPs presented in section 3.3, determination of their localization within the H_2Pc molecule (on the basis of the sequences of the normalized band intensities of the resonantly enhanced totally symmetric A_g and their localization within the H_2Pc molecule mode by using the approach first reported in ref 44 for RRS) and on specification of the mechanisms of GERS operating in both SERS + GERS and GERS of H_2Pc in the 532−830 nm range.

First, the electronic absorption band giving rise to the 633 nm maximum on both SERS + GERS and GERS EPs of H_2Pc (Figures 5A and 6A,B) is attributed to the $Q_y(0-0)$ electronic transition of H_2Pc on the basis of the previously reported electronic absorption spectra and EPs.[24,26−30] Furthermore, the same sequences of the normalized band intensities in the SERS + GERS and GERS EPs of the three selected H_2Pc bands (Figure 6 and section 3.3) encountered at the 633 and 647 nm excitations indicate that the 647 nm excitation also falls into the contour of the $Q_y(0-0)$ electronic absorption band. The markedly larger normalized band intensities at 633 than at 647 nm excitation (Figures 5A and 6), together with the ∼10 nm value of the $Q_y(0-0)$ band half-width determined by detailed SERRS EPs of this electronic transition in Ag NSs/H_2Pc hybrid system[26] (as the largest reported half-width of this electronic transition), indicate that the maximum of this electronic transition in both the glassI/AgNPs/SLG/H_2Pc-(ML) and the glassI/SLG/H_2Pc(ML) systems is located between the 633 and 647 nm excitations (mutually distanced by 14 nm), but closer to the 633 nm excitation, that is, within ca. 633−639 nm interval. In contrast to the normalized band intensities in GERS of H_2Pc, which maximize at 633 nm excitation (Figure 6A), the GERS EFs (Table 3) were determined to be larger at 647 nm (average EF = 4) than at 633 nm excitation (average EF = 3). This observation is consistent with broadening and a small blue shift (vide infra) of this electronic absorption band in both the glassI/AgNPs/SLG/H_2Pc(ML) hybrid system and the glassI/SLG/H_2Pc-(ML) reference system, in comparison to the graphite/H_2Pc(ML) second reference system. These changes in the position and half-width of the $Q_y(0-0)$ electronic absorption band are attributed to the SLG−H_2Pc(ML) interaction, and they are responsible for the GERS enhancement experienced by H_2Pc spectral modes in both the probed hybrid system and the reference system at 633 and 647 nm excitations, respectively (Table 3).

Furthermore, the 1540 > 1143 > 683 cm^{-1} sequence of the normalized band intensities established in both SERS + GERS

DOI: 10.1021/acs.jpcc.8b06218
J. Phys. Chem. C 2018, 122, 20850−20860

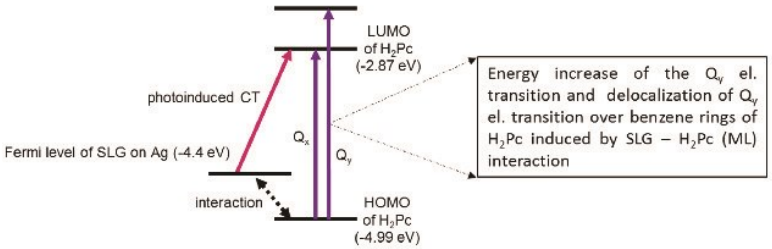

Figure 7. Schematic depiction of two mechanisms of GERS identified in SERS + GERS of H_2Pc measured from the glassI/AgNPs/SLG/H_2Pc(ML) hybrid system as well as in GERS of H_2Pc obtained from the glassI/SLG/H_2Pc(ML) system at excitations in the 532−830 nm range. The energy of the Fermi level of SLG was determined to be ca. −4.4 eV in both systems.

and GERS of H_2Pc at 633 and 647 nm together with the assignment of the H_2Pc vibrational modes in Table 1 and the detailed analysis of the complete GERS + SERS EPs (presented as Text S2 in the Supporting Information) indicate a preferential enhancement of the higher wavenumber modes, mainly the C−C stretching vibrations localized on benzene and pyrrole rings, the combined C−N−C stretch known as the cavity size marker,[45] and the C−H deformation modes localized on the outer benzene rings. By contrast, this electronic transition has been reported to be localized preferentially on the tetrapyrrole macrocycle for a free H_2Pc molecule owing to the preferential enhancement of macrocycle breathing and deformation modes.[46] The change in localization of the $Q_y(0-0)$ resonant electronic transition within the H_2Pc molecule represents another manifestation of GERS in SERS + GERS of H_2Pc in the glassI/Ag NPs/SLG/H_2Pc(ML) system as well as in GERS of H_2Pc in the glassI/SLG/H_2Pc(ML) reference system at 633 and 647 nm excitations, and it is also attributed to the SLG−H_2Pc(ML) interaction (Figure 7).

The second resonance which manifests itself by the relative intensity increase at 830 nm excitation has no analogue in the previously reported electronic absorption spectra of H_2Pc in solutions and matrices.[26−30] On the other hand, the energy difference between the Fermi level of SLG (positioned at ca. −4.4 eV) and LUMO of H_2Pc (at −2.87 eV[29]) is 1.53 eV, that is, 810 nm. This calculated value of the maximum of a CT from the Fermi level of SLG to the LUMO of H_2Pc at 810 nm suggests that the 830 nm excitation is in resonance with this CT electronic transition (Figure 7). Such a CT transition has been theoretically predicted as one of the four possible mechanisms of GERS.[21]

Finally, to evaluate the importance of the same doping, that is, of the same position of Fermi level of SLG in the hybrid system probed for SERS + GERS and in the reference system providing GERS of H_2Pc, we have investigated the effect of the ca. 0.1 eV difference in the position of Fermi level of SLG on the operation and manifestations of the mechanisms of GERS of H_2Pc by comparing GERS EFs and EPs of H_2Pc vibrational modes in two glass/SLG/H_2Pc(ML) hybrid systems: the glassI/SLG/H_2Pc(ML) system reported in this work with the Fermi level of SLG at ca. −4.4. eV (further denoted as system I) and the glassII/SLG/H_2Pc(ML-*X*) system reported previously in ref 24 in which the Fermi level of SLG is at ca. −4.3 eV (system II). The distinct features common to both systems are manifestation of two resonances on the EPs of H_2Pc vibrational modes and nearly the same localization of each of the two resonant electronic transitions within the H_2Pc molecule, which, in turn, indicates that the same mechanisms of GERS operate in both systems in the 532−830 nm range. On the other hand, the following differences between the two systems were found. First, the maxima of EPs in the visible spectral region have been encountered at different excitation wavelengths, namely, at 633 nm for system I and at 647 nm for system II. Furthermore, the average GERS EFs of H_2Pc vibrational modes are markedly lower for system I than for system II at both 633 and 647 nm excitations, namely, 3 and 4, respectively, for system I (this paper) and 9 and 8, respectively, for system II.[24] We have also noticed that the average GERS EF is slightly higher at 647 nm excitation for system I and at 633 nm excitation for system II. These differences are consistent with a slight blue shift of the maximum of the electronic absorption band for system I reported in this paper (but not encountered for system II[24]). This shift is tentatively attributed to a closer proximity of the Fermi level of SLG to the highest occupied molecular orbital of H_2Pc (calculated as −4.99 eV[29]) in system I than in system II, which, in turn, can allow a weak interaction of these two energy levels in the former system. The second difference between the two systems is a more pronounced increase of the normalized band intensities of H_2Pc vibrational modes at 830 nm excitation encountered for system I in comparison to system II. This difference is explained by a closer proximity of the 830 nm excitation wavelength to the maximum of the CT electronic transition from the Fermi level of SLG to the LUMO of H_2Pc in the former case (the calculated max. at 810 nm) than in the latter one (the calculated max. at 867 nm). Although all the above-mentioned differences between systems I and II could possibly be viewed as minor, their importance largely increases in the case when they are employed as reference systems for combined SERS + GERS. For example, should the system II have been used as the reference system in this study instead of system I, these differences could be erroneously attributed to the combination of SERS with GERS of H_2Pc.

4. CONCLUSIONS

Evidence for a simultaneous operation of GERS and SERS experienced by the free-base phthalocyanine (H_2Pc) molecular ML localized on the top of SLG deposited over an array of annealed Ag NPs has been obtained. Preparation and characterization of the glassI/AgNPs/SLG/H_2Pc(ML) hybrid systems together with the glassI/SLG/H_2Pc(ML) and graphite/H_2Pc(ML) reference systems and their micro-Raman spectral mapping at five excitations in the 532−830 nm range, followed by the determination of SERS, GERS, and SERS + GERS EFs and construction of SERS + GERS and GERS EPs of H_2Pc vibrational modes, have emerged as an appropriate strategy for a detailed elucidation of the combined mechanism of SERS + GERS. Importantly, the same positions

DOI: 10.1021/acs.jpcc.8b06218
J. Phys. Chem. C 2018, 122, 20850−20860

of Fermi level of SLG (at −4.4 eV) were obtained in the glassI/Ag NPs/SLG/H_2Pc(ML) hybrid system probed for SERS + GERS and in the glassI/SLG/H_2Pc(ML) reference system probed for GERS. This was achieved by employment of the appropriate glass substrate, which induces a small negative doping of SLG comparable to the doping of SLG by Ag.

GERS, SERS, and GERS + SERS EF values have provided evidence that the combined SERS + GERS of H_2Pc is observed at all excitations in the 532−830 nm range. This observation is attributed to a proper selection of the array of annealed Ag NPs as the plasmonic enhancer operating in the broad wavelength range. In addition to that, the mechanisms of SERS and GERS in combined SERS + GERS were found to operate additively (i.e., their EFs are simply multiplicative) at 633 and 647 nm excitations. Furthermore, the comparison of SERS + GERS and GERS EPs of H_2Pc vibrational modes has revealed that the two distinct resonance features, that is, the maximum at 633 nm and the normalized intensity increase from 785 to 830 nm excitation encountered in GERS EPs, remain preserved in the SERS + GERS EPs as well. In this respect, the SERS + GERS EPs resemble the SERRS EPs, the shapes of which are modulated by RRS of chromophoric molecules.

The particular mechanisms of GERS operating in both SERS + GERS and GERS of H_2Pc in our probed and reference hybrid systems, respectively, at different excitation wavelengths have been identified and found to be consistent with two of the four theoretically predicted mechanisms of GERS.[21] In particular, modification of localization of the resonant $Q_y(0-0)$ electronic transition (with maximum at ca. 633−639 nm) within the H_2Pc molecule together with broadening and a small blue shift of its spectral band has been ascertained and ascribed to the SLG−H_2Pc(ML) interaction. The resonance observed at 830 nm excitation is attributed to the CT electronic transition from the Fermi level of SLG to the LUMO of H_2Pc with the calculated maximum at ca. 810 nm. A slightly less pronounced (but still clearly detectable) manifestation of this CT transition in the SERS + GERS EPs in comparison to GERS EPs is the only difference between the SERS + GERS and GERS EPs of H_2Pc encountered under the conditions of our experiment, that is, upon the same position of Fermi level of SLG in the probed and reference systems, respectively.

The importance of the last mentioned experimental condition was further demonstrated by the comparison of GERS EPs and EFs of two glass/SLG/H_2Pc hybrid systems (system I in this work and system II in ref 24), for which the mutual difference in the position of Fermi level was established to be ∼0.1 eV. Distinct differences in the GERS EP shapes and GERS EF values were found between the two systems. Therefore, provided that system II would have been taken as the reference system instead of system I, these differences could be incorrectly ascribed to the mutual coupling of SERS with GERS.

In summation, observation of the combined SERS + GERS in a plasmonic NS/SLG/aromatic molecules hybrid system is conditioned by the overlap between the wavelength range of the plasmon resonance of the particular plasmonic NS and the range of wavelengths in which one of the mechanisms of GERS operates for a particular molecule. Another important aspect of SERS + GERS combination stems from the (now well established) fact that the GERS mechanism operation is, for any molecule, strongly dependent on the actual position of the Fermi level of SLG, which, in turn, is set to a particular value by doping of SLG by the plasmonic metal in the plasmonic NS/SLG/molecules hybrid system. This aspect has to be taken into account upon designing and probing hybrid systems for SERS + GERS of aromatic molecules as well as upon selection of an appropriate substrate/SLG/molecule reference system for the evaluation of the GERS mechanism contribution to combined SERS + GERS.

■ ASSOCIATED CONTENT

Supporting Information

The Supporting Information is available free of charge on the ACS Publications website at DOI: 10.1021/acs.jpcc.8b06218.

Electronic absorption spectrum of H_2Pc, preparation scheme of H_2Pc(ML) deposition, additional optical images and SERS + GERS spectral maps of the glassI/AgNPs/SLG/H_2Pc(ML) hybrid system, SERS + GERS EFs of individual H_2Pc spectral bands, and complete sequences of normalized band intensities in SERS + GERS EPs (PDF)

■ AUTHOR INFORMATION

Corresponding Author

*E-mail: vlc@natur.cuni.cz.

ORCID

Veronika Sutrová: 0000-0001-8320-2078
Ivana Šloufová: 0000-0002-4757-6029
Peter Mojzeš: 0000-0002-9952-6939
Zuzana Melníková: 0000-0001-5582-9236
Martin Kalbáč: 0000-0001-9574-4368
Blanka Vlčková: 0000-0003-0553-3722

Notes

The authors declare no competing financial interest.

■ ACKNOWLEDGMENTS

I.S., P.M., and B.V. thank the Czech Science Foundation for the financial support by the 17-05007S grant. V.S. acknowledges the financial support by the 892217 students grant awarded by the Grant Agency of Charles University. M.K. and Z.M. acknowledge the support from MSMT project ERC-CZ (LL1301). The authors also acknowledge the assistance provided by the Research Infrastructure NanoEnviCz, supported by the Ministry of Education, Youth and Sports of the Czech Republic under project no. LM2015073 and project no. CZ.02.1.01/0.0/0.0/16_013/0001821. The authors also thank Jana Vejpravova (Charles University) for helpful discussions.

■ REFERENCES

(1) Procházka, M. *Surface-Enhanced Raman Spectroscopy-Bioanalytical, Biomolecular and Medical Applications*; Springer International Publishing: Switzerland, 2016.

(2) Aroca, R. *Surface-Enhanced Vibrational Spectroscopy*; John Wiley and Sons, Ltd.: Chichester, U.K., 2006.

(3) Cotton, T. M. Applications of SERS to Biomolecular Systems. In *Spectroscopy of Surfaces*; Clark, R. J. H., Hester, R. E., Eds.; Wiley: New York, 1988; pp 91−153.

(4) Matějka, P.; Vlčková, B.; Bednárová, L.; Maloň, P. Advances and Challenges in Optical Molecular Spectroscopy Including Surface Plasmon Resonance-Based Methods for Bioanalysis. In *Natural Products Analysis: Instrumentation, Methods and Applications*; Havlíček, V., Spížek, J., Eds.; John Wiley and Sons: Hoboken, N.J., USA, 2014; pp 163−238.

DOI: 10.1021/acs.jpcc.8b06218
J. Phys. Chem. C 2018, 122, 20850−20860

(5) Vlčková, B.; Matějka, P.; Šimonová, J.; Čermaková, K.; Pančoška, P.; Baumruk, V. Surface-enhanced resonance Raman spectra of free base 5,10,15,20-tetrakis(4-carboxyphenyl)porphyrin and its silver complex in systems with silver colloid: direct adsorption in comparison to adsorption via molecular spacer. *J. Phys. Chem.* **1993**, *97*, 9719−9729.
(6) Weitz, D. A.; Garoff, S.; Gersten, J. I.; Nitzan, A. The Enhancement of Raman Scattering, Resonance Raman Scattering, and Fluorescence from Molecules Adsorbed on a Rough Silver Surface. *J. Chem. Phys.* **1983**, *78*, 5324−5338.
(7) Kokošková, M.; Procházka, M.; Šloufová, I.; Vlčková, B. SERRS Spectra and Excitation Profiles of Ru(II) Polypyridine Complexes Attached to Ag Nanoparticle Aggregates: Structural, Electronic, and Resonance Damping Effects of Chemisorption. *J. Phys. Chem. C* **2013**, *117*, 1044−1052.
(8) Xu, W.; Ling, X.; Xiao, J.; Dresselhaus, M. S.; Kong, J.; Xu, H.; Liu, Z.; Zhang, J. Surface Enhanced Raman Spectroscopy on a Flat Graphene Surface. *Proc. Natl. Acad. Sci. U.S.A.* **2012**, *109*, 9281−9286.
(9) Xu, W.; Mao, N.; Zhang, J. Graphene: A Platform for Surface-Enhanced Raman Spectroscopy. *Small* **2013**, *9*, 1206−1224.
(10) Zaretski, A. V.; Marin, B. C.; Moetazedi, H.; Dill, T. J.; Jibril, L.; Kong, C.; Tao, A. R.; Lipomi, D. J. Using the Thickness of Graphene to Template Lateral Subnanometer Gaps between Gold Nanostructures. *Nano Lett.* **2015**, *15*, 635−640.
(11) Zhang, N.; Tong, L.; Zhang, J. Graphene-Based Enhanced Raman Scattering toward Analytical Applications. *Chem. Mater.* **2016**, *28*, 6426−6435.
(12) Dai, Z.-g.; Xiao, X.-h.; Wu, W.; Zhang, Y.-p.; Liao, L.; Guo, S.-s.; Ying, J.-j.; Shan, C.-x.; Sun, M.-t.; Jiang, C.-z. Plasmon-Driven Reaction Controlled by the Number of Graphene Layers and Localized Surface Plasmon Distribution During Optical Excitation. *Light: Sci. Appl.* **2015**, *4*, No. e342.
(13) Zhang, X.; Dai, Z.; Si, S.; Zhang, X.; Wu, W.; Deng, H.; Wang, F.; Xiao, X.; Jiang, C. Ultrasensitive SERS Substrate Integrated with Uniform Subnanometer Scale "Hot Spots" Created by a Graphene Spacer for the Detection of Mercury Ions. *Small* **2017**, *13*, 1603347.
(14) Weiss, J. E.; Costa, S.; Frank, O.; Fridrichová, M.; Vlčková, B.; Vejpravová, J.; Kalbáč, M. SERS of Isotopically Labeled 12C/13C Graphene Bilayer−Gold Nanostructured Film Hybrids: Graphene Layer as Spacer and SERS Probe. *J. Phys. Chem. C* **2017**, *121*, 11680−11686.
(15) Hao, Q.; Wang, B.; Bossard, J. A.; Kiraly, B.; Zeng, Y.; Chiang, I.-K.; Jensen, L.; Werner, D. H.; Huang, T. J. Surface-Enhanced Raman Scattering Study on Graphene-Coated Metallic Nanostructure Substrates. *J. Phys. Chem. C* **2012**, *116*, 7249−7254.
(16) Kang, L.; Chu, J.; Zhao, H.; Xu, P.; Sun, M. Recent Progress in the Applications of Graphene in Surface-Enhanced Raman Scattering and Plasmon-Induced Catalytic Reactions. *J. Mater. Chem. C* **2015**, *3*, 9024−9037.
(17) Xu, S.; Man, B.; Jiang, S.; Wang, J.; Wei, J.; Xu, S.; Liu, H.; Gao, S.; Liu, H.; Li, Z.; Li, H.; Qiu, H. Graphene/Cu Nanoparticle Hybrids Fabricated by Chemical Vapor Deposition as Surface-Enhanced Raman Scattering Substrate for Label-Free Detection of Adenosine. *ACS Appl. Mater. Interfaces* **2015**, *7*, 10977−10987.
(18) Gopal, J.; Abdelhamid, H. N.; Huang, J.-H.; Wu, H.-F. Nondestructive detection of the freshness of fruits and vegetables using gold and silver nanoparticle mediated graphene enhanced Raman spectroscopy. *Sens. Actuators, B* **2016**, *224*, 413−424.
(19) Xu, S.; Jiang, S.; Wang, J.; Wei, J.; Yue, W.; Ma, Y. Graphene Isolated Au Nanoparticle Arrays with High Reproducibility for High-Performance Surface-Enhanced Raman Scattering. *Sens. Actuators, B* **2016**, *222*, 1175−1183.
(20) Ling, X.; Xie, L.; Fang, Y.; Xu, H.; Zhang, H.; Kong, J.; Dresselhaus, M. S.; Zhang, J.; Liu, Z. Can Graphene Be Used as a Substrate for Raman Enhancement? *Nano Lett.* **2010**, *10*, 553−561.
(21) Barros, E. B.; Dresselhaus, M. S. Theory of Raman Enhancement by Two-Dimensional materials: Applications for Graphene-Enhanced Raman Spectroscopy. *Phys. Rev. B: Condens. Matter Mater. Phys.* **2014**, *90*, 035443.
(22) Ling, X.; Huang, S.; Deng, S.; Mao, N.; Kong, J.; Dresselhaus, M. S.; Zhang, J. Lighting Up the Raman Signal of Molecules in the Vicinity of Graphene Related Materials. *Acc. Chem. Res.* **2015**, *48*, 1862−1870.
(23) Huang, S.; Ling, X.; Liang, L.; Song, Y.; Fang, W.; Zhang, J.; Kong, J.; Meunier, V.; Dresselhaus, M. S. Molecular Selectivity of Graphene-Enhanced Raman Scattering. *Nano Lett.* **2015**, *15*, 2892−2901.
(24) Uhlířová, T.; Mojzeš, P.; Melníková, Z.; Kalbáč, M.; Sutrová, V.; Šloufová, I.; Vlčková, B. Raman Excitation Profiles of Hybrid Systems Constituted by Single-Layer Graphene and Free Base Phthalocyanine: Manifestations of Two Mechanisms of Graphene-Enhanced Raman Scattering. *J. Raman Spectrosc.* **2017**, *48*, 1270−1281.
(25) Sutrová, V.; Šloufová, I.; Melníková, Z.; Kalbáč, M.; Pavlova, E.; Vlčková, B. Effect of Ethanethiolate Spacer on Morphology and Optical Responses of Ag Nanoparticle Array-Single Layer Graphene Hybrid Systems. *Langmuir* **2017**, *33*, 14414−14424.
(26) Brotman, A.; Burstein, E. Raman Scattering-Excitation Profiles of Molecules Adsorbed on Metal Surfaces: Free-Base Phthalocyanine on Silver. *Phys. Scr.* **1985**, *32*, 385−390.
(27) Murray, C.; Dozova, N.; McCaffrey, J. G.; Shafizadeh, N.; Chin, W.; Broquier, M.; Crépin, C. Visible Luminescence Spectroscopy of Free-Base and Zinc Phthalocyanines Isolated in Cryogenic Matrices. *Phys. Chem. Chem. Phys.* **2011**, *13*, 17543−17554.
(28) Cook, M.; Chambrier, I. *The Porphyrin Handbook: Phthalocyanines: Properties and Materials*; Kadish, K., Guilard, R., Smith, K. M., Eds.; Academic Press, 2003; Chapter Phthalocyanine Thin Films: Deposition and Structural Studies; Vol. *17*, pp 37−128.
(29) Nilson, K.; Åhlund, J.; Brena, B.; Göthelid, E.; Schiessling, J.; Mårtensson, N.; Puglia, C. Scanning tunneling microscopy study of metal-free phthalocyanine monolayer structures on graphite. *J. Chem. Phys.* **2007**, *127*, 114702.
(30) Menaa, B.; Takahashi, M.; Tokuda, Y.; Yoko, T. Dispersion and Photoluminescence of Free-Metal Phtalocyanine Doped in Sol-Gel Polyphenylsiloxane Glass Film. *J. Photochem. Photobiol., A* **2008**, *194*, 362−366.
(31) Kaya, E. N.; Basova, T.; Polyakov, M.; Durmuş, M.; Kadem, B.; Hassan, A. Hybrid Materials of Pyrene Substituted Phthalocyanines with Single-Walled Carbon Nanotubes: Structure and Sensing properties. *RSC Adv.* **2015**, *5*, 91855−91862.
(32) Ochsner, M. Photophysical and Photobiological Processes in the Photodynamic Therapy of Tumors. *J. Photochem. Photobiol., B* **1997**, *39*, 1−18.
(33) Xu, H.; Xie, L.; Zhang, H.; Zhang, J. Effect of Graphene Fermi Level on the Raman Scattering Intensity of Molecules on Graphene. *ACS Nano* **2011**, *5*, 5338−5344.
(34) Joo, Y.; Kim, M.; Kanimozhi, C.; Huang, P.; Wong, B. M.; Roy, S. S.; Arnold, M. S.; Gopalan, P. Effect of Dipolar Molecule Structure on the Mechanism of Graphene-Enhanced Raman Scattering. *J. Phys. Chem. C* **2016**, *120*, 13815−13824.
(35) Michl, M.; Vlčková, B.; Mojzeš, P. Ag colloid-ethanethiol films: spacer-modified substrates for surface-enhanced resonance Raman scattering spectroscopy of chromophoric molecules. *Vib. Spectrosc.* **1999**, *19*, 239−242.
(36) Kalbáč, M.; Frank, O.; Kavan, L. The Control of Graphene Double-Layer Formation in Copper-Catalyzed Chemical Vapor Deposition. *Carbon* **2012**, *50*, 3682−3687.
(37) Hallam, T.; Berner, N. C.; Yim, C.; Duesberg, G. S. Strain, Bubbles, Dirt, and Folds: A Study of Graphene Polymer-Assisted Transfer. *Adv. Mater. Interfaces* **2014**, *1*, 1400115.
(38) Giovannetti, G.; Khomyakov, P. A.; Brocks, G.; Karpan, V. M.; van den Brink, J.; Kelly, P. J. Doping Graphene with Metal Contacts. *Phys. Rev. Lett.* **2008**, *101*, 026803.
(39) Jorio, A.; Saito, R.; Dresselhaus, G.; Dresselhaus, M. S. *Raman Spectroscopy in Graphene Related Systems*; Wiley-VCH Verlag GmbH & Co. KGaA: Weinheim, Germany, 2011.

DOI: 10.1021/acs.jpcc.8b06218
J. Phys. Chem. C 2018, 122, 20850−20860

(40) Ferrari, A. C.; Basko, D. M. Raman Spectroscopy as a Versatile Tool for Studying the Properties of Graphene. *Nat. Nanotechnol.* **2013**, *8*, 235−246.
(41) Dissanayake, D. M. N. M.; Ashraf, A.; Dwyer, D.; Kisslinger, K.; Zhang, L.; Pang, Y.; Efstathiadis, H.; Eisman, M. D. Spontaneous and Strong Multilayer Graphene n-Doping on Soda-Lime Glass and its Applications in Graphene-Semiconductor Junctions. *Sci. Rep.* **2016**, *6*, 21070.
(42) Murray, C.; Dozova, N.; McCaffrey, J. G.; FitzGerald, S.; Shafizadeh, N.; Crépin, C. Infra-red and Raman Spectroscopy of Free-Base and Zinc Phthalocyanines Isolated in Matrices. *Phys. Chem. Chem. Phys.* **2010**, *12*, 10406−10422.
(43) Lin, W.-L.; Gholami, M. F.; Beyer, P.; Severin, N.; Shao, F.; Zenobi, R.; Rabe, J. P. Strongly Enhanced Raman Scattering of Cu-Phthalocyanine Sandwiched between Graphene and Au(111). *Chem. Commun.* **2017**, *53*, 724−727.
(44) Clark, R. J. H.; Dines, T. J. Resonance Raman Spectroscopy, and Its Application to Inorganic Chemistry. New Analytical Methods (27). *Angew. Chem., Int. Ed. Engl.* **1986**, *25*, 131−158.
(45) Tackley, D. R.; Dent, G.; Smith, W. E. Phthalocyanines: Structure and Vibrations. *Phys. Chem. Chem. Phys.* **2001**, *3*, 1419−1426.
(46) Heutz, S.; Salvan, G.; Silaghi, S. D.; Jones, T. S.; Zahn, D. R. T. Raman Scattering as a Probe of Crystallinity in PTCDA and H2Pc Single-Layer and Double-Layer Thin Film Heterostructures. *J. Phys. Chem. B* **2003**, *107*, 3782−3788.

DOI: 10.1021/acs.jpcc.8b06218
J. Phys. Chem. C 2018, 122, 20850−20860

SUPPORTING INFORMATION

Excitation Wavelength Dependence of Combined Surface- and Graphene-Enhanced Raman Scattering Experienced by Free-base Phthalocyanine Localized on Single Layer Graphene-Covered Ag Nanoparticle Array

Veronika Sutrová[a,d] Ivana Šloufová[a] Peter Mojzeš[b], Zuzana Melniková[c] Martin Kalbáč[c], Blanka Vlčková[a*]

[*] Correspondence to: Blanka Vlčková, Charles University, Faculty of Science, Department of Physical and Macromolecular Chemistry, Hlavova 8, Prague 2, 128 40, Czech Republic, vlc@natur.cuni.cz

[a] Charles University, Faculty of Science, Department of Physical and Macromolecular Chemistry, Hlavova 8, Prague 2, 128 40, Czech Republic

[b] Charles University, Faculty of Mathematics and Physics, Institute of Physics, Ke Karlovu 5, Prague 2, 121 16, Czech Republic

[c] J. Heyrovsky Institute of Physical Chemistry of the ASCR, v.v.i, Dolejškova 3, 182 21 Prague 8, Czech Republic

[d] Institute of Macromolecular Chemistry AS CR, Heyrovsky Sq. 2, 162 06 Prague 6, Czech Republic

CONTENT:

Figure S1 – page S2

Figure S2 – page S2

Text S1 – page S3

Figure S3 – page S4

Table S1 – page S4

Text S2 – page S5 - S6

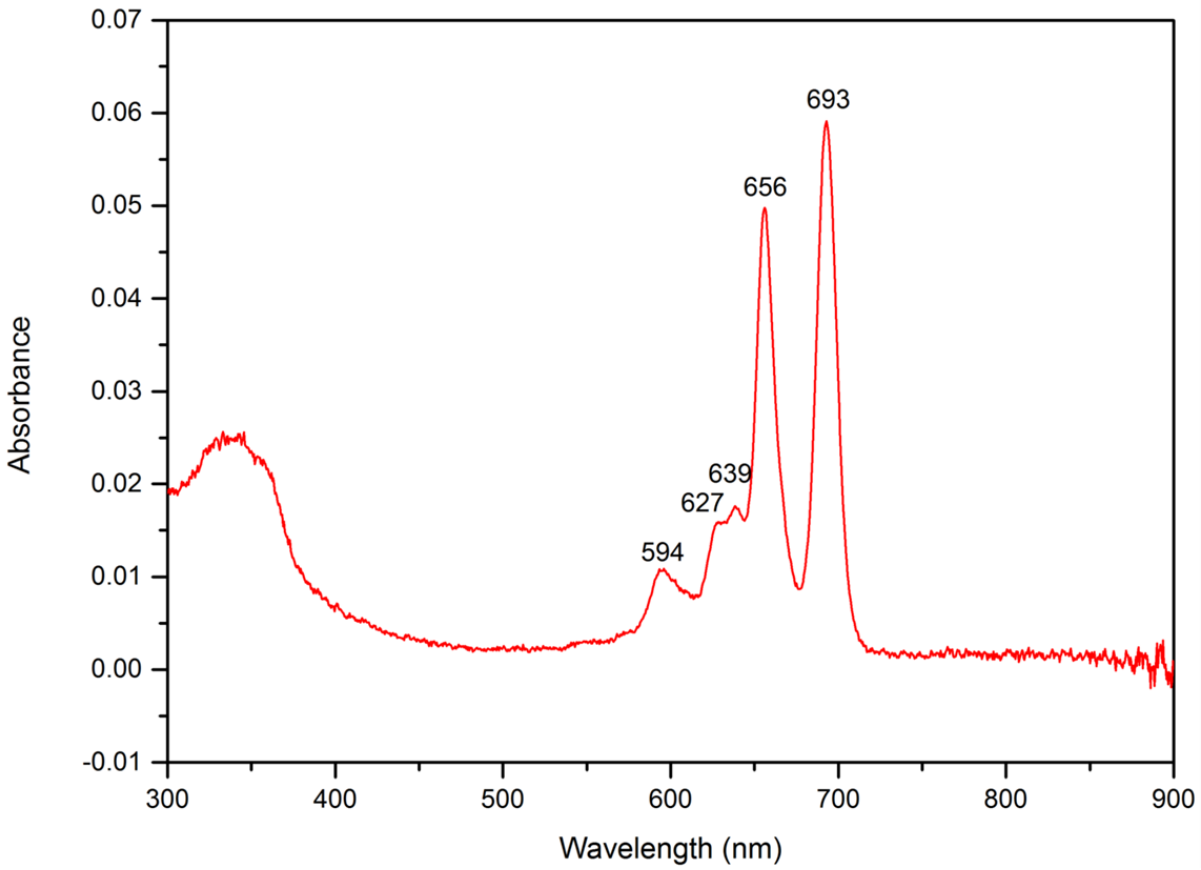

Figure S1 Electronic absorption spectrum of a filtered saturated (<5x10^{-5} M) solution of H_2Pc in toluene.

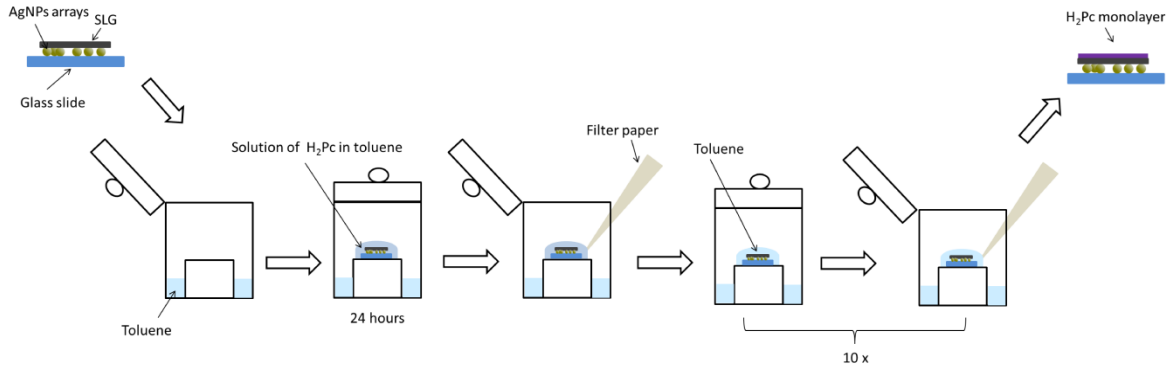

Figure S2 Schematic depiction of the final step of the glassI/AgNPs/SLG/H_2Pc(ML) hybrid system preparation: overdeposition of the glassI/AgNPs/SLG hybrid system by a monolayer (ML) of H_2Pc molecules.

Text S1

A generally known formula for calculation of the standard deviation for a function *u* of two variables *(x,y)*, each of which suffers from random errors:

$$u = u(x, y)$$

$$s_{\bar{u}} = \sqrt{\left(\frac{\partial u}{\partial x}\right)^2 s_{\bar{x}}^2 + \left(\frac{\partial u}{\partial y}\right)^2 s_{\bar{y}}^2}$$

has been adapted for calculations of the average standard deviations of the average values of enhancement factors (EFs) and of the normalized band intensities. As an example, the formula for calculation of the average standard deviations of the average values of SERS EFs is provided:

$$s_{E_F} = E_F \sqrt{\left(\frac{s_{I_{SERS}}}{I_{SERS}}\right)^2 + \left(\frac{s_{I_{RRS}}}{I_{RRS}}\right)^2}$$

where

s_{EF} = average standard deviation of the average value of SERS EF

E_F = average value of SERS EF

I_{SERS} = average value of SERS spectral bands intensity

I_{RRS} = average value of RRS spectral bands intensity

$s_{I_{SERS}}$ = average standard deviation of the average SERS spectral bands intensity

$s_{I_{RRS}}$= average standard deviation of the average RRS spectral bands intensity

The average spectral band intensity was calculated as an average of spectral band intensities at each of the 50 x 50 points of a 25 μm x 25 μm microRaman spectral map, and the average standard deviations were calculated as the average values of differences between the particular spectral band intensity at each point of the map and the average spectral band intensity. The values of the average standard deviations thus reflect the degree of heterogeneity of the microRaman spectral maps on μm scale.

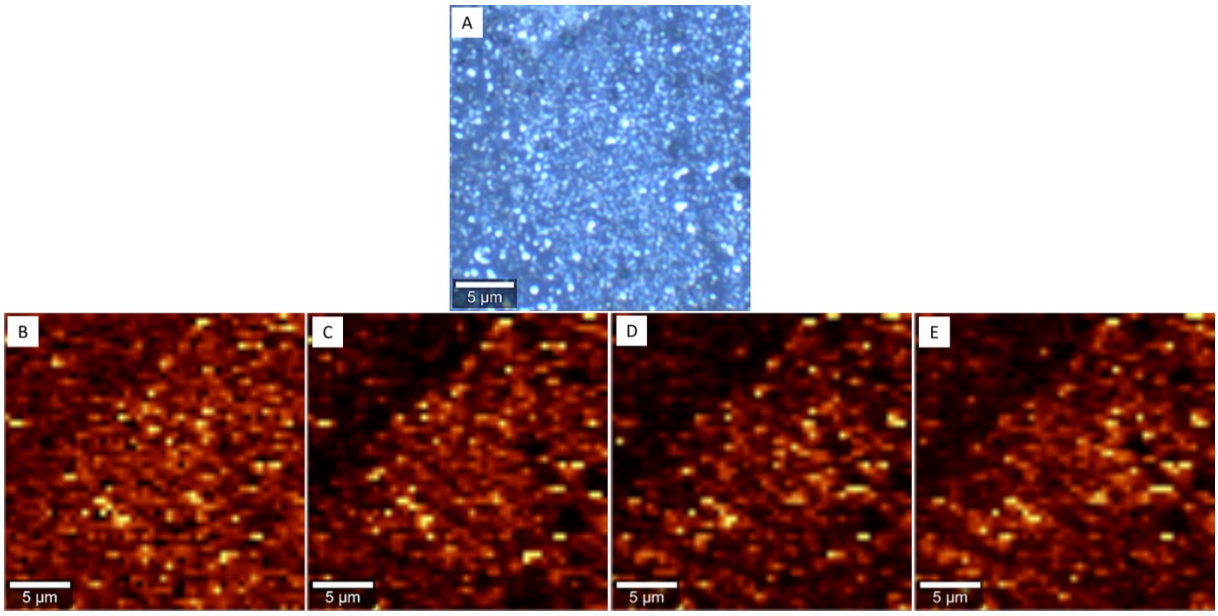

Figure S3 (A) - an optical image of the glassI/AgNPs/SLG/H_2Pc(ML) area of the sample; **(B)** and **(C) -** SERS spectral maps of the G mode (1590 cm^{-1}) and 2D (2595 cm^{-1}) mode of SLG; **(D)** and **(E) -** SERS+GERS spectral maps of the 683 cm^{-1} and 1540 cm^{-1} modes of H_2Pc. The spectral maps **(B)-(D)** were acquired from the same area as the optical image **(A)** at 785 nm excitation.

Table S1 SERS+GERS enhancement factors experienced by Raman modes of the H_2Pc molecule localized in the glassI/AgNPs/SLG/H_2Pc(ML) hybrid system.

Peak position [cm^{-1}]	**EFs GERS + SERS vs RR**	
	633 nm	**647 nm**
484	26 ± 6	25 ± 4
683	34 ± 7	25 ± 6
726	14 ± 5	20 ± 3
798	22 ± 5	28 ± 5
1085	32± 8	27± 5
1143	46 ± 7	53 ± 12
1343	39 ± 5	33 ± 8
1452	67 ± 6	72 ± 9
1540	107 ± 15	88 ± 13

Text S2

Detailed analysis of the sequences of normalized band intensities in SERS+GERS EPs of the spectral bands of H_2Pc localized in glassI/AgNPs/SLG/H_2Pc(ML) hybrid systems

The sequences of the normalized band intensities in SERS+GERS excitation profiles (EPs) of the spectral bands of H_2Pc localized in glassI/AgNPs/SLG/H_2Pc(ML) were determined at 633 and 647 nm excitations from the complete EPs presented in Figure 5A and at 830 nm excitation from the detailed EPs depicted in Figure 5B. The sequences of the normalized band intensities were analyzed in terms of the symmetry of the corresponding vibrations and their localization within the H_2Pc molecule. For the totally symmetric normal vibrations (A_g), their normalized relative band intensities are proportional to the magnitude of changes of their normal coordinates upon the resonant electronic transition. Their evaluation thus allows for determination of the localization of the resonant electronic transitions within a molecule. [24,44] The sequence of the most intense bands (maxima in cm^{-1}) in EM SERS+GERS of H_2Pc at 633 nm excitation was determined as follows: 1540 (A_g) > 1343 (A_g) > 1143 (A_g) > 1452 (A_g) > 799 (A_g) ~ 726 (A_g) > 683 (A_g) > 1085 (B_{1g}) ~ 484 (B_{1g}). At 647 nm excitation, the sequence of the most intense bands was found to be: 1540 (A_g)> 1343 (A_g) > 1143 (A_g) > 726 (A_g) ~1452 (A_g) ~ 683 (A_g) ~ 799 (A_g) > 1085 (B_{1g}) > 484 (B_{1g}). The common feature of both sequences of the spectral bands is a preferential enhancement of the totally symmetric A_g modes over the B_{1g} modes, and a preferential enhancement of higher wavenumber A_g modes of localized on the pyrrole and on the benzene rings over the low wavenumber A_g macrocycle modes (the latter aspect being more pronounced at 633 than at 647 nm excitation). Importantly, the sequences of the most enhanced bands are similar to those reported for GERS of H_2Pc in ref.[24] and they indicate that both the 633 and the 647 nm excitations fall into the electronic absorption band of the Q_y 0-0 electronic transition within the H_2Pc molecules assembled into a monolayer on the surface of SLG, i.e. upon the conditions of the SLG-H_2Pc (ML) interaction.

The sequence of the most intense bands at 830 nm excitation was established as: 683 (A_g) > 726 (A_g) > 1343 (A_g) ~484 (B_{1g}) > 1143 (A_g) ~ 1540 (A_g) > 1452 (A_g) > 799 (A_g) > 1086 (B_{1g}). In contrast to the previously established sequences of the most enhanced bands at 633 and 647 nm excitation, the low wavenumber bands of the H_2Pc macrocycle are among the most enhanced bands in SERS-GERS of H_2Pc. This effect is analogous to that observed for GERS of H_2Pc in ref.[24], however, the preferential

enhancement of the low wavenumber bands of the H_2Pc macrocycle is even more pronounced in the SERS-GERS EPs presented in this paper (Figure 5B) than in the GERS ones [24], since the low wavenumber 684 and 726 cm^{-1} bands show the largest normalized band intensities of all bands at 830 nm excitation. This observation thus provides a clearcut evidence that the LUMO of H_2Pc is populated by a different electronic transitions at 830 nm excitation than at 633 and 647 nm excitations (as depicted in Figure 7). The former electronic transition is attributed to the charge transfer (CT) electronic transition from the Fermi level of SLG to LUMO of H_2Pc (first reported in ref.[24] for GERS of H_2Pc).

References [24,44] are the same as those listed in the MS text, in particular:

(24) Uhlířová, T. Mojzeš, P. Melniková, Z.; Kalbáč, M.; Šloufová, I.; Vlčková, B. Raman Excitation Profiles of Hybrid Systems Constituted by Single-layer Graphene and Free Base Phthalocyanine: Manifestations of Two Mechanisms of Graphene-enhanced Raman Scattering. *J. Raman Spectrosc.* **2017**,*48*, 1270-1281.

(44) Clark, R. J. H.; Dines, T. J. Resonance Raman Spectroscopy, and its Applications to Inorganic Chemistry. *Angew. Chem. Int. Ed. Engl.* **1986,** *25*, 131-158.